THE
PHYSICAL REVIEW
A Journal of Experimental and Theoretical Physics Established by E. L. Nichols in 1893
VOL. 52, NO. 11 DECEMBER 1, 1937 SECOND SERIES

Neutrons from the Disintegration of Nitrogen by Deuterons

WILLIAM E. STEPHENS, KAMAL DJANAB
W. K. Kellogg Radiation Laboratory, California Institute of Technology, Pasadena, California
AND
T. W. BONNER, *Rice Institute, Houston, Texas*
(Received October 5, 1937)

The energy distribution of the neutrons resulting from the disintegration of nitrogen by 0.93 MV deuterons has been investigated in a high pressure cloud chamber. Three groups of recoil protons were found with maximum enegies of 5.7 MV, 2.7 MV and 1.9 MV and with relative intensities of 2 : 1 : 3. The 2.7 MV group is attributed to deuterium contamination on the target. The other two groups are from the reaction

$$_7N^{14}+{}_1H^2={}_8O^{15}+{}_0n^1+Q_1$$

where $Q_{10}=5.1\pm0.2$ MV and $Q_{11}=1.1\pm0.2$ MV.

INTRODUCTION

WHEN nitrogen is bombarded with deuterons, three reactions are known to take place

$$_7N^{14}+{}_1H^2={}_8O^{15}+{}_0n^1+Q_1, \quad (1)$$
$$_8O^{15}={}_7N^{15}+{}_+e+Q_e,$$

$$_7N^{14}+{}_1H^2={}_7N^{15}+{}_1H^1+Q_2, \quad (2)$$

$$_7N^{14}+{}_1H^2={}_6C^{12}+{}_2He^4+Q_3. \quad (3)$$

The neutron reaction was first detected by the radioactivity of O^{15} [1] which has a half-life of 126 seconds[2] and a maximum positron energy of 1.7 MV.[3] The neutrons have been observed,[2, 4] but have not been measured heretofore. The protons and alpha-particles have been observed[5] and accurately measured,[6] giving values of

$$Q_{20}=8.53\pm0.1 \text{ MV}, \quad Q_{21}=3.25\pm0.07 \text{ MV},$$
$$Q_{30}=13.22\pm0.1 \text{ MV}, \quad Q_{31}=8.93\pm0.03 \text{ MV}.$$

Gamma-rays have been found to accompany these reactions.[7] At 0.5 MV energy of the deuterons, these reactions have about the same yields,[6] while at 1.4 MV, the alpha-particles are thirty times as numerous as the protons.[5]

It was the purpose of this experiment to investigate the energy distribution of the neutrons from reaction (1).

EXPERIMENTAL PROCEDURE

The high pressure cloud chamber used has been described by Brubaker and Bonner.[8] The

[1] Henderson, Livingston and Lawrence, Phys. Rev. **45**, 428 (1934).
[2] Livingston and McMillan, Phys. Rev. **46**, 437 (1934).
[3] Fowler, Delsasso and Lauritsen, Phys. Rev. **49**, 561 (1936).
[4] Cockcroft, Gilbert and Walton, Proc. Roy. Soc. **A148**, 225 (1935).
[5] Lawrence, McMillan and Henderson, Phys. Rev. **47**, 273 (1935).
[6] Cockcroft and Lewis, Proc. Roy. Soc. **A154**, 261 (1935).
[7] Crane, Delsasso, Fowler and Lauritsen, Phys. Rev. **48**, 100 (1935).
[8] Brubaker and Bonner, Rev. Sci. Inst. **6**, 143 (1935).

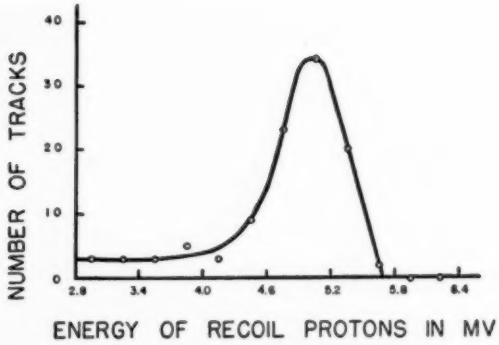

FIG. 1. The energy distribution of the high energy recoil protons observed when nitrogen was bombarded with deuterons.

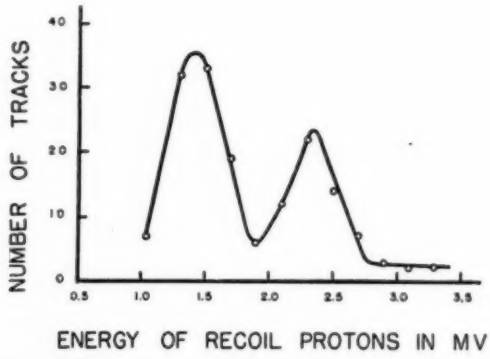

FIG. 2. The energy distribution of the low energy recoil protons observed when nitrogen was bombarded with deuterons.

method of determining neutron energies by measuring the ranges of recoil protons in the cloud chamber has also been discussed.[9–12]

Targets of $NaNO_2$ melted onto copper were bombarded with 0.93 MV deuterons from a short ion path a.c. tube built by one of us (W.E.S.). The target was bombarded only for the 1/10 of a second that the chamber was sensitive and was changed after about 2000 expansions to avoid carbon and deuterium contamination. The current was of the order of 100 to 200 microamperes of unresolved ions. According to a magnetic analysis made on a similar ion source, the ratio of deuterium ions to molecules may be 1 to 10.[13] The gas used in the ion source was 95 percent deuterium, 4.5 percent hydrogen, and 0.5 percent nitrogen which can now be bought in tanks.[14]

To investigate the high energy neutrons, the chamber was filled with illuminating gas to 10.2 atmospheres. The initial composition of the gas was known from the gas company's analysis. We assumed that the composition was not altered by putting it in the chamber except for the methane-ethane ratio. This should change due to the different solubilities of methane and ethane in the 500 cc of ethyl alcohol in the chamber. To determine this ratio, a sample was drawn from the chamber after the run and its specific gravity measured. The percentage of methane had changed from 82 to 89 percent. The stopping power was then calculated using Mano's values.[15] This calculated stopping power of 0.93 per atmosphere was then checked by determining the mean range of polonium alpha-particles in the chamber at one atmosphere pressure of the same gas. To resolve the low energy neutron groups, another run was made with 11.4 atmospheres of hydrogen in the chamber. Here the stopping power was determined directly by measuring polonium alpha-particle tracks in the chamber at the same time as the recoil proton tracks.

RESULTS

9500 stereoscopic pictures were taken with methane in the cloud chamber and the tracks within 8° of the forward direction were measured. The energy number curve for these is shown in Fig. 1. 5500 of these pictures were measured carefully enough to resolve the low energy groups and to the tracks from them were added the tracks from 7500 pictures taken with hydrogen in the chamber. The energy number curve for these low energy tracks is shown in Fig. 2. (The ordinates of the two curves are not directly comparable.) It is apparent from these curves that there are three distinct groups of neutrons with maximum energies of 5.7 MV, 2.7 MV and 1.9 MV.

Since the 2.7 MV group has the same energy as would be expected from deuterons on deuterium,[11] it was suspected of being due to

[9] Bonner and Brubaker, Phys. Rev. **47**, 910 (1935).
[10] Bonner and Brubaker, Phys. Rev. **48**, 742 (1935).
[11] Bonner and Brubaker, Phys. Rev. **49**, 19 (1936).
[12] Bonner and Brubaker, Phys. Rev. **50**, 308 (1936).
[13] R. B. Roberts, Phys. Rev. **51**, 810 (1937).
[14] Stuart Oxygen Company, 211 Bay Street, San Francisco.
[15] G. Mano, J. de phys. et rad. **5**, 628 (1934).

deuterium contamination on the target. To check this, 2500 pictures were taken with methane in the chamber and everything the same as in the first run except that the bombarding energy was 0.72 MV instead of 0.93 MV. The yield from deuterium (D_3PO_4), as determined under similar conditions, decreases only 20 percent[11] in reducing the voltage from 0.9 MV to 0.7 MV, while the yield from nitrogen would be expected to decrease faster even than from beryllium (which decreases 70 percent[11]). Hence the relative intensity of the 2.7 MV group to the 5.7 MV group would be expected to increase by a factor greater than 2.5 if the 2.7 MV group were from deuterium. If they were both from nitrogen, the relative intensity should not be greatly altered. Actually the ratio increased by a factor of 10. Further confirmation of the presence of deuterium contamination is gotten from previous work on carbon[12] where deuterium neutrons were present in similar numbers under similar conditions. Also in a run with a target of NaOH to check the background, only deuterium neutrons were observed. Hence there is little doubt that this group is from deuterons on deuterium. Since the number of deuterium neutrons does not seem to increase appreciably with time of bombardment, it may be that most of the deuterium in this case is not driven into the target from the beam, but is adsorbed on the surface of the target from the deuterium in the tube. The energy Q_D calculated from this peak is $Q_D=3.2$ MV, slightly less than the more accurate value $Q_D=3.35$ MV recently found.[16] The difference is probably due to the fact that with an a.c. tube and with such a slowly rising excitation function, the effective bombarding energy is slightly smaller than the peak energy (by about 0.2 MV).

The 5.7 MV and 1.9 MV groups have approximately the same energies as the neutrons attributed to the reaction ${}_6C^{13}+{}_1H^2={}_7N^{14}+{}_0n^1$.[12] If these neutrons were due to carbon contamination on the target, then the C^{12} neutrons (energy 0.35 MV[12] or 0.46 MV[17]) would be 100 times as numerous. A run with one atmosphere of methane in the chamber showed no C^{12} neutrons. Furthermore, the number of neutrons from $NaNO_2$ was greater than the number of C^{13} neutrons produced under similar conditions by bombarding a pure carbon target.[12]

The Q's for the nitrogen reaction come out $Q_{10}=5.1$ MV and $Q_{11}=1.1$ MV with the errors of ± 0.2 MV due to uncertainty in the stopping power and uncertainty in interpretation of the end points. The observed end-points of the proton groups were corrected by subtracting the probable error in measuring the track length. The maximum mean range was then gotten by subtracting the calculated straggling. This range was converted to energy using the energy-range curve of Mano's.[15] The disintegration energies were calculated in the usual manner, assuming that the maximum energy neutrons came off at an angle of 80° to the direction of the deuteron (since the neutrons were observed at $90°\pm 10°$ to the direction of the incident deuterons).

The relative intensity of the 5.7 MV group to the 1.9 MV group is 2 : 3. The relative intensity of the 5.7 MV group to the deuterium group is 2 : 1 at 0.9 MV and 1 : 5 at 0.7 MV. These relative intensities were corrected for the area in which a track could start and still not hit the wall, and for the collision cross section.[10]

A very few recoil protons with energies greater than 7 MV were observed. These may have been from N^{15} or from Na^{23}.[18]

$$ {}_7N^{15}+{}_1H^2={}_8O^{16}+{}_0n^1+9.9 \text{ MV},$$
$$ {}_{11}Na^{23}+{}_1H^2={}_{12}Mg^{24}+{}_0n^1+8.3 \text{ MV}.$$

Discussion

These two groups of neutrons imply an excited level in O^{15} at 4.0 ± 0.3 MV. The normal level in O^{15} is supposed to be a ${}^2P$,[19] and since 4 MV seems large for doublet separation, this excited level may be a D state. If we suppose the excited level in N^{15} at 5.28 MV[6] is a similar level, then the energies of these two states should differ only by the perturbation caused by the Coulomb field of the extra proton in O^{15}. It is somewhat surprising that this difference is so great when

[16] T. W. Bonner, Phys. Rev. **52**, 685 (1937).
[17] Lewis and Burcham; unpublished (see Cockcroft, Proc. Roy. Soc. **A161**, 450 (1937)).
[18] E. O. Lawrence, Phys. Rev. **47**, 17 (1935).
[19] Feenberg and Wigner, Phys. Rev. **51**, 95 (1937).

in the similar case of C^{11} and B^{11} the difference is[12, 20]

$$2.2\pm0.2-2.1\pm0.1=0.1\pm0.3 \text{ MV}.$$

The gamma-rays observed[7] are at least consistent with a gamma-ray of 4 MV, but the spectrum is very complex and assignments are impractical.

According to Bohr's idea of the nucleus,[21] low energy neutrons should have much more probability of escape than higher energy neutrons. That this is not so in this case implies some compensating probability in favor of the higher energy neutrons. If the high energy neutrons came out with no angular momentum and the low energy ones had an angular momentum of one, the increased probability of escape with zero angular momentum would balance the increased probability of escape with low energies.

If we subtract Eq. (2) from Eq. (1) we get

$$Q_e=Q_2-Q_1-({}_0n^1-{}_1H^1)-2e.$$

Using the values $Q_1=5.1\pm0.2$ MV, $Q_2=8.53\pm0.1$ MV[6] and $({}_0n^1-{}_1H^1)=0.85$ MV[12] we can calculate Q_e, the maximum energy of the O^{15} positrons. This comes out $Q_e=1.56\pm0.2$ MV, which agrees within the errors with the observed end point 1.7 ± 0.2 MV.[3] This is in accord with the cases of N^{13}, C^{11}, F^{17} and P^{30} where also the calculated value is slightly lower but in agreement within the experimental errors with the observed end point rather than the Konopinski-Uhlenbeck extrapolated end point.[22]

If we use the mass-spectroscopic value for the doublet $(N^{14}H^1-N^{15})$,[23] and the photodisintegration value for the binding energy of the deuteron[24] and substitute in Eq. (1),

$(N^{14}H^1-N^{15})-\text{binding of deuteron}-2e=Q_1+Q_e$,

where

$$(N^{14}H^1-N^{15})=10.0\pm0.2 \text{ MV},$$
$$\text{binding of deuteron}=2.22 \text{ MV},$$
$$2e=1.02 \text{ MV},$$
$$Q_1=5.1\pm0.2 \text{ MV};$$

then $$Q_1+Q_e=6.76\pm0.2 \text{ MV}$$

or $$Q_e=1.66\pm0.3 \text{ MV}.$$

This also is in much better agreement with the observed end point of 1.7 MV, than with the Konopinski-Uhlenbeck extrapolated end-point of 2.0 MV.

Livingston and Bethe[25] ascribe the 4/35 MV neutron group obtained by bombarding boron with deuterium to C^{12} instead of to C^{11}, thus not leaving any evidence for a 2 MV excited level in C^{11}. If this is so, there is no experimental reason to expect similar levels in nuclei differing by interchange of a neutron and proton to have closely the same energy.

We wish to thank Dr. C. C. Lauritsen for continued encouragement, Dr. Walter Elsasser for a discussion of the theoretical aspects, and the Seeley W. Mudd Fund for financial support.

[20] Cockcroft and Lewis, Proc. Roy. Soc. **A154**, 246 (1936). *Note added in proof:* It should be pointed out that it is not certain that the 4.35 MV neutron group appearing when boron is bombarded with deuterons is to be associated with C^{11} rather than C^{12}. So the existence of a 2.2 MV level in C^{11} is not definitely established.

[21] N. Bohr, Nature **137**, 344 (1936).

[22] J. D. Cockcroft, Proc. Roy. Soc. **A161**, 450 (1937).

[23] Jordan and Bainbridge, Phys. Rev. **50**, 98 (1936).

[24] Feather, Nature **136**, 467 (1935); Bethe and Bacher, Rev. Mod. Phys. **8**, 123 (1936).

[25] Livingston and Bethe, Rev. Mod. Phys. **9**, 333 (1937).

Molecular Viewpoints in Nuclear Structure

JOHN ARCHIBALD WHEELER[1]
University of North Carolina, Chapel Hill, North Carolina
(Received August 17, 1937)

A study of the transition between the H_2^+ molecule and the corresponding three-body nucleus shows (1) that it is useful to regard the system as composed of two parts (heavy particle; heavy and light particles) between which acts an effective potential; (2) that this potential depends more and more on the relative velocity of the two parts as the masses of the light and heavy particles approach equality; (3) that the wave equation and the potential for the relative motion are obtained in a consistent manner by requiring that a certain form of approximate wave function give the best possible representation of the motion of the three particles, in the sense of the variation principle. This wave function represents a state in which the system resonates between the groupings atom-ion and ion-atom. It is adapted to the treatment of the scattering of neutrons in deuterium and is also used in the text to calculate the binding energy of H^3. Application of the same type of approximate wave function to the description of nuclear structure in general, gives rise to the concept of resonating group structure. This picture regards the constituent neutrons and protons as divided into various groups (such as alpha-particles) which are continually being broken and reformed in new ways. Group theory gives information as to which groupings are most important in describing a particular state of a given nucleus. The interchange of neutrons and protons between the groups is rapid. It is largely responsible for the intergroup forces, but also prevents one from attributing any well-defined individuality to the groups except as follows: If the time required for a particle to diffuse between two parts of the nucleus vibrating in opposite phase (in the language of the liquid droplet model) is large in comparison with the period of the vibration, then the particles of the nucleus may be divided into groups which preserve their identity long enough to make possible a simple description of the nuclear motion in terms of the relative displacements of these clusters. Arguments are given to show that the diffusion condition is satisfied for low excitation energies. When the nuclear energy is higher, the groups have significance only in providing a suitable mathematical scheme to treat the nuclear motion (see following paper). Allowed types of motion and energies for low states of Be^8, C^{12}, and O^{16} are calculated in terms of the relative motion of alpha-particle groups, using the methods familiar in molecular structure. The modes of vibration are closely related to those given by the liquid model of Bohr and Kalckar, but many low levels are excluded on symmetry grounds. The general methods outlined here for the description of nuclear structure are to a large extent independent of the nature of the forces between elementary particles. A discussion of the possible existence of many-body forces is given (i.e., forces which cannot be described by a potential that is a sum of potentials involving two particles at a time). The observed variation of nuclear binding energy with atomic number is found not to give sufficient evidence from which to draw any general conclusion. Electron positron theory indicates that a part of the nuclear forces consists of many-body interactions.

UNDERSTANDING of certain features of nuclear constitution has been gained by applying, with proper limitations, concepts native to atomic structure. To these ideas we wish in the following to add some points of view more closely related to molecular structure. If atomic structure be characterized by a central force dominating the motion of almost independent particles, and nuclear constitution, by those collective types of motion which Bohr and Kalckar[2] liken to the modes of vibration and rotation of a liquid droplet, then the feature which distinguishes molecular structure from these is its division of the constituent particles into more or less well-defined groups, between which it is a good approximation to say that inter- "atomic" forces act. It is the usefulness, and limitations, of this concept of group structure that we wish to study in connection with the mechanical description of the atomic nucleus.

THE THREE-BODY PROBLEM

We consider in illustration first the three-body problem (Fig. 1), because here the differences between the treatments of atom, nucleus, and molecule are not accentuated sufficiently that the similarities escape notice. In both the atomic and the nuclear systems, there is no one particle which provides a dominating center of force; and

[1] I am indebted to the University of North Carolina for leave of absence, December 15, 1936 to March 15, 1937, to the Institute for Advanced Study, where part of this work was done, for its hospitality, and to the other members of the 1937 Washington Conference on Theoretical Physics for discussion of some of the results.
[2] N. Bohr and F. Kalckar, Kgl. Dansk Viden. Selskab, in press.

FIG. 1.

introduction of a time average field to represent the action of two particles on the third is not satisfactory because the two speeds involved are comparable. These difficulties, which distinguish the helium atom among other atomic systems, are the same ones experienced in approaching the description of nuclear constitution in general by the Hartree central field approximation.

In the molecular three-body problem, on the other hand, the rapidity of the electronic motion in comparison with the displacement of the heavy particles is known to allow an approximate separation[3] of the system into (1) electronic motion with fixed force centers and (2) slow nuclear motion in the time average field determined by (1). In contrast to the situation in the helium problem, we have here a relatively simple basis from which to approach the nuclear three-body system.

As the mass of the light particle is gradually increased in the transition from molecule to nucleus, two new features reveal themselves. First, the molecular potential acts not from nucleus to nucleus but from the center of gravity of a pair consisting of a heavy and a light particle to the other heavy particle. Second, the velocity of approach of these two parts of the system has an influence on the interaction which grows as the mass of the light particle is increased and its speed becomes more comparable with that of the intermolecular motion.

We shall find it possible to bring both of the above facts into evidence by dividing the original molecular potential into two parts:

V, an ordinary potential; and

K, a velocity dependent potential, represented for quantum-mechanical purposes by an integral operator.[4] In addition, we introduce

$\mathbf{X}$, a vector with components X, Y, Z, representing the separation between one heavy particle (which, not stated!) and the center of gravity of the other two particles;

$\boldsymbol{\xi}=(\xi, \eta, \zeta)$, simply a vector variable of integration, which however is shown below to be interpretable as the separation between the second heavy particle and the center of gravity of the other two particles (see Fig. 1); and

μ_{12}, the reduced mass associated with the relative motion of the two groups of particles composing the system:

$$\mu_{12}^{-1}=M^{-1}+(M+m)^{-1}.$$

Then the equation we use to describe the integroup motion is

$$(\hbar^2/2\mu_{12})\nabla^2\psi(\mathbf{X})+E\psi(\mathbf{X})=V(\mathbf{X})\psi(\mathbf{X})+\int K(\mathbf{X}, \boldsymbol{\xi})\psi(\boldsymbol{\xi})d\boldsymbol{\xi} \quad (1)$$

(an equation which is derived independently in Appendix I). Rapid motion means many nodes in ψ and a diminished contribution from the integral; thus the velocity dependence of the potential. Integration over $\boldsymbol{\xi}$, $\mathbf{X}$ remaining constant, is seen from the figure to represent a type of averaging over the different internal configurations of a pair consisting of a heavy and a light particle. In the limiting case where the mass of the light particle approaches zero, the average difference between $\boldsymbol{\xi}$ and $-\mathbf{X}$ becomes smaller and smaller. Thus, for fixed value of $\mathbf{X}$, the function $K(\mathbf{X}, \boldsymbol{\xi})$ is different from zero in a more and more limited range of values of $\boldsymbol{\xi}$ near the point $\boldsymbol{\xi}=-\mathbf{X}$, and eventually becomes representable as a delta-function:

$$K(\mathbf{X}, \boldsymbol{\xi})\rightarrow W(\mathbf{X})\delta(\mathbf{X}+\boldsymbol{\xi}).$$

In this limit, the molecular potential is now $V(\mathbf{X})+W(\mathbf{X})$; as in the customary treatment of molecular binding, it shows no dependence on velocity. The very deep narrow "trough" presented by the interaction kernel $K(\mathbf{X}, \boldsymbol{\xi})$ in the molecular case, widens out as the mass of the light particle is increased. In the nuclear limit, the half-width of K as a function of $\boldsymbol{\xi}+\mathbf{X}$, so far as this concept is definable, is of the same order as the average distance between the heavy particles.

The relation of molecular ideas to the nuclear three-body problem, brought out by the introduction of velocity dependent forces, is more

[3] To the order $(m/M)^{\frac{1}{2}}$, m and M being electronic and nuclear masses. M. Born and J. R. Oppenheimer, Ann. d. Physik **84**, 457 (1927).

[4] A discussion of the quantum mechanics of velocity dependent forces is given in Phys. Rev. **50**, 643 (1936). Cf. also J. H. Van Vleck, Phys. Rev. **48**, 367 (1935), and appendix of Ostrofsky, Breit, Johnson, Phys. Rev. **49**, 196 (1936). A distinction must be made between possible velocity dependence of the forces between the fundamental particles themselves, and the variation of intergroup forces with velocity, of which we speak here.

easily visualized with the help of the concept of resonance. Just as the general diatomic molecule is said to resonate between a condition of ionic binding and one of atomic binding, so the three particles in the nucleus may be regarded as spending part of their time in the grouping (13)2 and part in the configuration (23)1. In the corresponding mathematical treatment, the nuclear wave function, $\Psi(\mathbf{r}_1, \mathbf{r}_2, \mathbf{r}_3)$, is approximated by a linear combination of terms associated with the two groupings:

$$\Psi=\psi\left(\mathbf{r}_2-\frac{M\mathbf{r}_1+m\mathbf{r}_3}{M+m}\right)\Phi(\mathbf{r}_3-\mathbf{r}_1)$$
$$\pm\psi\left(\mathbf{r}_1-\frac{M\mathbf{r}_2+m\mathbf{r}_3}{M+m}\right)\Phi(\mathbf{r}_3-\mathbf{r}_2). \quad (2)$$

The first product represents light particle 3 bound to heavy particle 1, and heavy particle 2 interacting with the center of gravity of 1 and 3. The sign joining the two products depends upon the kind of statistics obeyed by the heavy particles. As a starting point for the treatment of the molecular and nuclear three-body problem, Eq. (2) is independent of special assumptions as to the nature of the binding forces.

The concept of resonating group structure leads directly to the introduction of velocity dependent forces. If we require that a wave function of the form (2) give the best possible representation of the nuclear motion, in the sense of the variation principle, then we find indeed exactly the wave equation (1), containing a potential, part of which is expressed in the form of an integral operator. The proof of this fact and the explicit calculation of the interaction between the two groups of the system is carried out in Appendix I, where the relationship to the Heitler-London procedure is also traced.

Three features characterize the method just described for treating nuclear structure. First, it supplies a rational basis for the customary type of variational calculation of nuclear binding energies. The calculation in the appendix, for example, gives -6.4 mMU (milli-mass-units) for the binding energy of H^3, in contrast to the value -5.6 mMU obtained with the same force constants but a two parameter variational function of the form $\exp[-\nu(3-1)^2-\nu(3-2)^2-\mu(2-1)^2]$. Second, the form of the wave function is adapted to the description of excited states of the nucleus as well as its ground level; in particular, collision processes, involving states in the continuous spectrun, fall under this classification. Third, the method has the disadvantage of not explicitly taking into account the effect of polarization of one group by the other. To be sure, we could introduce into the internal group wave function Φ of (2) a dependence on the position of the third particle, but the mathematical treatment would become unduly complicated (see discussion at end of following paper). On the other hand, for certain states of the total system, the two terms of (2) are already correlated in such a way as partially to allow for the action of polarization.

Resonating Group Structure

The method of resonating group structure shows a new characteristic when applied to the nuclear four-body system. In contrast to the preceding example, which shows only a single type of grouping, the alpha-particle may be divided into two deuterons, triton and neutron, and He^3 plus proton. The wave function is therefore expressed as a linear combination of six terms, of which the first corresponds to one possible grouping into deuterons, and the second is its mate, with sign chosen as in (2) so the two form a combination antisymmetrical in neutrons and in protons; the other four terms are divided into two similar pairs, associated with the second and third types of grouping. The relative importance of each term may be regarded as determined by the fraction of the time the whole system remains in the corresponding configuration. Three simultaneous wave equations are now needed to determine the relative motion of the groups in the three different configurations. These equations may be used to describe both disintegration processes and elastic scattering. For the detailed calculations for the nuclear four-body problem, reference is made to the work of Parker.[5]

The general mathematical details of applying the method of resonating group structure to the description of the motion in a nucleus containing

[5] H. Parker, Phys. Rev. **51**, 683 (1937) and M. A. thesis, University of North Carolina (1937).

many neutrons and protons are given in the following paper. Below, however, we are interested in the question: Which of the unmanageable number of possible types of grouping into which a large nucleus may be divided are most suited to describing approximately the actual state of the system?

Characteristic of the heavy nucleus is the close binding of the constituent particles. Viewed classically, the motion of a typical particle is a rapid zigzag motion superimposed on a general random drift. The velocity of the motion of general drift is so low that it contributes little to the total energy. The rapid motion with respect to nearest neighbors, however, represents the same type of exchange phenomena which is responsible for the binding between the two groups in the three- and four-body problems. The local nature of the binding in a heavy nucleus can for our purposes be best described by a division into groups of contiguous particles, between which act intergroup velocity dependent forces.

Let us pick out of all the particles in the nucleus those neutrons whose spins at a certain instant[5a] are all $+\frac{1}{2}$. The Pauli principle assures us that the wave function of the nucleus is antisymmetrical in these particles and hence has a node wherever two of these neutrons approach each other. To make the kinetic energy of the system as low as possible, the various nodes space themselves as far apart as is consistent with considerations of potential energy. Close to each of the neutrons just mentioned, a neutron with opposite spin finds a position of lowest potential energy, and similarly protons of both spins tend to follow the structural plan of the original neutrons. This follows most directly from our present information on nuclear forces: Unlike particles, and like particles of opposite spin, attract each other when the wave function is symmetric with respect to interchange of their coordinates, but not when it is antisymmetric. The configuration of the nucleus which we have just described, represents a grouping into alpha-particles, but alpha-particles of continually changing individuality. The interchange of neutrons and protons between the groupings, in fact, furnishes the bonds that tie the groups together.

The usefulness of the group structure picture for a description of nuclear vibration and rotation, along molecular lines, depends on the extent to which the groups remain well defined during the period of one vibration. For this reason, application of the method of resonating group structure to the nuclear three-body problem, although as suitable there as the idea of resonance is in the case of molecular structure, is not to be justified on the basis of any clear-cut physical division of the system into deuteron and neutron, any more than the molecular treatment can be founded on a sharp distinction between atomic and ionic binding. On the other hand, division of a large nucleus into a few groups, each containing many particles, represents an extreme case where the identities of the clusters remain relatively sharp even after several periods of vibration. It is just this fact that Bohr has recognized in his division of nuclear excitation into rotational energy and energy of volume and surface tension vibrations. We shall see that many of these modes of excitation find a simple representation in terms of the motion of alpha-particle groups.

Alpha-Particle Groups

Before describing any mode of nuclear motion in terms of the displacements of alpha-particle groupings, we require that the following two conditions be satisfied: (a) the half wave-length of the disturbance must be larger than the group, and (b), the period, τ, of vibration must be shorter than the average interval, t, required for a moving alpha-particle to exchange a neutron or proton with a part of its surroundings moving in the opposite phase. The quantity t is a property of the mode of vibration in question, and may be termed "characteristic diffusion time:" it is in order of magnitude the time required for a particle to diffuse a distance, ρ, of one-half wavelength: $\rho=\lambda/2$.

There appears to be no method by which to calculate the characteristic diffusion time quantum mechanically without entering into the details of the problem. An estimate on the basis of the classical diffusion theory is limited in its validity to energies much higher than those in

[5a] In mathematical terms, we suppose the nuclear wave function to be known as a function of spins and coordinates; we give the spins of the various particles fixed values and then investigate the dependence of the wave function on coordinates.

which we are interested; namely, the following conditions must be satisfied: (1) the uncertainty in the position of the particle due to its finite wave-length must be less than the effective mean free path, λ_d, for diffusion; (2) the average momentum transfer per collision must be larger than that uncertainty in the momentum of the particle which is conditioned by our knowledge of its position; (3) potential barriers surrounding the given particle, due to interaction with its neighbors, must be low in comparison with the available energy of the particle. In spite of its limitations, such an estimate is instructive. The classical equation gives

$$\rho^2=(\lambda_d v/3)t \tag{3}$$

for the mean square distance of diffusion in terms of the average speed, v, of the particle. We insert $\rho=\lambda/2$, where λ is of the order $2\pi R/n$ for the nth characteristic mode of surface tension vibration (R=nuclear radius), and using $\lambda_d\sim 2\times 10^{-13}$ cm, $M_p v^2/2\sim 25$ Mev, $R\sim 2\times 10^{-13}A^{\frac{1}{3}}$ cm, we obtain

$$t\sim n^{-2}A^{\frac{1}{3}}\times 10^{-21}\text{ sec.} \tag{4}$$

The period of the surface oscillation, on the other hand, is given by[6]

$$\tau=2\pi/\omega,$$
$$\omega^2=n(n-1)(n+2)(G/S)(4\pi/3M_pA), \tag{5}$$

where G/S is the surface tension and A the atomic number of the nucleus. Using for G/S the value estimated[7] from the empirical variation of binding energy with atomic number, we find

$$\tau\sim n^{-\frac{1}{2}}A^{\frac{1}{3}}2\times 10^{-21}\text{ sec.}, \tag{6}$$

which is in general considerably larger than the classical estimate of the characteristic diffusion time.

In the above classical estimate of the diffusion time the interaction between the particle in question and its neighbors was brought into evidence only through the assumption of an effective mean free path between collisions. But when the average energy of the particle is small in comparison with the height of the surrounding potential barriers due to nearby particle, there is only a small probability that the particle will, by fluctuations in the distribution of energy, acquire the amount required to surmount the ridge. Eyring[8] has shown that diffusion coefficients can be calculated by the same methods which are used in treating other absolute reaction rates. The probability that the required amount of energy be concentrated on one particle is represented in Eyring's formula by the factor $e^{-\epsilon/kT}$, where ϵ is an activation energy associated with the height of the barrier. Allowance must be made also for the possibility that the particle will penetrate through the potential hill. Eyring has shown that, even in ordinary liquids (diffusion of D_2O in H_2O, for example) the value of the activation energy has an important influence on the rate of the diffusion; and it is dominating, of course, for a solid body.

In the nucleus, the local potential barriers encountered by a typical particle may be estimated very roughly to be of the order of 30 Mev. The typical particle has a zero-point energy of possibly 20 Mev and in addition a fluctuating fraction of the nuclear excitation energy. It is essentially only this latter energy which is available for concentration, by chance, on the particle in whose diffusion we are interested. We would estimate, then an activation energy of roughly 10 Mev. A more plausible way of stating this is as follows: the binding energy per particle is 10 Mev; the saturation character of nuclear forces means that the given particle is bound as tightly to its close neighbors as to the whole of the nucleus; hence an energy of the above order of magnitude is required to overcome their attraction.

The nuclear excitation in ordinary transmutation experiments is ordinarily never enough to raise the nuclear temperature, kT, above 2 Mev. As the activation energy appears to be considerably larger than this amount, we have to expect a very strong dependence of the rate of diffusion upon excitation energy. When the nuclear excitation is low the simple classical treatment for this reason undoubtedly overestimates the rate of diffusion (cf. Eq. (4)) very considerably. It seems safe to say that actually the characteristic time of diffusion, t, is then definitely smaller that the period of nuclear vibration, τ, (Eq. (6)) and that the condition is satisfied for applying the simple

[6] Following Lord Rayleigh, *Scientific Papers*, Vol. I (Cambridge, 1899), Eq. (40), p. 401. I am indebted to Professor Bohr for reference to this paper.

[7] Cf. for example H. Bethe, Rev. Mod. Phys. 9, 69 (1937), Eq. (314).

[8] H. Eyring, J. Chem. Phys. 4, 283 (1936).

group structure picture of the nucleus mentioned above. With higher and higher nuclear excitation, on the other hand, the influence of diffusion becomes progressively stronger, and predictions based on a simple group structure treatment gradually lose close correspondence with the actual properties of the nucleus.

In accordance with the preceding considerations on the special stability of alpha-particle groupings and on the influence of diffusion, we shall use a simple alpha-particle model on molecular lines to describe low states of excitation of the nucleus. It is necessary to distinguish between such a model, which must assume the forces between alpha-particles to be given beforehand, and a direct application of the method of resonating group structure, which starts out from first principles, and only introduces the alpha-particle concept in setting up a suitable approximate wave function for the nucleus. The two treatments are, of course, closely related.

The wave function of the whole system has the proper antisymmetry when written in the form

$$\Psi(1,\cdots\mathbf{N})=\sum_{\text{dist}} F\left(\frac{1+2+3+4}{4},\ \frac{5+6+7+8}{4},\cdots\right)\Phi(1234)\Phi(5678)\cdots \quad (7)$$

Here Φ is the wave function for a single alpha-particle, completely antisymmetrical[9] with respect to interchange of any two particles; $F(\mathbf{X}_{\mathrm{I}}, \mathbf{X}_{\mathrm{II}}, \cdots)$ is a symmetric function of the coordinates of the centers of gravity of the various α-particles $(4\mathbf{X}_{\mathrm{I}}=\mathbf{r}_1+\mathbf{r}_2+\mathbf{r}_3+\mathbf{r}_4=1+2+3+4)$; and the sum runs over all those even permutations of the N particles which give really different distributions into alpha-particles. It is in F that we are interested; it describes the rotation and vibration of the framework of alpha-particle groupings. We write F as the product $\psi_R\psi_V$ of a rotational and vibrational wave function, and apply the results of molecular theory to determine the allowed rotational and vibrational quantum numbers for the nuclei Be^8, C^{12}, and O^{16}.

TABLE I. *Number of allowed vibration-rotation levels for three alpha-particles, determined from symmetry characters of ψ_R and ψ_V.*

$n_1=0,1,2,\cdots; n_2=$			0	1	2	3	4
J	K	Character	α	γ, δ	α, γ, δ	$\alpha, \beta, \gamma, \delta$	$\alpha, 2(\gamma, \delta)$
0	0	α	1	0	1	1	1
1	1	γ, δ	0	1	1	1	2
1	0	β	0	0	0	1	0
2	2	γ, δ	0	1	1	1	2
2	1	γ, δ	0	1	1	1	2
2	0	α	1	0	1	1	1
3	3	α, β	1	0	1	2	1
3	2	γ, δ	0	1	1	1	2
3	1	γ, δ	0	1	1	1	2
3	0	β	0	0	0	1	0

[9] For simplicity, we treat neutrons and protons as different spin states of the same particle. See Heisenberg, *Rapport du VII^me Congres Solvay* (Paris, 1934), for proof of equivalence to the treatment in which two different types of particles are used.

Low Levels of Beryllium, Carbon and Oxygen[9a]

A. Allowed states

a. Two alpha-particles.—The rotational energy is given by the well-known expression

$$E_R=(\hbar^2/2A)J(J+1). \quad (8)$$

Here the moment of inertia, A, is somewhat greater than the moment, I, of a spherical nucleus of the same density and mass: $A=I/g$ defines a dimensionless number $g<1$. ψ_R is symmetric for even J, antisymmetric for odd J; ψ_V is symmetric for all vibrational quantum menbers; hence only levels with $J=0, 2, 4, \cdots$ are allowed. As a matter of fact, owing to the stability of Be^8, only the lowest vibrational level has a life long enough to be observable. It seems likely that rotational levels, too, above $J=4$ are too much widened by dissociation to be of interest. We therefore consider only the three levels

$$E=E_0,\ E_0+6g(\hbar^2/2I),\ E_0+20g(\hbar^2/2I). \quad (J=0, 2, 4). \quad (9)$$

b. Three alpha-particles.—Neglecting for the moment the influence of vibration on rotation, we consider the centers of gravity of the alpha-particles located at the vertices of an equilateral triangle. The moments of inertia about the axis of symmetry and about a line in the plane of the triangle we write, respectively, $C=I/g_2$ and $A=I/g_1$, where I is the moment of inertia which

[9a] Considerations on the influence of alpha-particle symmetry upon allowed nuclear levels had occurred to Professor E. Teller independently, and were mentioned to the author in conversation.

TABLE II. *Symmetry characters of wave functions belonging to the vibrations ω_2 and ω_3.*

n_2 \ n_3	0	1	2
0	A_1 (1)	F_2 (3)	A_1+E+F_2 (6)
1	E (2)	F_1+F_2 (6)	$A_1+A_2+2E+F_1+F_2$ (12)
2	A_1+E (3)	F_1+2F_2 (9)	$2A_1+A_2+3E+F_1+2F_2$ (18)
3	A_1+A_2+E (4)	$2F_1+2F_2$ (12)	$2A_1+2A_2+4E+2F_1+2F_2$ (24)

would belong to a spherical nucleus of the same density and mass. g_2 and g_1 depend on the distribution of mass; for an ellipsoid of revolution with major axis ρ times the minor axis, $g_2=\rho^{-2/3}$, $g_1=2/(\rho^{2/3}+\rho^{-4/3})$. The rotational energy of the system is

$$E_R=(h^2/2I)[g_1J(J+1)-(g_1-g_2)K^2], \quad (10)$$

where K is the quantized projection of the total angular momentum, J, along the symmetry axis.

Two types of vibration are possible: a doubly degenerate vibration (ω_2), in which one side of the triangle shrinks and at the same time moves away from the third alpha-particle; and a dilatation vibration (ω_1) in which the triangle expands and contracts isotropically. The latter vibration is symmetric in the three alpha-particles. The symmetry character of the wave function of the system therefore does not depend on the vibrational quantum number n_1. On the other hand, associated with any value of n_2, there are n_2+1 different states having the vibrational energy $(n_2+1)h\omega_2$. For even values of n_2, one of these states[10] is symmetric (α) and the others divide up into $n_2/2$ pairs of states having doubly degenerate symmetry character (γ, δ). For odd values of n_2 greater than 2, we have in addition a completely antisymmetric state (symmetry character β).

We combine a given vibrational state with a rotational state of the symmetry character necessary to make the total wave function completely symmetrical in the three particles.[11] This has been done in Table I. Example: For any value of n_1, and for $n_2=4$, the rotational state $J=1$, $K=0$ is not allowed; but two states $J=1$, $K=1$ exist. (Each splits into $2J+1=7$ states in a magnetic field!) These two states have the same energy until we allow for the coupling of vibration and rotation. Neglecting this and similar refinements, we have

$$E=E_0+E_R(J, K)+n_1h\omega_1+n_2h\omega_2 \quad (11)$$

for the energy of C^{12}.

c. Four alpha-particles.—The system has tetrahedral symmetry and the following types of vibration occur: a single vibration (ω_1), corresponding to isotropic dilation of the nucleus; a doubly degenerate vibration (ω_2) in which the alpha-particles are paired into two dumbbells twisting with respect to each other; and a triply degenerate vibration (ω_3) in which one dumbbell shortens, the other lengthens, but no tipping occurs. In addition there exists the possibility that one alpha-particle will push through or around the other three and invert the pyramid. This motion is not associated with a new degree of freedom but there is a finite probability for it to occur when the amplitudes of the above nine vibrations are as large as they are in the nucleus. Splittings, $\Delta E=2\epsilon$, will occur in the energy level system proportional to the frequency with which such inversions occur.

The wave function representing a particular one of the three modes of vibration belongs to one of the five representations[12] of the tetrahedral rotation reflection group:

A_1; function unchanged in sign by any rotation or reflection.
A_2; only reflection at a symmetry plane changes the sign of the function.
E; the function is paired with another; neither is altered by rotation about a twofold axis; other operations transform the two functions among each other.
F_1; function paired with two others; transform among each other for all operations of the group; character of reflection in a plane drawn through two alpha-particles is -1.
F_2; like F_1, except the reflection has character $+1$.

TABLE III. *Allowed states for four alpha-particles.*

$n_1=0,1,\cdots$; $(n_2,n_3)=$		(0,0)		(0,1)		(0,2)		(1,0)		(1,1)		(2,0)		(2,1)		(3,0)	
J	Character R	+	−	+	−	+	−	+	−	+	−	+	−	+	−	+	−
0	A	0	1	0	0	0	1	0	0	0	1	0	1	0	0	1	1
1	F	0	0	0	1	0	1	0	0	1	1	0	0	1	2	0	1
2	$E+F$	0	0	0	1	1	2	1	0	1	1	1	1	1	2	1	1
3	$A+2F$	0	1	0	2	0	3	0	0	2	2	0	1	2	4	1	1
4	$A+E+2F$	0	1	0	2	1	4	1	1	2	2	1	2	2	4	2	2
5	$E+3F$	0	0	0	3	1	4	1	1	2	3	1	1	2	6	1	1

[10] Here and below we follow the terminology and use the results of Hund, Zeits. f. Physik **43**, 805 (1927), presented in convenient form by Dennison, Rev. Mod. Phys. **3**, 340 (1931).

[11] The combination rules are given in simple form by Dennison, reference 10.

[12] We use here the notation and results of L. Tisza on the symmetry of the vibrations of polyatomic molecules, Zeits. f. Physik **82**, 67 (1932).

The character of the vibration ω_1 is A_1 (symmetric) for all values of n_1, and thus has no influence on the symmetry of the total wave function. Table II gives the types of vibrational wave functions occurring for any given state of excitation of ω_2 and ω_3; thus, for $n_1=n_1$, $n_2=0$, $n_3=2$, we have a single symmetric vibrational state, a doubly degenerate state, and a triply degenerate state of type F_2, making 6 different wave functions altogether, provided we consider only small amplitudes of displacement. But for large amplitudes, inversion occurs, and a wave function will or will not change sign according as it belongs to the representation A_1 or A_2 of the inversion operation. A function of the latter type possesses one additional node and therefore has an energy slightly higher than one of the type A_2. Recalling that $A_2A_1=A_2$, $A_2E=E$, $A_2F_2=F_1$, we therefore actually obtain for $n_1=n_1$, $n_2=0$, $n_3=2$ six energy levels, consisting of three close pairs: A_1, A_2; E, E; F_2, F_1, the first member of the pair having in each case the lowest energy.

We now combine the vibrational wave function with the rotational function to obtain a state completely symmetric in the four alpha-particles. Table III gives the number of such allowed states for any value of n_1 and the tabulated values of n_2, n_3, and the rotational quantum number J. Example: For $n_1=n_1$, $n_2=0$, $n_3=1$, $J=2$, we have one allowed level (which splits into $2J+1$ in a magnetic field); this level is symmetric with respect to inversion of the tetrahedron, and therefore has an energy slightly less (cf. minus sign in table) than it would othereise possess. Neglecting interaction of rotation with vibration, we have for the energy of O^{16} the following expression:

$$E=E_0+(\hbar^2/2I)J(J+1)+n_1\hbar\omega_1+n_2\hbar\omega_2 +n_3\hbar\omega_3\pm\epsilon. \quad (12)$$

If, in the example, we had had $n_2=1$, $n_3=0$, we should have had the plus sign as well as the minus sign occurring in the energy expression (ϵ proportional to frequency of inversion).

B. Relation to the treatment by Bohr and Kalckar

a. Types of motion.—Bohr and Kalckar[13] divide the nuclear motion into rotation and volume and surface vibrations of the nuclear material. They calculate the frequency of these vibrations as for a fluid substance. The legitimacy of this treatment depends upon the extent to which diffusion can be neglected during the period of one vibration, which condition is also essential to the considerations in the preceding section.

The modes of vibration of the fluid model bear a close relation to those discussed in A from the alpha-particle point of view, but characteristic differences are present due to the clustering which we have attributed to the nucleus. For example, the first surface tension oscillation, $n=2$, represents a motion in which the nucleus shrinks at the equator and expands at top and bottom. The degeneracy is $2n+1$ or 5-fold, corresponding to the different possible orientations of the pole of the motion. On transition to the alpha-particle picture, say for O^{16}, three of these vibrations go over into the first excited level ($n_2=1$) of ω_3, in which the tetrahedron shrinks about a line which is normal to both a twofold and a threefold symmetry axis, and at the same time expands along this line. The other two surface tension oscillations go over to the level $n_1=1$ of ω_2, in which the flattening of the nucleus is brought about by the twisting of the two dumbbells towards the same plane (see Fig. 3). Similar considerations hold for other levels. It is to be expected that the actual position of the low nuclear levels which are observed will lie between these two extremes.

Once the connection is established between the types of motion characteristic of the liquid and the alpha-particle models, it becomes clear that a great many of the levels predicted by the former treatment have been excluded on symmetry grounds in the latter. For example, when the nucleus O^{16} is in its normal vibrational state, all values of the rotational quantum number, J, are allowed according to the homogeneous drop model, whilst we find that the permitted levels are limited to $J=0, 3, 4, 6, \cdots$. Even those states that occur have a weight much lower than predicted by the semi-classical model ($2J+1=7$ for $J=3$ as compared with $(2J+1)^2=49$ for the same value of J). The physical reality of the restrictions which symmetry puts on the energy level scheme depends upon the extent to which

[13] N. Bohr and F. Kalckar, reference 2. I am indebted to Professor Bohr and Mr. Kalckar for valuable discussions of the liquid model of the nucleus.

the identities of the alpha-particles are preserved during the course of the motion. The higher the energy level, the greater is the amount of diffusion which occurs, during one period of vibration, between parts of the system moving in opposite phase, and the more the symmetry restrictions break down. The influence of symmetry considerations on the energy level system, it now becomes clear, is in actual fact only one of degree rather than one of kind.[14] The types of low levels which were excluded on the alpha-particle picture are to be found in the energy spectrum, but pushed upwards by some millions of volts from the position predicted by the treatment in terms of a homogeneous classical liquid. Those modes of motion which are forbidden on the alpha-particle picture can attain the required antisymmetry in neutrons and protons by modifications in the motion equivalent to excitation of one of the alpha-particles or to other divisions of the neutrons and protons into clusters (i.e., 5+3 +4+4 instead of 4+4+4+4). The excitation energy associated with such changes is large in proportion as the alpha-particle type of grouping is well defined. On the other hand, for volume and surface tension oscillations of progressively shorter wave-length, the definition of the group structure in the nucleus becomes less and less distinct under the influence of diffusion of neutrons and protons between parts of the nucleus moving in opposite phase.

To summarize, we may divide the nuclear energy level spectrum into two parts. In the first, extending from the ground level up to an excitation of perhaps four to eight million volts, the effect of the nonhomogeneous structure of the nucleus is to modify the types of motion predicted by the liquid model and in addition to push to higher energies many of the levels which on the classical model would be low lying,[15] but which cannot be described quantum mechanically as being symmetric in terms of alpha-particles or similar stable structures. In the second region of the spectrum, the group structure becomes more and more washed out and the liquid model should give a progressively more correct picture of the nuclear excitation. We are, in fact, approaching the region of high quantum numbers where, according to the correspondence principle, the quantum-mechanical description approaches the classical treatment, and the predictions of the liquid model become valid to the extent that any system of classical particles can be replaced by a continuum.

TABLE IV. *Normal vibrations of* Be^8, C^{12}, *and* O^{16}, *and constants of rotational energy, using "large radius" for nucleus. (Energies in thousands of a mass unit.)*

NUCLEUS	$\hbar\omega_1$	$\hbar\omega_2$	$\hbar\omega_3$	$\hbar\omega_4$	$\hbar^2/2I$
Be^8	(5.2)	—	—	1.9	0.41
C^{12}	2.9_2	2.0_6	—	1.5_4	0.21
O^{16}	2.3_0	1.1_5	1.6_3	1.3_3	0.13

[14] This is not true for the statistical weights, however.

[15] It is the intention in a later paper with E. Teller to extend these considerations to the low energy levels of heavy nuclei, in connection with the problem of nuclei having the same atomic number and atomic weight but different properties (such as distinct half-lives).

b. Vibration frequencies and other constants.— Comparison with the theory of Bohr and Kalckar now gives a control with which to check the simplest assumption we can make regarding the various vibrations of the alpha-particle model. In default of a more satisfactory treatment (cf., however, Section E below) we assume, namely, that a reasonable approximation is obtained by calculating the characteristic frequencies as if quasi-elastic central forces acted between the alpha-particles. (In accordance with the saturation character of nuclear binding, we do not assume that these "equivalent forces" between alpha-particles are the same within different nuclei.) Using $V(\mathbf{r})=V(\mathbf{r}_0)+k(\mathbf{r}-\mathbf{r}_0)^2/2$ for the effective potential between alpha-particles, we readily find for the vibrations of C^{12},

$$\begin{aligned}\omega_1'(\text{dilatation}) &= 3^{\frac{1}{2}}(k'/4M),\\ \omega_2'(\text{tipping}) &= (\tfrac{3}{2})^{\frac{1}{2}}(k'/4M)^{\frac{1}{2}};\end{aligned} \qquad (13)$$

and for O^{16},

$$\begin{aligned}\omega_1''(\text{dilatation}) &= 2(k''/4M)^{\frac{1}{2}},\\ \omega_2''(\text{twisting}) &= (k''/4M)^{\frac{1}{2}},\\ \omega_3''(\text{flattening}) &= 2^{\frac{1}{2}}(k''/4M)^{\frac{1}{2}},\end{aligned} \qquad (14)$$

where M is the proton mass. We obtain an order of magnitude estimate for k by equating $(k/2)(R/2)^2$ (R = nuclear radius) to the energy required to break an alpha-alpha bond. Allowing for the share of the zero-point kinetic energy[16]

[16] In view of the roughness of potential approximation, it does not seem justifiable to attempt to make a more detailed estimate, allowing for the difference in the zero point energies of the nuclei A and $A-4$ and for the different state of internal binding of a free and a bound alpha-particle.

belonging to one alpha-particle, we obtain

$$\begin{aligned} &2(k'R'^4/8)-\hbar(\omega_1'+2\omega_2')/6 \\ &\quad\sim 8.0080+4.0040-12.0043(\text{MU}), \\ &3(k''R''^4/8)-\hbar(\omega_1''+2\omega_2''+3\omega_3'')/8 \\ &\quad\sim 12.0043+4.0040-16.0000(\text{MU}), \end{aligned} \quad (15)$$

whence, with $R'=4.1\times10^{-13}$, $R''=5.2\times10^{-13}$,[17] we find the vibrational excitation energies given in Table IV. For comparison, we give the energy, $\hbar\omega_s$, of the lowest surface-tension vibration ($n=2$) of the liquid model, as calculated from Eq. (5), using for the surface tension the value estimated from the empirical variation of nuclear binding energy with atomic number (Bethe, reference 7, Eq. (314)). As was to be expected from our considerations on the transition between the liquid and the alpha-particle model, ω_s for oxygen lies between ω_2 and ω_3. The favorable comparison indicates a general agreement between two quite different methods of estimating the nuclear surface tension.

We obtain the moment of inertia of the nucleus of atomic weight A from $I=(2/5)MAR^2$. Using units $e^2/mc^2=2.80\times10^{-13}$ cm for length and mMU for energy, we have

$$\hbar^2/M=5.56,$$

and

$$\begin{aligned} \hbar/2I&=(5/4)5.56\,(2.80\times10^{-13}/2.05\times10^{-13})^2A^{-5/3} \\ &=13.0A^{-5/3}\ \text{mMU (milli-mass-units)} \end{aligned} \quad (16)$$

as given in Table IV. A rough estimate of the flattening of C^{12} is long diameter = 1.5 times short axis, whence the form factors $g_1=1.06$, $g_2=0.76$ (Eq. (10)). Similarly, we estimate for Be^8 long axis = 1.5 times short diameter, $g=0.80$ (Eq. (9)). The uncertainty in the g's is unimportant compared to that of I: a 30 percent decrease of the nuclear radius from $R=2.05\times10^{-13}A^{1/3}$ increases $\hbar^2/2I$ by a factor of two.

c. Dissociation.—The mean square displacement of a harmonic oscillator of circular frequency ω and equivalent mass m, when in the nth state of vibration, is known to be given by

$$(x^2)_{Av}=(n+\tfrac{1}{2})(\hbar^2/m)(\hbar\omega)^{-1}. \quad (17)$$

[17] In default of any certain way of deciding between alternative theories of nuclear radii, we use throughout this paper for definiteness the values given by Bethe, Rev. Mod. Phys. 9, 166 (1937). It appears that the most reliable estimate of nuclear radii will be obtained from observations on the spacing of low rotational energy levels.

If we assume a quasi-elastic character for the alpha-particle oscillations of C^{12}, we find for the mean square displacement of one alpha-particle from equilibrium the expression

$$(X^2)_{Av}=(2n_1+1)(0.282)^2+(2n_2+1)(0.336)^2 \quad (18)$$

(units $e^2/mc^2=2.80\times10^{-13}$ cm for distance). The frequencies ω_1 and ω_2 are incommensurable, however, and when the two vibrations happen to be in phase with respect to the radial motion of one alpha-particle, we shall have

$$(\delta R^2)^{\frac{1}{2}}_{Av}=(2n_1+1)^{\frac{1}{2}}0.282+(2n_2+1)^{\frac{1}{2}}0.336. \quad (19)$$

Energy enough for disintegration being available in the nucleus, the probability for the emission of an alpha-particle will be of the order of magnitude of the number of times per second that δR exceeds the range of nuclear attraction, provided that the energy is still not so high that diffusion completely destroys the identity of the alpha-particle during the period of vibration. In particular, this condition requires that the available energy of the system be small in comparison with the amount required for the release of a neutron or proton.

Although the range of validity of the simple alpha-particle description of disintegration is much limited for nuclei of light and medium atomic weight by the energy restrictions above, nevertheless the resemblance to the evaporation concept used in the liquid model is apparent. Thus, on both pictures, emission of a particle from the nucleus occurs when by chance the amounts of kinetic energy associated with the various modes of collective motion of the nucleus have become concentrated on one particle to the extent required to break its binding to the nucleus.

For heavy nuclei, the conditions are improved with respect to the applicability of the alpha-particle picture of disintegration, above all when spontaneous disintegration can occur. In the latter case, each alpha-particle already has the energy required for release, and penetration through the potential barrier is the factor which determines the nuclear lifetime. Whether observed disintegration constants can be used in conjunction with the Gamow penetration formula to calculate nuclear radii is, of course, another question, in view of the ambiguity due to the size of the alpha-particle itself. Application of the method of resonating group structure should

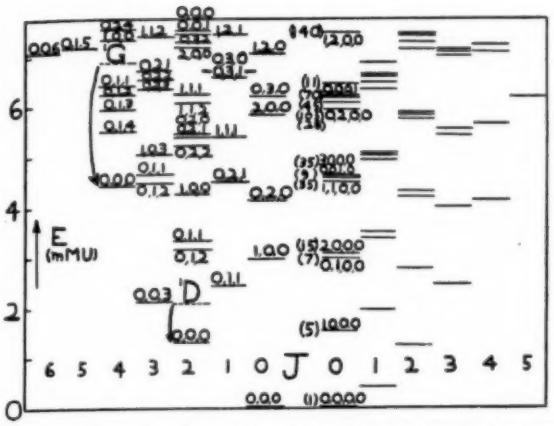

FIG. 2. Low levels predicted for the nucleus C^{12}. Excitation energy in thousands of a mass unit. Jh gives total nuclear angular momentum. At left, the states given by simple alpha-particle model. Labels refer, respectively, to quantum numbers n_1 and n_2 for vibration and K for rotation about symmetry axis of the triangle of alpha-particles. Weight of levels is $2J+1$. Arrows show correspondence with dotted levels calculated by Hartree-Fock procedure (Feenberg, Wigner, Phillips). At right, levels given by the liquid droplet model. Weight given by number in parenthesis times $(2J+1)^2$. Labels refer to degree of excitation of the surface tension vibrations $n=2, 3, 4, 5$, respectively.

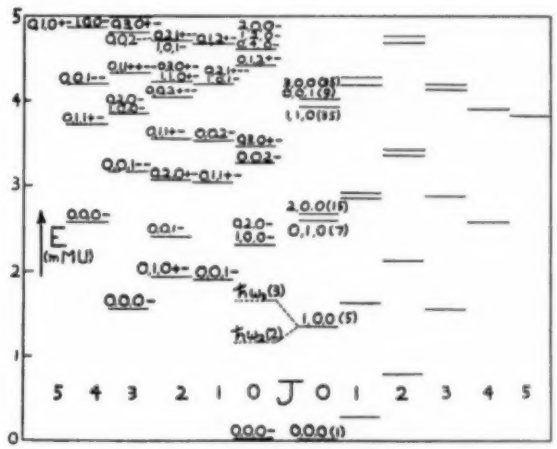

FIG. 3. Low levels of O^{16}. At left, according to simple alpha-particle model; at right, on liquid droplet model. Numbers at left are vibrational quantum numbers for dilatation (ω_1), twisting (ω_2), and flattening (ω_3) of the tetrahedron, respectively. Levels marked with a minus sign are slightly lowered with respect to those marked with a plus sign because the wave function for the minus levels does not change sign on inversion of the tetrahedron. For numbers at right, see Fig. 2. The dotted lines exemplify how a state of the liquid model becomes modified under the influence of a tendency to form alpha-particle groups. In the example, however, the two dotted levels are excluded in the alpha-particle treatment on symmetry grounds, and therefore would also be missing in a refined liquid drop theory. The left portion of the diagram shows similar examples of how profoundly symmetry considerations influence the appearance of the lower part of the nuclear energy level spectrum.

make it possible to eliminate this ambiguity by a mathematical treatment which goes beyond the Gamow model and treats the disintegration from first principles (cf. in this connection a following paper on the interaction between two alpha-particles).

It does not seem possible, however, to justify the so-called "many-body" picture[17a] of spontaneous alpha-particle disintegration. In this treatment, the probability of penetration through the potential barrier is multiplied by a factor which is termed "probability for concentration of energy on an alpha-particle," and is identified in order of magnitude with the similar factor encountered in the theory of the disintegration of a nucleus which is normally stable but has been excited. The two cases are actually quite different. In the latter, it is essential that the remainder of the nucleus lose energy if one particle is to have energy enough to escape. We must allow for the time required for the various degrees of freedom to concentrate the energy on the particle in question, by a favorable fluctuation. In the former case, the vibrations associated with the various modes of collective motion in the nucleus are all in their lowest state; the zero point energy is distributed almost uniformly among the various particles; and we do not have to wait for the concentration of energy to occur.

[17a] For details, cf. H. Bethe, Phys. Rev. **50**, 977 (1936).

C. Energy level spectrum

a. Beryllium.—With the values of the constants given above, we have $E_R=0.33J(J+1)$ for Be^8. The alpha-particle treatment therefore predicts a normal S level ($J=0$), a D state ($J=2$) at an excitation of 2.0 mMU (milli-mass-units), and a G level ($J=4$) at 6.7 mMU above the ground level. The first excited level has been observed[18] to lie at 3.0 mMU, and to have a width of 0.8 mMU. There also exists evidence[19] for an even broader level at about 10 mMU, which it seems reasonable to attribute to $J=4$. The same normal and excited levels are predicted by Feenberg and Wigner[20] and their energies are calcu-

[18] Oliphant, Kempton and Rutherford, Proc. Roy. Soc. **150**, 241 (1935).

[19] See paper on the scattering of alpha-particles in helium, to be published in the *Physical Review*.

[20] E. Feenberg and E. Wigner, Phys. Rev. **51**, 101 (1937); cf. also E. Feenberg and M. Phillips, Phys. Rev. **51**, 597 (1937).

lated on the basis of a perturbation treatment using $1s$ and $2p$ harmonic oscillator functions for individual neutrons and protons: $E(G)-E(S)=6.9$ mMU, $E(D)-E(S)=2.1$ mMU. The two theoretical treatments fail by about the same amount. To obtain agreement of the alpha-particle model with experiment, it is necessary to decrease the nuclear radius from $2.05\times10^{-13}A^{\frac{1}{3}}$, used above, to $1.67\times10^{-13}A^{\frac{1}{3}}$ cm.

b. Carbon.—The alpha-particle model in the form used above gives

$$E(C^{12})=2.92n_1+2.06n_2+0.22J(J+1)-0.06K^2(\text{mMU}). \quad (20)$$

Fig. 2 presents the low allowed energy levels, and shows for comparison the states predicted by the semi-classical droplet model. The effect of symmetry considerations is excluding low levels is very marked. The high lying levels given by the alpha-particle model will certainly be strongly modified by the growing effect of diffusion discussed in *B*. More confidence can be placed in the general feqtures of the spectrum predicted at lower energies. It should be stated that the smaller nuclear radius suggested by the case of Be^8 would increase the rotational energies of C^{12} states by a factor 1.5 and vibrational energies by a factor ~1.2.

In view of the number of excited levels, it appears that a comparison of the spectrum with the three gamma-rays if C^{12} known at present would not yield any useful information. Observations on the fine structure of low levels would be of interest; the separation of levels differing only in the quantum number K depends upon the extent to which the nucleus is flattened by grouping into the alpha-particles.

The dotted levels on the diagram are those predicted by Feenberg and Wigner. Their approximate calculations place the levels at the same position in C^{12} as in Be^8.

c. Oxygen.—The model which we have discussed gives for four alpha-particles

$$E(O^{16})=2.03n_1+1.15n_2+1.63n_3+0.13J(J+1), \text{ (mMU)} \quad (21)$$

with uncertainties in the constants similar to those mentioned in the case of carbon. The low lying allowed terms are shown in the left-hand portion of Fig. 3. The dotted lines for $J=0$ indicate the two levels $n_1=0$, $n_2=1$, $n_3=0$ and $n_1=0$, $n_2=0$, $n_3=1$, which are forbidden on symmetry grounds. If symmetry did not exclude them, then on our altering the nuclear forces in such a way as to leave no tendency to grouping into alpha-particles, we should find these two levels merging into the first excited level, $n_{s2}=1$, of the lowest mode, $n=2$, of surface tension oscillation of the liquid model. Other levels of the alpha-particle model show similar correlation properties. Whether observation gives a scheme of vibrational levels corresponding more to the one model or the other will give important information on the extent to which the group structure of the nucleus is affected by diffusion.

D. Relation to Hartree-Fock type of calculation

Wigner[21] has shown that the symmetry character of the total nuclear wave function comes first in determining the energy of the nucleus; next come the finer details of dependence on coordinates and spin. The symmetry character is described by a certain partition of A, the number of particles in the nucleus; the nucleus has its lowest energy for the partition containing the largest possible number of 4's: $A=4+4+\cdots$.

The partition of lowest energy is automatically given by the alpha-particle treatment, which is not adapted as it stands, however, to the description of the highly excited nuclear states belonging to other partitions.

The Hartree-Fock description of the nuclear motion, on the other hand, (1) starts out with an equivalent central field to represent the interaction of a particle with its neighbors; (2) builds up out of single particle states in this field a wave function of the desired symmetry character for the whole system; and (3) by a perturbation calculation attempts to allow for the difference between the equivalent field and the actual field. In principle, such a treatment is no more (or less) complicated for one partition than for another. Carried through to a finish, it would yield a wave-function which recognized the collective types of motion common to the liquid and the alpha-particle models of the nucleus. In point of fact the perturbation calculation just mentioned is either carried out only to a low order of approximation,

[21] E. Wigner, Proc. Nat. Acad. **22**, 662 (1936).

where it gives a false picture of the nuclear state of motion; or with more labor, is made to yield a better wave function, which is, however, too complicated in form to have its meaning read or its accuracy certified.

The relationship of the Hartree-Fock type of wave function to the alpha-particle description of the nucleus is most easily seen in the case of the ground state of oxygen. We compare the resonating group wave function of Eq. (7) with the zero-order wave function of the central field treatment:

$$\Psi(1,\cdots 16)=\begin{vmatrix} (sa|1) & (sb|1) & (sc|1) & \cdots & (p_1d|1) \\ (sa|2) & & & & \\ \cdots & & & & \\ \cdots & & & & \\ (sa|16) & \cdots & \cdots & \cdots & (p_1d|16) \end{vmatrix}. \tag{22}$$

In the determinant, **2** stands for the spatial, ordinary spin, and isotopic spin coordinates of particle 2 (which may be either a neutron or a proton).[9] The function $(p_1a|1)$ represents a single particle behaving as a proton with spin $+\frac{1}{2}$ and moving in a $2p$ state with $m_l=1$; b, c, d, refer, respectively, to a proton state of spin $-\frac{1}{2}$ and neutron states with spin $+\frac{1}{2}$ and $-\frac{1}{2}$; s indicates the $1s$ state. We add and subtract rows of the determinant without changing its value and obtain

$$\Psi=\begin{vmatrix} (\mathrm{I}a|1) & \cdots & (\mathrm{IV}d|1) \\ \cdot & & \\ \cdot & & \\ \cdot & & \\ (\mathrm{I}a|16) & \cdots & (\mathrm{IV}d|16) \end{vmatrix}, \tag{23}$$

where the new states I, II, III, IV exhibit the same type of tetrahedral symmetry (cf. Slater, Pauling, etc.) which characterizes the bond eigenfunctions of a carbon atom:

$$\begin{aligned} (\mathrm{I}|\ )&=2^{-1}\{(s|\ )+(x|\ )+(y|\ )+(z|\ )\},\\ (\mathrm{II}|\ )&=2^{-1}\{(s|\ )-(x|\ )-(y|\ )+(z|\ )\},\\ (\mathrm{III}|\ )&=2^{-1}\{(s|\ )+(x|\ )-(y|\ )-(z|\ )\},\\ (\mathrm{IV}|\ )&=2^{-1}\{(s|\ )-(x|\ )+(y|\ )-(z|\ )\}. \end{aligned} \tag{24}$$

Here the states x, y, z are defined by

$$\begin{aligned} (x|\ )&=2^{-1}\{(p_{-1}|\ )-(p_{+1}|\ ),\\ (y|\ )&=i2^{-1}\{p_{-1}|\ )+(p_{+1}|\ ),\\ (z|\ )&=(p_0|\ ). \end{aligned} \tag{25}$$

In the form (23), the Hartree-Fock zero-order wave function is adapted to recognize the same spatial arrangement which the alpha-particle model attributed to the oxygen nucleus: the form of Ψ indicates that in the region of space near each vertex of a tetrahedron there exists a large probability of finding the building material of an alpha-particle—a pair of protons of opposite spins and a similar pair of neutrons. The wave function does not, however, seize this opportunity actually to construct alpha-particles; the exceedingly strong interaction between the four particles in the same region of space is not recognized by any dependence of the wave function upon the mutual separations of the neutrons and protons and the result is much the same as we should obtain on attempting to describe a helium nucleus in terms of particles moving in a central field. The initial advantage being lost by this neglect, a practicable series of perturbation calculations can regain it only in the case of light nuclei. For example, Inglis[22] has shown that successive approximations to the binding energy of He^4 converge well (E = −27.6 mMU in first order, −28.8 mMU in second order), but that for Li^6 higher order contributions fall off less rapidly ($E=-14.9$ mMU in first order, −27.7 mMU in second order). Already in the case of O^{16} a first-order calculation[20] misses the observed binding energy by 100 mMU. That the weakness of the central field procedure really lies in neglecting the alpha-particle type of correlation follows most readily from the fact that internal binding of four free alpha-particles is already 122 mMU, only 16 mMU less than the binding energy of the same neutrons and protons in oxygen.

Description of excited levels of the nucleus by the Hartree-Fock procedure in general requires

[22] D. R. Inglis, Phys. Rev. **51**, 531 (1937).

the introduction in the wave function of terms representing the excitation of individual neutrons and protons to higher states. The dotted levels in Fig. 2 (carbon), for example, were obtained by considering[20] only $1s$ and $2p$ states of the individual particles in a central field. The next excited single particle states, $2s$ and $3d$, lie about 10 mMU higher. At the least the ten states just mentioned must be taken into account if the central field calculation is to account for the levels of whose existence and approximate position the alpha-particle model informs us. There does not seem to be any physical argument to justify one in believing that this degree of approximation in the Hartree-Fock treatment will give one generally correct energy level differences, since the difference is so great between the starting point of the calculation and the actual modes of collective motion which characterize the nucleus. For example, the three low energy levels predicted by the central field approximation for Be^8 and C^{12} have been shown (Feenberg and Phillips, reference 20, Eq. (3a)) to satisfy the relation $E=E_0+L(L+1)K'$, which has the same form as the rotational energy given by the liquid model of the nucleus. Nevertheless, the constant K' represents an integral of potential energy rather than the influence of altered kinetic energy; moreover, K' has the same value for Be^8 and C^{12}, although the moment of inertia with which we should expect it to be correlated differs for the two nuclei by a factor between 1.6 and 2.

The lack of any valid picture of the nucleus with which to visualize the results of the Hartree-Fock treatment means unfortunately that one must depend on convergence arguments rather than physical insight to recognize in what cases one can rely on the results of the central-field calculation for binding energies and term differences. This emphasizes the desirability of developing a mathematical procedure more closely related to nuclear models which recognize the collective nature of the nuclear motion.

E. Refinement of the alpha-particle model

The alpha-particle model used in A and B above must be distinguished from a thoroughgoing application of the method of resonating group structure. The latter treatment takes explicitly into account the interchange of neutrons and protons between the various groupings, and allows us to derive the energies of the various nuclear levels directly from our information about the forces between elementary particles. The former description, of course, tacitly recognizes that such interchanges do go on and that they are in principle responsible for the forces between alpha-particles. Nevertheless, it depends for its validity on the assumption that the diffusion does not go on at such a rate that the alpha-particles altogether lose their identity during one characteristic period of the nuclear motion. We have seen that this assumption is reasonable for low nuclear excitation but grows progressively worse at high energies. It then becomes necessary to adopt the true method of resonating group structure to obtain a satisfactory treatment. It will be a good approximation to limit the groupings we consider to alpha-particles alone, if we are interested in nuclear levels of the symmetry type $4+4+\cdots$; levels of this kind in fact dominate the nuclear spectrum below 10 Mev. We wish now to indicate how our mathematical procedure can be simplified by taking over the results of the alpha-particle model as regards modes of vibration and allowed levels.

a. Analytic expression for alpha-particle wave function.—For definiteness, let us treat that level of C^{12} which in the simple alpha-particle model is described by the quantum numbers $n_1=2$, $n_2=0$, $J=3$, $K=3$, $m_J=3$. The system has six degrees of freedom exclusive of translation; they are associated with the three Eulerian angles φ, θ, χ of a symmetric top, the normal coordinate, ξ, of the dilatation vibration, and the coordinates η and ζ of the doubly degenerate tipping vibration. In terms of our molecular picture, the nuclear level in question would be described by the wave function

$$(\sin^6(\theta/2)e^{-3i\varphi}-\cos^6(\theta/2)e^{3i\varphi})e^{3i\chi}H_2(\xi')\times H_0(\eta')H_0(\zeta')e^{-\frac{1}{2}(\xi'^2+\eta'^2+\zeta'^2)}. \quad (26)$$

Here the H's are the usual Hermitian polynomials encountered in the oscillator problem; ξ' is an abbreviation for $(m_\xi\omega_1/h)^{\frac{1}{2}}\xi$; η', for $(m_\eta\omega_2/h)^{\frac{1}{2}}\eta$ etc., where m_ξ is defined by $m_\xi\dot{\xi}^2$ = classical kinetic energy of the first mode of vibration.

In the method of resonating group structure, we write the nuclear wave function as an expres-

sion completely antisymmetric in the twelve neutrons and protons:

$$\Psi(1,\cdots,12)=\sum_{\text{perm}} F\left(\frac{1+2+3+4}{4},\cdots,\cdots\right)$$
$$\times\Phi(1\,2\,3\,4)\Phi(5\,6\,7\,8)\Phi(9\,10\,11\,12). \quad (27)$$

The wave functions Φ describing the internal motion of the alpha-particles are taken to be fixed, while $F(\mathbf{X}_{\mathrm{I}}, \mathbf{X}_{\mathrm{II}}, \mathbf{X}_{\mathrm{III}})$ varies from state to state of the system, and corresponds in our problem to the wave function (26). Our procedure is (1) to write down a suitable analytical expression for F, having approximately the same symmetry and transformation properties as (26), but containing certain adjustable parameters; (2) to adjust these parameters to obtain the best possible wave function Ψ in the sense of the variation principle; that is, Ψ shall be orthogonal to all lower states of the same J and m_J value, and at the same time shall minimize the energy of the system:

$$\int \Psi^* H\Psi d\tau \Big/ \int \Psi^*\Psi d\tau = E = \text{a minimum.}$$

The function F exactly satisfying the condition of minimum energy (i.e., containing an infinite number of adjustable parameters) is found by solution of a wave equation, which is derived in the following paper and applied to the treatment of collision and disintegration problems. Here, however, F is taken to depend on a relatively small number of parameters, and to have a mathematical form which is at the same time simple enough to make practicable the analytic calculation of the energy of the system, and yet sufficiently flexible to give a good description of the nuclear motion. What is the most convenient form for F depends on the manner in which Φ and the nuclear interactions depend upon distance. We shall assume that the potential between elementary particles varies with distance as $\exp(-b^2\mathbf{r}_{ij}^2)$, and shall use for the alpha-particle wave function, Φ, an exponential expression which allows in the simplest manner for the close interaction between the four constituent particles:

$$\Phi(1\,2\,3\,4)=24^{-\frac{1}{2}}\begin{vmatrix} a(1) & \cdots & a(4) \\ \cdot & & \cdot \\ \cdot & & \cdot \\ d(1) & \cdots & d(4) \end{vmatrix} 8(2\alpha/\pi)^{9/4}$$
$$\times\exp -\alpha(\mathbf{r}_{12}^2+\mathbf{r}_{13}^2+\mathbf{r}_{14}^2+\mathbf{r}_{23}^2+\mathbf{r}_{24}^2+\mathbf{r}_{34}^2) \quad (28)$$

where a, b, c, and d are the four spin states defined in D. Then simplest of all choices for F is an e power with the exponent a second degree function of the Cartesian coordinates of the three alpha-particles:

$$\mathbf{F}\sim\exp\{-\sum_{i,j=1}^{\mathrm{III}}\sum_{x}^{x}(ijx)X_iX_j-\sum_{i=1}^{\mathrm{III}}\sum_{x}^{x}(ix)X_i\}. \quad (29)$$

Here the (ix) and (ijx) are numerical parameters; also $(ijx)=(jix)$, etc. The typical term in such an integral as

$$\int \Psi_m^* H\Psi_n d\tau \quad \text{or} \quad \int \Psi_m^*\Psi_n d\tau,$$

when expressed in terms of the coordinates of the twelve neutrons and protons, is thus representable as the product of three exponential integrals, associated respectively with the x, y, and z axes. The exponent of the first integral is a function of the Cartesian coordinates $x_1,\cdots,x_{12}$ and depends in addition on the constants α and b^2, the nine parameters $(ijx)_m$ and $(ix)_m$ of Ψ_m, and nine similar parameters belonging to Ψ_n:

$$I_x=\int \exp(-P_x)d\tau,$$

$$\text{where} \quad P_x=\sum_{k,l}^{12}[klx]x_kx_l+\sum_{k=1}^{12}[kx]x_k \quad (30)$$

and the brackets are combinations of the above-mentioned parameters. The integration gives at once

$$I_x=\pi^{12/2}\Delta^{-\frac{1}{2}}\exp\Delta^{-1}\sum_{k,l}^{12}[kx][lx]\frac{\partial\Delta}{\partial[klx]}, \quad (31)$$

$$\text{where} \quad \Delta=\begin{vmatrix} [1,1x] & \cdots & [1,12x] \\ \cdot & & \cdot \\ \cdot & & \cdot \\ [12,1x] & \cdots & [12,12x] \end{vmatrix}$$

and in the differentiation, $[klx]$ and $[lkx]$ are regarded as independent, being afterwards set equal to each other.

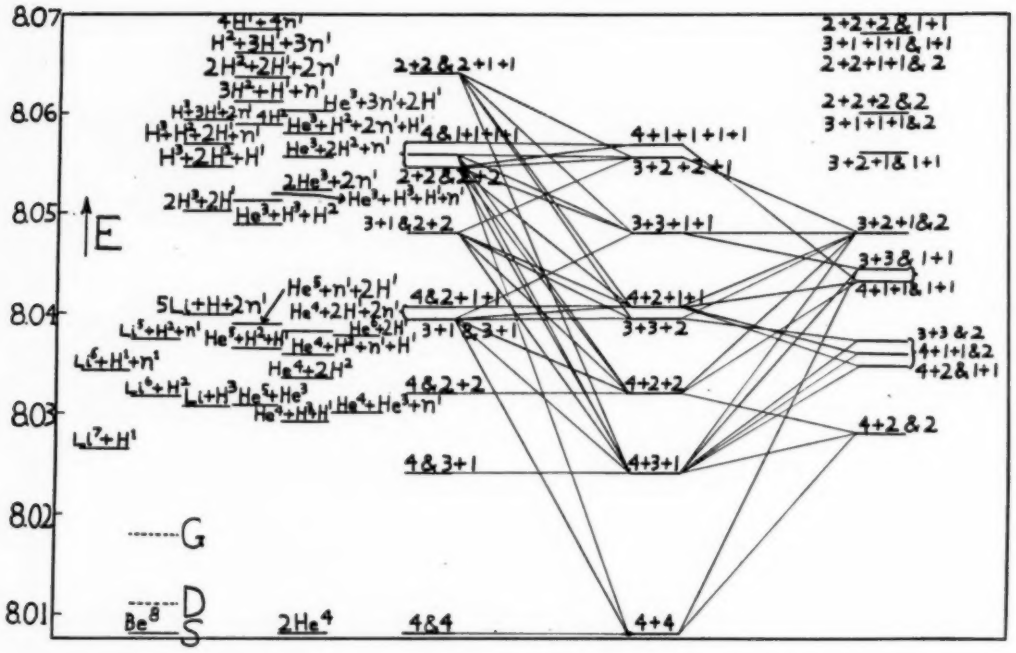

FIG. 4. At right: correlation (on long range force model) between levels of Be^8 (b) and those of groups into which the nucleus can be decomposed. Energy of levels is completely determined in this approximation by partition. The two groups whose energies are combined at (a) each contain four particles; those at (c), six and two particles. In the method of resonating group structure, states of Be^8 belonging to a particular partition are built up from those states of the various groups with which the given state is connected by correlation lines. The lowest states of Be^8 (partition 4+4) may be described approximately in terms of the normal states of two alpha-particles alone, since all other group states possess so much higher energy. At left: The experimental values for the normal energies of the constituent nuclei give a useful but less detailed guide to the choice of groups to represent a given state of the compound nucleus. (Energies in mass units.) Dotted levels predicted by alpha-particle model and by Hartree-Fock treatment.

Evaluation of the expressions

$$\mathbf{H}_{mn}=\int \Psi_m^* H \Psi_n d\tau \quad \text{and} \quad \mathbf{I}_{mn}=\int \Psi_m^* \Psi_n d\tau$$

actually requires calculation of a number of integrals of the above type, since Ψ contains $(12!/(4!\,4!\,4!\,3!))=5775$ terms $F\Phi\Phi\Phi$ corresponding to the different ways twelve particles can be grouped into alpha-particles. Symmetry arguments easily reduce the 5775 integrals entering I_{mn} to only nine, and in the same way enormously simplify the work of evaluating H_{mn}. The nine integrals all contain as first member of the integrand the expression $F_m((1+2+3+4)/4, \cdots, \cdots)\Phi(1\,2\,3\,4)\Phi(5\,6\,7\,8)\Phi(9\,10\,11\,12)$; in the last member, which contains F_n, the 12 particles have been interchanged. The 5775 integrals divide up as follows, according to the type of rearrangement:

1	belonging to the original arrangement
48	belonging to grouping (5234)(1678)(9 10 11 12)
128	..... (9234)(1678)(5 10 11 12)
54	..... (5634)(1278)(9 10 11 12)
576	..... (5934)(1678)(2 10 11 12)
216	..... (9 10 34)(1278)(5 6 11 12)
1728	..... (9234)(1 10 78)(5 6 11 12)
1728	..... (9634)(1 10 78)(52 11 12)
1296	..... (569 10)(127 11)(3 4 8 12).

The result of our choice of mathematical expression for F,

$$\mathbf{F}_m \sim \exp\{-\sum(ijx)_m X_i X_j - \sum(ix)_m X_i\}, \quad (32)$$

is to give simple analytical formulae for H_{mn}, I_{mn}, and the energy $E_m=\mathbf{H}_{mm}/\mathbf{I}_{mm}$, in terms of the parameters $(ijx)_m$, $(ix)_m$, $(ijx)_n$, and $(ix)_n$. We now observe that these three formulae, once obtained with the aid of the "generating functions" $\mathbf{F}_m$ and $\mathbf{F}_n$, enable us readily to find the corresponding quantities H_{mn}, I_{mn}, and E_m for any other pair of functions F_m and F_n. In fact, we

have only to differentiate $\mathbf{F}_m$ a suitable number of times with respect to the parameters $(ijx)_m$ and $(ix)_m$, and then carry out linear combinations to build up a function F_m consisting of a general polynomial in the alpha particle coordinates, multiplied by the same exponential as occurs in $\mathbf{F}_m$ (cf. for example Eq. (35) below). But since the parameters behave as constants in those integrations over coordinates which gave H_{mn} and I_{mn}, the values of H_{mn} and I_{mn} are obtained by carrying out the same processes of differentiation and linear combination which produced F_m from $\mathbf{F}_m$ and F_n from $\mathbf{F}_n$. This point explains the motive for giving the exponent of the generating function a dependence on alpha-particle coordinates which is more general than allowed by symmetry and the requirements of proper transformation under rotation and translation. In fact, after the differentiations just referred to, the (ix) are set equal to zero, the diagonal coefficients (iix) are all equated to one constant, and the off-diagonal coefficients (ijx) are all identified with a second constant. The parameters which really make the wave function flexible are those which enter in the formation of the linear combinations referred to above.

c. Application of alpha-particle model to construction of wave functions.—We have obtained in (*b*) a relatively simple method for the determination of the matrix elements of the energy and of unity with respect to any two wave functions. We now have the problem of actually building up from the generating function $\mathbf{F}$ the proper type of wave function to represent a given state of the system.

Let us first take as example the ground state of C^{12}. There is no rotation of the nucleus, and only zero-point vibration. It is clear that the wave function $F(\mathbf{X}_{\mathrm{I}}, \mathbf{X}_{\mathrm{II}}, \mathbf{X}_{\mathrm{III}})$ has its maximum value when the three alpha-particles are equidistant from each other and at some equilibrium distance, a_0, from the center of gravity of the nucleus. Moreover, for a uniform dilatation of the triangle of alpha-particles, the wave function will fall off approximately as $e^{-\xi'^2/2}$ or as $1-(m_\xi\omega_1/2\hbar)\xi^2$, where ξ is the normal coordinate for the given mode of motion; a similar falling off will occur for the deformations of the triangle described by the normal coordinates η and ζ (cf. *a*, above). A suitable form for the ground state wave function, having the above properties, and expressible as a linear combination of generating functions, is the following:

$$F_0 = e^{-\beta(1-\mu)(R_1^2+R_2^2+R_3^2)} \times \{e^{-(\beta\mu/3)R_{12}^2} - e^{-(\beta/3)(\mu+\epsilon)R_{12}^2}\} \times \{e^{-(\beta\mu/3)R_{13}^2} - e^{-(\beta/3)(\mu+\epsilon)R_{13}^2}\} \times \{e^{-(\beta\mu/3)R_{23}^2} - e^{-(\beta/3)(\mu+\epsilon)R_{23}^2}\}. \quad (33)$$

The first factor tends to keep the alpha-particles near the center of the nucleus, whilst each successive factor represents a given pair of alpha-particles seeking to preserve a certain equilibrium separation. F_0 reaches its maximum value when $R_1=R_2=R_3=a_0$, where $\beta a_0^2=\epsilon^{-1}\ln(1+\epsilon)$; and in the neighborhood of the maximum we have

$$F_0 = \epsilon^3(1+\epsilon)^{-3-3/\epsilon}\{1-6(1+\epsilon)\beta a_0^2\beta\xi^2 - 3(1+\epsilon)\beta a_0^2\beta(\eta^2+\zeta^2)\}.$$

Minimization of the energy of the ground state with respect to β, ϵ, and μ fixes these parameters, from which we estimate directly $a_0=[\beta^{-1}\epsilon^{-1}\ln(1+\epsilon)]^{\frac{1}{2}}$ and $\hbar\omega_1\sim(\hbar^2/M_p a_0^2)\epsilon^{-2}(1+\epsilon)\ln^2(1+\epsilon)$.

Let us now consider as a more general example the state to which we referred in (a): $n_1=2$, $n_2=0$, $J=3$, $K=3$, $m_J=3$. To represent in terms of Cartesian coordinates the angular part of the wave function given by the alpha-particle model, we note that

$$(1/4)(\sin^6\theta/2e^{-3i\varphi}-\cos^6\theta/2e^{3i\varphi})e^{3ix} \sim(X_1+iY_1)(X_2+iY_2)(X_3+iY_3)/a^3, \quad (34)$$

where $a\sim a_0+\xi$. To introduce the factors $X+iY$ into the wave function (33) used in the preceding example, we have only to operate on

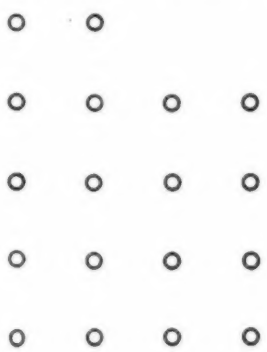

FIG. 5.

the generating function (29) with the differential expression

$$\left\{\frac{\partial}{\partial(1x)}+i\frac{\partial}{\partial(1y)}\right\}\left\{\frac{\partial}{\partial(2x)}+i\frac{\partial}{\partial(2y)}\right\}\times\left\{\frac{\partial}{\partial(3x)}+i\frac{\partial}{\partial(3y)}\right\}. \quad (35)$$

The proper dependence of the wave function on the normal coordinate ξ' which enters in the factor $H_2(\xi')=4\xi'^2-2$ is introduced by analogous differential operators.

In summary, then, we use the method of resonating group structure as follows to calculate the position of the levels predicted by the alpha-particle model: (1) we build up the type of wave function suggested by the simple model, by operating on a generating function with the proper combination of differentiation and linear superposition; (2), we calculate the matrix element of unity between this state (s) and any lower state (t) of the same J and m_J value by carrying out on the generator $\mathbf{I}_{mn}$ the same set of operations which give F_s and F_t from the generating function $\mathbf{F}$; (3), we put on the parameters of F_s the condition that this matrix element shall vanish (requirement of orthogonality to lower states); (4), we obtain the diagonal matrix elements H_{ss} and I_{ss} by a similar operational procedure; (5), we minimize the energy $E_s=H_{ss}/I_{ss}$ by varying the parameters in F_s, subject to condition (3); (6) we then have the energy and wave function of the state s in a form which (a) bears a close relation to the results of the alpha-particle model, but (b) maintains its validity even when the rate of exchange of neutrons and protons between alpha-"particles" is very rapid, and in fact (c) brings into evidence the fact that the forces between alpha-particles are intimately bound up with this interchange phenomenon.

Relative Importance of Various Groupings

The usefulness of the alpha-particle model treated above, and the importance of alpha-particle groupings in the description of the nucleus by the method of resonating group structure, both depend on those properties of nuclear forces (cf. p. 1085) which make the alpha-particle grouping particularly stable. Other types of group structure must be taken into account, however, if we desire a more accurate treatment of a nucleus of the type $4N$, or if we wish to apply our method to nuclei which cannot be built up from alpha-particles alone. In general, the various groups in which we may be interested will be characterized by their state of excitation as well as by the number of neutrons and protons they contain. In the following we develop with the aid of group theory and energy considerations some general qualitative arguments as to which types of grouping will be most important for the description of a certain state of a given nucleus.

We can discuss the general relationship between the energy levels of a compound nucleus (C) and the nuclei (A and B) from which it is synthesized with the aid of group theory alone, if we adopt a model of the nucleus (Wigner's[23] model (1)) in which the forces depend only on space coordinates and are the same between all pairs of particles. Then the eigenfunctions have the form

$$\psi^{(R)}(\mathbf{x}_1\sigma_1\tau_1,\cdots,\mathbf{x}_n\sigma_n\tau_n)=\sum_{k=1}^{\chi(E)} f_k{}^{(R)}(\sigma_1\tau_1,\cdots,\sigma_n\tau_n)u_k{}^{(R')}(\mathbf{x}_1,\cdots\mathbf{x}_n). \quad (36)$$

Here x_i denotes the position and σ_i and τ_i, the ordinary and isotopic spin variables, of the ith particle. $\chi(E)$ is the character of the identity operation. The $f_k{}^{(R)}$ constitute the normalized orthogonal basis of an irreducible representation, R, through unitary matrices, of the group H_n of permutations on n symbols. Similarly, the $u_k{}^{(R')}$ compose the substratum of that matrix representation, R', the "associate" of R, obtained by changing the sign of $(-1)^{\frac{1}{2}}$ and multiplying by ϵ_p(-1 for odd, $+1$ for even permutations P).

With each irreducible representation of H_n is associated, according to Young, a certain "symmetry pattern" constructed by arranging n dots in rows and columns, all rows starting at a fixed vertical axis and extending to the right, all columns running upwards from a fixed base line. Successive columns do not increase in length, nor is a given row ever longer than the rows beneath it. (Fig. 5 represents that symmetry pattern of H_{18} which is said to correspond to the partition

[23] E. Wigner, Phys. Rev. **51**, 107 (1937).

4+4+4+4+2 or 4^42.) Start with any function of n variables, put the n labels on the blocks in any order, symmetrize the function with respect to the variables associated with the rows, antisymmetrize with respect to the columns. The result (if not identically zero) gives a function belonging to the corresponding representation of the symmetry group. The pattern of the associated representation, R', is obtained by rotating the pattern R by 180° about the diagonal which begins at the lower left-hand corner. Since the pair of numbers σ, τ take on only four sets of values, it follows that the spin functions $f_k^{(R)}(\sigma_1 \cdots \tau_n)$ belong to a symmetry pattern whose columns do not exceed four dots in length. The rows of physically allowed partitions R' therefore never contain more than four dots.

The interaction of n_1 particles in nucleus A with n_2 particles in nucleus B will be described to the first order in terms of the zero-order wave functions of the individual systems. In their dependence on spin, these functions are linear combinations of products of the type

$$f_i^A(\sigma_1, \cdots, \tau_{n_1}) f_j^B(\sigma_{n_1+1}, \cdots, \tau_n), \quad (37)$$

obtained by distributing the $n=n_1+n_2$ pairs of variables $\sigma\tau$ between A and B in the $n!/n_1!n_2!$ possible different ways. The $\chi^A(E)\chi^B(E)n!/n_1!n_2!$ products give a representation of H_n. Broken into its different irreducible parts, this representation provides the proper linear combinations of wave functions for treating the energy levels of C. To find the symmetry patterns belonging to these allowed levels of C from the patterns of A and B, we make use of the following procedure given by Littlewood and Richardson[24] and drop those compound patterns not physically possible:

"Take the tableau (pattern) A intact, and add to it the symbols (dots) of the first (bottom) row of B. These may be added to one row of A, or the symbols may be divided (proceeding from the left, and) not disturbing their order, into any number of sets, the first set being added to one row of A, the second set to a subsequent (higher) fow, the third to a row subsequent to this, and so on. After the addition no row must contain more symbols than a preceding (lower) row, and no two of the added symbols may be in the same column.

"Next add the second row of symbols from B, according to the same rules, with this added restriction. Each symbol from the second row of B must appear in a later (higher) row of the compound tableau (pattern) than the symbol (if any) from the first row (of B which now lies) in the same column (of the compound pattern).

"Similarly add each subsequent row of symbols from B, each symbol being placed in a later row of the compound tableau than the symbol in the same column (which came originally) from the preceding row of B, until all the symbols of B have been used."

The application of this simple rule is based upon Wigner's observation that the gross structure of the nuclear energy level system appears to be determined by the symmetry of the wave function, the splitting into a multiplicity of levels arising from the finer details of the dependence of the wave function on coordinates and spins. Assuming an exactly saturated mixture of ordinary and Majorana long range forces (so that the splitting is negligible) he has in fact shown that the energy levels of an n particle system are given by

$$E=-J[(1/4)-\chi^{(R)}(2)/\chi^{(R)}(E)]n(n-1)/2 + \text{kinetic energy}. \quad (38)$$

Here J is the constant of the two-body interaction $V=-J[(\frac{1}{4})+P_M]$. R indicates the representation to which the spin part of the wave function belongs and $\chi(2)$ is the character of a transposition in this representation[25] (see Table V in Appendix). In this simplified model it is very easy to trace the relation between the energy levels of the compound nucleus and those of the groups into which it can be decomposed. Fig. 4 gives the correlation diagram for the lower "gross structure" levels of a system of eight particles.

Decrease of the range of the forces and introduction of electrostatic and spin interactions splits up the levels in the correlation diagram and complicates the tracing of correspondences. Also,

[24] D. E. Littlewood and A. R. Richardson, Proc. Lond. Math. Soc. **A233** (1934).

[25] Reference is made to F. D. Murnaghan, J. Am. Math. Soc. **59**, 437 (1937), for a treatment of the properties of the symmetric group in a form convenient for application to nuclear theory. I am indebted to Professor Murnaghan for informing me of his results before publication.

the symmetry character of the wave function is no longer an exact integral of the equations of motion. Nevertheless, it is approximately an integral, and dominates the discussion of the composition of the compound wave function from the wave functions of the constituent groups. Particularly, in applying the method of resonating group structure in its simplest form to approximate the description of a certain level of C, we can neglect all but the lowest of the "symmetry levels" of the groups A and B into which C may be decomposed. The usefulness of this approximation is based on the relatively enormous dependence of the energy of the system on the symmetry character, in comparison to other effects.

With the above considerations as a guide, we are able to make an approximate estimate as to which types of groupings are most important in describing a given state of a given nucleus. This is particularly important for the development of the following paper, in which the mathematical treatment starts out with the assumption that the important groupings are already known.

Two-Body and Many-Body Forces

So far we have applied the concepts of resonating group structure to the nucleus in a way which has been independent of all but the simplest assumptions about the properties of the interactions between elementary particles. Nevertheless, the question of the detailed nature of these interactions must have an essential, if indirect, connection with the types of collective motion occurring in the nucleus.

Can nuclear properties be accounted for by forces acting between pairs of particles, or is a field theory necessary from the beginning in any reasonably accurate account of nuclear properties? Although present theory supplies no answer, we can at least expect *a priori* an intimate connection between electron theory and forces within the nucleus. The disturbance of the electron-positron field near the heavy nuclear particles owing to the rapidly alternating electromagnetic fields within the nucleus necessarily counter induces a reaction of the electron positron distribution upon the heavy particles. In the terminology of the quantum theory, we may say that virtual pairs induce forces between the heavy particles in the same sense in which we speak of virtual quanta being responsible for the Coulomb interaction.

It is instructive in this connection to recall the method by which we may abstract from the existence of the electromagnetic field to obtain the ordinary expression for the interactions in a system of charged particles: from the fields $\mathbf{E}_i$ and $\mathbf{H}_i$ of the individual particles we obtain the total fields $\mathbf{E}=\Sigma\mathbf{E}_i$ and $\mathbf{H}=\Sigma\mathbf{H}_i$ and thence that part of the field energy which does not contain self-energy terms:

$$(8\pi)^{-1}\int(\mathbf{E}^2+\mathbf{H}^2-\Sigma\mathbf{E}_i^2-\Sigma\mathbf{H}_i^2)d\tau. \quad (39)$$

In the static case the result is

$$\sum_{i<j}e_ie_j/r_{ij},$$

and also in general it is the sum of terms, each of which represents the interaction between only two particles, a consequence of the quadratic expression for the field energy.

A similar calculation of how much the electron-positron field contributes to the interaction of a system of particles might be made in the same way if it were not that a general expression for the energy density, U', of the field is lacking. However, even in the expansion for U' given by Euler and Kockel[26]

$$\begin{aligned}U'=&(180\pi^2)^{-1}mc^2(h/mc)^{-3}\\&\times\{(\tfrac{1}{2})(\mathbf{f}^2-\mathbf{g}^2)(3\mathbf{f}^2+\mathbf{g}^2)+(7/2)(\mathbf{f}\cdot\mathbf{g})^2\\&+(2/7)(\mathbf{f}^2-\mathbf{g}^2)^2(5\mathbf{f}^2+\mathbf{g}^2)\\&\qquad+(13/7)(\mathbf{f}\cdot\mathbf{g})^2(3\mathbf{f}^2-\mathbf{g}^2)+\cdots\} \quad (40)\\&[(h/mc)e\mathbf{E}=mc^2\mathbf{f};\quad(h/mc)e\mathbf{H}=mc^2\mathbf{g}],\end{aligned}$$

valid only for not too strong or too rapidly varying fields,

$$(h/mc)|\text{grad }\mathbf{F}|\ll|\mathbf{F}|,\quad(h/mc^2)|\dot{\mathbf{F}}|\ll|\mathbf{F}|, \quad (41)$$

it is clear that that part of the interaction energy of a group of particles at nuclear distances ($|\mathbf{f}|, |\mathbf{g}|\gg1$) which is due to the electron positron field involves many-body forces and two-body forces of the same order of magnitude.

The observed dependence of nuclear binding on numbers of neutrons and protons gives little un-

[26] H. Euler and B. Kockel, Naturwiss. **23**, 246 (1935); also W. Heisenberg and H. Euler, Zeits. f. Physik **38**, 714 (1936).

ambiguous information on the question of the existence of many-body forces. Nevertheless, if we adopt the long range force model by which Wigner[21] freed the group theory discussion of nuclear binding from complications due only to the dependence of forces on distance and spin, we can draw one important conclusion; namely, that no compromise is available between two-body forces and many-body forces. More precisely, to account for observed binding energies, either (a) , the many-body forces must be much weaker than the two-body forces; or (b), with increasing number of particles in the nucleus, each successive group of many-body forces coming into action must make a contribution comparable with the total binding energy. Excluded is situation (c): 2, 3, $\cdots$, k-body forces strong ($238 \gg k > 2$), t-body forces negligible ($t > k$). This result can be seen in a general way from a comparison of the number of adjustable force constants with the requirements of observation: saturation character of nuclear binding, observed energy differences between isotopes, relative stability of nuclei of the types $4N$, $4N+1$, $4N+2$, $4N+3$, How it comes about in detail is shown in the appendix for the cases $k=3$ and $k=4$.

It must be emphasized[27] that the above conclusion depends on the (incorrect) assumption that nuclear forces are of long range; for example, it does not follow that the conclusion is true for short range many-body forces; and it is probably false if the many-body forces depend on velocity. Our arguments, in fact, are not quite general enough to allow us the satisfaction of dividing possible theories of nuclear forces into two sharply differentiated groups: (1), the usual, and plausible, description in terms of two-body forces; and (2), a description whose mathematical formulation requires from the beginning essentially a complete field theory of nuclear forces.

That many particle forces are consistent with our present information about the nucleus emphasizes the almost insuperable mathematical difficulties in the way of attempts to make nuclear spectroscopy alone yield any complete and unambiguous account of nuclear *forces*. Concerning the symmetry properties and certain other general features of the nuclear *wave function*, however, it appears possible to draw definite conclusions which depend on only a few very general assumptions about the exchange nature of nuclear forces—not, for example, on the number of particles involved in the interactions, nor particularly on the way the forces may vary with velocity. Although the nuclear liquid model of Bohr and Kalckar does not attempt to take account of symmetry properties, the qualitative correspondence in other respects between the modes of nuclear motion predicted by this and by the alpha particle treatment emphasizes to what a small extent the details of the interactions really enter into the determination of the general structure of the nuclear energy level spectrum. From this point of view, the most permanent value of detailed calculations based on special types of two-body forces is the correlation achieved between the properties of nuclear wave functions or states of motion and energy level systems.

Appendix I. Treatment of the Nuclear Three-Body Problem by the Method of Resonating Group Structure

Particles **1** and **2** are protons (neutrons); **3** is a neutron (proton). Consider the system as composed of proton (neutron) plus deuteron. The spin of the deuteron has three possible orientations:

$$\Phi_1(2,3)=\alpha(2)\alpha(3)\varphi(3-2),$$
$$\Phi_0(2,3)=2^{-\frac{1}{2}}[\alpha(2)\beta(3)+\alpha(3)\beta(2)]\varphi(3-2),$$
$$\Phi_{-1}(2,3)=\beta(2)\beta(3)\varphi(3-2). \quad (42)$$

In these deuteron wave functions, $\varphi(3-2)$ is supposed to be a known function, depending only on the separation $r=|3-2|$ of neutron and proton, and to be normalized so that $\int\varphi^2(r)4\pi r^2dr=1$.

According as $S=\frac{3}{2}$ or $S=\frac{1}{2}$ for the combined system $He^3(H^3)$, we have two types of antisymmetric total wave function, typified, respectively, by

$$\Psi(1,2,3)=2^{-\frac{1}{2}}\alpha(1)\alpha(2)\alpha(3)[F((2+3)/2-1)\varphi(3-2) - F((1+3)/2-2)\varphi(3-1)] \quad (43)$$

and

$$\Psi(1,2,3)=12^{-\frac{1}{2}}[\alpha(1)\alpha(2)\beta(3)+\alpha(1)\beta(2)\alpha(3) -2\beta(1)\alpha(2)\alpha(3)]F((2+3)/2-1)\varphi(3-2) -12^{-\frac{1}{2}}[\alpha(2)\alpha(1)\beta(3)+\alpha(2)\beta(1)\alpha(3) -2\beta(2)\alpha(1)\alpha(3)]F((1+3)/2-2)\varphi(3-1). \quad (44)$$

With the help of these expressions, we calculate in terms of F the average energy of the system:

$$E=\int\Psi(T+V)\Psi d\tau/\int\Psi^2d\tau.$$

[27] I am indebted to Professor Wigner for making this observation.

We represent the interactions between the constituent particles by combinations of Majorana and Heisenberg forces.[28] We find by integration

$$E=\{(3\hbar^2/4M)\int(\nabla F)^2 d\mathbf{X} + E_0\int F^2(\mathbf{X})d\mathbf{X}+\int F^2(\mathbf{X})\,V(\mathbf{X})d\mathbf{X} + \int\int F(\mathbf{X})J(\mathbf{X},\xi)F(\xi)d\mathbf{X}d\xi\}/ \{\int F^2(\mathbf{X})d\mathbf{X}+\int\int F(\mathbf{X})I(\mathbf{X},\xi)F(\xi)d\mathbf{X}d\xi\}. \quad (45)$$

Here M represents the proton mass and E_0 the average energy of a free deuteron described by the wave function φ:

$$E_0=(\hbar^2/M)\int(\nabla\varphi)^2 d\boldsymbol{\sigma}-B\int\varphi^2(\boldsymbol{\sigma})\exp(-b^2\boldsymbol{\sigma}^2)d\boldsymbol{\sigma}. \quad (46)$$

Brackets are used below to represent the dependence of the ordinary interaction potential V and the integral operators I and J upon spin; the upper component belongs to $S=\frac{3}{2}$, the lower to $S=\frac{1}{2}$. $\mathbf{X}$, ξ, $\boldsymbol{\sigma}$ are vectors, as are also $\mathbf{u}=(4\xi+2\mathbf{X})/3$ and $\mathbf{v}=(4\mathbf{X}+2\xi)/3$.

$$I(\mathbf{X},\xi)=(64/27)\begin{pmatrix}-1\\1/2\end{pmatrix}\varphi(\mathbf{u})\varphi(\mathbf{v}), \quad (47)$$

$$V(\mathbf{X})=(1-2g)B\begin{pmatrix}1/3\\-2/3\end{pmatrix}\int\varphi^2(\boldsymbol{\sigma})\exp[-b^2(\mathbf{X}-\boldsymbol{\sigma}/2)^2]d\boldsymbol{\sigma} + e^2\int\varphi^2|\mathbf{X}-\boldsymbol{\sigma}/2|^{-1}d\boldsymbol{\sigma}, \quad (48)$$

$$J(\mathbf{X},\xi)=(64/27)\varphi(\mathbf{u})\varphi(\mathbf{v})[-B\begin{pmatrix}4/3-2g/3\\11/6-19g/6\end{pmatrix} \exp[-b^2(\mathbf{u}-\mathbf{v})^2]+B\begin{pmatrix}1\\-1/2\end{pmatrix}[\exp(-b^2\mathbf{u}^2) +\exp(-b^2\mathbf{v}^2)]-\begin{pmatrix}1\\-1/2\end{pmatrix}e^2|\mathbf{u}-\mathbf{v}|^{-1} +(256\hbar^2/81M)\begin{pmatrix}1\\-1/2\end{pmatrix}[\varphi(\mathbf{u})\nabla^2\varphi(\mathbf{v}) +\varphi(\mathbf{v})\nabla^2\varphi(\mathbf{u})+\nabla\varphi(\mathbf{u})\cdot\nabla\varphi(\mathbf{v})]. \quad (49)$$

Before proceeding further, we investigate how accurate a treatment of the binding energy of H^3 is possible with the simplest analytical expressions for the deuteron wave function and the intergroup wave function:

$$\varphi(\boldsymbol{\sigma})=\exp(-\alpha\boldsymbol{\sigma}^2); \quad F(\mathbf{X})=\exp(-\beta\mathbf{X}^2). \quad (50)$$

No electrostatic terms enter this problem. The state of the system is ^2S. The energy becomes a simple function of α and β. Its minimum value, -6.4mMU, is reached when $\alpha=0.87(mc^2/e^2)^2$, $\beta=0.68(mc^2/e^2)^2$. In comparison, a wave function of the form

$$\Psi(\mathbf{1},\mathbf{2},\mathbf{3})=2^{-\frac{1}{2}}\alpha(\mathbf{3})[\alpha(\mathbf{2})\beta(\mathbf{1})-\alpha(\mathbf{1})\beta(\mathbf{2})]N \times\exp[-(\nu/2)(\mathbf{r}_{13}^2+\mathbf{r}_{23}^2)-(\mu/2)\mathbf{r}_{12}^2] \quad (51)$$

gives an expression[29] for the energy of H^3, whose minimum value, -5.6 mMU, is obtained when $\mu=0.8$ and $\nu=1.0(mc^2/e^2)^2$. (The same values of the force constants are used in both calculations. We estimate by the equivalent two-body method that an accurate calculation using these constants would give $E=-8.7$ mMU for the binding energy.) We compare the spatial parts of the wave function (51) and the resonating group wave function (44):

$$\exp\{-(\mu+\nu)\mathbf{X}^2/2-(\mu+5\nu)\boldsymbol{\sigma}^2/8+(\mu-\nu)\mathbf{X}\cdot\boldsymbol{\sigma}/2\} \leftrightarrow\exp\{-\beta\mathbf{X}^2-\alpha\boldsymbol{\sigma}^2\}. \quad (52)$$

The polarization term, $\mathbf{X}\cdot\boldsymbol{\sigma}$, in the first function is in the right direction to allow for polarization of the deuteron by the neutron, but is small owing to the near equality of μ and ν. That the second function gives a binding 0.8 mMU better than the first in this problem must be attributed mainly to its having a better form of spin dependence, built up from deuteron spin functions (cf. discussion below).

How can one find the best possible wave function of the form (44), supposing φ to be given? We use the variation principle, varying $F(\mathbf{X})$ to make the expression (45) for the energy a minimum. The necessary and sufficient condition for stationary E is found to be [30] that F satisfy the wave equation[31]

$$(3\hbar^2/4M)\nabla^2F(\mathbf{X})+(E-E_0)F(\mathbf{X})=V(\mathbf{X})F(\mathbf{X}) +\int[J(\mathbf{X},\xi)-EI(\mathbf{X},\xi)]F(\xi)d\xi. \quad (53)$$

Thus the relative motion of deuteron and neutron is governed by an ordinary potential $V(\mathbf{X})$ and a velocity dependent potential, represented by an integral operator with the kernel $K(\mathbf{X},\xi)=J-EI$. The three dimensional equation of motion (53) is reduced[32] to a radial equation by expressing $\mathbf{X}$ and ξ in polar coordinates r, θ, φ and ρ, ϑ, τ and making the substitutions

$$F(\mathbf{X})=r^{-1}f_L(r)P_L(\cos\theta); \quad \cos(\mathbf{X},\xi)=\mu; \quad K(\mathbf{X},\xi)=\Sigma(2L+1)K_L(r,\rho)P_L(\mu)/4\pi r\rho. \quad (54)$$

For S states ($L=0$) we find

$$(3\hbar^2/4M)d^2f/dr^2+(E-E_0)f(r)=V(r)f +\int[J_0(r,\rho)-EI_0(r,\rho)]f(\rho)d\rho, \quad (55)$$

which is thus the wave equation applying to the ground states of H^3 and He^3.

We determine the dependence of neutron-deuteron interaction on distance by substituting into (47–49) the expression $(2\alpha/\pi)^{\frac{3}{4}}\exp(-\alpha r^2)$ for the deuteron wave-function, with $\alpha=0.87$ (see Fig. 6*d*). We find

$$V(r,\rho)=-(2B/3)(1-2g)(1+b^2/8\alpha)^{-\frac{3}{2}} \times\exp[-b^2r^2(1+b^2/8\alpha)^{-1}]; \quad (56)$$

$$I_0(r,\rho)=(8/3)(2\alpha/\pi)^{\frac{3}{4}}\sinh(32\alpha r\rho/9) \times\exp[-(20\alpha/9)(r^2+\rho^2)]; \quad (57)$$

$$J_0(r,\rho)=-(8/3)(2\alpha/\pi)^{\frac{3}{4}}(1+b^2/4\alpha)^{-1}B(11/3-19g/3) \cdot\sinh(32\alpha/9+8b^2/9)r\rho\exp[-(20\alpha/9+4b^2/9) \times(r^2+\rho^2)]-(8/3)(2\alpha/\pi)^{\frac{3}{4}}(1+b^2/2\alpha)^{-1}B\sinh (32\alpha/9+16b^2/9)r\rho\cdot\{\exp[-(20\alpha/9+4b^2/9)r^2 -(20\alpha/9+16b^2/9)\rho^2]+\exp[-(20\alpha/9+16b^2/9)r^2 -(20\alpha/9+4b^2/9)\rho^2]\}+(64\hbar^2\alpha/9M)(2\alpha/\pi)^{\frac{3}{4}} \times\exp[-(20\alpha/9)(r^2+\rho^2)]\{[(11/4 -(56\alpha/9)(r^2+\rho^2)]\sinh(32\alpha r\rho/9) +(104\alpha r\rho/9)\cosh(32\alpha r\rho/9)\}. \quad (58)$$

V, I_0 and J_0 are charted in Fig. 6.

The function $f(r)=r\exp(-\beta r^2)$, with $\beta=0.68$, represents an approximate solution of the radial equation. Curve A in Fig. 6 shows how this function is related to the range of the neutron-deuteron interaction.

[28] Eqs. (22a, b, c), "The Interaction Between Two Normal Alpha-Particles," give the exact expressions used. (To be published in the *Physical Review*.)

[29] E. Feenberg, Phys. Rev. **47**, 854 (1935), Eq. (14).

[30] For the variational calculation, see following paper, Eq. (17).

[31] In a recent paper [Proc. Phys. Math. Soc. Japan 19, 542 (1937)], Yukawa and Sakata discuss the scattering of neutrons in deuterium and derive an integro-differential equation which is similar to (53) but contains no term analogous to I, since their treatment was not based on the variation principle.

[32] Wheeler, Phys. Rev. **50**, 647 (1936), Eq. (10).

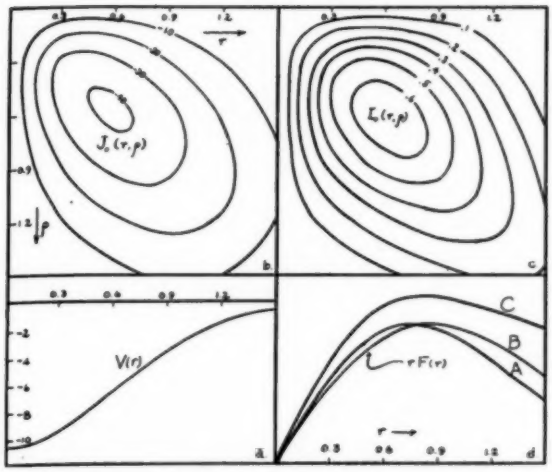

FIG. 6. Interaction of neutron and deuteron in ^3S states of H^3. (*a*) Ordinary potential $V(r)$ in mMU as a function of r (in units $e^2/mc^2=2.80\times10^{-13}$ cm). (*b*) Contour map of the kernel, $J_0(r,\rho)$, of the velocity dependent interaction, in units mMU $(e^2/mc^2)^{-1}$, as function of r and ρ. As one carries through the transition from the nuclear to the molecular three-body problem, the trough in J_0 becomes deeper and narrows down in the ratio $m/M=1/1840$, representing finally an interaction nearly independent of velocity. (*c*) $I_0(r,\rho)$, in units $(e^2/mc^2)^{-1}$. (*d*) *B*, approximate solution of the radial wave equation for relative motion of neutron and deuteron. *A*, internal wave function of deuteron used in calculating V, I_0, and $J_0(r\varphi(r)=Kr\exp(-\alpha r^2))$. *C*, exact wave function of free deuteron, for comparison. (*A*, *B*, and *C* not normalized.)

A calculation of V, I_0 and J_0 using for φ the exact wave function for a free deuteron, although complicated, would not give interactions very different from those shown in the figure, as one sees from a comparison of curves *B* and *C*. This choice of φ, however, makes one essential simplification: the wave function (44) for the three-body problem has exactly the right asymptotic behavior to describe dissociation and scattering. Solution of (53) then gives phase shifts and scattering cross sections.

The connection between the method of resonating group structure and the Heitler-London procedure is easily traced. The forces between 3 and 1, and 3 and 2, no longer depend appreciably on spin. In contrast to the deuteron, the atom has stable states of both the singlet and triplet type. Out of these we can build up two types of doublet wave functions, for the molecule, one of the form (44), the other being

$$2^{-1}\alpha(1)[\alpha(2)\beta(3)-\alpha(3)\beta(2)]G(\mathbf{X}_{\mathrm{I}})\chi(3-2)$$
$$-2^{-1}\alpha(2)[\alpha(1)\beta(3)-\alpha(3)\beta(1)]G(\mathbf{X}_{\mathrm{II}})\chi(3-1). \quad (59)$$

The states of the whole system are actually represented by linear combinations of the two types of doublet function. In the nuclear problem, the slight admixture of the second type was neglected, although our treatment would have been improved by taking into account the virtual ^1S level of the deuteron, describable by χ. In the molecular case, the atomic wave functions χ and φ are to be identified, as the dynamical effect of spin is negligible. The proper linear combinations are easily found: $F=(3^{\frac{1}{2}}/2)F_1$, $G=-(\frac{1}{2})F_1$ gives the molecular state built on a singlet state of the two protons; the doublet state built on a triplet is obtained when $F=(\frac{1}{2})F_3$, $G=(3^{\frac{1}{2}}/2)F_3$. It is to the former that the nuclear ground state is most closely related. The associated wave functions are

$$\Psi_1=2^{-1}[\alpha(1)\beta(2)-\alpha(2)\beta(1)]\alpha(3)[F_1(\mathbf{X}_{\mathrm{I}})\varphi(3-2)+F_1(\mathbf{X}_{\mathrm{II}})\varphi(3-1)],$$
$$\Psi_3=12^{-\frac{1}{2}}[2\alpha(1)\alpha(2)\beta(3)-\alpha(1)\beta(2)\alpha(3)-\alpha(2)\beta(1)\alpha(3)]\cdot[F_3(\mathbf{X}_{\mathrm{I}})\varphi(3-2)-F_3(\mathbf{X}_{\mathrm{II}})\varphi(3-1)]. \quad (60)$$

In addition we also have four quartet states built on triplet states of the two protons. These are like (43) in spin dependence, and have the same coordinate dependence as Ψ_3.

The different spin dependence of atomic and nuclear forces governed the just mentioned changes in the spin part of the compound wave function, changes which had nothing to do, however, with the decrease of the mass of particle 3 from M to $m=M/1839$. At the end of the latter transition, in the limit $m/M\to0$, the separation of particle 1 from group (23), namely, $\mathbf{X}_{\mathrm{I}}=(M\mathbf{x}_2+m\mathbf{x}_3)/(M+m)-\mathbf{x}_1$, approaches the negative of the complementary separation $\mathbf{X}_{\mathrm{II}}$. The calculation of the energy of the system in this limit is very simple and gives the same type of expression as occurred in the nuclear problem, (Eq. (45)), with $\hbar^2/M$ as coefficient of the kinetic energy term and

$$V(\mathbf{X})=J(\mathbf{X})+e^2/|\mathbf{X}|,$$
$$J(\mathbf{X},\boldsymbol{\xi})=\delta(\mathbf{X}+\boldsymbol{\xi})[2K(\mathbf{X})+D(\mathbf{X})e^2/|\mathbf{X}|-\hbar^2/2m\nabla^2D(\mathbf{X})],$$
$$I(\mathbf{X},\boldsymbol{\xi})=\delta(\mathbf{X}+\boldsymbol{\xi})D(\mathbf{X}) \quad (61)$$

(for singlet states; I and J have opposite sign for triplet states). Here D is the orthogonality integral, and J and K the direct and exchange integrals, which are familiar from the Heitler-London approximation:

$$D(\mathbf{X})=\int\varphi(-\mathbf{X}/2+\boldsymbol{\lambda})\varphi(\mathbf{X}/2+\boldsymbol{\lambda})d\boldsymbol{\lambda},$$
$$J(\mathbf{X})=\int\varphi^2(-\mathbf{X}/2+\boldsymbol{\lambda})\frac{e^2}{|\mathbf{X}/2+\boldsymbol{\lambda}|}d\boldsymbol{\lambda},$$
$$K(\mathbf{X})=\int\varphi(-\mathbf{X}/2+\boldsymbol{\lambda})\frac{e^2}{|\mathbf{X}/2+\boldsymbol{\lambda}|}\varphi(\mathbf{X}/2+\boldsymbol{\lambda})d\boldsymbol{\lambda}. \quad (62)$$

The velocity dependence of the interaction between the two groups has degenerated in the molecular problem to a kernel which is approximately a δ function. Two cases are possible: (1), $F(\mathbf{X})$ an even function of $\mathbf{X}(L=0,2,\cdots)$. Then $\int\delta(\mathbf{X}+\boldsymbol{\xi})F(\boldsymbol{\xi})d\boldsymbol{\xi}=F(\mathbf{X})$; the effective molecular potential represents attraction for singlet states (ionized parahydrogen), instability for triplets (derived from orthohydrogen); (2), $L=1,3,\cdots$; $\int\delta(\mathbf{X}+\boldsymbol{\xi})F(\boldsymbol{\xi})d\boldsymbol{\xi}=-F(\mathbf{X})$; and the roles of the ortho- and parahydrogen molecular ion are interchanged.

If φ is the exact wave function for the ground state, E_0, of the hydrogen atom, we have

$$-(\hbar^2/2m)\nabla^2D(\mathbf{X})=E_0D(\mathbf{X})-K(\mathbf{X})$$

and the wave equation (53) can be put in a form which exhibits the usual Heitler-London molecular potential:

$$(1\pm D)^{-1}(\hbar^2/M)\nabla^2F+(E-E_0)F=\left[\frac{e^2}{|\mathbf{X}|}+\frac{J\pm K}{1\pm D}\right]F. \quad (63)$$

TABLE V. *Table for determining the character ratios* $\chi(2)/\chi(E)$, $\chi(3)/\chi(E)$, $\chi(4)/\chi(E)$, $\chi(2^2)/\chi(E)$ *for certan simple partitions. Example: For the partition* $(t+1)^3t$ *of the number* $n=4t+3$, $\chi(2)/\chi(E)=(4t^2-10t-6)/n(n-1)$.

Partition (spin)	Adjoint (coordinate)	Order n	$n!\chi(2)/(n-2)!\chi(E)$			$n!\chi(3)/(n-3)!\chi(E)$				$n!\chi(4)/(n-4)!\chi(E)$					$n!\chi(2^2)/(n-4)!\chi(E)$				
			t^2	t	1	t^3	t^2	t	1	t^4	t^3	t^2	t	1	t^4	t^3	t^2	t	1
t^4	4^t	$4t$	4	−16	0	4	−48	+68	0	4	−96	+404	−336	0	16	−144	+416	−264	0
$(t+1)^2t^2$	4^t1	$4t+1$	4	−14	0	4	−45	+56	0	4	−92	+356	−268	0	16	−128	+344	−232	0
$(t+1)^2t^2$	4^t2	$4t+2$	4	−12	−2	4	−42	+38	0	4	−88	+296	−172	0	16	−112	+264	−128	0
$(t+1)^3t$	4^t3	$4t+3$	4	−10	−6	4	−39	+14	+6	4	−84	+224	−24	0	16	−96	+176	+24	0
$(t+2)t^3$	4^t1^2	$4t+2$	4	−12	+2	4	−42	+50	0	4	−88	+320	−236	0	16	−112	+296	−272	0
$(t+2)(t+1)t^2$	4^t21	$4t+3$	4	−10	0	4	−39	+32	−3	4	−84	+260	−156	0	16	−96	+224	−168	0
$(t+2)^2t^2$	4^t2^2	$4t+4$	4	−8	0	4	−36	+20	−12	4	−80	+212	−136	0	16	−80	+176	−136	+24
$(t+2)(t+1)^2t$	4^t31	$4t+4$	4	−8	−4	4	−36	+8	0	4	−80	+188	−24	+8	16	−80	+144	−24	−8
$(t+2)^2(t+1)t$	4^t32	$4t+5$	4	−6	−4	4	−33	−4	−12	4	−76	+140	−20	+24	16	−64	+104	−8	+24
$(t+2)^2t$	4^t3^2	$4t+6$	4	−4	−6	4	−30	−22	−24	4	−72	+80	+12	+72	16	−48	+56	+48	+72

That the factor $(1\pm D)^{-1}$ occurs in (63), although absent in the customary molecular treatment, is due to the fact that we have consistently applied the variation principle. Indeed, without this factor, the wave functions Ψ derived from F's for two different energies would not have the proper orthogonality. The modification which the above factor introduces in the mass of the system gives an improvement, in principle, on the H−L approximation. Although the Born-Oppenheimer theory[3] requires use of the customary value for the reduced mass, this does not contradict our conclusions, for this theory assumes an accurate calculation of the molecular potential.

Appendix II. Two-, Three- and Four-Body Long Range Exchange Forces

A number of important consequences were drawn by Wigner[21] by considering a Hamiltonian arising from long range two-body interactions, linear combinations of ordinary and Majorana forces, equal between all pairs of particles:

$$H=\sum_{i<j}[-J_0-J(ij)]. \tag{64}$$

The symbol (ij) represents the Majorana coordinate exchange operator. The J's are numerical constants. The expression

$$H=\sum_{\text{pairs}}[-J_0-J(ij)]+\sum_{\text{triples}}[-K_0-K(ijk)]+\sum_{\text{quadruples}}[-L_0-L(ijkl)]+\sum_{\text{double pairs}}[-M_0-M(ij)(kl)] \tag{65}$$

represents the corresponding Hamiltonian operator if forces exist between larger groups of particles. The permutations are defined by equations like

$$(ijk)u(\mathbf{x}_1\cdots\mathbf{x}_i\cdots\mathbf{x}_j\cdots\mathbf{x}_l\cdots)=u(\mathbf{x}_1\cdots\mathbf{x}_l\cdots\mathbf{x}_i\cdots\mathbf{x}_j). \tag{66}$$

In terms of the number, n, of particles and the characters, χ, of the representation of the symmetric group, H_n to which the coordinate part of the wave function belongs, the energy, W, of the system is given exactly by

$$W=[-J_0-J\chi(2)/\chi(E)]n(n-1)/2+[-K_0-K\chi(3)/\chi(E)]n(n-1)(n-2)/6+[-L_0-L\chi(4)/\chi(E)]n(n-1)(n-2)(n-3)/24+[-M_0-M\chi(2^2)/\chi(E)]\times n(n-1)(n-2)(n-3)/8. \tag{67}$$

From Table V one finds that exact saturation requires that

$$M_0=-M/16,\ L_0=L/64,\ M=\mathrm{L}/4,\ K_0=-K/16,\ J_0=J/4+45K/48+575L/512,$$

J, K, and L being arbitrary. Under these conditions, the normal energy level of the system is given by

$$\begin{aligned}
-W&=n(15J/8+75K/32+915L/768) && (n=4N)\\
&=n(15J/8+90K/32+945L/768)\\
&\quad-(15J/8+90K/32+6750L/768) && (n=4N+1)\\
&=n(15J/8+95K/32+1195L/768)\\
&\quad-(20J/8+160K/32+2000L/768) && (n=4N+2)\\
&=n(15J/8+90K/32+1305L/768)\\
&\quad-(15J/8+150K/32+2745L/768)\\
&&& (n=4N+3)
\end{aligned} \tag{68}$$

and when $n=4N$, the first excited level is determined by

$$-W=n(15J/8+107K/32+1363L/768)-(32J/8+256K/32+3584L/768), \tag{69}$$

the partition being $4+4+\cdots+4+3+1$. The excitation energy

$$W=4J+(8-n)(K+7L/12) \tag{70}$$

corresponds in the case of actual nuclei to the difference of binding energies in pairs such as ${}_3\mathrm{Li}^8$, ${}_4\mathrm{Be}^8$. Allowance being made in the experimental values for electrostatic energy, this difference does not change by as much as 50 percent in the light nuclei up to $n=16$, whence

$$|K+7L/12|<J/8. \tag{71}$$

From the almost periodic manner in which the binding energy of light nuclei is observed to vary with atomic number, we conclude by the same type of argument that K and L individually cannot exceed approximately 10 percent of J. In conclusion: if a mixture of two-, three-, and four-body exchange and ordinary forces is to account for the characteristic features of nuclear structure, the two-body forces must be responsible for at least 90 percent of the binding energy of the light nuclei up to oxygen, provided first, that the forces are of long range, and second, that they do not depend on velocity.

On the Mathematical Description of Light Nuclei by the Method of Resonating Group Structure

JOHN A. WHEELER
University of North Carolina, Chapel Hill, North Carolina
(Received August 17, 1937)

The wave function for the composite nucleus is written as a properly antisymmetrized combination of partial wave functions, corresponding to various possible ways of distributing the neutrons and protons into various groups, such as alpha-particles, *di*-neutrons, etc. The dependence of the total wave function on the intergroup separations is determined by the variation principle. The analysis is carried out in detail for the case that the configurations considered contain only two groups. Integral equations are derived for the functions of separation. The associated Fredholm determinant completely determines the stable energy values of the system (Eq. (33)), Eq. (48) connects the asymptotic behavior of an arbitrary particular solution with that of solutions possessing a standard asymptotic form. With its help, the Fredholm determinant also determines all scattering and disintegration cross sections (Eqs. (50)···(54) and (57)), without the necessity of actually obtaining the intergroup wave functions. The expressions (43) and (60) obtained for the cross sections, taking account of spin effects, have general validity. Details of the application of the method of resonating group structure to actual problems are discussed.

INTRODUCTION

Resonating group structure

A DESCRIPTION[1] of the nucleus which regards the neutrons and protons as spending part of their time in configurations corresponding, for example, to interacting alpha-particles, part of their time in other groupings, already takes into account to a large extent that intimate interaction between nuclear particles which is so entirely different from the situation in atomic structure, where the concept of average field is a reasonable approximation. In contrast to the Hartree-Fock procedure, the method of "resonating group structure" builds up a wave function for the whole nucleus out of partial wave functions which describe the close interaction within the individual groups. It is clear that in this way we take advantage from the beginning of the saturation character of nuclear binding, by which much the largest part of the energy of the compound nucleus is accounted for by the internal binding of the separate groups. On the other hand, the fact that the total wave function is built of a properly antisymmetrized combination of partial wave functions, corresponding to the various possible types of groupings, shows that we are far from the picture which regards alpha-particles, for example, as having any real existence within the nucleus.

It is the purpose of this paper to derive the wave equation for resonating group structures and to show how the interaction integrals can be evaluated and how solutions can be obtained which give the positions of nuclear energy levels and the cross sections for scattering and disintegration. We start out by considering a system of m protons and n neutrons described by the $m+n=N$ coordinates[2a] $\mathbf{x}_1, \sigma_1; \mathbf{x}_2, \sigma_2; \cdots \mathbf{x}_m, \sigma_m; \mathbf{y}_1, \tau_1; \cdots \mathbf{y}_n, \tau_n$, ($\sigma$'s are proton spins, τ's are neutron spins) which we may abbreviate as simply $\mathbf{1}, \mathbf{2}, \cdots, \mathbf{N}$. In the approximation given by the method mentioned, the wave function Ψ of the whole system is written as the sum of parts, of which a given term represents the N particles sorted into groups in a particular way (configuration). Such a term is the product of wave functions Φ describing the motion of the particles within each group, multiplied by a function F which depends on the positions, $\mathbf{X}$, and spin variables, m_S, of the different groups (the word spin referring here to the total internal

[1] Cf. preceding paper, where Appendix I gives an example which illustrates the following considerations. For a preliminary account of the present work, cf. Phys. Rev. **51**, 683 (1937).

[2a] In this paper, neutrons and protons are treated as different particles. Nothing essential is changed, however, if one uses the formalism of the isotopic spin variable and treats neutrons and protons as different states of one type of particle.

angular momentum of a group). The various unknown functions F^i belong to different configurations—thus, for Li^6, F^1 might represent the relative motion of a normal alpha-particle and a normal deuteron; F^2 might similarly represent excited Li^5 plus neutron, etc. The properly antisymmetrized wave function for the whole system has the form [2b]

$$\Psi(12\cdots\mathbf{N})=(k_\mathrm{I}^1!\cdots l_\mathrm{I}^1!\cdots m!n!)^{-\frac{1}{2}}$$
$$\times\sum_{\text{perm}}(\pm1)\sum_{m^1}F^1(\mathbf{X}_\mathrm{I}^1, m_\mathrm{I}^1; \mathbf{X}_\mathrm{II}^1, m_\mathrm{II}^1; \cdots).$$
$$\Phi_{\mathrm{I}^1, m_\mathrm{I}}(1, 2, \cdots\mathbf{k}_\mathrm{I}^1; \mathbf{m}+1, \mathbf{m}+2, \cdots\mathbf{m}+\mathbf{l}_\mathrm{I}^1)$$
$$\times\Phi_{\mathrm{II}^1, m_\mathrm{II}}(\mathbf{k}_\mathrm{I}^1+1, \cdots; \mathbf{m}+\mathbf{l}_\mathrm{I}^1+1, \cdots)\cdots$$
$$+(k_\mathrm{I}^2!\cdots l_\mathrm{I}^2!\cdots m!n!)^{-\frac{1}{2}}\sum_{\text{perm}}(\pm1)$$
$$\sum_{m^2}F^2(\mathbf{X}_\mathrm{I}^2, m_\mathrm{I}^2; \cdots)\Phi^2{}_{\mathrm{I}, m_\mathrm{I}}(1, 2, \cdots\mathbf{k}_\mathrm{I}^2; \cdots)\cdots$$
$$+\text{terms in } F^3, F^4, \cdots F^c. \quad (1)$$

The symbol $\sum_{\text{perm}}(\pm1)$ indicates a summation running over all $m!$ permutations of the protons and $n!$ permutations of the neutrons, with a change in sign for odd permutations; the function Ψ as written is not normalized but the numerical factors simplify the normalization.[3] The $\mathbf{X}$'s are of the form

$$\mathbf{X}_\mathrm{I}^1=(\mathbf{x}_1+\mathbf{x}_2+\cdots+\mathbf{x}_{k_\mathrm{I}}+\mathbf{y}_1+\mathbf{y}_2+\cdots+\mathbf{y}_{l_\mathrm{I}})/(k_\mathrm{I}+l_\mathrm{I}).$$

The subscript m_II on $\Phi_\mathrm{II}{}^1$ singles out that particular wave function for group II^1 (possessing spin S_II') which represents the z component of its angular momentum as having the value m_II; the sum over the m's is to give a partial wave function Ψ^1 corresponding to definite values of the angular momentum of the whole system and its projection along the z axis (the same, of course, for all Ψ^i's). Group I of configuration 1 is not in general the same as group I of configuration 2, etc. The Φ's, among which there are, for example, alpha-particle wave functions, are antisymmetric in neutrons and in protons.[4] Each Φ is normalized, and the Φ's representing different states of the same group are orthogonal; thus,

$$\sum_{\sigma_1,\,\sigma_2,\,\tau_8,\,\tau_9}\int\Phi_\alpha{}^*(1, 2, 8, 9)\times\Phi_\beta(1, 2, 8, 9)d\tau_{1,\,2,\,8,\,9}=\delta_{\alpha\beta}, \quad (2)$$

where by $\int\cdots d\tau$ we mean here the integral with respect to any three independent variables, keeping the center of gravity fixed:

$$d\tau=d(\mathbf{x}_1, \mathbf{x}_2, \mathbf{y}_8, \mathbf{y}_9)/d\mathbf{X}_{1289}.$$

The Φ's may depend explicitly on the $\mathbf{X}$'s ("polarization").

Outline of procedure

The problem centers on the calculation of the functions F^i, which we determine uniquely by the condition that they shall give the best possible wave function of the form (1) in the sense of the variation principle:

$$\delta E=0 \quad \left(E=\int\Psi^*H\Psi d\tau\Big/\int\Psi^*\Psi d\tau\right). \quad (3)$$

Our program is as follows: We express (Eq. (13)) $\int\Psi^*H\Psi d\tau$ and $\int\Psi^*\Psi d\tau$ in terms of the F^i and certain quantities representing the Hamiltonians of the individual configurations and the interactions responsible for the resonance of the nucleus between different configurations; then (specializing to the case of only two groups in each configuration) we vary E in (2) separately with respect to each of the c functions F^i, and obtain from the variation principle c simultaneous integro-differential equations ((17) and (25)) on the F^i; through the use of a generalized Green's function we transform these equations to integral equations (Eq. (30)) of a well-known type; the condition that the Fredholm determinant of this set of equations shall vanish is found to determine energy levels, and also, phase shifts and transmutation probabilities, without calculation of the F^i themselves; finally, we go into some details of the numerical calculation of the Fredholm determinants encountered.

[2b] The following is simplified on first reading by supposing that the groups have no spin, as is the case for α-particles.

[3] The terms of the first sum are identical in sets of $u^1=k_\mathrm{I}^1!\cdots l_\mathrm{I}^1!\cdots$ at a time because of the antisymmetry of the Φ's; there are $v^1=m!n!/k_\mathrm{I}^1!\cdots l_\mathrm{I}^1!\cdots$ different distributions of the neutrons and protons into the groupings I^1, II^1, etc.; if the different distributions were orthogonal, the normalizing factor for the first sum would be exactly $(v^1)^{-\frac{1}{2}}(u^1)^{-1}$.

[4] When a group consists only of a single particle, Φ is simply a δ function.

Integration over Internal Degrees of Freedom

Normalization integral

We have to express the integral $\int \Psi^* \Psi d\tau$ and similar energy integrals in terms of the F's. The contribution coming from $\Psi^{i*}\Psi^j$ reduces to the integral of

$$(k_{\mathrm{I}}{}^i! k_{\mathrm{II}}{}^i! \cdots l_{\mathrm{I}}{}^i! \cdots k_{\mathrm{I}}{}^j! k_{\mathrm{II}}{}^j! \cdots l_{\mathrm{I}}{}^j! \cdots)^{-\frac{1}{2}}$$
$$\times \sum_{m^j} F^i(\mathbf{X}_{\mathrm{I}}{}^i, m_{\mathrm{I}}{}^i; \mathbf{X}_{\mathrm{II}}{}^i, \cdots)$$
$$\Phi^i{}_{\mathrm{I}m_{\mathrm{I}}}{}^i(\mathbf{1}, \mathbf{2}, \cdots \mathbf{k}_{\mathrm{I}}{}^i; \mathbf{m}+\mathbf{1}, \cdots \mathbf{m}+\mathbf{l}_{\mathrm{I}}{}^i)$$
$$\times \Phi^i{}_{\mathrm{II}m_{\mathrm{II}}}{}^i(\mathbf{k}_{\mathrm{I}}{}^i+\mathbf{1}, \cdots \mathbf{k}_{\mathrm{I}}{}^i+\mathbf{k}_{\mathrm{II}}{}^i; \mathbf{m}+\mathbf{l}_{\mathrm{I}}{}^i+\mathbf{1}, \cdots) \cdots$$
$$\sum_{\text{perm}} (\pm 1) \sum_{m^j} F^j(\mathbf{X}_{\mathrm{I}}{}^j, \cdots) \Phi^j{}_{\mathrm{I}m_{\mathrm{I}}}{}^j(\mathbf{1}, \cdots \mathbf{k}_{\mathrm{I}}{}^j; \cdots) \cdots \quad (4)$$

owing to the complete antisymmetry of the individual configuration wave functions Ψ^i. Imagine $a_{\mathrm{I\,I}}$ protons to be withdrawn from the $k_{\mathrm{I}}{}^i$ in group I of configuration i and placed in the group I of configuration j, $a_{\mathrm{I\,II}}$ to be removed from the same source to II^j, and so on; similarly we transfer $b_{\mathrm{I\,I}}$ neutrons from I^i to I^j, etc. Then the set of numbers a_{rs}, b_{tu} describes a certain shifting of particles which may call the *linkage* $\{ab\}$ from configuration i to j. Clearly

$$\sum_s a_{rs} = k_r{}^i; \quad \sum_r a_{rs} = k_s{}^j;$$
$$\sum_u b_{tu} = l_t{}^i; \quad \sum_t b_{tu} = l_u{}^j.$$

(In the example following Eq. (26), for $i=1$, $j=2$, we have $a_{\mathrm{I\,I}}=a_{\mathrm{II\,I}}=b_{\mathrm{I\,I}}=b_{\mathrm{I\,II}}=0$, $a_{\mathrm{I\,II}}=a_{\mathrm{II\,II}}=b_{\mathrm{II\,I}}=b_{\mathrm{II\,II}}=1$).

All $a_{\mathrm{I\,I}}!\, a_{\mathrm{I\,II}}! \cdots b_{\mathrm{I\,I}}!\, b_{\mathrm{I\,II}}! \cdots$ terms in $\sum_{\text{perm}}$ which belong to the same linkage are identical; terms belonging to a different set of values of the a's and b's are different from these [unless there are two or more group wave functions among either the $\Phi^i{}_{\mathrm{I}m_{\mathrm{I}}}{}^i$, $\Phi^i{}_{\mathrm{II},m_{\mathrm{II}}}{}^i$, $\cdots$ or the $\Phi^j{}_{\mathrm{I}m_{\mathrm{I}}}{}^j$, $\Phi^j{}_{\mathrm{II}m_{\mathrm{II}}}{}^j$, $\cdots$, which are actually the same. When this situation occurs, the same linkage will be said to include those sets of values of the a_{rs}, b_{tu} which arise by permuting the subscripts of identical states of individual groups in configuration i and by changing about the labels I, II, $\cdots$ of those states $\Phi^j{}_{\mathrm{I}m_{\mathrm{I}}}{}^j$, $\Phi^j{}_{\mathrm{II}m_{\mathrm{II}}}{}^j$, $\cdots$ which are really the same. If λ^i and λ^j are, respectively, the numbers of such permutations, which do not actually have any effect on the distribution of particles into groups, then we introduce $1/\lambda^i$ and $1/\lambda^j$ as additional normalizing factors for the parts Ψ^i and Ψ^j of Ψ Eq. (1). Then the procedure goes through exactly as below, where we explicitly assume that all groups are different, so as to avoid unessential complications]. By defining numerical factors

$$g_{\{ab\}} = \frac{a_{\mathrm{I\,I}}!\, a_{\mathrm{I\,II}}! \cdots b_{\mathrm{I\,I}}! \cdots}{[k_{\mathrm{I}}{}^i! \cdots l_{\mathrm{I}}{}^i! \cdots k_{\mathrm{I}}{}^j! \cdots]^{\frac{1}{2}}},$$

we conveniently combine all terms belonging to the same linkage:

$$\int \Psi^* \Psi d\tau = \sum_{i,j} \sum_{m^i m^j} \sum_{\{ab\}_{ij}} g_{\{ab\}_{ij}}$$
$$\times \int F^{i*}(\mathbf{X}_{\mathrm{I}}{}^i, m_{\mathrm{I}}{}^i, \cdots) \Phi^i{}_{\mathrm{I}m_{\mathrm{I}}}{}^i(\mathbf{1}, \mathbf{2}, \cdots) \cdots$$
$$\times F^j(\mathbf{X}_{\mathrm{I}}{}^j, \cdots) \Phi^j{}_{\mathrm{I}m_{\mathrm{I}}}{}^j(\cdots) \cdots d\tau. \quad (5)$$

When in (5) $\{ab\}_{ij}$ is the identical linkage ($a_{\mathrm{I\,I}}=k_{\mathrm{I}}$, $a_{\mathrm{I\,II}}=0$, etc.), then the normalization and orthogonality of the Φ's reduces the corresponding terms in the sum to

$$\delta_{ij} \sum_{m^i} \int F^{i*}(\mathbf{X}_{\mathrm{I}}{}^i, m_{\mathrm{I}}{}^i, \cdots) F^i(\mathbf{X}_{\mathrm{I}}{}^i, m_{\mathrm{I}}{}^i, \cdots)$$
$$\times d(\mathbf{X}_{\mathrm{I}}{}^i, \cdots)/d\mathbf{A}, \quad (6)$$

where $\mathbf{A}$ represents the (vector) coordinate of the center of gravity and we have used the identity

$$\frac{d(\mathbf{1}, \cdots \mathbf{k}_{\mathrm{I}}{}^i; \mathbf{m}, \cdots)}{d\mathbf{X}_{\mathrm{I}}{}^i} \frac{d(\mathbf{k}_{\mathrm{I}}{}^i+\mathbf{1}, \cdots)}{d\mathbf{X}_{\mathrm{II}}{}^i} \cdots$$
$$\times \frac{d(\mathbf{X}_{\mathrm{I}}{}^i, \mathbf{X}_{\mathrm{II}}{}^i, \cdots)}{d\mathbf{A}} = \frac{d(\mathbf{1}, \cdots, \mathbf{N})}{d\mathbf{A}}.$$

(In general, $\dfrac{d\{f_1(xyz), f_2(xyz), f_3(xyz)\}}{dx}$ is defined to be $\dfrac{\partial(f_1, f_2, f_3)}{\partial(x, y, z)} dydz$.)

For all other linkages in the sum (5), the $\mathbf{X}^i$'s, regarded as functions of the neutron and proton coordinates, will not all be the same as the $\mathbf{X}^j$'s. As it is complicated to carry out the treatment

from this stage on in detail in the general case, we specialize now to the case that there are only two groups in each of the c configurations. Then when $\{ab\}$ is not the identical linkage, clearly the vectors $\mathbf{X}_{\mathrm{II}}{}^i-\mathbf{X}_{\mathrm{I}}{}^i=\mathbf{X}_{\{ab\}}$ and $\mathbf{X}_{\mathrm{II}}{}^j-\mathbf{X}_{\mathrm{I}}{}^j=\boldsymbol{\xi}_{\{ab\}}$ are independent of each other. We can therefore express the coordinates $\mathbf{x}_1, \cdots \mathbf{x}_m, \mathbf{y}_1, \cdots \mathbf{y}_n$ in terms of $\mathbf{A}$, $\mathbf{X}_{\{ab\}}$, $\boldsymbol{\xi}_{\{ab\}}$, and $N-3$ independent (vector) variables $\mathbf{u}_4, \cdots, \mathbf{u}_N$ by a linear substitution. The differential element $d\tau$ becomes

$$\frac{\partial(1, \cdots \mathbf{N})}{\partial(\mathbf{A}, \mathbf{X}, \boldsymbol{\xi}, \mathbf{u}_4, \cdots \mathbf{u}_N)} d\mathbf{X} d\boldsymbol{\xi} d\mathbf{u}_4 \cdots d\mathbf{u}_N.$$

Since the $\mathbf{u}$'s do not enter in the F's, and moreover we take the F's to be independent[5] of $\mathbf{A}$, it follows that the integral in which we are interested reduces after integration over the $\mathbf{u}$'s to the form

$$\sum_{m^i,\, m^j} \sum_{\{ab\}_{ij}} \int\int F^{i*}(\mathbf{X}_{\{ab\}_{ij}};\, m_{\mathrm{I}}{}^i,\, m_{\mathrm{II}}{}^i) \times \mathbf{I}_{\{ab\}_{ij}}(\mathbf{X}_{\{ab\}},\, m_{\mathrm{I}}{}^i,\, m_{\mathrm{II}}{}^i;\, \boldsymbol{\xi}_{\{ab\}},\, m_{\mathrm{I}}{}^j,\, m_{\mathrm{II}}{}^j) \times F^j(\boldsymbol{\xi}_{\{ab\}};\, m_{\mathrm{I}}{}^j,\, m_{\mathrm{II}}{}^j) d\mathbf{X}_{\{ab\}} d\boldsymbol{\xi}_{\{ab\}}. \quad (7)$$

We regard the functions $F^i(\mathbf{X},\, m_{\mathrm{I}},\, m_{\mathrm{II}})$ which are obtained when the two m's run over their allowed values ($m_{\mathrm{I}}{}^i=-S_{\mathrm{I}}{}^i, \cdots, S_{\mathrm{I}}{}^i-1, S_{\mathrm{I}}{}^i$; etc.) as components of a single spin vector $\mathbf{F}_i(\mathbf{X})$, and similarly consider the quantities I in Eq. (7) as components of a spin matrix $\mathbf{I}_{\{ab\}_{ij}}(\mathbf{X}, \boldsymbol{\xi})$. The $\mathbf{X}$'s and $\boldsymbol{\xi}$'s in the sum of integrals in Eq. (7) are dummy variables in the sense that they drop out of the integrated answer. Consequently, in spite of their different physical origin, we sum the spin matrices $\mathbf{I}_{\{ab\}_{ij}}$ over all the different linkages joining the given configurations i and j (except the identical linkage), and denote the result as $\mathbf{I}_{ij}(\mathbf{X}, \boldsymbol{\xi})$ ("overlapping integral"). On using a dot to indicate the inner product of spin vectors, we have finally

$$\int \Psi^* \Psi d\tau = \sum_{i=1}^{c} \int \mathbf{F}_i{}^*(\mathbf{X}) \cdot \mathbf{F}_i(\mathbf{X}) d\mathbf{X} + \sum_{i,\, j}^{c} \int\int \mathbf{F}_i{}^*(\mathbf{X}) \cdot \mathbf{I}_{ij}(\mathbf{X}, \boldsymbol{\xi}) \cdot \mathbf{F}_j(\boldsymbol{\xi}) d\mathbf{X} d\boldsymbol{\xi}, \quad (8)$$

[5] It being most convenient to calculate cross sections in the frame of reference in which the center of gravity is at rest: $\mathbf{P}=\mathbf{0}$ in the factor $\exp(i\mathbf{PA}/\hbar)$ of F.

where the I's are in principle known functions of $\mathbf{X}$ and $\boldsymbol{\xi}$, the form of the dependence being determined by the nature of the group wave functions Φ.

Kinetic and potential energy integrals

The calculation of the kinetic energy follows the preceding division into the cases of identical and nonidentical linkages. In the first case we express the k_{I} $\mathbf{x}$'s and l_{I} $\mathbf{y}$'s of the particles of the first group in terms of $\mathbf{A}$, $\mathbf{X}$ and additional variables $\mathbf{v}_2, \mathbf{v}_3, \cdots, \mathbf{v}_{k_{\mathrm{I}}+l_{\mathrm{I}}}$ by a linear orthogonal substitution, and similarly put in the coordinates of the particles of the second group as functions of $\mathbf{A}$, $\mathbf{X}$, $\mathbf{w}_2, \mathbf{w}_3, \cdots, \mathbf{w}_{k_{\mathrm{II}}+l_{\mathrm{II}}}$. Then

$$\frac{\partial}{\partial \mathbf{x}_1} = \frac{1}{N}\frac{\partial}{\partial \mathbf{A}} - \frac{1}{k_{\mathrm{I}}+l_{\mathrm{I}}}\frac{\partial}{\partial \mathbf{X}} + \frac{\partial \mathbf{v}_2}{\partial \mathbf{x}_1}\frac{\partial}{\partial \mathbf{v}_2} + \cdots,$$

and the kinetic energy operator becomes

$$T=(\hbar^2/2M)\{N^{-1}\boldsymbol{\nabla}_A \cdot \boldsymbol{\nabla}_A + [(k_{\mathrm{I}}+l_{\mathrm{I}})^{-1}+(k_{\mathrm{II}}+l_{\mathrm{II}})^{-1}]\boldsymbol{\nabla}_X \cdot \boldsymbol{\nabla}_X + \sum_\alpha c_\alpha \boldsymbol{\nabla}_{\mathbf{v}_\alpha} \cdot \boldsymbol{\nabla}_{\mathbf{v}_\alpha} + \sum_\alpha d_\alpha \boldsymbol{\nabla}_{\mathbf{w}_\alpha} \cdot \boldsymbol{\nabla}_{\mathbf{w}_\alpha}\}, \quad (9)$$

where the c_α and d_α are numbers depending on the choice of the $\mathbf{v}$'s and $\mathbf{w}$'s and the first and second gradients in each pair act on $\mathbf{F}_i{}^*(\mathbf{X})\Phi_{\mathrm{I}}{}^{i*}\Phi_{\mathrm{II}}{}^{i*}$ and $\mathbf{F}_j(\mathbf{X})\Phi_{\mathrm{I}}{}^j\Phi_{\mathrm{II}}{}^j$, respectively. In terms of the reduced mass $\mu_i=\mu_j$ of the two groups, the kinetic energy integral for the identical linkage reduces to an expression of the form

$$\delta_{ij}(\hbar^2/2\mu_i)\int \boldsymbol{\nabla}_X \mathbf{F}_i{}^*(\mathbf{X}) \cdot \boldsymbol{\nabla}_X \mathbf{F}_i(\mathbf{X}) d\mathbf{X} + \int \mathbf{F}_i{}^*(\mathbf{X}) \cdot \mathbf{T}_{ij}(\mathbf{X})\, \mathbf{F}_j(\mathbf{X}) d\mathbf{X}, \quad (10)$$

provided either that we do not allow the Φ's to depend on $\mathbf{X}$ (no explicit polarization effects) or that we do not have in Ψ any configurations differing only by the internal state of excitation of the individual groups. [In the latter case, where the Φ's may involve $\mathbf{X}$ as well as the $\mathbf{u}$'s and $\mathbf{v}$'s, we arrange that no terms occur in (10) which arise from derivatives of the type $(\boldsymbol{\nabla}_X \mathbf{F}^*) \cdot \int \Phi_{\mathrm{I}}{}^{i*}(\boldsymbol{\nabla}_X \Phi_{\mathrm{I}}{}^i) d\mathbf{v}\mathbf{F}$, by suitably choosing the arbitrary multiplicative functions exp (if $(\mathbf{X})$) left free by the normalization and orthogonality conditions on the Φ's. There will however be

terms typified by $\nabla_X\Phi_{\rm I}{}^{i*}\cdot\nabla_X\Phi_{\rm I}{}^j$, which are included in $\mathbf{T}_{ij}(\mathbf{X})$ along with the contributions of the proper internal kinetic energy operator $(\hbar^2/2M)\sum_{\alpha c}\nabla_{v_\alpha}\cdot\nabla_{v_\alpha}$ of group I.] It is quite natural that there should be this exclusive relation between treatment by excited states and by explicit polarization of the groups, for the two are to a large extent equivalent methods of describing the same phenomenon.

Kinetic energy terms belonging to nonidentical linkages are reducible to expressions containing the F's alone by use of the variables $\mathbf{A}$, $\mathbf{X}_{[ab]}$, $\boldsymbol{\xi}_{[ab]}$, $\mathbf{u}_4, \cdots \mathbf{u}_N$ introduced above. The transformation is not in general orthogonal and consequently the kinetic energy operator (center of gravity at rest) becomes the linear combination of operators of the form

$$\nabla_X\cdot\nabla_X,\quad \nabla_X\cdot\nabla_\xi,\quad \nabla_X\cdot\nabla_{u_\alpha},\quad \nabla_{u_\alpha}\cdot\nabla_{u_\beta}.$$

The first gradient in each pair acts on $\mathbf{F}_i{}^*(\mathbf{X})\Phi_{\rm I}{}^{i*}\Phi_{\rm II}{}^{i*}$, the second on $\mathbf{F}_j(\xi)\Phi_{\rm I}{}^j\Phi_{\rm II}{}^j$. From $\nabla_X\cdot\nabla_X$ originate the terms

$$[\nabla_X\mathbf{F}_i{}^*(\mathbf{X})]\Phi_{\rm I}{}^i\Phi_{\rm II}{}^i\mathbf{F}_j(\xi)[\nabla_X\Phi_{\rm I}{}^j\Phi_{\rm II}{}^j]$$

and

$$\mathbf{F}_i(\mathbf{X})[\nabla_X\Phi_{\rm I}{}^i\Phi_{\rm II}{}^i]\mathbf{F}_j(\xi)[\nabla_X\Phi_{\rm I}{}^j\Phi_{\rm II}{}^j].$$

By partial integration of the first term with respect to $\mathbf{X}$, and use of the boundary condition[6] that $\mathbf{F}_i(\mathbf{X})$ must vanish at infinity, we transform the first term to one where $\mathbf{F}_i$ and $\mathbf{F}_j$ appear undifferentiated. Continuing in this way with all the operators above, and then introducing new variables $\mathbf{X}$, ξ, $\mathbf{u}$ to treat the next linkage, etc., we obtain finally the kinetic energy integral for all nonidentical linkages in the form

$$\sum_{i,j}\int\mathbf{F}_i{}^*(\mathbf{X})\cdot\mathbf{T}_{ij}(\mathbf{X},\xi)\cdot\mathbf{F}_j(\xi)d\mathbf{X}d\xi. \quad (11)$$

The remaining terms in the integral $\int\Psi^*H\Psi d\tau$ come from the potential energy. If the forces between the elementary particles were ordinary interactions, the above analysis of the linkages would be valid, but the presence of exchange potentials will change some of the identical linkages to nonidentical linkages, and *vice versa*. Nevertheless, for each term there will be a suitable transformation of variables, either of the type $\mathbf{A}$, $\mathbf{X}$, $\mathbf{v}$, $\mathbf{w}$ or of the type $\mathbf{A}$, $\mathbf{X}$, ξ, $\mathbf{u}$, which will finally reduce the total potential energy to the form

$$\sum_{i,j}\int\mathbf{F}_i{}^*(\mathbf{X})\cdot\mathbf{U}_{ij}(\mathbf{X})\cdot\mathbf{F}_j(\mathbf{X})d\mathbf{X}$$
$$+\sum_{i,j}\int\int\mathbf{F}_i{}^*(\mathbf{X})\cdot\mathbf{U}_{ij}(\mathbf{X},\xi)\cdot\mathbf{F}_j(\xi)d\mathbf{X}d\xi, \quad (12)$$

regardless of the type of the forces.[7]

For large values of $\mathbf{X}$ and ξ, it follows from the finite extension of the individual group wave functions Φ that the $\mathbf{U}_{ij}(\mathbf{X},\xi)$ and $\mathbf{T}_{ij}(\mathbf{X},\xi)$ tend to zero. At the same time, owing to the normalization and orthogonality of the Φ's, $\mathbf{U}_{ij}(\mathbf{X})+\mathbf{T}_{ij}(\mathbf{X})$ approaches δ_{ij} times E_i, the energy attributable to the internal binding of the separated groups of configuration i. We therefore write $\mathbf{U}_{ij}(\mathbf{X})+\mathbf{T}_{ij}(\mathbf{X})=E_i\boldsymbol{\delta}_{ij}+V_{ij}(\mathbf{X})$ and also combine the interchange integrals:

$$\mathbf{U}_{ij}(\mathbf{X},\xi)+\mathbf{T}_{ij}(\mathbf{X},\xi)=\mathbf{J}_{ij}(\mathbf{X},\xi).$$

Summarizing the above considerations, we find that in the approximation given by the method of resonating group structure, the energy of the compound system is

$$E=N/D,$$

where

$$N=\sum_i(\hbar^2/2\mu_i)\int\nabla_X\mathbf{F}_i{}^*(\mathbf{X})\cdot\nabla_X\mathbf{F}_i(\mathbf{X})d\mathbf{X}$$
$$+\sum_iE_i\int\mathbf{F}_i{}^*(\mathbf{X})\cdot\mathbf{F}_i(\mathbf{X})d\mathbf{X}$$
$$+\sum_{i,j}\int\mathbf{F}_i{}^*(\mathbf{X})\cdot\mathbf{V}_{ij}(\mathbf{X})\cdot\mathbf{F}_j(\mathbf{X})d\mathbf{X}$$
$$+\sum_{i,j}\int\int\mathbf{F}_i{}^*(\mathbf{X})\cdot\mathbf{J}_{ij}(\mathbf{X},\xi)\cdot\mathbf{F}_j(\xi)d\mathbf{X}d\xi,$$

and

$$D=\sum_i\int\mathbf{F}_i{}^*(\mathbf{X})\cdot\mathbf{F}_i(\mathbf{X})d\mathbf{X}+\sum_{i,j}\int\int\mathbf{F}_i{}^*(\mathbf{X})$$
$$\cdot\mathbf{I}_{ij}(\mathbf{X},\xi)\cdot\mathbf{F}_j(\xi)d\mathbf{X}d\xi. \quad (13)$$

[6] Only in the derivation do we make this restriction, which would, for the continuous spectrum, require us to deal always with a finite if small energy spread in the wave-function (which is of course physically correct), but in the actual calculations with the integro-differential equation below it is permissible to deal in the usual way with sharp energy values and waves which extend to infinity.

[7] They may be many-body interactions, for example.

The Wave Equation

Application of variation principle

It is known[8] that the Schroedinger wave equation may be derived from the variation principle $\delta E=0$, and that any improvement in an approximate wave function lowers the corresponding value of the energy.

We therefore determine the unknown functions $\mathbf{F}$ by the condition that they shall give the best possible total wave function Ψ of the form (1) in the sense of the variation principle

$$\delta E=\delta(N/D)=0. \tag{14}$$

The variation in N caused by a change $\delta\mathbf{F}_i\delta(\mathbf{X}-\mathbf{X}_0)$ in the value of $\mathbf{F}_i(\mathbf{X})$ at the point $\mathbf{X}_0$ is found by partial integration to be[9] $2\delta\mathbf{F}_i$ times

$$-(\hbar^2/2\mu_i)\nabla_X{}^2\mathbf{F}_i(\mathbf{X})+E_i\mathbf{F}_i(\mathbf{X})+\sum_j\mathbf{V}_{ij}(\mathbf{X})\cdot\mathbf{F}_j(\mathbf{X})$$
$$+\sum_j\int\mathbf{J}_{ij}(\mathbf{X},\xi)\cdot\mathbf{F}_j(\xi)d\xi \tag{15}$$

evaluated at $\mathbf{X}=\mathbf{X}_0$. Similarly, the change in D is $2\delta\mathbf{F}_i$ times

$$\mathbf{F}_i(\mathbf{X})+\sum_j\int\mathbf{I}_{ij}(\mathbf{X},\xi)\cdot\mathbf{F}_j(\xi)d\xi. \tag{16}$$

E is stationary with respect to all variations of the $\mathbf{F}$'s only if the ratio $\delta N/\delta D$ is the same as $N/D=E$ for all values of $\mathbf{X}_0$ and all values of i, whence we have the system of simultaneous linear integro-differential equations

$$[(\hbar^2/2\mu_i)\nabla_X{}^2+E-E_i]\mathbf{F}_i(\mathbf{X})$$
$$=\sum_j\Big[\mathbf{V}_{ij}(\mathbf{X})\cdot\mathbf{F}_j(\mathbf{X})+\int\{\mathbf{J}_{ij}(\mathbf{X},\xi)-E\mathbf{I}_{ij}(\mathbf{X},\xi)\}$$
$$\cdot\mathbf{F}_j(\xi)d\xi\Big]. \tag{17}$$

If the right member of (17) were zero, the solution of our equations would give simply the free relative motion of the different groups of a given configuration; the terms with $j=i$ on the right determine the interaction between these groups, and the nondiagonal terms take into account the resonance between different configurations—in particular, the possibility of transmutations. From the fact that the energy of the system is always real we have[10]

$$\mathbf{V}_{ij}(\mathbf{X})=\mathbf{V}_{ji}{}^*(\mathbf{X}),\quad \mathbf{J}_{ij}(\mathbf{X},\xi)=\mathbf{J}_{ji}{}^*(\xi,\mathbf{X}),$$
$$\mathbf{I}_{ij}(\mathbf{X},\xi)=\mathbf{I}_{ji}{}^*(\xi,\mathbf{X}). \tag{18}$$

Angular dependence

Owing to the intimate interaction which occurs in the compound nucleus, neither the internal angular momenta of the groups nor their mutual angular momentum L will be constant, but only the total angular momentum J and its projection m_J along a fixed space axis. We build up an eigenstate for a given J and m_J in two steps: S_I, $S_\mathrm{II}\to S$; S, $L\to J$. To form a wave function corresponding to a particular value of the total internal group angular momentum, S, we have to take a definite[11] linear combination of the sets of states belonging to S_I and S_II:

$$\Phi^i{}_{S,m_S}=\sum_{m_\mathrm{I}(m_\mathrm{II})}\{S^i,S_\mathrm{I}{}^i,S_\mathrm{II}{}^i;m_S,m_\mathrm{I},m_\mathrm{II}\}$$
$$\times\Phi^i{}_{\mathrm{I},m_\mathrm{I}}\Phi^i{}_{\mathrm{II},m_\mathrm{II}}. \tag{19}$$

The coefficients $\{\ \}$ are pure numbers; they vanish unless $m_\mathrm{II}=m_S-m_\mathrm{I}$, for which reason m_II is put in parenthesis in the sum.

We combine the Φ's for a given S with functions belonging to a definite state of relative angular momentum L (and projection m) of the two groups and express the separation vector X in polar coordinates r, θ, φ. The function

$$(1/r)f_J(i,L,S,r)\sum_{m(m_S)}\{JLS;m_Jmm_S\}$$
$$\times Y_L{}^{(m)}(\theta,\varphi)\Phi^i{}_{Sm_S} \tag{20}$$

belongs to a given value of the total angular momentum J and its projection m_J, and $\mathbf{F}_i(\mathbf{X})\Phi_\mathrm{I}{}^i\Phi_\mathrm{II}{}^i$ will be made up of the sum of such functions over all values of L and S which are

[8] E. Schroedinger, Ann. d. Physik **79**, 362 (1926); cf. also R. Courant and D. Hilbert, *Methoden der Mathematischen Physik I*, second edition (Berlin, 1931), p. 159.

[9] We carry out the derivation as if the $\mathbf{F}$'s, $\mathbf{V}$'s, $\mathbf{J}$'s, and $\mathbf{I}$'s were all real; the result is however true in general. Cf. W. Heisenberg, *The Physical Principles of the Quantum Theory* (Chicago, 1930), p. 163.

[10] The star of a spin matrix indicates here its conjugate transposed.

[11] Cf. E. Wigner, *Gruppentheorie*, Eqs. (18a) and (27). (Braunschweig, 1931), p. 206. It is supposed that the normalizing constants in the Φ's are chosen with the proper sign. Three choices of sign for the related spherical harmonics $Y_L{}^{(m)}$ are given in the literature; for that consistent with (19), and for tables of the $\{\ \}$, cf. Condon and Shortley, *The Theory of Atomic Spectra* (Cambridge, 1935), p. 52, p. 75.

consistent with $S_{\rm I}$, $S_{\rm II}$, and J according to the vector rule of addition of angular momenta. Consequently, for the given J and m_J, the $m_{\rm I}$, $m_{\rm II}$ component of the spin vector $\mathbf{F}_i$ is

$$F^i(\mathbf{X}, m_{\rm I}, m_{\rm II}) = \sum_{\substack{L,\ S \\ (m),\ (m_S)}} (1/r) f_J(iLSr) \times \{JLS; m_J m m_S\} Y_L^{(m)}(\theta, \varphi) \times \{SS_{\rm I}S_{\rm II}; m_S, m_{\rm I}, m_{\rm II}\} \quad (21)$$

with suitably chosen f_J.

Clearly the left member of the ith integro-differential Eq. (17) will have the same form as (21) except that the $f_J(iLSr)$ will appear operated on by

$$(1/r)[(\hbar^2/2\mu_i)((d^2/dr^2) - L(L+1)/r^2) + E - E_i]. \quad (22)$$

We now multiply this number by $rY_L^{(m)*}(\theta, \varphi) \times \sin\theta d\theta d\varphi \{SS_{\rm I}S_{\rm II}; m_S m_{\rm I} m_{\rm II}\}$, integrate over θ and φ, sum over $m_{\rm I}$ and $m_{\rm II}$, make use of the orthogonality and normalization of the spherical harmonics and the relation[12]

$$\sum_{m_{\rm I}(m_{\rm II})} \{SS_{\rm I}S_{\rm II}; m_S m_{\rm I} m_{\rm II}\} \times \{S'S_{\rm I}S_{\rm II}; m_S m_{\rm I} m_{\rm II}\} = \delta_{SS'}, \quad (23)$$

and end up with a single one of the $f_J(iLSr)$ on the left-hand side of the integro-differential equation. The right-hand member of this equation will, in general, contain radial functions $f_J(jL'S'r)$ from all configurations and from values of L' and S' not necessarily the same as L and S. We can say at once from the invariance of the nuclear wave equation with respect to space rotations: firstly, that J and m_J have the same value on both sides of the equation; and secondly, that the equation for $f_J(iLSr)$ must be independent of m_J—i.e., the right-hand side of the equation must contain as a factor the same expression $\{JLS; m_J m m_S\}$ which appears on the left. (This could of course be proven with more difficulty directly from the expressions for $\mathbf{V}_{ij}$, $\mathbf{J}_{ij}$, $\mathbf{I}_{ij}$). On introducing ρ, σ, τ for polar coordinates of ξ (like the polar coordinates r, θ, φ of $\mathbf{X}$), and defining the Jth components of $\mathbf{V}$, $\mathbf{J}$ (and similarly $\mathbf{I}$) as follows:

$$\{JLS; m_J m m_S\} V_J(iLS; jL'S'; r) = \int \sin\theta d\theta d\varphi \sum_{m_{\rm I}(m_{\rm II})} \sum_{m_{\rm I}'(m_{\rm II}')} Y_L^{(m)*}(\theta, \varphi) \times \{SS_{\rm I}{}^i S_{\rm II}{}^i; m_S m_{\rm I} m_{\rm II}\} \mathbf{V}_{ij}(\mathbf{X}; m_{\rm I} m_{\rm II}; m_{\rm I}' m_{\rm II}') \times \{JL'S'; m_J m' m_S'\} Y_{L'}^{(m')}(\theta, \varphi) \times \{S'S_{\rm I}{}^j S_{\rm II}{}^j; m_S' m_{\rm I}' m_{\rm II}'\};$$

$$\{JLS; m_J m m_S\} \mathbf{J}_J(iLSr; jL'S'\rho) = r\rho \int\int \sin\theta d\theta d\varphi \sin\sigma d\sigma d\tau \sum\sum \cdots \times \mathbf{J}_{ij}(\mathbf{X} m_{\rm I} m_{\rm II}; \xi m_{\rm I}' m_{\rm II}') \cdots, \quad (24)$$

we obtain the radial wave equations of the method of resonating group structure:

$$[(\hbar^2/2\mu_i)(d^2/dr^2 - L(L+1)/r^2) + E - E_i] f_J(iLSr) = \sum_{jL'S'} \int H_J(iLSr; jL'S'\rho) f_J(jL'S'\rho) d\rho = g_J(iLSr), \quad (25)$$

where $g_J(iLSr)$ is an abbreviation for

$$\sum_{jL'S'} \{V_J(iLS; jL'S'; r) f_J(jL'S'r) + \int [J_J - E I_J(iLSr; jL'S'\rho)] f_J(jL'S'\rho) d\rho\}. \quad (26)$$

Integral Equations

Reduction of integro-differential equations

In the radial integro-differential equations (25), we write

$$(2\mu_i/\hbar^2)(E - E_i) = -\kappa_i^2 \quad \text{for } E < E_i \text{ (configuration } i \text{ stable)},$$

$$(2\mu_i/\hbar^2)(E - E_i) = k_i^2 \quad \text{for } E > E_i \text{ (dissociation possible)}. \quad (26)$$

We have the following cases to consider:

(*A*) All $E_i > E$. Completely stable nucleus. Sharp energy values.

(*B*) Only one $E_i < E$. Elastic collisions between groups I^i and II^i; lifetime of compound nucleus determined by probability of a single mode of dissociation.

(*C*) More than one $E_i < E$. Elastic scattering; also transmutation processes $\mathrm{I}^i + \mathrm{II}^i \rightleftarrows \mathrm{I}^j + \mathrm{II}^j$.

As illustration, Table I gives the configurations which may be used to describe the compound nucleus $_2\mathrm{He}^4$:

[12] Wigner, reference 11, Eq. (28), p. 206.

TABLE I. *Configurations of* $_2He^4$.

i	I^i	$S_I{}^i$	II^i	$S_{II}{}^i$	E_i (mMU)
1	H^1	$\frac{1}{2}$	H^3	$\frac{1}{2}$	−9.1
2	n^1	$\frac{1}{2}$	He^3	$\frac{1}{2}$	−8.1
3	H^2	1	H^2	1	−4.8

In case A (stable $_2He^4$) the radial functions f must fall off exponentially for large r for all configurations; in addition, the f's must satisfy the usual boundary condition $f(0)=0$ at the origin. On considering the right hand members of (25) to be known functions[13] of r, we can immediately obtain expressions for the f_i satisfying the proper boundary conditions. We introduce the "regular" and "irregular" solutions of the homogeneous equation

$$[d^2/dr^2-\kappa^2-L(L+1)/r^2]f=0 \qquad (27)$$

as follows:

$$\rho=\kappa r;\quad F_L(\rho)=\rho^{L+1}\left(\frac{1}{\rho}\frac{d}{d\rho}\right)^L(\rho^{-1}\sinh\rho)$$

$$=\{\rho^{L+1}/1\cdot3\cdots(2L+1)\}\{1+\rho^2/2(2L+3)+\cdots\};$$

$$G_L(\rho)=(-1)^L\rho^{L+1}\left(\frac{1}{\rho}\frac{d}{d\rho}\right)^L(\rho^{-1}\exp(-\rho))\sim e^{-\rho};$$

$$\frac{dF_L}{d\rho}G_L-F_L\frac{dG_L}{d\rho}=1; \qquad (28a)$$

and for later use write down also the regular and irregular solutions of the equation obtained by replacing $-\kappa^2$ in (27) by k^2:

$$\rho=kr;\quad F_L(\rho)=(-1)^L\rho^{L+1}\left(\frac{1}{\rho}\frac{d}{d\rho}\right)^L(\rho^{-1}\sin\rho)$$

$$=\{\rho^{L+1}/1\cdot3\cdots(2L+1)\}\cdot\{1-\rho^2/2(2L+3)+\cdots\}$$

$$\sim\sin(\rho-L\pi/2);$$

$$G_L(\rho)=(-1)^L\rho^{L+1}\left(\frac{1}{\rho}\frac{d}{d\rho}\right)^L(\rho^{-1}\cos\rho)\sim$$

$$\sim\cos(\rho-L\pi/2);$$

$$\frac{dF_L}{d\rho}G_L-F_L\frac{dG_L}{d\rho}=1. \qquad (28b)$$

The uniquely determined solution of the inhomogeneous equation is

$$f_J(iLSr)=-(2\mu_i/\hbar^2\kappa_i)\left\{\int_0^r F_L(\kappa_i\sigma)G_L(\kappa_i r)\right.$$

$$\left.+\int_r^\infty F_L(\kappa_i r)G_L(\kappa_i\sigma)\right\}g(iLS\sigma)d\sigma. \qquad (29)$$

As the g's are however given in terms of the f's, we have cross relations which will not in general be consistent with each other—except for those special values of E which represent stable levels of the compound system. We write out (29) as a system of linear integral equations on the f's:

$$f_J(iLSr)+\sum_{jL'S'}\int_0^\infty S_J(iLSr;jL'S'\rho)$$

$$\times f_J(jL'S'\rho)d\rho=0, \qquad (30)$$

where the kernel S_J is given by

$$S_J(iLSr;jL'S'\rho)=(2\mu_i/\hbar^2\kappa_i)$$

$$\times\left\{\int_0^r G_L(\kappa_i r)F_L(\kappa_i\sigma)+\int_r^\infty F_L(\kappa_i r)G_L(\kappa_i\sigma)\right\}$$

$$\times H_J(iLS\sigma;jL'S'\rho)d\sigma, \qquad (31)$$

and is therefore in principle known as soon as the **V**'s, **J**'s, and **I**'s have been evaluated. We know from the theory[14] of integral equations that (30) has a characteristic solution only when the Fredholm determinant of the equation vanishes:

$$D(E)=|\delta_{ij}\delta_{LL'}\delta_{SS'}\delta(r-\rho)$$

$$+S_J(iLSr;jL'S'\rho;E)|=0. \qquad (32)$$

Eq. (32) determines the stable levels of the system. In diagonal expansion, it runs

$$D(E)=1+\sum_{iLS}\int S(iLSr;iLSr)dr+(1/2!)\sum_{iLS}\sum_{jL'S'}\int\int\begin{vmatrix}S(iLSr;iLSr) & S(iLSr;jL'S'\rho)\\ S(jL'S'\rho;iLSr) & S(jL'S'\rho;jL'S'\rho)\end{vmatrix}drd\rho$$

$$+\cdots=0, \qquad (33)$$

[13] Cf. Mott and Massey, *The Theory of Atomic Collisions* (Oxford, 1933), p. 151, for an analogous method of conversion to an integral equation.

[14] Lovitt, *Linear Integral Equations* (New York, 1924), p. 41.

where for brevity the suffix J and the argument E have been omitted from S.

Elastic Scattering

The collision of H^1 and H^3 with energy too small to form n^1+He^3 comes under case B. For every given E, Eqs. (25) will now possess a solution. The wave functions for configurations 2 and 3 must still fall off exponentially for large r, but the $f(1LSr)$, which also satisfy the boundary condition at the origin, behave asymptotically for large r as combinations of $\sin(k_1r)$ and $\cos(k_1r)$.[15]

A proton and triton without spin would be described at large distances by one function $f_J(1J0r)$. If this function is so normalized that that part of it which corresponds to the incoming wave $e^{-i(k_1r-J\pi)}$ has amplitude $-(1/2i)$, then the amplitude of the outgoing wave e^{ik_1r} must have the same absolute value and may be written $(1/2i)e^{2iK_J}$. Here K_J is the so-called "phase shift," which is completely determined (up to $\pm n\pi$) by the collision energy and form of the interaction, and which in turn, along with the other K_J's, determines the differential cross section $\sigma_{11}(\theta)$ for elastic scattering through the well known formula[16]

$$\sigma_{11}(\theta)=(4k_1^2)^{-1} \times\Big|\sum_{L=0}^{\infty}(2L+1)(e^{2iK_L}-1)P_L(\cos\theta)\Big|^2. \quad (34)$$

Effect of spin

The specific dynamic[17] action of nuclear spin splits up an incoming wave

$$-(1/2i)\exp[-i(k_1r-L\pi)],$$

containing two groups in one state JLS of specified spin orientation and given mutual angular momentum, into a number of outgoing waves representing these groups separating with altered spin orientations and changed mutual angular momentum. The particular solution $f^{L,S}$ associated with the given initial conditions is a set of functions, g_J in number, having the asymptotic form:

$$\begin{aligned} f_J{}^{LS}(1LSr)&\sim-(1/2i)\exp[-i(k_1r-L\pi)] \\ &\quad+(1/2i)c_J(LS;LS)\exp[ik_1r], \\ f_J{}^{LS}(1L'S'r)&\sim(1/2i)c_J(L'S';LS)\exp[ik_1r] \\ &\quad(L',S'\neq L,S). \end{aligned} \quad (35)$$

Another particular solution is obtained by letting the groups approach in a different initial state $JL\bar{S}$; altogether there are g_J such independent particular solutions for a given value of J. We therefore need $g_J{}^2$ complex numbers $c_J(L'S';LS)$ to characterize completely the behavior at infinity of the independent solutions associated with a given component H_J of the interaction operator. For these large distances the waves associated with the stable configurations 2, 3, $\cdots$ have fallen to zero, and the total wave function for a state described by the quantum numbers J, m_J, L, S is obtained from

$$\chi_{Jm_J}{}^{LS}(\mathbf{1},\mathbf{2},\cdots,\mathbf{N})=\sum_{L'S'}(1/kr)f_J{}^{LS}(1L'S'r) \sum_{m_{S'}(m')}\{JL'S';m_Jm'm_{S'}\}Y_{L'}{}^{(m')}(\theta,\varphi)\Phi^{1}{}_{S',m_{S'}} \quad (36)$$

by antisymmetrizing according to the procedure discussed earlier. However, in deriving the scattering cross section, as in the next paragraph, we are justified in dealing with the unsymmetrized χ's because: (1), the f_J's are solutions of wave equations in which the H_J's already include all dynamical effects of symmetrization (exchange interactions); and (2), those scattered waves in the total wave function which come from χ's differing by an interchange of particles between the constituent groups cannot interfere with each other at distances large in comparison with the size of the groups.

We consider a state typified by

$$\exp(ik_1z)\Phi^{1}{}_{S,m_S}+\text{scattered waves}. \quad (37)$$

The proper linear combination of the $\chi_{Jm_J}{}^{LS}$ required to give this state is found most easily by comparing the coefficients of $\exp[-i(k_1r$

[15] Provided we assume any coulomb fields to be broken off beyond some suitable distance r. The question of the most convenient procedure in this connection is discussed in more detail below.

[16] Mott and Massey, reference 13, p. 24.

[17] The *statistical* effect of the spin in a problem where two groups are identical (Mott, Proc. Roy. Soc. **A126**, 259 (1930)) is already taken into account in our treatment before the wave equation is reduced to radial form.

$-L\pi)]$ in the asymptotic expansions of the χ's and the advancing plane wave

$$\exp(ik_1z)\sim\sum_L(2L+1)P_L(\cos\theta)(1/2ikr)\times[-e^{-i(k_1r-L\pi)}+e^{ik_1r}]. \quad (38)$$

For the comparison we use Eqs. (19) and (36). We find by application of the orthogonality relation[18]

$$\sum_J\{JLS;m_Jmm_S\}\{JLS;m_Jm'm_S'\}=\delta_{mm'}\delta_{m_Sm_S'} \quad (39)$$

and the equations of definition,

$$Y_L^{(m)}(\theta,\varphi)=\Theta_L^{(m)}(\theta)(2\pi)^{-\frac{1}{2}}e^{im\varphi},$$
$$\Theta_L^{(0)}(\theta)=(L+1/2)^{\frac{1}{2}}P_L(\cos\theta), \quad (40)$$

that the desired coefficient of $\chi_{Jm_J}^{LS}$ is

$$\{JLS;m_S\,0\,m_S\}\delta_{m_Sm_J}[4\pi(2L+1)]^{\frac{1}{2}}. \quad (41)$$

The difference between the resultant linear superposition of solutions and the advancing plane wave is the scattered wave

$$(e^{ik_1r}/2ik_1r)\sum_L[4\pi(2L+1)]^{\frac{1}{2}}\times\{\sum_{JL'S'}\sum_{m_S'(m')}c_J(L'S';LS)\{JLS;m_S\,0\,m_S\}\times\{JL'S';m_Sm'm_S'\}Y_{L'}^{(m')}(\theta,\varphi)\Phi^1{}_{S'm_S'}-Y_L^{(0)}(\theta,\varphi)\Phi^1{}_{Sm_S}\}. \quad (42)$$

We square the absolute value of the coefficient of $(e^{ik_1r}/r)\Phi^1{}_{S',m_S'}$ and thus get the differential cross section for the process: groups in spin state $\Phi^1{}_{S,m_S}$ collide and go off in the direction θ,φ in the spin state $\Phi^1{}_{S',m_S'}$. The observable collision cross section, per unit solid angle, is obtained by averaging this over all $(2S_{\rm I}+1)(2S_{\rm II}+1)$ initial modes of orientation and summing over all possible final values $S'm_S'$:

$$\sigma_{\rm II}(\theta)=[(2S_{\rm I}+1)(2S_{\rm II}+1)4k_1^2]^{-1}\sum_{S,\,m_S}\sum_{S',\,m_S'}\Big|\sum_L\{\sum_{JL'}c_J(L'S';LS)\{JLS;m_S0m_S\}\times\{JL'S';m_S,m_S-m_S',m_S'\}(4L+2)^{\frac{1}{2}}\times\Theta_{L'}^{(m_S-m_S')}(\theta)-\delta_{SS'}\delta_{m_Sm_S'}(2L+1)P_L(\cos\theta)\}\Big|^2. \quad (43)$$

[18] Wigner, reference 11, Eq. (28).

Determination of scattering matrix

Our next steps are based on the hope that all the desired quantities $c_J(L'S';LS)$ (for a fixed J) can be obtained by consideration of a single generalized Fredholm determinant, without the necessity of actually constructing and investigating explicitly the asymptotic behavior of the solutions $f_J^{LS}(1L'S'r)$. We observe first of all that the transition from a set of integro-differential equations to a set of integral equations goes through as in the case of stable energy levels (Eq. (25) to Eq. (30)), since the two independent zero field solutions for positive energies (28b) have that same relation to their derivatives which made possible the building up of a Green's function in the earlier case. Only now the integral equations (30) are not unique, for the combination $G_L(k_1r)+[\mathrm{ctg}\,K]F_L(k_1r)$, as well as G_L itself, satisfies (28b), and both are equally satisfactory in their asymptotic behavior for large r. Consequently, the kernel of (30) not only depends on the energy but in general also contains g_J undetermined "phase shifts" $K_J(LS)$:

$$S_J(iLSr;jL'S'\rho)=(2\mu_i/\hbar^2k_i)\Big\{\int_0^r G_L(k_ir)F_L(k_i\sigma)+\int_r^\infty F_L(k_ir)G_L(k_i\sigma)+[\mathrm{ctg}\,K_J(iLS)]\int_0^\infty F_L(k_ir)F_L(k_i\sigma)\Big\}\times H_J(iLS\sigma;jL'S'\rho)d\sigma. \quad (44)$$

In this expression, the F's and G's represent the positive energy zero field solutions (28b) when $E-E_i$ is positive (i.e., for configuration 1); but when $E-E_i$ is negative (configurations 2, 3, $\cdots$), we understand k_i to be replaced by κ_i (Eq. (26)), and F's and G's to be the negative energy solutions (28a), and the ctg $K_J(iLS)$ to be put equal to zero. We next remark that for *any* given energy the Fredholm determinant

$$D(E;K_J(1\cdots),\cdots,K_J(1LS),\cdots)=|\delta(iLSr;jL'S'\rho)+S(iLSr;jL'S'\rho)| \quad (45)$$

can be made to vanish, because we now have the K's free to adjust, in contrast to the situation in the case of stable energy values. The equation $D(E,K)=0$ determines a g_J-1 dimensional

surface in the g_J dimensional space of the K's. Every point on this surface corresponds to a particular solution for the radial wave functions $f_J(iLSr)$. This solution must be a linear combination with certain (complex) coefficients $a_J{}^{LS}$ of the g_J particular solutions $f_J{}^{LS}(iLSr)$ defined by Eq. (35). By comparison of the asymptotic behavior of the superposition of states,

$$\sum_{L,\,S} a_J{}^{LS} f_J{}^{LS}(iL'S'r) \sim -(1/2i)\delta_{i1} a_J{}^{L'S'} \times \exp\left[-i(k_1 r - L\pi)\right] + (1/2i)\delta_{i1} \exp\left[ik_1 r\right] \sum_{LS} c_J(L'S';LS) a_J{}^{LS}, \quad (46)$$

with that of the solution of the integral equations (30) belonging to the kernel (44),

$f_J(iL'S'r)$ asymptotically proportional to

$$\delta_{i1}\{G_{L'}(k_1 r) + [\operatorname{ctg} K_J(1L'S')] F_{L'}(k_1 r)\}$$

or to

$$\delta_{i1}\left\{-(1/2i)\exp\left[-i(k_1 r - L\pi)\right] + (1/2i)\exp\left[ik_1 r\right]\frac{i\operatorname{ctg} K - 1}{i\operatorname{ctg} K + 1}\right\}, \quad (47)$$

we find

$$\sum_{L',\,S'} c_J(LS;L'S') a_J{}^{L'S'} = \exp\left[2iK_J(1LS)\right] a_J{}^{LS} \quad (48)$$

as the equations of connection between the coefficients $a_J{}^{LS}$ and the points on the $g_J - 1$ dimensional surface in the space of the K's. It is seen that the constants c completely define the surface in question. The c's form a unitary matrix, for the equality which must exist between the numbers of incoming and outgoing groups in the state (46) for arbitrary choice of the a's,

$$k_1 \sum_{LS} |a_J{}^{LS}|^2 = k_1 \sum_{LS} \Big| \sum_{L'S'} c_J(LS;L'S') a_J{}^{L'S'} \Big|^2, \quad (49)$$

is just the necessary and sufficient condition[19] for unitary character.

Our problem is: To determine the unitary scattering matrix $\|c_{mn}\|$ (we abbreviate by using $m = 1, 2, \cdots, g$ to indicate the possible values of the pair L, S), being given: (1), the surface

$$D(K_1, \cdots, K_g) = 0 \quad (50)$$

(from the Fredholm determinant of the integral equation); and (2), the equations

$$\sum_{a=1}^{g} c_{ma} a_a = e^{2iK_m} a_m \quad (m = 1, 2, \cdots, g) \quad (51)$$

(which we have seen to be an equivalent way of representing the surface). We first eliminate the a's by the condition that Eqs. (51) possess a solution:

$$\begin{vmatrix} c_{11} - e^{2iK_1} & c_{12} & \cdots & c_{1g} \\ c_{21} & c_{22} - e^{2iK_2} & \cdots & c_{2g} \\ \cdots & \cdots & \cdots & \cdots \\ c_{g1} & c_{g2} & \cdots & c_{gg} - e^{2iK_g} \end{vmatrix} = 0. \quad (52)$$

Eq. (52) is a condition on the c's which must be satisfied at every point $K = (K_1, K_2, \cdots, K_g)$ on the surface $D(\mathbf{K}) = 0$. In the actual applications the question of procedure depends upon whether the Fredholm determinant is available only by numerical calculations for each particular set of values of the K's, or whether an analytic expression is obtainable for D. In the first case it is desirable for simplicity in the computations to restrict the K's to real values, which, however, are not the most convenient in solving (52) for the c's. In the second case, where we have an analytic expression for D, it is simplest to consider first those points on the surface which are defined by $\operatorname{ctg} K = i$ for all K's except a particular K_m. The (complex) value of $K_m = K_m'$ is then fixed by $D(K) = 0$, and from (52) we have at once $c_{mm} = e^{2iK_m'}$. In this way we find all diagonal elements of the unitary matrix. Next we let two K's at a time vary freely, determining all other K's by $\operatorname{ctg} K = i$. Again we use (52) and find

$$c_{mn} c_{nm} = (c_{mm} - e^{2iK_m})(c_{nn} - e^{2iK_n}), \quad (53)$$

or in the limiting case $\operatorname{ctg} K_n \to i$, where we can neglect c_{nn} in comparison with e^{2iK_n},

$$c_{mn} c_{nm} \to \left[e^{2iK_m'} - e^{2i(K_m' + \delta K_m)}\right] \frac{1 - i(i + \delta \operatorname{ctg} K_n)}{1 + i(i + \delta \operatorname{ctg} K_n)};$$

that is,

$$c_{mn} c_{nm} = -4 c_{mm} \frac{\partial K_m}{\partial(\operatorname{ctg} K_n)} = 4 c_{mm} \left[\frac{\partial D_m}{\partial(\operatorname{ctg} K_n)} \Big/ \frac{\partial D}{\partial K_m}\right]_{\operatorname{ctg} K_n = i} \quad (m' \neq m). \quad (54)$$

[19] A. Wintner, *Spektraltheorie der Unendlicher Matrizen* (Leipzig, 1929), p. 34.

If $D(K_1, \cdots, K_g)$ reduces to the product of two functions $D'(K_1, \cdots, K_a)$ and $D''(K_{a+1}, \cdots, K_g)$, then the matrix $\|c_{mn}\|$ breaks down to two square blocks along the diagonal, for from (54) and the unitary nature of c it follows that all elements c_{mn} connecting the one set of K's with the other must be zero.

There is more than one[20] set of values for the c's satisfying Eq. (52) for all points on the given surface: for example, the substitution $u_{ik}=c_{ki}$ in general gives a new unitary matrix which is an equally good solution. Two matrices c and u both satisfy (52) only if the chain conditions

$$\begin{aligned} &u_{ii}=c_{ii}, \\ &u_{ij}u_{ji}=c_{ij}c_{ji}, \qquad (55a) \\ &u_{ij}u_{jk}u_{ki}+u_{ik}u_{kj}u_{ji}=c_{ij}c_{jk}c_{ki}+c_{ik}c_{kj}c_{ji}, \text{ etc.}, \end{aligned}$$

are fulfilled for all values of the indices.

We suppose now that no off-diagonal elements vanish (trivial modifications ensue in the following if some are zero). We write the second chain condition, for $i=1$, in the form

$$\begin{aligned} &u_{1j}=\varphi_1^{-1}c_{1j}\varphi_j, \\ &u_{j1}=\varphi_j^{-1}c_{j1}\varphi_1 \quad [=(\varphi_1 c_{11}/c_{11})c_{1j}(\varphi_j c_{1j}/c_{j1})^{-1}], \end{aligned} \qquad (55b)$$

where the quantity φ_1 is arbitrary and may be put equal to unity. Inserting (55b) in the third chain condition, with $i=1$, and using $u_{jk}u_{kj}=c_{jk}c_{kj}$, we find that there exist only two possible values for u_{jk}:

$$u_{jk}=\varphi_j^{-1}c_{jk}\varphi_k, \qquad (55c)$$

$$u_{jk}=(\varphi_j c_{1j}/c_{j1})^{-1}c_{kj}(\varphi_k c_{1k}/c_{k1}). \qquad (55d)$$

Similar solutions exist for u_{k1}, etc. Using the third chain condition in its general form, and recalling that the φ's are arbitrary, we find that if u_{jk} is given by (55c), then all other u's are given by the corresponding solution; and similarly for the second solution. In matrix language: If d is an arbitrary diagonal matrix with the general diagonal element $d_{jj}=\varphi_j$ or $d_{jj}=\varphi_j c_{1j}/c_{j1}$, then the most general matrix u consistent with (52) is given by either

$$u=d^{-1}cd \quad \text{or} \quad u=d^{-1}c'd. \qquad (55e)$$

We still have the information that u, as well as c and c', is unitary, whence

$$\sum_j |c_{ij}|^2\{|\varphi_j|^2-|\varphi_i|^2\}=0 \quad (i=1, 2, \cdots, g).$$

With $c_{ij}\neq 0$ for all $i\neq j$ (cf. remark above), it follows by simple algebra that all $|\varphi_j|^2$ must be equal; and since $\varphi_1=1$, we conclude that our diagonal matrix must be a phase matrix: $d_{jj}=\varphi_j=e^{i\vartheta_j}$. Therefore, given the Fredholm determinant (51), we can determine the scattering matrix $\|c_{mn}\|$ uniquely up to a transformation by an arbitrary phase matrix and a possible interchange of rows and columns. In the trivial special cases mentioned above, where the off-diagonal elements of c vanish in such a way as to allow the scattering matrix to be broken up into submatrices, each block can have rows and columns interchanged independently of the other blocks.

When the conditions are satisfied for the time reversal of nuclear processes (absence of external magnetic fields, etc.), the matrix c shows a certain symmetry property equivalent to the principle of microscopic reversibility. The operation of time reversal,[21] in fact, converts a given wave function Ψ into a new one, $K\Psi$:

$$\begin{aligned} &K\Psi(\mathbf{x}_1, \sigma_1, \cdots, \mathbf{x}_m, \sigma_m, \mathbf{y}_1, \tau_1, \cdots, \mathbf{y}_n, \tau_n) \\ &=\mathbf{s}_{1x}\cdots\mathbf{s}_{mx}\mathbf{t}_{1x}\cdots\mathbf{t}_{nx}\Psi^*(\mathbf{x}_1, \sigma_1, \cdots, \mathbf{y}_n, \tau_n) \\ &=(-i)^{m+n}\sigma_1\cdots\sigma_m\tau_1\cdots\tau_n\Psi^*(\mathbf{x}_1, \sigma_1, \cdots, \mathbf{y}_n, \tau_n), \end{aligned}$$

which, under the conditions stated, will be a linear combination of the old wave functions. We go back to (46), put $a_J{}^{LS}=\mathfrak{C}_J(L'S'; LS)$, and obtain then solutions whose radial parts have the asymptotic behavior

$$\begin{aligned} f_J(iLSr)\sim{}&\mathfrak{C}_J(L'S'; LS)(1/2i) \\ &\times\exp[-i(k_1r-L\pi)] \\ &+(1/2i)\exp[ik_1r]\delta_{L'L}\delta_{S'S}. \end{aligned} \qquad (56a)$$

The corresponding total wave function, after being operated on by the time reversal operator K, will also be a solution of the wave equation in the absence of external magnetic fields, etc., under which conditions we may suppose that the

[20] I am indebted to Professor H. Weyl and Professor J. H. M. Wedderburn for discussions of the arbitrariness in the c's.

[21] Cf. E. Wigner, Göttingen Nachrichten **31**, 546 (1932), Eq. (10).

group functions satisfy

$$i^{2m}K\Phi_m=\Phi_{-m} \tag{56b}$$

(cf. Wigner's Eq. (21)). Then, using the relation[21a]

$$\{JLS; m_J m_L m_S\}=(-1)^{J-L-S} \times\{JLS; -m_J, -m_L, -m_S\}, \tag{56c}$$

and referring to Eqs. (19) and (20), we have for the radial components of the new wave function

$$f_J^{(\text{new})}(iLSr)\sim(-1)^{J-S_\text{I}-S_\text{II}}(-i)^{2m_J} \times\{-(1/2i)\delta_{L'L}\delta_{S'S}\exp[-i(k_1r-L\pi)] +(1/2i)c_J(L'S';LS)\exp[ik_1r]\}. \tag{56d}$$

Comparison with the corresponding old radial wave function (35) gives

$$c_J(L'S';LS)=c_J(LS;L'S'). \tag{57}$$

This relation shows that $\|c_{mm}\|$ is a symmetric matrix, and with the help of (54) demonstrates that each element of the matrix is determined up to a factor ±1.

From the results of the last two paragraphs, we conclude that a knowledge of the Fredholm determinant (51) of our integral equations is sufficient, in the absence of external magnetic fields, to determine all elements of the scattering matrix up to a transformation by a diagonal matrix whose elements d_{ii} are ±1. Once this 2^{g-1}-fold arbitrariness in choice of signs has been resolved for one energy, perhaps by explicit solution of the integral equations,[22] the principle of continuity with respect to variation of the energy is sufficient to determine the c's completely for all energies from the Fredholm determinant, $D(E; K_1, \cdots, K_g)$ of the integral equation.

Transmutation

Cross sections giving the number and angular distribution of disintegration products may be calculated on the same line as the scattering probabilities considered above. The kernel of the integral equation is in fact given by the previous expression (44), where now, however, several of the quantities $E-E_s$ are positive, corresponding to the several possible unstable configurations or modes of disintegration of the compound nucleus. Associated with each unstable configuration i there are the phase shifts $K_J(iLS)$, related by the condition

$$D(E; K_J(1\cdots), \cdots, K_J(iLS), \cdots)=0. \tag{58}$$

From the shape of the corresponding surface in K space and possibly by making explicit solutions of the integral equations in certain cases (see preceding discussion) we find the elements of a unitary matrix $\|c_J(jL'S';iLS)\|$ whose elements describe the asymptotic behavior of the particular solutions $f_J^{iLS}(jL'S'r)$ of the wave equation:

$$f_J^{iLS}(jL'S'r)\sim-(1/2i)\delta_{ij}\delta_{LL'}\delta_{SS'} \times\exp[-i(k_jr-L\pi)]+(1/2i)(k_i/k_j)^{\frac{1}{2}} \times c_j(jL'S';iLS)\exp[ik_jr]. \tag{59}$$

The cross section per unit solid angle for the process in which groups I^i and II^i (for example, ${}_2\text{He}^3$ and ${}_0n^1$) collide with random spin orientation and groups I^j and II^j (${}_1\text{H}^3$ and ${}_1\text{H}^1$) separate along a line oriented at an angle θ with respect to the original direction is

$$\sigma_{ij}(\theta)=[(2S_\text{I}{}^i+1)(2S_\text{II}{}^i+1)4k_ik_j]^{-1}\sum_{S,\,m_S}\sum_{S',\,m_{S'}} \times\Big|\sum_{J,\,L,\,L'}c_J(jL'S';iLS)\{JLS;m_S\,0\,m_S\} \times\{JL'S';m_Sm_S-m_S'm_S'\}(4L+2)^{\frac{1}{2}} \times\Theta_{L'}{}^{(m_S-m_S')}(\theta)\Big|^2 \quad (i\neq j),$$

$$\sigma_{ii}(\theta)=\sigma_{ii} \quad \text{(Eq. (43))}. \tag{60}$$

Discussion

Validity of treatment

The connection which we have obtained between the scattering and disintegration cross sections and a certain surface

$$D(E; K_1, \cdots, K_g)=0$$

defined by the Fredholm determinant of an integral equation, does not depend for its

[21a] This relation was suggested by Professor Wigner, who has also been kind enough to clear up several points in connection with Eqs. (55e) and (57).

[22] Cf. remarks in discussion.

validity on the accuracy of what we have called the method of resonating group structure. The derivation, in fact, made use only of certain quite general asymptotic properties of the solution of the wave equation. Consequently, the same method of treatment goes through also in the case where that kernel is employed in the integral equation (30) which will give the rigorous solution of the problem in question—i.e., a kernel S, built up somewhat as (44), but from the accurate wave functions of the individual groups and the accurate solutions of the problem of N *free* neutrons and protons, followed by the energy operator H representing individual particle rather than group interactions. It appears feasible to carry out such a treatment of the nuclear three-body problem in detail.

Numerical calculations

However the fundamental integral equation is derived, the central problem from the computational point of view is to evaluate the associated Fredholm determinant. A diagonal expansion on analytic lines, following Eq. (33), is not in general possible, although the possibility is not excluded of finding a suitable analytic approximation to S, such that the powers, S^n, can be evaluated explicitly.

A straightforward numerical calculation offers another procedure, which can always be carried through to a finish. For a simple illustration, we suppose that the system in question is to be described by a single configuration, in which the two groups have no spin. The range of values of the intergroup separation, $r=0$ to $r=r^*$, over which the interaction departs appreciably from its asymptotic value, is replaced by the set of points $r_1=a$, $r_2=2a$, $\cdots$, $r_p=pa$, the spacing, a, being taken sufficiently small. The integral equation

$$f(r)+\int S(r,\rho)f(\rho)d\rho=0 \qquad (30')$$

may then, by Simpson's rule, be replaced approximately by the set of linear equations

$$f_i+\sum_{\alpha=1}^{p} S_{i\alpha}f_\alpha=0, \quad (i=1, 2, \cdots, p), \quad (30'')$$

where

$$f_1=f(a), \quad f_2=f(2a), \quad \cdots$$

and

$$S_{11}=(2a/3)S(a,a), \quad S_{12}=(4a/3)S(a,2a),$$
$$S_{13}=(2a/3)S(a,3a), \quad \cdots \qquad (30''')$$
$$S_{21}=(2a/3)S(2a,a), \quad \cdots, \quad \text{etc.}$$

The kernel S may itself be calculated by a similar procedure of approximation to Eq. (44):

$$S_{mn}=\sum_{\alpha=1}^{p} G_{m\alpha}H_{\alpha n}. \qquad (44'')$$

Here the matrix $\|G_{mn}\|$ bears the same type of relation to the function

$$\begin{aligned} G(r,\rho)&=(2\mu/h^2k)\{G_L(kr)F_L(k\rho) \\ &\quad +\operatorname{ctg} KF_L(kr)F_L(k\rho)\} \quad (\rho<r) \\ &=(2\mu/h^2k)\{G_L(k\rho)F_L(kr) \\ &\quad +\operatorname{ctg} KF_L(kr)F_L(k\rho)\} \quad (\rho>r) \end{aligned} \qquad (44''')$$

that $\|S_{mn}\|$ bears to $S(r,\rho)$, except for one detail. Since $G(r,\rho)$ has a kink (discontinuous first derivative) at the point $\rho=r$, the Simpson coefficients 2/3, 4/3, etc., must be slightly modified to make the summation (44'') give the best agreement with the integration of (44). Written following the order of (30'''), the proper coefficients for the calculation of the matrix G are

$$\begin{array}{llllllll} 2a/3, & 4a/3, & 2a/3, & 4a/3, & 2a/3, & 4a/3, & 2a/3, & \cdots \\ 9a/8, & 6a/8, & 9a/8, & 9a/8, & 17a/24, & 4a/3, & 2a/3, & \cdots \\ 2a/3, & 4a/3, & 2a/3, & 4a/3, & 2a/3, & 4a/3, & 2a/3, & \cdots \\ 17a/24, & 9a/8, & 9a/8, & 6a/8, & 9a/8, & 9a/8, & 17a/8, & \text{etc.} \end{array}$$

In order for (30'') to possess a solution, the Fredholm determinant

$$D(E,K)=\begin{vmatrix} 1+S_{11} & S_{12} & \cdots & \cdots \\ S_{21} & 1+S_{22} & \cdots & \cdots \\ \cdots & \cdots & \cdots & 1+S_{pp} \end{vmatrix}$$

must vanish. For stable states ($E<0$, $\operatorname{ctg} K=0$) the Fredholm determinant is evaluated for one energy value, then another, and so on; the curve $D(E)$ as a function of energy crosses the horizontal axis at the eigenwerte. The case of scattering (and in general, disintegration) is treated in the same way.

Though laborious, it is quite feasible to deal with determinants of the 30th order. The proce-

dure of evaluation is straightforward on a calculating machine:[23] The lowest row $(d_{p1}, d_{p2}, \cdots, d_{pp})$ (we abbreviate $\delta_{ik}+S_{ik}$ by d_{ik}) is multiplied by $(d_{p-1,\,p}/d_{pp})$ and subtracted from the $(p-1)$th; by $(d_{p-2,\,p}/d_{pp})$ and subtracted from the $(p-2)$nd row, etc. When all elements in the pth column are reduced to zero, (except d_{pp}), the (new) second row is used in the same way to eliminate all elements in the $(p-1)$ the column except $d_{p,\,p-1}$ and $d_{p-1,\,p-1}$; and so on. The value of the determinant is given by the product of the diagonal elements of the final matrix: $D=d_{11}'d_{22}'\cdots d_{pp}'$. If this vanishes, the wave function (vector) f may easily be found, if desired, by recursive solution: $f_1=1$; $f_2=-d_{21}'f_1/d_{22}'$; $f_3=-(d_{31}'f_1+d_{32}'f_2)/d_{33}'$, etc. The smoothness of the curve $f(r)$ drawn through the values so obtained furnishes a good check on the calculations.

Modifications in procedure

So far we have assumed that the interaction falls off rapidly. If it follows the Coulomb law for large distances, then in the calculations we may take it to be broken off at $r=r^*$. The asymptotic form of the wave functions we obtain in this way corresponds to zero field from r^* to ∞; we then fit the Coulomb functions on at r^*, in such a way[24] as to have the same logarithmic derivative as those combinations of zero field solutions described by the phase shifts K. This procedure determines the phase shifts K' of the solution for the actual field, measured with respect to the solutions for a pure Coulomb field. The scattering cross section is known[25] in terms of K', for the case of elastic collisions with zero spin, and may be derived for scattering and disintegration processes involving groups with spin along the lines described above. An alternative procedure, using for F_L and G_L the Coulomb wave functions, would require more detailed tables of these functions than are now available.

In the actual problems treated so far by the method we have described, it appears to be a general rule that the larger the number of particles involved, the more closely

$$\int \sum_{jL'S'} I_J(iLSr;jL'S'\rho)f_J(jL'S'\rho)d\rho$$

approaches to being the negative of $f_J(iLSr)$, although of course the operator $\delta_{ij}\delta_{LL'}\delta_{SS'}\delta(r-\rho)+I_J(\cdots)$ is always positive definite. This behavior is connected with the large number of nodes present in the total wave function Ψ owing to its antisymmetry properties. In fact, $\int\Psi^*\Psi d\tau$ is very much smaller than the integral $\int\chi^*\chi d\tau$ of any one of the (not antisymmetrized) parts χ (Eq. (36)) from which Ψ is built up, and this comes to expression in the feature we have mentioned. The appearance of the operator $\delta+I$ in the denominator of the expectation value of the energy has the consequence that calculations are sensitive to the accuracy with which $\int\int f^*(r)[\delta(r-\rho)+I(r,\rho)]f(\rho)drd\rho$ is determined. This would suggest that $\varphi=[\delta+I]^{\frac{1}{2}}f$ be introduced as dependent variable, instead of f itself; for φ has the same asymptotic behavior as f and gives $\int\varphi^*(r)\varphi(r)dr$ for the integral in question. The method is known by which the positive square root of a positive definite Hermitian matrix may be obtained,[26] but we do not carry out here the consequences of this possible improvement on the procedure we have already described.

The development above was given in detail only for configurations consisting of two groupings. When three groupings interact, one approximate mode of description is to regard the configuration as composed of two groupings, the internal wave function of one of which is in turn determined by the method of resonating group structure. More accurate, also more symmetric, is the direct extension to three bodies of the type of kernel we have used for two. Instead of the functions F_L, G_L of one variable, r, we must then have a combination of functions of three variables r_{12}, r_{13}, r_{23} built up into a Green's function for the "radial" motion of three free bodies, the angular part of the motion having been separated out by known[27] methods.

[23] Cf. James and Coolidge, J. Chem. Phys. **1**, 834 (1933).
[24] See John A. Wheeler, "Wave Functions for Large Arguments by the Amplitude Phase Method," Phys. Rev. **52**, 1123 (1937).
[25] Cf. Mott and Massey, reference 13, p. 275.
[26] Cf. M. Born and P. Jordan, *Elementare Quantenmechanik* (Berlin, 1930), p. 69.
[27] Cf. G. Breit, Phys. Rev. **35**, 569 (1930), and especially J. O. Hirschfelder and E. Wigner, Proc. Nat. Acad. **21**, 113 (1935), where the corresponding separation of angles is treated in the case of N bodies.

By introducing a dependence of the individual group wave functions on the intergroup distances, we get an approximation to the total wave function which corresponds to better values for the absolute energy than is otherwise obtained. In some ways this modification is analogous to a polarization effect, but it must be remembered that the interaction between the various groups is far too intimate for such a simple change to make the total wave function really approach in full detail to the accurate solution of the given quantum mechanical problem. Rather such a refinement is to be taken in the spirit of the method of resonating group structure, in which we try to build up a suitable description of the whole system from what we know of its parts, being guided throughout by the variation principle. Use of a "polarized" group wave function appears to be especially suitable in treating such a problem as that of proton-deuteron collisions. On the other hand there are situations (as when the available energy is large) where it is more convenient, and indeed absolutely necessary, to take into account excited group states in making the proper allowance for the interaction between the various groups (we use the word "group" here in the extended sense employed throughout the present discussion, in which there is no one to one correspondence between a given group and definite neutrons and protons picked out of the total system). Analogy with the polarization problem in atomic physics make it clear that explicit dependence of wave functions on separation, and excitation of higher states are to a considerable extent even in the nuclear problem equivalent ways of allowing for the same thing, and indeed the mathematical treatment given above indicated that it was practically impossible to introduce both methods of description at the same time in a consistent manner. The question as to which excited states of the individual groups are most important in the description of the compound system is of course an important one in the actual applications, and has received so far only a very general kind of answer.[28]

A thoroughgoing treatment of collision processes for nuclei of medium and high atomic weight in the detail we have mentioned in this paper appears to be out of the question. The considerations of Bohr[29] point rather to a statistical approach, based on the analogy between nuclear structure and the liquid state, as more fruitful. For this reason a study of the detailed correspondence between the two viewpoints would be very valuable. In this connection the importance of symmetry arguments has already been pointed out.[28]

For sufficiently light nuclei, on the other hand, the connection between nuclear forces and observations on collisions and transmutations can be traced out with sufficient accuracy to make possible definite conclusions about the interactions involved. The method of resonating group structure described above has been used to treat the interaction between two normal alpha-particles,[30] and is being applied to other problems,[31] where further details will be given.

---

[28] Preceding paper.

[29] Niels Bohr, Nature **137**, 344 (1936); also unpublished lectures summarized in Science **86**, 161 (1937).

[30] To be published.

[31] Four-particle problem: preliminary report, Hermon Parker, Paper No. 3, Chapel Hill-Durham meeting of the American Physical Society, Feb. 19–20, 1937. Five-particle problem: Miss K. Way, University of North Carolina, in progress.

Wave Functions for Large Arguments by the Amplitude-Phase Method

JOHN A. WHEELER
University of North Carolina, Chapel Hill, North Carolina
(Received August 17, 1937)

The two independent solutions of the radial wave equation required in the treatment of collision problems may be expressed in terms of a common amplitude and phases differing by $\pi/2$, following a method due to Milne. The determination of phase shifts is simplified by this procedure. Analytical expressions for the amplitude and phase and their derivatives are given in the case of zero field for $L=0, 1, 2, 3, 4$. In other cases these quantities may rapidly be determined for large arguments by numerical integration of Eqs. (7) and (5b). Values of the amplitude and phase of the coulomb functions needed in the treatment of the scattering of alpha-particles in helium for $L=0$ and $L=2$ were obtained in this way and are tabulated.

IN the treatment of questions of nuclear scattering and disintegration and similar problems in atomic physics,[1] the radial wave function describing the relative motion of the two particles under consideration may be divided into two parts. The first part, $F^*(r)$, defined over the region from the origin out to a certain separation r^*, depends upon the special nature of the interaction between the two particles or systems, whilst the second, extending from r^* to infinite distance, requires for its determination the solution of the Schroedinger equation for some relatively simple analytic law of force.

Characteristic of the problems mentioned is the requirement that both independent solutions of the wave equation be known for $r>r^*$—the so-called "regular" and "irregular" functions. Difficulty in obtaining numerical values of the irregular function and its derivative often occurs as a serious obstacle in applying collision theory to actual problems. Adequate tables must give both functions and their derivatives at intervals relatively small in comparison with the wavelength, since these quantities change rapidly even in regions where they do not oscillate. However, the calculation of the two wave functions and their derivatives for a single value of r for a given impact energy is often a time-taking process, especially if r is large and the customary power series calculation is employed.

The introduction of slowly varying functions, representing essentially the amplitude and phase of the two functions, makes it possible to increase the size of the interval of tabulation by a large factor, gives a method of computing the wave function for large arguments which is often much more rapid than expansion in power series about the origin, and in addition makes a certain simplification in the calculation of phase shifts in scattering problems.

The functions under consideration may be defined as follows:

F (regular function) satisfies the wave equation; vanishes at $r=0$ when prolonged inward to the origin; has unit amplitude at $r=\infty$. Example: $F(r)=(kr)^{-1}\sin kr-\cos kr$ (scattering of a neutron with one unit of angular momentum).

G (irregular function) satisfies same equation; has unit amplitude and is 90° in advance of F at infinity. (In example, $G(r)=(kr)^{-1}\cos kr+\sin kr$). From the definitions of F and G and the properties of the Schroedinger equation it follows that

$$GdF/dr-FdG/dr=k(\equiv[2\mu E/\hbar^2]^{\frac{1}{2}}). \quad (1)$$

In applications, the equations of fit are applied at $r=r^*$:

$$aF+bG=F^*, \quad (2a)$$

$$adF/dr+bdG/dr=dF^*/dr \quad (r=r^*), \quad (2b)$$

and the values found for a and b are used to evaluate the collision cross section (determined by the phase shift $K=\operatorname{arc\,cotg}\, a/b$) and the probability of interpenetration (proportional to $[a^2+b^2]^{-1}$) of the two particles of given angular momentum.

Milne[2] has shown that a simple differential

[1] Cf. Mott and Massey, *The Theory of Atomic Collisions* (Oxford, 1933).

[2] W. E. Milne, Phys. Rev. **35**, 864 (1930). Cf. also L. A. Young, Phys. Rev. **38**, 1612 (1931), who has given the name "local momentum" to the quantity $P(r)=A^{-2}(r)$ and shown its natural connection with the Bohr-Sommerfeld quantum conditions.

equation (essentially (5a) below) is satisfied by the amplitude function $A(r)=[F^2(r)+G^2(r)]^{\frac{1}{2}}$, and has used this equation to obtain solutions of the wave equation for certain problems in the discrete spectrum. We introduce in addition a phase function $\Phi(r)$ defined as follows:

$$F(r)=A(r)\sin\Phi(r);\quad G(r)=A(r)\cos\Phi(r);\quad \Phi(0)=0. \tag{3}$$

If a satisfactory method is already available for obtaining F and G, Eq. (3) is needed only for purposes of interpolation; otherwise, the following differential equations may readily be deduced[3] for the direct determination of A and Φ:

$$d^2A/dr^2+2\mu/\hbar^2[E-V(r)]A-(d\Phi/dr)^2A=0, \tag{4a}$$

$$1/kd\Phi/dr=1/A^2. \tag{4b}$$

On combining and introducing $\rho=kr$ for independent variable, we have equations by which first A and then Φ may be determined:

$$d^2A/d\rho^2+(1-V/E-1/A^4)A=0,\quad A(\infty)=1,\ dA/d\rho(\infty)=0, \tag{5a}$$

$$d\Phi/d\rho=1/A^2,\ \Phi(0)=0. \tag{5b}$$

These equations clearly reduce to the Jeffreys-W.K.B. approximation on neglecting

$$1/Ad^2A/d\rho^2.$$

Functions in Field Free Space

When there is no interaction between the two particles, we have $V(r)=L(L+1)\hbar^2/2\mu r^2$, representing the effect of centrifugal force alone. The analytical expressions for F and G are in this case well known,[4] and the expressions for A and Φ can be obtained directly from the equations of definition. The asymptotic value of Φ for large ρ is $\rho-L\pi/2$; we therefore write $\Phi=\rho-L\pi/2+\varphi$; also $z=\rho^{-1}=(kr)^{-1}$.

$$L=0.\quad A=1,\quad \varphi=0,\quad \frac{r}{A}\frac{dA}{dr}=0,\quad r\frac{d\varphi}{dr}=0,$$

$$L=1.\quad A=(1+z^2)^{\frac{1}{2}},\quad \operatorname{tg}\varphi=z,\quad \frac{r}{A}\frac{dA}{dr}=-\frac{z^2}{1+z^2},\quad r\frac{d\varphi}{dr}=-\frac{z}{1+z^2},$$

$$L=2.\quad A=(1+3z^2+9z^4)^{\frac{1}{2}},\quad \operatorname{tg}\varphi=\frac{3z}{1-3z^2},\quad \frac{r}{A}\frac{dA}{dr}=-\frac{3z^2+18z^4}{1+3z^2+9z^4},\quad r\frac{d\varphi}{dr}=-\frac{3z+9z^3}{1+3z^2+9z^4},$$

$$L=3.\quad A=(1+6z^2+45z^4+225z^6)^{\frac{1}{2}},\quad \operatorname{tg}\varphi=\frac{6z-15z^3}{1-15z^2},\quad \frac{r}{A}\frac{dA}{dr}=-\frac{6z^2+90z^4+675z^6}{1+6z^2+45z^4+225z^6}, \tag{6}$$

$$r\frac{d\varphi}{dr}=-\frac{6z+45z^3+225z^5}{1+6z^2+45z^4+225z^6},$$

$$L=4.\quad A=(1+10z^2+135z^4+1575z^6+11025z^8)^{\frac{1}{2}},\quad \operatorname{tg}\varphi=\frac{10z-105z^3}{1-45z^2+105z^4},$$

$$\frac{r}{A}\frac{dA}{dr}=-\frac{10z^2+270z^4+4725z^6+44100z^8}{1+10z^2+135z^4+1575z^6+11025z^8},\quad r\frac{d\varphi}{dr}=-\frac{10z+135z^3+1575z^5+11025z^7}{1+10z^2+135z^4+1575z^6+11025z^8}.$$

Numerical Integration

Ordinarily solutions of (5) for a given $V(r)$ cannot be obtained in terms of polynomials or simple analytical expressions. As we are primarily interested in the solution of the wave equation for large arguments, we solve Eq. (5a) by numerical integration from infinity inward.

[3] We make use of the fact that the real part of $G+iF=A\exp(i\Phi)$ satisfies the wave equation to get (4a) and derive (4b) from condition (1).

[4] $F=(\pi kr/2)^{\frac{1}{2}}J_{L+\frac{1}{2}}(kr)$; $G=(\pi kr/2)^{\frac{1}{2}}J_{-L-\frac{1}{2}}(kr)$, in terms of Bessel functions.

Hartree has already pointed[5] out that the non-linear nature of a second-order differential equation causes no difficulties in the calculations; the essential point is to see that the equation involves no first derivatives. Hence, if we introduce $z=1/\rho$ as new independent variable suitable for integrating (5a) inward, we must also change the dependent variable to $M=zA$ to compensate the first derivatives which would otherwise creep into the equation. We then obtain

$$M''=M^{-3}-M(1-V/E)z^{-4},\ M(0)=0,\quad M'(0)=1 \qquad (7)$$

on using dashes to represent differentiation with respect to z.

In the numerical computation, the range of z of interest is divided into equal intervals (say $z=0.00,\ 0.05,\ 0.10,\ \cdots$ to 0.50) and a power series expansion for M in the neighborhood of $z=0$ is used to start the integration. The first few steps of the calculation must be made with high accuracy, since M'' appears as the small difference between large quantities. A rapid procedure for integrating second order differential equations which are free of first derivatives, together with a discussion of stability and accuracy, is given in Hartree's paper.[5]

The most convenient check on the calculation of M may be made by means of Φ, provided one knows from other considerations the value of the constant C in the asymptotic expression for the phase:

$$\Phi\sim\int^{\rho}(1-V/E)^{\frac{1}{2}}d\rho+C \quad (\rho\to\infty).$$

(For example, it follows[6] from the asymptotic expansion of the contour integrals for the Coulomb functions that

$$\Phi\sim\rho-\eta\ln 2\rho-L\pi/2+\sigma_L,$$

where $\sigma_L=\arg\Gamma(L+1+i\eta)$.) Starting with this value for Φ at $\rho=\infty$, and integrating (5b) inwards toward the origin, it is easy to determine how closely $\Phi(\rho)$ approaches to having the value zero at the origin; this gives a direct check on the calculation of Φ and hence (from (5b)) on the accuracy of A.

[5] D. R. Hartree, Memoirs and Proc. Manchester Lit. and Phil. Soc. **77**, 91 (1932–33).

[6] Cf., for example, reference 1, p. 39.

TABLE I. *Coulomb functions for $L=0$. $F, G=A$ sin, cos Φ. $\Phi=\rho-\eta\ln 2\rho+\sigma_0+\varphi$; $\eta=1/ak$; $z=1/kr$. Last digit uncertain.*

$L=0$	$ak=1.25$		$\sigma_0=-.3044$		$ak=1.50$		$\sigma_0=-.2873$		$ak=1.75$		$\sigma_0=-.2657$		$ak=2.00$		$\sigma_0=-.2440$		$ak=2.25$		$\sigma_0=-.2245$	
z	A	φ	$\rho-p d\Phi/dp$	$-(\rho/A)dA/dp$	A	φ	$\rho-p d\Phi/dp$	$-(\rho/A)dA/dp$	A	φ	$\rho-p d\Phi/dp$	$-(\rho/A)dA/dp$	A	φ	$\rho-p d\Phi/dp$	$-(\rho/A)dA/dp$	A	φ	$\rho-p d\Phi/dp$	$-(\rho/A)dA/dp$
.00	1.0000	0.0000	0.8000	0.0000	1.0000	0.0000	0.6667	0.0000	1.0000	0.0000	0.5714	0.0000	1.0000	0.0000	0.5000	0.0000	1.0000	0.0000	0.4444	0.0000
.05	1.0210	.0157	.8155	.0217	1.0174	.0108	.6772	.0178	1.0148	.0079	.5790	.0151	1.0129	.0060	.5057	.0131	1.0114	.0047	.4488	.0116
.10	1.0442	.0308	.8293	.0466	1.0362	.0210	.6862	.0377	1.0306	.0152	.5852	.0317	1.0265	.0114	.5101	.0273	1.0234	.0089	.4521	.0240
.15	1.0697	.0449	.8403	.0746	1.0564	.0303	.6931	.0583	1.0474	.0216	.5895	.0493	1.0409	.0161	.5130	.0421	1.0359	.0124	.4540	.0368
.20	1.0974	.0577	.8484	.1044	1.0779	.0385	.6970	.0824	1.0650	.0272	.5917	.0677	1.0558	.0201	.5142	.0575	1.0488	.0153	.4546	.0500
.25	1.1270	.0688	.8505	.1362	1.1007	.0455	.6986	.1057	1.0834	.0318	.5921	.0861	1.0712	.0232	.5139	.0727	1.0621	.0175	.4538	.0629
.30	1.1587	.0781	.8506	.1685	1.1244	.0512	.6969	.1289	1.1023	.0354	.5901	.1044	1.0869	.0256	.5116	.0877	1.0755	.0190	.4517	.0756
.35	1.1930	.0856	.8462	.1995	1.1490	.0555	.6929	.1516	1.1217	.0380	.5864	.1221	1.1029	.0271	.5082	.1022	1.0891	.0199	.4484	.0877
.40	1.2265	.0913	.8383	.2291	1.1741	.0587	.6866	.1734	1.1414	.0397	.5811	.1396	1.1191	.0279	.5036	.1158	1.1028	.0202	.4443	.0991
.45	1.2621	.0951	.8272	.2569	1.1998	.0605	.6785	.1937	1.1613	.0404	.5745	.1549	1.1353	.0280	.4981	.1287	1.1164	.0199	.4387	.1100
.50	1.2985	.0973	.8139	.2824	1.2257	.0613	.6688	.2126	1.1813	.0403	.5669	.1695	1.1525	.0275	.4916	.1396				
.55	1.3354	.0979	.7987	.3056	1.2518	.0610	.6580	.2299	1.2013	.0395	.5586	.1831								
.60	1.3727	.0971	.7823	.3253	1.2780	.0588	.6463	.2456												
.65					1.3041	.0576	.6339	.2599												
.70	1.4476	.0918	.7460	.3301	1.3301	.0547	.6211	.2726												
.75					1.3559		.6081	.2839												
.80	1.5220	.0823	.7104	.3872																

Coulomb Functions[7]

In the case of the interaction $V(r)=ZZ'e^2/r+L(L+1)\hbar^2/2\mu r^2$, we use the notation

$$a=\hbar^2/\mu ZZ'e^2$$

(characteristic radius), $\eta=1/ak=\lambda/2\pi a=\lambda/a$ (reduced wave-length). Expanding the solution of

$$M''=M^{-3}-M[1-2\eta z-L(L+1)z^2]/z^4 \quad (8)$$

in a power series about the point $z=0$,

$$M=z+a_1z^2+a_2z^3+\cdots, \quad (9)$$

we have for the first few coefficients

$$\begin{aligned}
&a_1=\eta/2\,;\quad a_2=5\eta^2/8+L(L+1)/4\,;\\
&a_3=15\eta^3/16+5\eta L(L+1)/8-\eta/8\,;\\
&a_4=195\eta^4/128+45\eta^2L(L+1)/32 \quad (10)\\
&\qquad -23\eta^2/16+5L^2(L+1)^2/32-3L(L+1)/8\,;\\
&a_5=663\eta^5/256-91\eta^3/16+195\eta^3L(L+1)/64\\
&\qquad +45\eta L^2(L+1)^2/64-23\eta L(L+1)/8\\
&\qquad\qquad +3\eta/4.
\end{aligned}$$

The choice of interval of integration is governed by the practical rate of convergence of the series for the value of η under consideration.

[7] Cf. F. L. Yost, John A. Wheeler, and G. Breit, Phys. Rev. **49**, 174 (1936), for analytic properties of these functions. For numerical values for $\rho<1$, cf. same authors, J. Terr. Magn. At. El., 443, Dec. (1935), and E. R. Wicher, J. Terr. Magn. At. El., 389, Dec. (1936).

In calculating the phase, we use as dependent variable the quantity φ defined by

$$\Phi(\rho)=\rho-\eta\ln 2\rho-L\pi/2+\arg\Gamma(L+1+i\eta)+\varphi(\rho), \quad (11)$$

and take $z=1/\rho$ for independent variable. The integration of the first-order differential equation for φ,

$$d\varphi/dz=(1-\eta z)/z^4-1/M^2, \quad (12)$$

is simple (cf. Hartree, for example). Near $z=0$ we have

$$d\varphi/dz=[L(L+1)+\eta^2]/2+\cdots.$$

Numerical values are given in Tables I and II for $L=0$ and $L=2$ for the range of values of interest in the problem of the scattering of alpha-particles in helium, and applicable also to scattering and disintegration problems involving other light nuclei. The last digit is uncertain.

Equations of Fit

In the amplitude phase notation, the general solution of the wave equation from r^* to ∞ has the form

$$cA(r)\sin[\Phi(r)+K], \quad (13)$$

where c and K are constants determined by the equations of fit ($2a$ and $2b$) at $r=r^*$. These equations may be put as follows:

Table II. *Coulomb functions for $L=2$. $F, G=A\sin,\cos\Phi$. $\Phi=\rho-\eta\ln 2\rho+\sigma_2-\pi+\varphi$; $\eta=1/ak$; $z=1/kr$. Last digit uncertain.*

$L=2$	$ak=1.25$ $\sigma_2-\pi=-2.3906$		$ak=1.50$ $\sigma_2-\pi=-2.5192$		$ak=1.75$ $\sigma_2-\pi=-2.6098$		$ak=2.00$ $\sigma_2-\pi=-2.6770$		$ak=2.25$ $\sigma_2-\pi=-2.7292$	
z	A	φ	A	φ	A	φ	A	φ	A	φ
0.00	1.0000	0.0000	1.0000	0.0000	1.0000	0.0000	1.0000	0.0000	1.0000	0.0000
.05	1.0252	.1689	1.0215	.1634	1.0189	.1601	1.0169	.1579	1.0154	.1564
.10	1.0633	.3437	1.0545	.3315	1.0485	.3240	1.0440	.3191	1.0406	.3156
.15	1.1192	.5235	1.1030	.5034	1.0920	.4912	1.0841	.4830	1.0782	.4772
.20	1.1991	.7050	1.1717	.6767	1.1534	.6594	1.1408	.6478	1.1312	.6396
.25	1.3128	.8836	1.2678	.8480	1.2388	.8257	1.2186	.8109	1.2036	.8003
.30	1.4673	1.0542	1.3967	1.0127	1.3524	.9866	1.3217	.9690	1.2993	.9562
.35	1.6692	1.2103	1.5639	1.1658	1.4987	1.1375	1.4540	1.1182	1.4220	1.1040
.40	1.9239	1.3481	1.7734	1.3039	1.6812	1.2754	1.6188	1.2555	1.5743	1.2410
.45	2.2342	1.4664	2.0278	1.4252	1.9023	1.3982	1.8179	1.3792	1.7581	1.3653
.50	2.6021	1.5657	2.3286	1.5297	2.1633	1.5058	2.0527	1.4888	1.9745	1.4762
.55	3.0281	1.6480	2.6763	1.6186	2.4677	1.5988	2.3236	1.5846	2.2241	1.5740
.60	3.5125	1.7156	3.0712	1.6935	2.8066	1.6786	2.6308	1.6678	2.5070	1.6595
.70	4.6568	1.8154	4.0019	1.8085	3.6115	1.8046	3.3533	1.8013	3.1722	1.7986
.80	6.0347	1.8807	5.1195	1.8892	4.5765	1.8959	4.2188	1.9003	3.9683	1.9034
.90	7.6460	1.9223	6.4229	1.9452	5.7001	1.9620	5.2254	1.9739	4.8936	1.9827
1.00	9.4910	1.9476	7.9115	1.9844	6.9813	2.0101	6.3271	2.0290	5.9468	2.0431
1.10	11.5701		9.5850	2.0112	8.4194	2.0450	7.6579		7.1269	2.0895

$$r d\Phi/dr \operatorname{ctg}(\Phi+K) = r/F^* dF^*/dr - r/A dA/dr; \quad (14a)$$

$$cA \sin(\Phi+K) = F^* \quad (r=r^*). \quad (14b)$$

Eq. (14a) determines the phase shift, K, of the wave function in the actual field of force with respect to the wave function which would describe the motion if the "outer" potential ($r>r^*$) extended in to the origin. In scattering problems only K is needed; in the treatment of nuclear interpenetration, K from (14a) is substituted into (14b) to find c, giving the ratio between the amplitudes of the wave function in the inner and outer regions. The derivatives appearing in (14a) are independent of scale:

$$r d\Phi/dr = \rho d\Phi/d\rho = -z d\Phi/dz,$$

etc. Eqs. (6) and Tables I and II give the information needed for applying the corresponding functions to collision problems.

DECEMBER 1, 1937 PHYSICAL REVIEW VOLUME 52

The Nuclear Moment of Barium

A. N. Benson and R. A. Sawyer
University of Michigan, Ann Arbor, Michigan

(Received October 20, 1937)

New data have been obtained on the hyperfine structure of several lines of barium. These have been studied in the attempt to determine more definitely the nuclear moment of the odd isotopes of barium, reported as $2\frac{1}{2}$ by Kruger, Gibbs and Williams, and as $1\frac{1}{2}$ by Schüler and by Murakawa. Studies of the separation of the $6^2S_{\frac{1}{2}}$ and $7^2S_{\frac{1}{2}}$ components from the center of gravity, and of the spacing and patterns of the 5^3D_3 and 6^3P_2 terms all lead to the conclusion that $I=1\frac{1}{2}$ is the correct value of nuclear moment.

IN spite of several researches on the subject, the value of the nuclear moment of the odd isotopes of barium remains in doubt. The various investigators differ both in experimental findings and in interpretation of the data. McLennan and Allen[1] first found hyperfine structure in a number of the arc and spark lines of barium, but their results have never been confirmed by other workers. Frisch[2] found all lines sharp. The first accurate observations were those of Ritschl and Sawyer[3] who observed structure in several lines and published measurements on the resonance lines of Ba II, $6^2S_{\frac{1}{2}}-6^2P_{\frac{1}{2},\frac{3}{2}}$, from which Schüler and Jones[4] deduced $1\frac{1}{2}$ as the nuclear moment of the odd isotopes. However, from their own measurements on the same lines, Kruger, Gibbs, and Williams[5] concluded that the moment is probably $2\frac{1}{2}$, while Murakawa,[6] from observations on these and other lines, considered $1\frac{1}{2}$ to be correct. Recent compilations of nuclear moments[7-9] have given $2\frac{1}{2}$ as the moment of barium but have indicated that uncertainty exists.

The difficulty in the determination of the moment from hyperfine structure observations arises from the fact that barium is a mixture of several isotopes. The recent measurements of Sampson and Bleakney[10] give for the isotopes and their percentage abundance:

mass number	130	132	134	135	136	137	138
percentage	0.16	0.015	1.72	5.7	8.5	10.8	73.1

The even isotopes thus make up 83.5 percent of the atoms and all observers are agreed that these even isotopes, in common with all observed even isotopes save N^{14}, have no hyperfine structure. In all barium h.f.s. patterns, the five even isotopes fall together in a very heavy central

[1] McLennan and Allen, Phil. Mag. **8**, 515 (1929).
[2] Frisch, Zeits. f. Physik **68**, 758 (1931).
[3] Ritschl and Sawyer, Zeits. f. Physik **72**, 36 (1931).
[4] Kallman and Schüler, Ergebn. d. Exakt. Naturwiss. **11**, 134 (1932).
[5] Kruger, Gibbs, and Williams, Phys. Rev. **41**, 322 (1932).
[6] Murakawa, Sci. Papers Tokyo I. P. C. R. **18**, 304 (1932).
[7] White, *Introduction to Atomic Spectra* (McGraw Hill, 1934), p. 372.
[8] Darrow, Bell Tech. J. **14**, 319 (1935).
[9] Bacher and Bethe, Rev. Mod. Phys. **8**, 82 (1936).
[10] Sampson and Bleakney, Phys. Rev. **50**, 456 (1936).

TABLE I. *Observed hyperfine structure in barium.*

	CLASSIFICATION	PLATE SEPARATIONS	POSITIVE COMPONENT	NEGATIVE COMPONENT
4554.0	Ba II $6^2S_{\frac{1}{2}}-6^2P_{1\frac{1}{2}}$	10	0.152 cm^{-1}	0.100 cm^{-1}
4934.1	Ba II $6^2S_{\frac{1}{2}}-6^2P_{\frac{1}{2}}$	10, 12	0.174	0.118
4579.7	Ba I $6s6p^3P_2-$"12"	10, 12, 17.5	0.100	0.098
4620.0	Ba I $6s6p^3P_0-6s8s^3S_1$	12	0.106	0.166
4691.6	Ba I $6s6p^3P_2-6p^2\,^3P_1$	10, 12, 22, 30	0.093	0.078
5519.1	Ba I $6s6p^3P_1-6s6d^3D_2$	12	0.078	0.045
5680.2	Ba I $6s5d^3D_2-$"5^0"	7.5, 22, 30		0.113
6110.8	Ba I $6s5d^3D_3-fd6p^3P_2$	17.5, 19.5, 30	0.055, 0.095	0.063

component which tends to obscure the detail of the structure due to the two odd isotopes.

EXPERIMENTAL

The barium spectrum was excited in a water-cooled hollow cathode discharge tube in an atmosphere of helium. The current used varied from one-tenth to one ampere on different plates. The spectrum was studied with a Fabry-Perot interferometer, with quartz plates. The plates were silvered by evaporation with an apparatus similar to that of Ritschl.[11] Various plate separations, from ten to thirty millimeters, were employed. The interferometer was used both with a large Littrow glass spectrograph and with a two-prism glass spectrograph.

Measurable hyperfine structure was found in a number of lines. Table I gives the results and shows, for each line, its classification, the plate separations used, and the separation of the components from the heavy central component due to the even isotopes. In each case, the result is the average of measurements from several plates.

DISCUSSION OF RESULTS

Since few of the barium hyperfine structure patterns are completely resolved and all are obscured by the heavy central component already mentioned, indirect methods must be used to determine the nuclear moment. Murakawa and Kruger, Gibbs, and Williams relied on the intensity ratios of the components of the 6^2S-6^2P lines of Ba II. This is, at best, a difficult and uncertain procedure and liable to errors due to plate background, plate calibration, and other experimental troubles which may easily lead to false conclusions, since the intensity ratios for different spins differ but little. Thus Schütz, in his work on the intensity ratios of the hyperfine structure of the blue caesium doublet, at first reported $I=1\frac{1}{2}$[12] and in a later correction[13] gave $4/2\leq I\leq 7/2$ with $I=2\frac{1}{2}$ as probable, while the correct value is now known to be $I=3\frac{1}{2}$.[14] Schüler and Jones do not explain their procedure but perhaps used the separations of the components of the Ba II resonance line $6^2S_{\frac{1}{2}}-6^2P_{1\frac{1}{2}}$ from the center of gravity. This method involves an assumption as to the presence of isotopic shift and is hardly adequate as a sole criterion. In the present work an attempt has been made to bring to bear evidence from several points of view in order to strengthen the conclusion.

The most direct method of approach is that mentioned above—the separations of the components of the $^2S_{\frac{1}{2}}$ terms from their center of gravity. The combination of a $^2S_{\frac{1}{2}}$ term with a term of no structure or unresolved structure gives rise to a pattern of only two components for all values of I, since the multiplicity is $(2J+1)$, but the relative intensities and separations depend on I. The intensities are proportional to $2F+1$ and the distances from the center of gravity are thus inversely proportional to $2F+1$. Since the F values are $I+\frac{1}{2}$ and $I-\frac{1}{2}$, the distances must be proportional to I and $I+1$. The line $6^2S_{\frac{1}{2}}-6^2P_{1\frac{1}{2}}$ is convenient for the test, since the structure of $6^2P_{1\frac{1}{2}}$ is probably small and has never been resolved. If we assume no isotope shifts, and no effect from the $6^2P_{1\frac{1}{2}}$ splitting, then the ratio of the distances of the hyperfine structure components should be equal to the ratio of I to $I+1$ and I may be computed.

[11] Ritschl, Zeits. f. Physik **69**, 578 (1931).

[12] Schütz, Naturwiss. **19**, 774 (1931).

[13] Schütz, Naturwiss. **19**, 1007 (1931).

[14] Kopfermann, Zeits. f. Physik **73**, 437 (1931).

The line, λ4554 has been examined by several observers with the results listed in Table II. The evidence clearly favors $I=1\frac{1}{2}$ over any other odd multiple of $\frac{1}{2}$. The variation in values indicates the difficulty of measuring these patterns, which are not completely resolved from the central component.

In the above calculation we have taken simply the distances of the unresolved components from the central components. In analyzing their data, Kruger, Gibbs, and Williams assumed that the $^2P_{1\frac{1}{2}}$ level had both a splitting of 0.033 cm^{-1} and an isotopic shift of 0.017 and concluded that, assuming no shift for $^2S_{\frac{1}{2}}$, its odd levels had separations of 0.113 and 0.159. These separations would lead to a value of I, by the above method, of 2.45. As a partial check, however, on this interpretation of $^2P_{1\frac{1}{2}}$ we may consider the line, $6^2P_{1\frac{1}{2}}-7^2S_{\frac{1}{2}}$, λ4899.9, which was resolved by Murakawa. He assigned the splitting, +0.043 and −0.027, to 7^2S. The above method of calculation gives, then, $I/I+1=0.027/0.043$ or $I=1.68$, in good agreement with the calculations on $6^2S_{\frac{1}{2}}$, and in support of the idea of small isotope shift and small $6^2P_{1\frac{1}{2}}$ splitting. The analysis of the $6^2P_{1\frac{1}{2}}-7^2S_{\frac{1}{2}}$ may also be studied graphically. In Fig. 1, is shown at the right, above, the level scheme, and below, the resulting grouping of the components about the central components for Murakawa's data and assignment. In Fig. 1 left, is shown the level scheme and line appearance on the assumption by Kruger, Gibbs, and Williams of no $7^2S_{\frac{1}{2}}$ splitting, and of splitting and isotope shift in $6^2P_{1\frac{1}{2}}$. In Fig. 1 center, is a combination of both Kruger's and Murakawa's idea. The former's value for $6^2P_{1\frac{1}{2}}$ splitting is used while Murakawa's $7^2S_{\frac{1}{2}}$ splitting is used but with a center of gravity corresponding to $I=2\frac{1}{2}$. It is clear that neither the left or central figures represent structures which are in accordance with Murakawa's data.

TABLE II. *Nuclear moment of barium computed from λ4554.*

OBSERVER	$I/(I+1)$	I
Murakawa	0.099/0.154=0.64	1.80
Kruger *et al.*	0.085/0.164=0.52	1.07
Ritschl and Sawyer	0.09 /0.16 =0.56	1.30
Benson and Sawyer	0.100/0.152=0.66	1.92
	Mean	$1.52\pm0.17(\pm\Sigma d/n^{1\frac{1}{2}})$

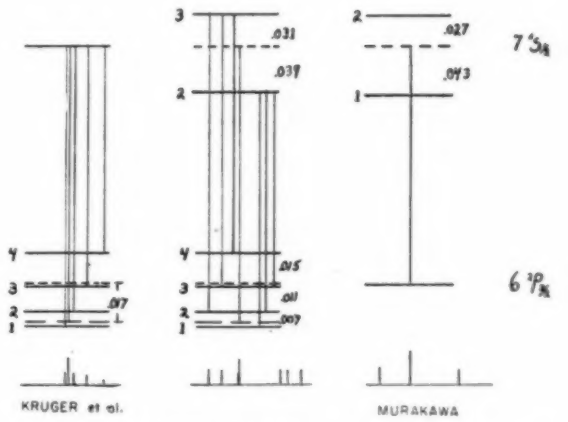

FIG. 1. Level scheme and line structure of $6^2P_{1\frac{1}{2}}-7^2S_{\frac{1}{2}}$, 4899.9. 1. According to Murakawa's data and assignment (right). 2. According to the Kruger, Gibbs, and Williams explanation of splitting and shift of the $6^2P_{1\frac{1}{2}}$ term (left). 3. According to a combination of the two assignments (center).

Further evidence on the nuclear moment of barium may be obtained from the Ba I line $6s5d^3D_3-5d6p^3P_2$, λ6110.8, which has been resolved into four components in this work, as well as by Murakawa and by Ritschl and Sawyer (unpublished material). The structure must be due to the $^3D_3$ term, for little structure would be expected in the $^3P_2$ term since it has no s electron. Furthermore, Murakawa found the same structure in $6s5d^3D_3-5d6p^3D_3$, λ6498.78, which is beyond the present range. The term $^3D_3$ should have four components for $I=1\frac{1}{2}$, or six for $I=2\frac{1}{2}$, but, if the interval rule is obeyed, the spacing should be quite different in the two cases. Fig. 2 shows how the $^3D_3$ level would appear if I were $1\frac{1}{2}$ and if it were $2\frac{1}{2}$. Since the center of the pattern is obscured by the even component, the best approach is to consider the ratio of the spacing of the two components with smallest F to the over-all width. From the Landé interval rule, for $I=1\frac{1}{2}$, this is $5/21=0.238$, while for $I=2\frac{1}{2}$, it is $3/55=0.085$. If, in the latter case, the farthest component was not observed, the ratio of the next two components to the total width would be $5/31=0.155$. The observations give:

Murakawa	0.037/0.156=0.238
Ritschl and Sawyer	0.032/0.147=0.218
Benson and Sawyer	0.038/0.156=0.244

The data points definitely to $1\frac{1}{2}$ as the value of the nuclear moment, and it may be emphasized

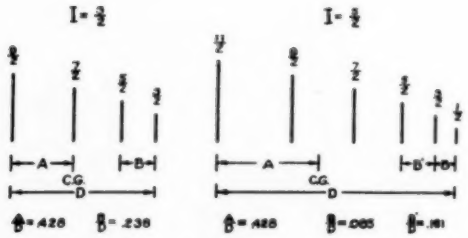

FIG. 2. Splitting of the $^3D_3$ term if $I=2\frac{1}{2}$ (right) and if $I=1\frac{1}{2}$ (left).

that the ratios used do not depend on the assumption that the isotope shift is zero. As proof that the outermost and weakest component was observed, we may consider the ratio of the separation of the strongest line from the center of gravity to the over-all width. The ratio is 0.428 both for $I=1\frac{1}{2}$ and $I=2\frac{1}{2}$, while, if the faintest component were missed, it would be 0.563 for $I=1\frac{1}{2}$ and 0.470 for $I=2\frac{1}{2}$. The measurements are:

Murakawa	0.060/0.156=0.348
Ritschl and Sawyer	0.057/0.147=0.388
Benson and Sawyer	0.063/0.156=0.404

The indication is that 0.428 is the ratio and that the isotope shift, if any, is small, since the amount of isotope shift required to bring the above ratios to exactly 0.428 is:

Murakawa	0.007
Ritschl and Sawyer	0.006
Benson and Sawyer	0.003

The conclusion is that the outermost component was observed, and the first ratios quoted give a very definite preference for $I=1\frac{1}{2}$ rather than $2\frac{1}{2}$, since the ratios are widely different in the two cases.

Further evidence from λ6110.8 is given in Fig. 3, which shows a graphical comparison of the expected and observed structures for a $^3D_3$ term. The lines above the horizontal line show the experimental values obtained by Murakawa and by the authors, while the lines below show the expected structure, drawn with the same over-all width for $I=1\frac{1}{2}$ and for $I=2\frac{1}{2}$. It will be noted that the experimental results are in good agreement with $I=1\frac{1}{2}$. The fact that the values fall a little to the left of the calculated positions with respect to the center of gravity (placed at the central even component) indicates a possible small isotopic shift.

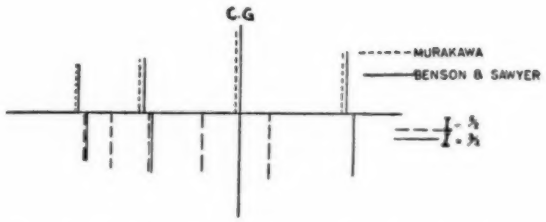

FIG. 3. The upper part shows the observed data of Murakawa and of Benson and Sawyer, for the line $6s5d^3D_3 - 5d6p^3P_2$, 6110.8. The lower part shows the expected structure, with the same over-all spread as observed, from a $^3D_3$ term if $I=1\frac{1}{2}$ and if $I=2\frac{1}{2}$.

Similarly the structure of the lines λ4691.6 ($6s6p^3P_2 - 5d6d^3P_1$) and λ4579.7 ($6s6p^3P_2 - 5d6d^1D_2$) is shown graphically in Fig. 4. Although the structure is slightly different, it may be safely assumed to arise essentially from the level 6^3P_2. The structures below the lines in the graph are those for $^3P_2$ with the over-all widths adjusted to be the same as those of the observed structures. It will be seen that only the structure for $I=1\frac{1}{2}$ can be brought into harmony with the observations.

The Goudsmit and Bacher constant a_1[12] has been calculated for several of the lines and comes out nearly a constant, both for $I=1\frac{1}{2}$ and for $I=2\frac{1}{2}$. The evidence is not directly in favor of either value of nuclear moment, but since, in two of the lines, the distance from center of gravity to the outer component was used, instead of over-all width, the agreement of the values means small isotope shifts. As we have seen, the assumption of small isotope shifts is in better accord with the correlation with $I=1\frac{1}{2}$ than with $I=2\frac{1}{2}$. The computed values for A and a_1 are given in Table III. It will be noted that the only considerable variations are in the ^3D terms. Similar deviations were noted by Goudsmit and

TABLE III. *Computed values of A and a_1 for barium.*

LINE	CONFIGURATION	EXP. TOTAL WIDTH	A FROM $I=1\frac{1}{2}$	A FROM $I=2\frac{1}{2}$	a_1 FROM $1\frac{1}{2}$	a_1 FROM $2\frac{1}{2}$
4620	$6s8s^3S_1$	0.274	0.068	0.045	0.100	0.067
4691	$6s6p^3P_2$	*	0.026	0.016	0.104	0.062
4579	$6s6p^3P_2$	0.198	0.026	0.016	0.106	0.066
6111	$6s5d^3D_3$	0.156	0.015	0.009	0.089	0.054
5680	$6s5d^3D_2$	*	0.038	0.023	0.152	0.090

* In the case of two of the lines above, the distance from the center of gravity to the strongest component, was measured and then from this value A was computed. In the other cases A was obtained from the over-all width.

Bacher in the ^3D terms of the analogous Tl II spectrum.

Conclusion

It has been assumed throughout the preceding discussion that the even isotopes have no spin and the line due to each of them falls undisplaced and unresolved at the center of gravity. These assumptions seem to be established within the limits of the resolution attained. The spectra of the two odd isotopes are also assumed to fall together and to have the same nuclear moment, as happens in most known similar cases. The evidence given on the basis of the separation of the components from the center of gravity, on the basis of the spacing, and on the basis of the patterns of the various lines, while not absolutely conclusive, when taken with the intensity measurements of Murakawa, seem to point quite convincingly to a value of $I=1\frac{1}{2}$ for the nuclear moment of the odd isotopes of barium.

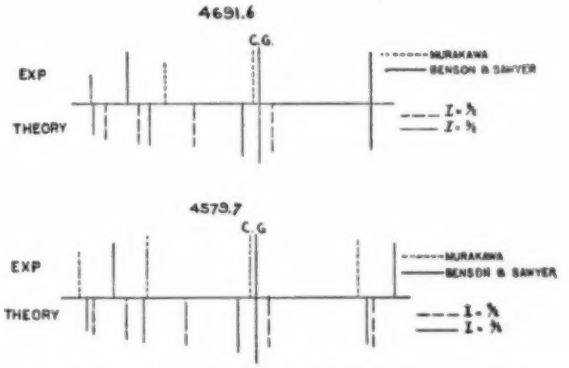

FIG. 4. The observed and expected structures are shown for $6s6p^3P_2-5d6d^3P_1$, 4691.6, and for $6s6p^3P_2-5d6d^1D_2$, 4579.7, on the assumption that the structure is due to the $^3P_2$ term. The calculated structures are given both for $I=1\frac{1}{2}$ and for $I=2\frac{1}{2}$ and are drawn to have the same over-all width as the observed patterns.

DECEMBER 1, 1937 PHYSICAL REVIEW VOLUME 52

The Production of Cosmic-Ray Showers at Great Depths

W. H. PICKERING
California Institute of Technology, Pasadena, California

(Received October 18, 1937)

Experiments are described which prove the existence of cosmic-ray showers consisting of at least three particles, at depths down to 30 meters of water below sea level. The experiments also show that the number of showers decreases in much the same way with depth as the number of vertical coincidences. Even in the first few meters of water there is no marked falling off in the relative number of showers. The effect of lead on the showers at great depths is also discussed.

EXPERIMENTS by various observers[1] have shown that as one ascends towards the top of the atmosphere the cosmic-ray showers measured by three Geiger counters placed below a thin lead plate, increase much more rapidly than the general radiation. The rate of increase is approximately exponential with an absorption coefficient of about 0.5 per meter of water. If an absorption at this rate continued below sea level, it is clear that a comparatively thin layer of water above the counters would eliminate the showers almost completely. Measurements of the showers at points below sea level have been made by Rossi,[2] Follett and Crawshaw,[3] Pickering,[4] and others. The published results, however, are not in good agreement, and in an attempt to clear up the matter further experiments have been performed by the writer.

As in the previous work, the counters were placed in a tunnel in the Morris Dam of the city of Pasadena. This tunnel goes straight down a 45° slope to the bottom of the lake behind the dam. At the top of the arch of the tunnel the minimum thickness of reinforced concrete varied from about 8 in. to 18 in. as one went down the

[1] Woodward, Phys. Rev. **49**, 711 (1936); Braddick and Gilbert, Proc. Roy. Soc. **156**, 570 (1936); and many others.

[2] Rossi, Ricerca Scient. **5**, 93 (1934).
[3] Follett and Crawshaw, Proc. Roy. Soc. **155**, 546 (1936).
[4] Pickering, Phys. Rev. **47**, 423 (1935).

TABLE I. *Observed counting rates; counts per minute.*

ARRANGEMENT OF COUNTERS	POSITION OF COUNTERS			
	WATER LEVEL	9 m WATER	13 m WATER	30 m WATER
Vertical	19.0 ±0.1	14.9 ±0.1	11.8 ±0.1	5.40±0.02
Shower, no lead	1.98±0.03	1.17±0.04	1.10±0.07	0.44±0.01
Shower, 0.6 cm Pb	1.80±0.06	1.1 ±0.13	—	0.51*±0.01
Shower, 1.6 cm Pb	1.92±0.04	1.21±0.02	—	0.49±0.01
Shower, 2.8 cm Pb	—	—	—	0.39±0.03
Horizontal, no lead.	—	—	0.41±0.01	0.18±0.01
Horizontal, 0.6 cm Pb	—	—	—	0.18±0.02
Horizontal, 1.2 cm Pb	—	—	0.33±0.01	0.21±0.03

* For this reading the area of the lead plate was larger than usual.

tunnel. For the experiments two sets of counters were used. One set, measuring showers, was placed with the counter axes horizontal and approximately in the center line of the tunnel. The other set, measuring the vertical intensity, was nearer the side of the tunnel, hence the radiation reaching this set, after passing through the same thickness of water, had to penetrate perhaps twice as much concrete as the radiation reaching the shower set. Readings were taken at four elevations: (1) just above the water level, (2) under about 9 meters of water, (3) under about 13 meters of water, and (4) under about 30 meters of water. At this last station a complication was introduced by the fact that an unknown quantity of rock had fallen on to the top of the tunnel from a slide above the tunnel entrance. Because of the depth of water at this point no attempt was made to estimate the amount of this rock.

The apparatus used in this work was that used in a sea-level study of the variation of the showers with latitude, and has been described elsewhere.[5] Although this equipment worked well on a long ocean voyage, the extreme humidity in the tunnel caused some trouble. The tunnel is primarily for drainage purposes and a great deal of water is carried through it. Under certain wind conditions a thick mist was formed, and this deposited moisture on all parts of the apparatus. The use of a heater helped matters somewhat, but even then trouble occurred. The arrangement of the counters and the lead was the same as that used in the sea level work. At two depths some readings were also taken with one set of counters arranged in a horizontal plane with about 25 cm separation between the outside counters. With this arrangement a thin lead plate could be put over the whole effective area of the counters.

[5] Neher and Pickering, Phys. Rev. (In preparation.)

In Table I the results are summarized. The counting rates in each case are counts per minute. The probable errors have been computed from the total number of counts in each reading. The accidental counting rate is very low, and furthermore it seemed to change with depth in roughly the same manner as the real coincidences, so that no effort has been made to correct for this. In order to show the effects of depth more clearly the readings have been adjusted with those at the highest elevation 1.00 in each case. These relative values are shown in Table II.

We first note that these results show definitely the existence of showers beneath great depths of water. Thus at the greatest depth, where a counting rate of about 0.5 per minute was obtained with the counters in the shower position, removing one of the counters to a great distance so lowered the counting rate that only one count was obtained in a 35 minute run. To exclude the possibility that the coincidences in this shower position were due to ordinary secondaries, for two particles could cause a coincidence with this arrangement, readings were taken with the counters in a horizontal plane. For a single particle to cause a coincidence in this case it has to make an angle of less than 20° with the horizontal. Because of the location of the dam in a deep canyon, such a ray would have to penetrate an enormous thickness of rock, and hence it can be definitely asserted that no single ray could pass through the three counters. There is still the possibility that two particles could cause a coincidence, but again, because of the geometry of the arrangement, this process can be excluded as being too rare to be significant. Hence (with this arrangement of the counters) all real coincidences must be due to showers of three or more particles originating in the material above the counters. Experimentally it was found that at the greatest depth the counting rate with two counters in the horizontal position and the third far removed was

TABLE II. *Relative counting rates.*

ARRANGEMENT OF COUNTERS	POSITION OF COUNTERS			
	WATER LEVEL	9 m WATER	13 m WATER	30 m WATER
Vertical	1.00	0.78	0.62	0.28
Shower, no lead	1.00	0.59	0.55	0.22
Shower, 0.6 cm Pb	1.00	0.6	—	0.28
Shower, 1.6 cm Pb	1.00	0.63	—	0.25

0.014 ± 0.003 per minute. With the three counters in position the rate was 0.18 ± 0.02 per minute, about 13 times the chance count. In view of this result it seems reasonable to ascribe most of the coincidences observed with the counters in the usual shower position, to real showers.

With the experimental evidence that showers exist at great depths conclusive, it follows that the shower producing radiation below sea level is not absorbed as fast as the absorption coefficient 0.5 per meter of water would indicate. The above experiments do not allow an accurate estimate of the rate of absorption of the radiation because of the irregular distribution of matter around the counters. However, the data do show that at depths somewhat below sea level the showers vary in much the same way as the vertical radiation. The ratio of vertical counting rate to the maximum shower counting rate at sea level is about 12, and at these points below sea level it is not very different from this value. If it is valid to make this comparison, then support is given to the results of Follett and Crawshaw,[3] rather than to those of Clay.[6] The latter found that the ratio went to twice its sea-level value, while the former observed no marked change.

An obvious feature of these measurements is the fact that the lead caused practically no change in the counting rates at all stations. In a previous paper the writer reported a similar result.[4] However, at that time this was interpreted as meaning that there were very few showers below sea level. The counting rates without lead were tacitly assumed to be solely due to the chance coincidences. The new data show that this was not correct, and that the number of showers produced in the lead is apparently not proportional to the intensity of the shower producing radiation. The reason for this lies in the fact that the concrete above the counters was heavily reinforced so that it could almost be regarded as an iron plate. That this is significant is beautifully shown by Schindler's transition curves,[7] which indicate that with large thicknesses of iron above an electroscope, the addition of lead between the iron and the electroscope causes an immediate decrease in the ionization. At intermediate thicknesses of iron no change is produced with small thicknesses of lead, and with very little iron, the addition of a thin lead plate increases the ionization. Since these transition effects are surely connected with the shower phenomena, one would expect the shower effects measures with Geiger counters to behave in the same way. A direct experiment with counters does indeed show a similar result. Thus, with a certain shower arrangement, the addition of lead above the counters caused a maximum increase in the counting rate of about 5 counts per hour. With 2 cm of iron above the lead the maximum increase was only 2 counts per hour, and furthermore, the thickness of lead required to produce this increase was about half the initial thickness. From these results it is easy to see that at the Morris Dam with the thickness of iron above the counters perhaps 20 cm, the addition of lead above the counters could cause no increase in the counting rate. It is perhaps worth noting that this explanation must almost certainly account for Rossi's results.[2]

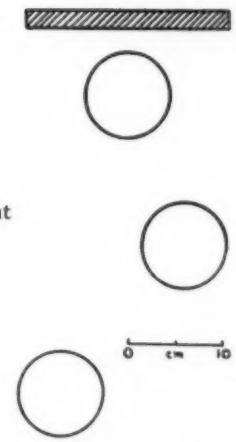

FIG. 1. Arrangement of counters.

Having shown that at depths somewhat below sea level the showers vary in much the same way as the vertical radiation, there still remains the interesting question: what happens in the first few meters of water? Earlier in this paper it was noted that the evidence seemed to indicate that the ratio of showers to vertical rays remained essentially constant at all points below sea level, but the validity of this conclusion rested on a somewhat doubtful comparison. In order to gain further information on the matter the following experiment has been performed.

Three counters were grouped as shown in Fig. 1. The whole arrangement could be rotated about

[6] Clay, Physica **2**, 1042 (1935).
[7] Schindler, Zeits. f. Physik **72**, 625 (1931).

TABLE III. *Observed counting rate; counts per minute.*

Zenith Angle	Counters in Line	Counters in Shower Position		
		No lead	With lead	Due to lead
0	25.6	1.34	3.00	1.66
30°	18.1	0.91	2.07	1.16
60°	6.12	0.44	0.88	0.44
90°	0.87	0.52	0.64	0.12

TABLE IV. *Relative counting rates.*

Zenith Angle	Counters in Line	Counts Due to Lead with Counters in Shower Position
0	1.00	1.00
30°	0.71	0.70
60°	0.24	0.26
90°	0.03	0.07

a horizontal axis parallel to the axes of the counters. By alternately finding the counting rates with and without the 1.6 cm lead plate above the counters, the number of showers from a direction making a given angle with the vertical could be found. By displacing the two lower counters laterally until the three were in a straight line, the corresponding distribution of the single rays about the vertical was readily obtained. The ratio of showers to single rays then gives the relative shower producing efficiencies of rays which have traveled through different thicknesses of air. This assumes of course, that in this case, with only air above the apparatus the number of showers emerging from a 1.6 cm lead plate gives a true picture of the intensity of the shower producing radiation.

The results of these measurements are given in Table III. The counting rates in each case are counts per minute. Again, to show the results more clearly, the relative values are shown in Table IV.

In considering these results due regard must be paid to the fact that the geometrical arrangements in the two cases are different. Undoubtedly the solid angle from which showers are received is larger than the angle from which the straight rays must come, however, the exact size of this angle is difficult to estimate, and for the present investigation it is not necessary. The effect of the larger solid angle is to make the intensity at the larger zenith angles seem larger, and the magnitude of the addition to the intensity is, to a first approximation, proportional to the sine squared of the zenith angle (see, for example, Janossy).[8] Hence in our case the correction is quite small, and will not affect the validity of our conclusions.

At Pasadena the water equivalent thickness fo the atmosphere is about 10.0 meters, so that the additional air at zenith angles of 30° and 60°, is equivalent to 1.5 and 10.0 meters of water respectively. The above data show that with these additional thicknesses of air above the apparatus, the decrease in intensity of the showers measured as described above, is almost exactly equivalent to the decrease in intensity of the single particles. This result again implies that the radiation that can penetrate to depths far below sea level is just as efficient at producing showers as the whole radiation at sea level.

The results of these experiments may be summed up as follows.

(1) The existence of showers at great depths below sea level is well established. The positive result obtained with three counters in a horizontal line is clear evidence of the presence of showers of at least three particles. Furthermore the comparatively large separation of the counters in this case shows that the shower particles are spread over a large solid angle.

(2) The negative result obtained when lead is added above the counters does not show an absence of showers, but is due to the presence of a considerable thickness of reinforced concrete above the apparatus.

(3) At all depths below sea level the decrease in the number of showers is almost exactly equivalent to the decrease in the number of vertical coincidences. Therefore, at a depth below the top of the atmosphere of 10 meters of water, or perhaps a little less than this, the absorption coefficient of the shower producing radiation changes quite rapidly from a value of about 0.5 per meter of water, to a value of about 0.07 per meter of water.

In conclusion I wish to thank the water department of the city of Pasadena for their generous cooperation in making possible the experiments at the Morris Dam. I also wish to acknowledge my appreciation of the financial assistance rendered by the Carnegie Corporation.

[8] Janossy, Zeits. f. Physik **99**, 369 (1936).

The Spectrum of SnF

F. A. JENKINS AND GEORGE D. ROCHESTER*
Department of Physics, University of California, Berkeley, California

(Received September 24, 1937)

Measurements of the absorption bands of SnF are reported for the first time. Analysis of the frequencies of the band heads shows the presence of four doublet systems, all due to transitions from a doublet normal state X, of separation 2317.3 cm^{-1}. The various states are as follows:

STATE	ν	ω_e	$x_e\omega_e$	PROBABLE TYPE
X	0.0	582.9	2.69	$^2\Pi$
	2317.3	587.6	2.65	
A	34,108.4	676.7	2.65	$^2\Sigma$
B	40,834	594	—	$^2\Delta$
C	44,161.6	688.2	4.65	$^2\Pi$
	45,498.9	688.2	4.65	
D	46,326	598	—	$^2\Delta$
	46,427	607	—	
E	~41,000	—	—	—
F	~53,000	—	—	—

The transitions $E \leftarrow X$ and $F \leftarrow X$ give continua. The second component of $B \leftarrow X$ is probably masked by $E \leftarrow X$. Resolution of the Sn isotope effect is observed for the first time. A carbon tube furnace for studying absorption spectra is described.

THIS is the first of a series of investigations of the ultraviolet absorption spectra of the heavy metal halides under high dispersion. Plates have already been obtained for a number of these, using a newly constructed carbon tube furnace, and a 30,000 line/in. aluminum grating of 21 foot radius which permits the ultraviolet spectrum to be studied as far as the limit of transmisson of air. The fluorides are the most satisfactory for investigating the nature of the electronic states involved, not only because of their smaller moment of inertia, but also because of their freedom from the isotope effect which complicates the chloride spectra.

EXPERIMENTAL

The furnace used for vaporizing the salts proved to be unusually efficient and convenient. As shown in Fig. 1, it is of the "cartridge" type, in which the large cylindrical vacuum chamber can be rolled away from the end plate, on which the carbon tube and its various heat shields are rigidly mounted. Since the heated portion is almost entirely surrounded by a water-jacket, a rubber gasket can be used for the vacuum seal. The heating element A is a graphite tube 12 in. long, of $\frac{1}{2}$ in. internal diameter, and wall thickness 3/32 in. This is tightly wedged in at the ends by the tapered graphite blocks F,F bearing on water-cooled copper surfaces. Surrounding it is a graphite tube B which acts as the primary heat shield. Immediately outside this is an iron tube C perforated around its circumference by a row of holes near its junction to the end plate. This reduces loss of heat by conduction. The water jacket E is made from two brass cylinders with a clearance of only 1/16 in. between them. The space D is packed with loosely fitting sheets of molybdenum, which greatly increase the efficiency of the heat shielding. The current leads are two heavy copper tubes with internal water cooling. Insulation of one of these leads, and of the main water jacket, from the end plate is accomplished by

* Commonwealth Fund Fellow. Now at the University of Manchester, England.

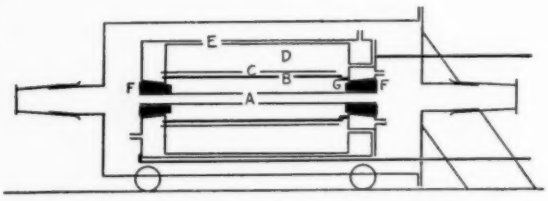

FIG. 1. Schematic diagram of furnace.

mica washers. The end of the graphite tube B is held in place by a lavite ring G.

The current is supplied at 15 or 20 volts by a large transformer. Temperatures were measured with an optical pyrometer, and preliminary trials showed that a temperature of 2000°C required a power of 9.1 kva, excluding transformer losses. For the present work it was found best to fill the furnace with nitrogen at atmospheric pressure to prevent diffusion of the fluoride vapor to the quartz windows.

The vapor of SnF was produced by heating equal parts of lead fluoride and metallic tin in a shallow graphite boat placed at the center of the heated tube. The source was a discharge through hydrogen at a pressure of 1 cm in a

TABLE I. *Band heads of SnF.*

$A \leftarrow X$ SYSTEM. HIGH FREQUENCY COMPONENT.

v' \ v''	0	1	2	3	4	5	6	7	8	9
0	34,155.3	33,577.6	33,005.3							
	144.8	568.1	32,996.6							
1	34,826.6	34,249.2	33,676.0	33,110.6						
	815.7	239.1	667.9	101.6						
2	35,493.0			33,777.2	—					
	481.0			768 5	33,208.1					
3	36,153.7	35,576.6	35,005.0			33,319.2				
	138.8	564.0	34,992.8			307.9				
4		36,232.8	35,661.0	35,094.2	34,533.5					
		219.4	649.2	084.0	524.3					
5	—	36,882.3	36,310.7	35,744.3	—	34,626.6				
	37,446.9	867.0	297.6	732.6	35,191.8	618.1				
6				36,389.6	35,827.1		34,721.3			
				376.4	814.6		711.9			
7				37,027.8	36,466.8	35,912.3		34,814.4		
				012.7	453.4	899.6				
8					37,100.8	36,544.1	35,993.7			
					085.8	531.9	981.5			
9						37,173.1	36,621.9	36,075.7		
						158.6	609.4			
10							37,244.3	36,699.3	36,158.4	
							230.4	687.7		
11								37,316.9	36,775.7	
								303.3		
12									37,388.6	36,852.3
									375.3	

$A \leftarrow X$ SYSTEM. LOW FREQUENCY COMPONENT.

v' \ v''	0	1	2	3	4	5	6
0	31,835.7	31,253.3	30,675.8				
	825.8	244.3	667.8				
1	32,507.4	31,925.7	31,347.9	30,775.9			
	496.8	916.1	339.3	768.2			
2	33,172.0	32,591.3		31,442.5	30,876.1		
	161.8	581.4		434.6	868.6		
3			32,675.4			30,973.9	
			664.9			965.6	
4			33,331.6	32,760.2			
			319.2	750.0			
5						32,282.3	
						273.8	
6							32,372.3
							362.3

$B \leftarrow X$ SYSTEM.

v' \ v''	0	1	2
0	38,522.8	37,941.5	
	516.2	933.9	
1	39,116.7	—	37,965.9
	106.9	38,528.2	958.2
2		—	
		39,093.3	
3			—
			39,067.3
4			
5			
6			

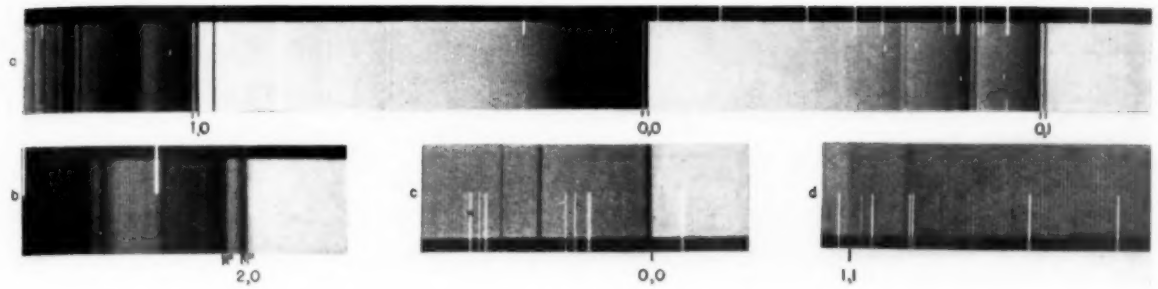

FIG. 2. (a) and (b) $^2\Sigma$, $^2\Pi$ system of SnF. (c) $^2\Pi$, $^2\Pi$ system of SnF. (d) V, N system of AgCl.

water cooled tube furnished with large aluminum electrodes in side tubes and having a quartz capillary of $2\frac{1}{2}$ mm internal diameter. With a current of 0.4 amp, suitably exposed plates were obtained from the grating in $\frac{1}{2}$ to 1 hour. Hilger Schumann plates were used in the region λλ2000–2600, and Eastman 40 plates for λλ2600–3800. The dispersion of the grating is 1.3 A/mm in this region of the first order. Three sets of plates were taken, at furnace temperature of 1320, 1480 and 1740°C, in order to bring out the strong and weak parts of the spectrum with suitable intensity for measurement. Measurements were made of all band heads, and of a few rotational lines, against iron arc standards.[1]

OBSERVATIONAL DATA

Whereas pure lead fluoride in the tube gave strong PbF bands, these are almost completely suppressed by the introduction of tin, and practically all of the molecular absorption observed appears to be due to SnF. Altogether seven band systems are found, of which six are definitely associated in pairs to form three doublet systems of wide separation. In addition, two strong continua occur, and it is probable that the other doublet component of the odd seventh system is obscured by (or perhaps represented by) one of these continua. All observed bands are degraded toward the further ultraviolet, and with the exception of one system ($C \leftarrow X$) all have fairly close double heads. It will be convenient to discuss these systems separately.

System $A \leftarrow X$, λλ2660–3260

This is the most extensive system observed, and its strongest bands begin to appear at a

TABLE I.—(*Continued*).

	$C \leftarrow X$ SYSTEM. HIGH FREQUENCY COMPONENT.					$C \leftarrow X$ SYSTEM. LOW FREQUENCY COMPONENT.		
v' \ v''	0	1	2	3	4	0	1	2
0	45,551.0	44,974.4	44,402.2					
1	46,228.9		45,080.9			42,573.1		
2	46,899.5	46,323.0			44,624.2	42,240.7	42,661.1	
3	47,560.3						43,320.6	
								43,403.0

	$D \leftarrow X$ SYSTEM. HIGH FREQUENCY COMPONENT.				$D \leftarrow X$ SYSTEM. LOW FREQUENCY COMPONENT.			
v' \ v''	0	1	2	3	0	1	2	3
0	46,351.3	45,774.2			44,118.4	43,536.2		
	343.2	767.4			110.8	528.6		
1	46,959.2	—	45,809.2		44,715.2	44,133.7	43,555.3	
	950.0	46,374.7	802.7		706.4	125.5	548.7	
2	47,536.3			45,852.3		44,728.4		43,573.7
	526.1			844.2		719.9		567.8

[1] W. F. Meggers and C. J. Humphreys, Nat. Bur. Stand. J. Research **18**, 543 (1937).

TABLE II. *Calculated and observed isotope shifts.*

BAND	MOLECULE	ρ^{-1}	$\Delta\nu_{calc}$	$\Delta\nu_{obs}$ (P HEADS)	$\Delta\nu_{obs}$ (Q HEADS)
2,0	$Sn^{116}F$	0.00235	3.02	2.8	2.7
	$Sn^{118}F$	0.00116	1.53	1.4	1.2
	$Sn^{120}F$	0.00000	—	—	—
	$Sn^{122}F$	−0.00112	1.58	1.6	1.4
	$Sn^{124}F$	−0.00221	3.22	3.2	3.0
1,0	$Sn^{124}F$	−0.00221	1.58	1.3	—
3,0	$Sn^{116}F$	0.00235	4.73	—	4.7
	$Sn^{118}F$	0.00116	2.33	—	2.3
4,1	$Sn^{116}F$	0.00235	4.87	4.5	5.0
	$Sn^{118}F$	0.00116	2.41	2.2	2.6
5,2	$Sn^{116}F$	0.00235	5.03	—	5.1
	$Sn^{118}F$	0.00116	2.49	2.5	2.5

furnace temperature of about 980°C. It consists of two electronic components, of separation 2317.3 cm^{-1}. The band structure and intensity distribution in the two components are exactly alike, but the high frequency component is much more intense. This shows that the doubling is in the lower state, and the observed ratio of intensities is consistent with the ratio 6 to 1 calculated from the Boltzmann factor for 1800°K.

Fig. 2(a) is an enlargement of the three strongest sequences as they are developed at 1600°C. Wave numbers of the band heads are given in Table I. The two values for each vibrational transition refer to the two heads, P and Q, observed for each band. The Q heads are represented by the equation

$$\nu = \left.\begin{matrix}34{,}108.4\\31{,}791.1\end{matrix}\right\} + 676.7u' - 2.65u'^2 - \left.\begin{matrix}582.9\\587.6\end{matrix}\right\}u'' + \left.\begin{matrix}2.69\\2.65\end{matrix}\right\}u''^2,$$

where $u=v+\frac{1}{2}$.

All heads except those of the 0,0 and 1,1 bands show evidence of the tin isotope effect. This is especially well resolved for the 2,0 band (Fig. 2(b)), where each head is split into five nearly equally spaced components, the two low frequency ones being much weaker than the other three. According to Aston, tin has 11 isotopes, but the above is just the pattern expected[2] when one takes into account only the more intense and favorably situated bands. Table II lists the observed and calculated isotope shifts for some of the more easily measured cases. For all bands on the short wave side of the system origin, the measurements of Table I refer to the first strong head, due to $Sn^{120}F$. For those on the long wave side, they probably represent $Sn^{116}F$ heads, but the isotope heads were not resolved on this side.

It was possible to measure a short series of structure lines between the P and Q heads of the 0,0 band in both components. These gave the same average second difference of 0.031 cm^{-1}, so that the value of $B'-B''$ is 0.015.

System $B\leftarrow X$, λλ2556–2635

This lies at the long wave end of the continuum $E\leftarrow X$ (see below), and is partly blotted out by it at the highest temperature. The vibrational constants are very nearly the same in the upper and lower states so that the bands in each sequence are very closely spaced. In fact, there appears to be a reversal in direction for the sequence $\Delta v=+1$. Under these conditions the band heads are a very poor representation of band origins, and there is little point in giving an equation for heads. Each band shows two heads, P and Q, with the Q head about half as intense as the P. Data for both are given in Table I, and indicate a value for $\Delta G_{\frac{1}{2}}'$ of about 594 cm^{-1}.

System $C\leftarrow X$, λλ2100–2350

The bands of this system (see Fig. 2(c)) have single heads, and the system as a whole is considerably less intense than those described above. It is about 1/10 as intense as the $D\leftarrow X$ system, which it overlies, and is well developed only at the highest temperature used. Only two sequences of the low frequency component could be found. This is presumably due to the others being masked by the $E\leftarrow X$ continuum. The v numbering for the observed bands is therefore somewhat uncertain, but that given in the table is indicated by both the intensity distribution in the sequences and by the ΔG values. There is a peculiar structure surrounding the two bands measured in the $\Delta v=+1$ sequence, consisting of what are apparently lines, band heads shaded in both directions, and regions of uniform absorp-

[2] A diagram of the predicted pattern is given by W. Jevons, Proc. Roy. Soc. **110A**, 387 (1926).

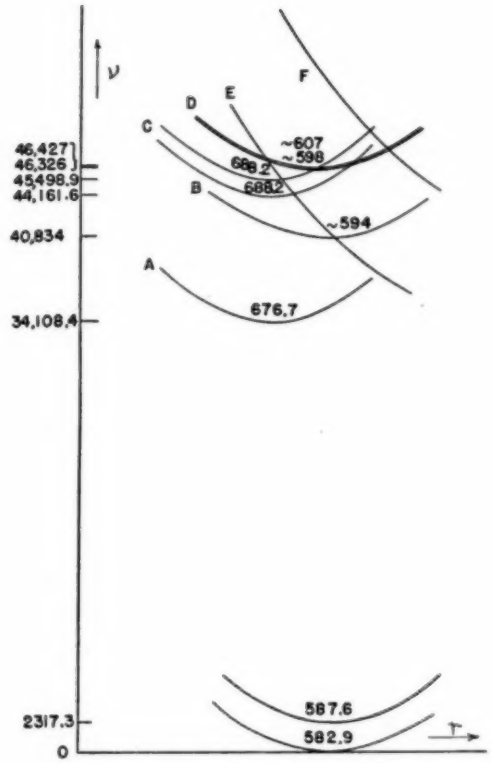

FIG. 3. Partial potential curves.

tion sharp on either edge. This is most likely due to strong perturbations. As in the case of the $A \leftarrow X$ bands, the low frequency component is much less intense. The heads of this system are given by the equations

$$\nu = 45{,}498.9 + 688.2u' - 4.65u'^2 - 582.9u'' + 2.69u''^2,$$

$$\nu = 41{,}844.3 + 688.2u' - 4.65u'^2 - 587.6u'' + 2.65u''^2.$$

The lower states are therefore the same as those of the $A \leftarrow X$ system.

A fairly long series of rotational lines could be measured in the 0,0 band (Fig. 2(c)). They gave an average second difference of $2(B'-B'') = 0.067$ cm^{-1}.

System $D \leftarrow X$, λλ2060–2300

This system is another wide doublet, with an intense high frequency component and a weak low frequency component. The bands are double headed, with the second head, or Q head, less intense. This difference in intensity is much more marked in the low frequency component. The system as a whole is of about the same intensity as the $A \leftarrow X$ system. Above 1480°C it is entirely masked by the overlapping $F \leftarrow X$ continuum (see below). The values of ΔG from the matrix diagram (Table I) do not show good agreement. Evidently this results from the fact that the heads are far from the origins, as was the case with $B \leftarrow X$. The approximate values of $\Delta G_1'$ are 607 and 598 cm^{-1} for the high and low frequency systems, respectively. The discrepancy between these values probably has little significance.

The isotope effect is evident in this system, as well as in all others discussed above, from a diffuseness of the heads further removed from the system origin. In the case of the 1,0 head of the present system, the isotope structure was resolved, and the isotope shifts were measured as 1.3 and 1.2 cm^{-1} for $Sn^{116}F$ and $Sn^{124}F$. These agree within the error of measurement with their computed values 1.47 and 1.38 cm^{-1}.

The continuous bands $E \leftarrow X$ and $F \leftarrow X$

These are two broad regions where the absorption is complete even at the lowest temperatures we used. Therefore all we can say about their intensity is that they are stronger than any of the discrete band systems. The width of the bands increases with temperature, and the approximate regions of absorption are as follows (estimated to half-absorption at either limit):

Temp.	$E \leftarrow X$	$F \leftarrow X$
1438°C	λλ2370–2500	−2010
1604	2360–2530	−2040
1860	2340–2580	−2300

It will be seen that the $F \leftarrow X$ continuum stretches toward short wave-lengths beyond the limit of observation, and that with increasing temperature it extends more rapidly toward long wave-lengths than does $E \leftarrow X$.

DISCUSSION

The spectrum of SnF should be analogous to the known spectra[3,4] of SnCl and of PbF. In SnCl, two band systems and two continua are known. The normal state is a wide doublet of

[3] W. Jevons, reference 2. Also W. F. C. Ferguson, Phys. Rev. **32**, 607 (1928).

[4] G. D. Rochester, Proc. Roy. Soc. **153A**, 407 (1936).

separation 2360.1 cm^{-1}, and shows the characteristics of a $^2\Pi$ state. In SnF the situation must be similar, since we observe wide doublet systems whose separation is of the above order of magnitude. To evaluate this separation, we must consider the nature of the excited states. The two known[5] excited states of SnCl are $^2\Delta$, at 28,665.3 and 28,939.2 cm^{-1}, and $^2\Sigma$, at 33,622.6 cm^{-1}. The $^2\Sigma$ state is much more tightly bound ($\omega_e=431.3$) than the $^2\Delta$($\omega_e=297.5$, 296.2).

The lower parts of the potential curves for the various states of SnF are shown in Fig. 3, approximately as they must lie according to our interpretation of the data. The curvature at the minimum was calculated from the observed ω_e, and the relative values of r_e estimated from the relation $\omega_e r_e^2=const.$ It will be seen that of the two lowest excited states one is more tightly bound than the other. We interpret state A as being $^2\Sigma$, and state B as $^2\Delta$, even though the order of the states is interchanged from the case of SnCl. It is difficult to say whether the $^2\Delta$ state is inverted with respect to $^2\Pi$ or not, because in either case the second component would probably not be observed. If the observed $B\leftarrow X$ system is the high frequency component, the low frequency one would be much weaker and probably masked by the $A\leftarrow X$ bands. On the other hand, if it is the low frequency component, the other component would fall in the $E\leftarrow X$ continuum. In Fig. 3 we have assumed the latter to be true, because no trace has been found of a lower frequency component, and because the observed $\Delta G''$ values are more nearly those of the upper $^2\Pi$ component. Neither of these reasons is conclusive, however, and actually the relative intensities of the P and Q heads is more nearly that expected for the high frequency component. A further reason for the above designation of states lies in the appearance of the bands. The $A\leftarrow X$ system resembles the $^2\Sigma\leftarrow{}^2\Pi$ system of SnCl. In both components the Q heads are about twice as strong as the P heads, as expected for this type of transition.

State C is unquestionably a second $^2\Pi$ state with a smaller doublet separation than that of the normal state. If the separation of the latter is taken as 2317.3 cm^{-1} from the $A\leftarrow X$ system, this upper $^2\Pi$ state must be inverted with respect to the lower one, with a splitting of 1337.3 cm^{-1}, since the observed separation of origins is 3654.6 cm^{-1}. This value is not too certain, however, for reasons mentioned earlier. The appearance of the bands is as expected for a $^2\Pi\leftarrow{}^2\Pi$ transition, since no evidence for a Q branch is present.

The bands of the $D\leftarrow X$ system have the appearance expected for a $^2\Delta\leftarrow{}^2\Pi$ transition. In particular, the lower relative intensity of the Q heads in the low frequency component[6] points to this conclusion. The general appearance of the system is much the same as that in the $^2\Delta\leftarrow{}^2\Pi$ bands of SnCl. Hence we may identify state D as another $^2\Delta$. It is not inverted, since the observed separation is 2216 cm^{-1}, leaving 101 cm^{-1} for the doublet separation of the state itself.

The potential curves for the repulsive states E and F are of course only drawn roughly in Fig. 3, but are so placed that the observed regions of absorption represent the range of most probable transitions.

No theoretical treatment has been given of the electronic states of the fluorides of the heavier metals near the middle of the periodic table. Further experimental data are obviously desirable.

[5] R. S. Mulliken, Rev. Mod. Phys. **4**, 59 (1932).

[6] See Ferguson, reference 3.

Extension of the Spectrum of AgCl

F. A. JENKINS AND GEORGE D. ROCHESTER*
Department of Physics, University of California, Berkeley, California
(Received September 24, 1937)

The absorption of AgCl vapor below λ2500 has been investigated with high dispersion. A new band system obeying the formula

$$\nu_{\text{head}} = 43{,}525.4 + 294.1u' - 1.70u'^2 - 342.8u'' + 2.14u''^2$$

has been found, and a fragment of another similar system. Strong continuous absorption is observed at higher pressures.

IT has been suggested by Mulliken[1] from a study of the electronic structures of the silver halides AgX that these molecules should show further absorption bands and continue below λ2500. The known spectrum of AgCl consists[2] of a single strong system in the region λλ3100–3400, designated by Mulliken $B \leftarrow N$. The positions and characteristics of the states above B are difficult to predict because of the strong interaction which is expected between them. The present investigation shows the existence of an extensive system covering the region λλ2100–2300, as well as part of another below λ2200 and a continuum at still shorter wave-lengths. Some of the characteristics of these transitions are in excellent agreement with Mulliken's predictions.

In exploring the absorption spectrum of AgCl vaporized in the carbon-tube furnace (see preceding article), we found on our low dispersion plates a set of rather faint bands below λ2300. These could only be seen when the temperature of the furnace was held between the rather narrow limits 1150 to 1220°C. At higher temperatures the system is blotted out by a continuous spectrum which extends to eventually join the absorption by the $B \leftarrow N$ system above 1700°C. The new 30,000-line/in. aluminum grating now in our 21-foot mounting proved admirably suited to the investigation of this region. With a hydrogen lamp of the conventional type, having a capillary of $2\frac{1}{2}$ mm internal diameter and carrying a current of 0.4 amp., it was possible to photograph the continuum on Schumann plates down to the beginning of the O_2 absorption bands at λ1950 with an exposure of $\frac{1}{2}$ hour. By carefully adjusting the current in the furnace, satisfactory plates of the AgCl absorption were obtained showing sharp bands as far as λ2100, below which they are masked by the continuous absorption.

The bands are all degraded toward the red and have a fairly open structure with the heads not pronounced. An enlargement of the 1,1 and 2,2 bands is shown in Fig. 2(*d*) of the preceding article. Resolution is not sufficient for an analysis by the combination principle. Measurements of the band heads were made against iron lines, using the new wave-lengths determined by Meggers and Humphreys.[3] The results are given in Table I, which includes all measured bands. Because of the indistinct character of the heads, some of the values are in error by several wave numbers. Many of the fainter heads appeared only as a rise in intensity of the structure lines from the preceding band, and the settings on these had to be made in a somewhat arbitrary manner.

The assignment of vibrational quantum numbers for the main system is definite. It is confirmed by the isotope effect, which, however, is not as clearly marked as in the longer wave-length system.[2] Each band has four heads, the pairs due to $Ag^{107, 109}$ having about one-ninth the separation of those due to $Cl^{35, 37}$. On the long wave-length side of the origin the Ag pairs were clearly resolved for the stronger bands, and the measurements of Table I refer to the first strong head, $Ag^{109}Cl^{35}$. On the short wave-length side the Ag pairs could not be separated, and the heads

* Commonwealth Fund Fellow. Now at the University of Manchester, England.

[1] R. S. Mulliken, Phys. Rev. **51**, 310 (1937).

[2] B. A. Brice, Phys. Rev. **35**, 960 (1930).

[3] W. F. Meggers and C. J. Humphreys, Nat. Bur. Stand. J. Research **18**, 543 (1937).

TABLE I. *Band heads of AgCl³⁵. The bands are shaded toward long wave-lengths.*

v' \ v''	0	1	2	3	4	5	6	7	8	9
0		43,162.0	42,823.8	42,487.7	42,154.1	41,823.0	41,490.4	41,168.0		
1		43,453.5	43,115.2	42,778.1	42,450.1			41,466.9	41,135.4	40,800.7
2	44,084.1	43,744.9	43,405.5			42,406.4	42,073.0			
3	44,372.8	44,032.1	43,693.1		43,025.3	42,693.1				
4	44,660.1	44,321.6		43,654.3	43,315.7					
5	44,945.6	44,608.0		43,930.4			42,935.3			
6	45,231.3									
7	45,512.7									
8	45,794.2									
9	46,070.5									
10	46,347.3									
11		46,283.2								
$v''\pm1$ \ v'	5	6	7	8	9					
0	47,466.4	47,138.8	46,814.2	46,490.2	46,165.6					
1		47,429.4	47,101.5							

due to Cl^{37} could only be measured with difficulty. Hence for these bands the measurements represent $Ag^{107}Cl^{35}$ heads. No correction has been made for this difference in view of the necessarily approximate character of many of the measurements. The measured isotope shifts are compared in Table II with their calculated values. The agreement is sufficient to establish the vibrational numbering and the carrier of the bands.

The band heads of the main system in Table I are represented by the equation

$$\nu = 43{,}525.4 + 294.1u' - 1.70u'^2 - 342.8u'' + 2.14u''^2,$$

where $u = v + \frac{1}{2}$. The constants for the vibrational energy G'' agree with those given by Brice[2] for the system $B \leftarrow N$, so that there can be no question that the two systems have the lower state N in common.

The vibrational intensity distribution is of the wide parabola type required by the Franck-Condon principle when there is a large change in moment of inertia between the initial and final states. The 0,0 band is entirely absent, and the intensity maxima in the $v'=0$ and $v''=0$ progressions come at $v''=4$ and $v'=6$, respectively. A rather marked secondary parabola appears below the main one.

In the lower part of Table I are given the data for seven additional bands which overlap the short wave end of the above system, and which apparently form part of a second system. The spacing and appearance of these bands are very similar to the above, and they probably form parts of two progressions $v'=0$ and 1, as indicated by the tentative assignment of quantum numbers in Table I. The assignments of v'' were made chiefly on the basis of the $\Delta G''$ values. Also there is a faint band 32.7 cm^{-1} to the violet of 0,6, which is probably the corresponding Cl^{37} head since the shift has about the right magnitude if the system origin is at about 48,800 cm^{-1}. If this system has a vibrational structure similar to the above, one could not observe bands of higher frequency than 0,5, because they are masked by the continuous absorption.

As regards the intensities of these systems as a whole, they are evidently much fainter than the

TABLE II. *Isotope shifts.*

v',v''	$\Delta\nu$(obs.)	$\Delta\nu$(calc.)
$Ag^{107}Cl^{35} - Ag^{107}Cl^{37}$ $\rho - 1 = -0.020577$		
6,0	29.1	34.30
5,0	26.0	28.72
4,0	22.5	23.01
$Ag^{109}Cl^{37} - Ag^{109}Cl^{35}$ $\rho - 1 = -0.020672$		
0,3	22.0	21.23
0,4	28.3	27.97
0,5	36.4	34.60
0,6	50.8	41.18
$Ag^{109}Cl^{35} - Ag^{107}Cl^{35}$ $\rho - 1 = -0.002264$		
1,3	2.1	1.67
0,4	2.9	3.06
0,5	3.8	3.79
1,8	5.4	5.26

$B \leftarrow N$ system. The latter is well developed at a furnace temperature of 1080°C, while no trace of our present bands is seen below 1150°C. The continuum has stronger absorption, as it begins to appear at the ultraviolet end at temperatures slightly below 1080°C.

Mulliken[1] predicts two transitions for this region, $V \leftarrow N$ and $Q_0 \leftarrow N$, of which the latter should probably give a continuum. The extended system described above is probably to be identified with $V \leftarrow N$. The bands are single-headed, as expected, and from the vibrational intensity distribution it can be concluded that r_e' is considerably greater than r_e''. This is also attested by some measurements of the rotational structure of the 1,1 band. A distinct series originating at the head could be measured, and followed the equation

$$\nu = 43{,}451.34 - 0.022M^2.$$

Thirty consecutive lines ($M = 16$ to 46) were measured. The value of $B' - B''$ is therefore -0.022, while B'' itself is of the order of 0.121 cm^{-1} according to Badger's relation I.[4] The most striking characteristic of our state V, however, is the fact that although r_e is much greater than in the normal state, ω_e is only very slightly less. Exactly the opposite behavior is observed in state B, which has nearly the same r_e as the normal state, but an ω_e which is even less than that we find for state V. These peculiarities of these states agree with the strong interaction between the various curves postulated by Mulliken.

It seems unlikely that our second system is $Q_0 \leftarrow N$, because it is so similar to $V \leftarrow N$. The strength of the continuum does not seem too great to ascribe it to $Q_0 \leftarrow N$.

[4] R. M. Badger, J. Chem. Phys. 2, 128 (1930).

DECEMBER 1, 1937 PHYSICAL REVIEW VOLUME 52

Temperature Determinations from Band Spectral Data

HAROLD P. KNAUSS AND MYRON S. MCCAY*
Mendenhall Laboratory of Physics, Ohio State University, Columbus, Ohio
(Received September 25, 1937)

A method of interpreting intensity distributions of lines in a band for determining the temperature of the emitter has been worked out which is independent of photometer calibration. The criterion used is the place in the band where adjacent lines of overlapping branches are of equal intensity, that is, the intersection of envelopes of the microphotometer records for the respective branches of a given band. The temperature is readily determined from graphs showing the temperature as a function of the J values at which the simultaneous requirements of equality of intensity and equality of frequency are satisfied in a given pair of branches. The method has been applied to the (0,1), (0,2), (0,3) and (0,4) bands of the Angstrom system of CO excited in the electrodeless ring discharge, both at room temperature and within a furnace at 365°C. Comparison of thermometer indications with the temperatures obtained by this method indicates (a) that the rotational energy distributions are characteristic of the temperature of the gas in the source, and (b) that the electrodeless ring discharge is a low temperature source of spectra. The error of the new method under favorable conditions may be as small as 5 percent of the absolute temperature.

INTRODUCTION

THE relative intensities of the lines in a band are determined by the proportionate numbers of molecules in the initial rotational states, and the transition probabilities for the states in question. If thermal equilibrium exists the intensity distribution can be computed from well-known formulas.[1] Even in cases where thermal equilibrium is obviously not attained, intensities may indicate a distribution of rotational energies corresponding to some effective rotational temperature. In particular, in a glow discharge where electronic bands requiring excitations of several volts are being emitted, the rotational energies may be in equilibrium with the unexcited molecules of the gas at a temperature only slightly above room temperature.

Although band intensity data have been used for estimating temperatures of both celestial and

* Now at Virginia Polytechnic Institute, Blacksburg, Va.
[1] W. Jevons, *Report on Band Spectra of Diatomic Molecules* (1932).

terrestrial sources, in only a few instances has the temperature been determined independently by conventional means. The investigation reported here was begun for the purpose of comparing rotational temperatures with thermometer readings in the electrodeless ring discharge maintained at various temperatures. Carbon monoxide gas was chosen for these experiments, because the bands of this molecule are so well known. The results for the Angstrom bands of CO are here presented, and a new method of interpreting the observations which uses the microphotometer essentially as a null instrument is described.

Experimental Procedure

A push-pull Hartley oscillator using two RCA 852 tubes operating at a frequency of 20 megacycles was the means of exciting the CO spectra studied. This oscillator was run at a power input of about 450 watts, the plate supply being furnished by a 2000-volt d.c. generator. The entire oscillator, including the tank coil within which the discharge tube was placed, was enclosed in a metal shield which limited radio-frequency radiation from the oscillator, thereby protecting sensitive devices elsewhere in the building.

The discharge tube had a plane quartz window and a quartz-to-Pyrex graded seal on one end, and a connection to the gas generator and vacuum system at the other end. The furnace around the discharge tube and tank coil was made up of double walls of asbestos board, with two 30 ohm, Nichrome heating units connected in parallel to the 110 volt a.c. line. Openings were provided for the light from the window and for the connection to the vacuum system. Temperatures were observed by simply placing a mercury thermometer within the tank coil near the discharge tube. With the heating current turned off, the enclosure nevertheless was hotter than room temperature because of heating by the discharge.

Carbon monoxide was produced by passing the vapor from concentrated formic acid (HCOOH) at reduced pressure over P_2O_5 which dehydrated the formic acid with the evolution of CO, and also eliminated most of the water vapor. A trap cooled by liquid air or dry ice removed all traces of vapor contaminations and no foreign spectra appeared in the CO discharge after baking the discharge tube and flushing it out several times with gas from the generator.

The gas generator and discharge tube were exhausted by means of a mercury diffusion pump backed by a Hyvac pump. A McLeod gauge was used to measure pressures. During a run the pumps were operated against a slow leak through a stopcock adjusted to maintain the desired pressure. This was held at an average value of 0.091 mm of Hg, with mean fluctuation of 0.003 mm, for an exposure of five hours.

Spectrograms were obtained by means of a 21-foot, 30,000 lines per inch grating in a Paschen-Runge mounting. This instrument has a mean dispersion in the visible wave-length range of 1.3 A/mm in the first order. For the region 2500–7000A in the first order Eastman 40 and hypersensitive panchromatic plates were used. The particular bands studied lie at the wave-lengths 4835, 5198, 5610, and 6080A. The slit was mounted at 13° from the normal to the grating, for minimum astigmatism [2]

Microphotometer traces for the bands investigated were made with a Moll, thermoelement instrument. The region covered by a single record was sufficient to include all the significant lines of a single band. For the purposes of this study, explicit intensity data were not required, and the indications of the microphotometer could be used without reducing them to true intensities, hence calibrations of the plates and of the photometer were dispensed with. In the following discussion, microphotometer deflections will occasionally be referred to as intensities for the sake of concise expression.

Temperature Determinations

Theory of band-line intensities

The intensity of a line in a band may be represented[1] by

$$I = \text{const.}\ \nu^4 i e^{-E_r/kT} \qquad (1)$$

if temperature equilibrium exists among the excited molecules at an absolute temperature, T. In this expression i is the intensity factor which

[2] H. Newhouse, Master's Thesis, Ohio State University (1935).

depends on the quantum-mechanical transition probability for the given line, E_r is the rotational energy of the initial state, and k is the Boltzmann constant. The constant of Eq. (1) holds for all branches of a particular band.

The Angstrom band system arises from transitions between the $B^1\Sigma$ and $A^1\Pi$ levels of CO. In each of these bands, extending for only a small wave-length range, the frequency factor, ν^4, may be considered constant. From wave mechanics the value of E_r is found to be $B_v hcJ(J+1)$ where B_v is the well-known molecular constant for the vibrational level in question, h is Planck's constant, c is the velocity of light in vacuum, and J is the rotational quantum number. By means of the intensity factors derived by Hönl and London[3] the following expressions are obtained for the intensities of the three branches of any one of these bands expressed in terms of the rotational quantum numbers of the final level:

$$I_P(J'') = \text{const.}\ (J''+1) \cdot \exp -(B_v' hcJ''(J''-1)/kT), \quad (2)$$

$$I_Q(J'') = \text{const.}\ (2J''+1) \cdot \exp -(B_v' hcJ''(J''+1)/kT), \quad (3)$$

$$I_P(J'') = \text{const.}\ (J'') \cdot \exp -(B_v' hc(J''+1)(J''+2)/kT), \quad (4)$$

$$J'' = 1, 2, 3, 4, \cdots.$$

The value of B_v' for the Angstrom bands studied here, which arise from the lowest vibrational state of the initial level, $B^1\Sigma$, is given by Hulthén[4] as 1.942 cm^{-1}.

Temperature from intensity maxima

The earliest use of the intensities of band lines for temperature estimates preceded the derivation of intensity expressions according to the new quantum theory, hence some of the analytical expressions used differ slightly from the relations accepted at present. However, the results are essentially the same.

By picking out the line of maximum intensity in a particular branch of a CN band, Birge[5] obtained temperatures of 70°C for active nitrogen, 4000°C for the solar reversal layer, and 3900°C to 4500°C for an arc with various currents and voltages. For the temperature of the underwater spark Wilson[6] found a value of 5000°C from the OH bands in absorption. In the case of the SiN bands excited by an active nitrogen source Mulliken[7] deduced a temperature of 80°C from the intensity maxima, which compares well with the value found by Birge for an active nitrogen source. Subsequently, Barton, Jenkins, and Mulliken[8] determined temperatures ranging from 290°K to 330°K from the beta-bands of NO as excited by active nitrogen.

More recently, by the use of the corrected formulas and quantum numbers, Johnson and Turner[9] found a rotational temperature of 750°K for the bands of He_2 excited by a condensed discharge. Richardson[10] studied temperatures in sunspots and in the reversing layer of the sun by applying this method to the Swan band of C_2 at 5165A.

It is obvious that the selection of the line of maximum intensity is independent of microphotometer calibration, and is thus convenient for such temperature measurements. However, the envelope at the maximum intensity is comparatively flat, and the maximum shifts only slightly with large changes in temperature. Hence, misinterpretations may arise because of these conditions and because of the blending of lines.

Expressions for the temperature in terms of the J values of the lines having greatest intensities in the different branches may be found by setting the first derivatives of the relations (2)–(4) equal to zero and simplifying. In Fig. 1 the graphs of these relations for the Angstrom bands which have the common initial vibrational state, $v'=0$, have been arranged. From the curves drawn there one may see that a change in temperature of 100° should change the point of maximum intensity by approximately one unit on the J'' scale for values in the neighborhood of 500°K.

[3] H. Hönl and F. London, Zeits. f. Physik **33**, 803 (1925).
[4] E. Hulthén, Ann. d. Physik **71**, 41 (1923).
[5] R. T. Birge, Astrophys. J. **55**, 273 (1922).
[6] E. D. Wilson, J. O. S. A. and Rev. Sci. Inst. **17**, 37 (1928).
[7] R. S. Mulliken, Phys. Rev. **26**, 319 (1925).
[8] H. A. Barton, F. A. Jenkins and R. S. Mulliken, Phys. Rev. **30**, 175 (1927).
[9] R. C. Johnson and R. C. Turner, Proc. Roy. Soc. **A142**, 574 (1933).
[10] R. S. Richardson, Astrophys. J. **73**, 216 (1931).

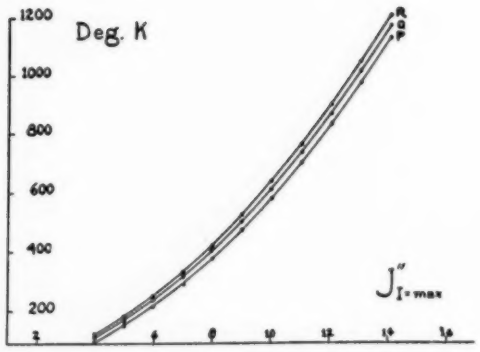

FIG. 1. Temperatures at which various J'' values designate lines of maximum intensity, computed for the P, Q, and R branches of Angstrom bands arising from the $v'=0$ level of the initial electronic state.

Temperature from intensity factor graphs

From the Eq. (3) it may be seen that a graph of $\ln [I_Q(J'')/(2J''+1)]$ against $J''(J''+1)$ should be a straight line of slope $(-B_v'hc/kT)$. This was introduced by Ornstein and van Wijk[11] as a method for measuring temperatures. In applying it to the light from an electric arc these investigators obtained a temperature of 5000°K from the CN bands and 2800°K from the bands of aluminum oxide. A comparison of the values found from the CN and C_2 bands simultaneously emitted by discharges through CH_4 and C_2H_2 was made by Lochte-Holtgreven.[12] Horst and Krygsman[13] made similar observations on the bands of these molecules as obtained by discharges in air. The same type of analysis has been applied in measuring effective discharge temperatures from bands of mercury hydride[14] and nitrogen,[15] and arc temperatures from the violet cyanogen and aluminum oxide bands [16, 17] The nitrogen band at 3914A was the subject of the studies made by Lindh[18] and by Thompson[19] for various excitation conditions in the low voltage arc, and the temperature of exploding aluminum wires was determined by Nagashima[20] from the AlH band at 4241A by means of this method.

Lochte-Holtgreven and Maecker[21] have pointed out certain influences which will distort such graphs. Surprisingly high temperatures have been derived in this manner by several investigators, and disagreement as to the interpretation of the true slope is found in some of the cited papers.

An application of this analysis for determining rotation temperatures requires accurate measurement of the individual line intensities using all the precautions essential to photometry of spectral lines. At best the method is very tedious to apply since so many quantities must be measured.

Temperature from frequency intensity equalities

In examining microphotometer records of an Angstrom band produced at two different temperatures, it was noticed that adjacent lines of the Q and R branches reached equal intensity in the tail of the band at room temperature, but at a higher temperature the place at which the two branches became equal in intensity occurred still farther away from the band origin. This observation suggested the possibility of using such points as a criterion for evaluating the rotational temperature. It has been found that the P and R branches also yield such a criterion.

If the envelopes for the microphotometer deflections are drawn for the respective branches, the points of intersection of the envelopes for the P and R branches will be points at which the conditions are simultaneously satisfied:

$$\nu_P=\nu_R, \tag{5}$$

$$I_P=I_R. \tag{6}$$

The frequencies and intensities may both be considered as continuous functions of J, the rotational quantum number for the lower level, since the observed J values, J_R and J_P, which satisfy these equations will not in general be integral numbers.

To find the temperature corresponding to an observed intersection the frequency equation

[11] L. S. Ornstein and W. R. van Wijk, Zeits. f. Physik **49**, 315 (1928).
[12] W. Lochte-Holtgreven, Zeits. f. Physik **64**, 443 (1930); **67**, 590 (1931).
[13] D. Th. J. ter Horst and C. Krygsman, Physica **1**, 114 (1933).
[14] W. Kapuściński and J. G. Eymers, Zeits. f. Physik **54**, 246 (1929).
[15] L. S. Ornstein and P. J. Haringhuizen, Zeits. f. Physik **77**, 788 (1932).
[16] L. S. Ornstein and H. Brinkman, Proc. K. Akad. Amst. **34**, 33 (1931).
[17] L. S. Ornstein and W. R. van Wijk, Proc. K. Akad. Amst. **33**, 44 (1930).
[18] A. E. Lindh, Zeits. f. Physik **67**, 67 (1931).
[19] N. Thompson, Proc. Phys. Soc. **46**, 436 (1934); **47**, 413 (1935).
[20] H. Nagashima, Tokyo B. D. Sci. Reports, Sec. **A1**, 219 (1932).
[21] W. Lochte-Holtgreven and H. Maecker, Zeits. f. Physik **105**, 1 (1937).

symbolized by (5) may be solved for one of the J values in terms of the other one alone. Substitution in the equation symbolized by (6) would then give an expression involving only the temperature and one J value of the intersection. Hence, the temperature is the only unknown if the value of either J at the intersection is determined from the observed band.

In practice, it is more convenient to proceed graphically. First, from a conventional Fortrat diagram, or from a plot of J numbers against wave-length, the value of J_P satisfying (5) can be found for any J_R. Next, a graph of temperatures against J_R may be prepared by substituting in Eq. (6) the various pairs of J values found in this manner. From this graph the temperature may be read directly, as soon as the J value of the intersection is found on the microphotometer record.

In order to test the accuracy of this procedure, temperatures were obtained from the intersections found on graphs of computed intensities plotted against wave-length, as in Fig. 2. These temperatures were compared with the values used in computing the plotted intensities, for the Angstrom (0,3) band at 5610A. The temperatures obtained by the method outlined came within one percent of the assumed values. This error is negligible in comparison with the error produced by the uncertainty in drawing the intensity envelopes.

In general, in a band with three branches there will be three intersections of intensity envelopes. For bands of the type considered here, the rotational temperature, T°K., corresponding to each

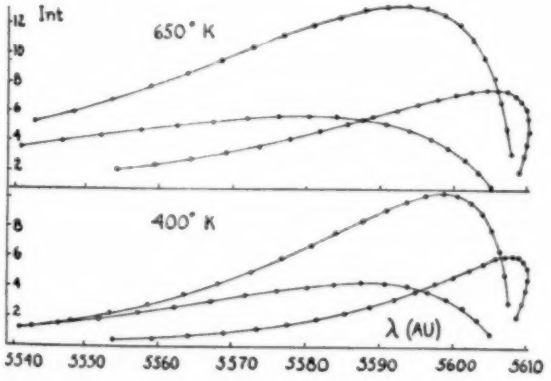

FIG. 2. Calculated intensities at temperatures of 650°K (above) and 400°K (below) for the lines of the Angstrom (0,3) band at λ5610, plotted against wave-length. Compare with microphotometer records, Fig. 4. An arbitrary scale of intensities is used.

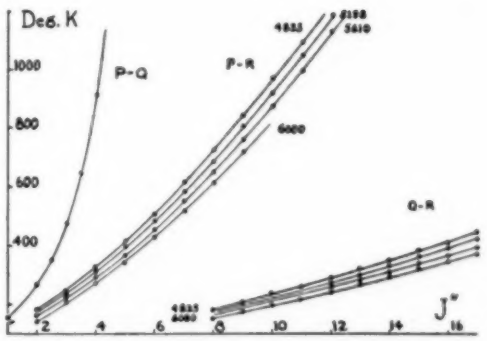

FIG. 3. Relationship between temperature and the J values of the intersections. For the P–R and Q–R curves, the abscissae are values of $J''(R)$; for the P–Q curve, $J''(Q)$. Computed for the Angstrom bands (0,1) λ4835, (0,2) λ5198, (0,3) λ5610, and (0,4) λ6080.

of these intersections is found by inserting in Eq. (6), and similar ones for the other intersections, the explicit formulas for intensities, and solving to obtain:

$$T=(B_v'hc/k)\cdot[J_P(J_P-1)-J_Q(J_Q+1)]/\ln[(J_P+1)/(2J_Q+1)], \quad (7)$$

$$T=(B_v'hc/k)\cdot[J_P(J_P-1)-(J_R+1)(J_R+2)]/\ln[(J_P+1)/J_R], \quad (8)$$

$$T=(B_v'hc/k)\cdot[J_Q(J_Q+1)-(J_R+1)(J_R+2)]/\ln[(2J_Q+1)/J_R], \quad (9)$$

where J_P, J_Q, and J_R refer to the J'' values *at the intersections*, which will not generally be integers but interpolations between the values belonging to the lines on either side of the intersection.

Graphs of Eqs. (7)–(9) are shown in Fig. 3 for four bands of the Angstrom system, except that for the P-Q intersection the curve is drawn for the 5610A, (0,3) band only, since the curves for the other three bands are very nearly coincident with this curve. From these graphs an impression may be gained of the sensitivity of this criterion to temperature changes.

RESULTS AND DISCUSSION

In Fig. 4 are shown two microphotometer traces of the 4835 (0,1) Angstrom band at ambient temperatures of 383° and 633°K respectively, illustrating the envelopes drawn, and showing intersections at A, B and C for the lower temperature, and A' and B' for the higher temperature, the Q-R intersection being hidden in the

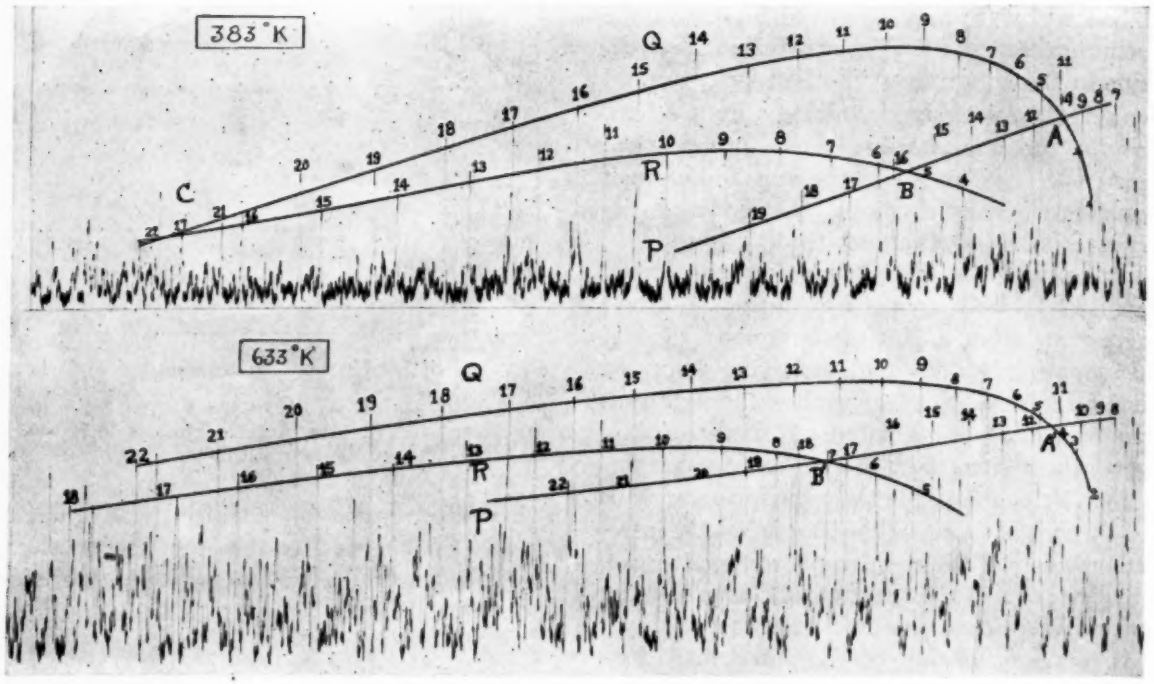

FIG. 4. Microphotometer records of the Angstrom band (0,1) λ4835, showing P–Q intersections at A,A'; P–R intersections at B,B', and Q–R intersection at C. Above, furnace cold; below, furnace hot. J'' values are given for the band lines.

background under the latter conditions. The band degrades toward the violet; that is, the wave-length increases toward the right. Attention is called to the way in which the envelopes are drawn, so as to touch the tops of the *less intense* lines. This procedure is based on the assumption that, in the absence of marked perturbations, no reason is known for finding a line less intense than called for by the formulas, but an excess intensity is quite probable, because of overlapping or "background." It will be noted that the P-Q intersection, at A and A', is near the head of the band where overlapping of the lines is prevalent; hence this intersection is not well adapted for temperature determinations. The Q-R intersection is unsuitable at the higher temperature. The P-R intersection is quite definite, and independent evaluations on duplicate microphotometer traces led to values of J differing by no more than 0.5, corresponding to temperature differences of 45°. If repeated trials are made, the average deviations indicate that the probable error is considerably less.

In Table I data are presented for four bands on each of four sets of plates, each plate consisting of a long and a short exposure, the latter being secured by covering up half of the plate during about four-fifths of the duration of the entire exposure. Rotational temperatures are entered for all the observed P-R intersections, and also for the J values of the maximum intensities of the Q branches. The mean values of the temperatures for a given set of conditions are shown, and also the average deviations both for the respective methods and for the respective bands. The temperatures indicated in the first column are readings of a thermometer placed within the furnace and helix against the outside of the discharge tube.

For comparison with furnace temperature, the rotational values under given conditions when averaged are found to be 88° higher with the furnace cold, and 8° lower with the furnace hot. The latter difference is less than the error in the rotational temperature, hence the conclusion is that the rotational temperature is characteristic of the furnace temperature when the latter is 638°K. For the "cold" furnace, 353° or 383°K, the temperature within the discharge tube may actually be that indicated by the rotational dis-

tribution, because of heating within the tube by the discharge itself, which absorbed about 300 watts from the oscillator.

The plates listed last in Table I were made with a considerable proportion of CO_2 in the discharge, to see if an anomalous distribution of rotational energies might be observed, produced by a process of simultaneous dissociation of the CO_2 molecule and excitation of the CO fragment. No such anomalies were observed, but the proportion of CO_2 was not controlled well enough to justify a conclusion that such an effect does not exist. Oldenberg[22] has studied this phenomenon in OH excited simultaneously with its dissociation from H_2O.

The experiments suggest that the intersections of microphotometer envelopes indicate rotational temperatures with an accuracy comparable with those found from locating maxima. However, the intersections can be located more conveniently, and they remain evident on plates which have been overexposed to the point where many lines in the region of the maximum are intense enough to reduce the galvanometer deflection uniformly to zero. Under suitable conditions, both criteria can be applied as they have been here, and the average values thereby have a probable error reduced by $2^{-\frac{1}{2}}$ in comparison with those from either criterion alone.

Reasons for abnormal distributions of intensities in bands have been considered by Lochte-Holtgreven and Maecker[21] with reference to bands from an arc in air at atmospheric pressure. The reasons are: (1) overlapping of lines; (2) inhomogeneity of temperature; (3) self-absorption by gas surrounding the discharge; and (4) self-reversal by cooler layers of gas, resulting in a change in the line contour because of the smaller Doppler widths of the lines absorbed by the cooler molecules. The first of these is clearly unavoidable unless bands with very open structure can

[22] O. Oldenberg, Phys. Rev. **46**, 210 (1934).

TABLE I. *Data on temperature measurements.*

Type of Discharge	Method of Measurement	Portion of Spectrogram	Temperature (Deg. K)					Mean Dev. from Mean
			4835 Band	5198 Band	5610 Band	6080 Band	Average	
CO at 638°K	From *Q* Branch Maxima	Strong	635	670	635	610	631	16
		Weak	619	615	—	—		
	P–R Intersections	Strong	616	660	585	—	629	32
		Weak	606	680	—	—		
CO at 383°K	*Q* Branch Maxima	Strong	500	450	400	500	477	32
		Weak	520	477	495	—		
	P–R Intersections	Strong	435	470	420	500	457	27
		Weak	470	480	420	—		
CO at 353°K	*Q* Branch Maxima	Strong	—	480	400	400	453	45
		Weak	500	500	490	400		
	P–R Intersections	Strong	440	455	385	435	423	39
		Weak	455	455	395	365		
CO_2 at 383°K	*Q* Branch Maxima	Strong	500	500	500	425	484	25
		Weak	510	450	500	500		
	P–R Intersections	Strong	480	540	420	435	473	31
		Weak	490	490	455	—		
Mean Deviation from the Means for given Conditions			17	18	30	16		

be chosen for study. The other three are far more serious in an arc than in a low pressure source. In locating maxima, overlapping may be more troublesome than in locating intersections. Inhomogeneity of temperature, which is to be expected only in sources at comparatively high pressure, clearly invalidates any assignment of rotational temperature. Self-absorption and self-reversal would not be expected to change the position of the maximum or the intersections, although these processes result in pronounced deviations from linearity in the intensity factor graphs. The layer of gas between the discharge and the window of the tube in our experiments was at a pressure of about 10^{-4} atmosphere, and about 10 cm long, hence no flattening of line contours was obtained on our plates.

A systematic study of rotational temperatures in comparison with temperatures measured by conventional means has been carried out by Thompson[19] for a low voltage arc in nitrogen, with respect to the negative nitrogen band at 3914A. He found rotational temperatures 300° higher than furnace temperatures of 600°K, and at higher furnace temperatures the discrepancy was less. It is clear from our data that the electrodeless discharge is a much cooler source than the low voltage arc, since the rotational temperature is within about 90° of the furnace temperatures of 353° and 383°K, and substantially equal to the furnace temperature at about 640°K. Although Thompson estimates the error of the determinations using the intensity factor graphs at 2 percent, his plotted points of differences between rotational and furnace temperatures show fluctuations as high as 20 percent. He offers no explanation for these fluctuations.

A possible use of band lines as calibration marks for photometry of spectrum plates is suggested by the great range of line intensities in a band, and the apparent reproducibility of the intensities under controlled temperature conditions. Our studies are not extensive enough to furnish sufficient evidence on this point, but the distributions obtained so far are remarkably consistent.

Acknowledgments

The authors acknowledge with thanks the aid of Mr. George E. Hansche in obtaining some of the spectra studied, and of Mr. H. W. Speicher in undertaking preliminary experiments. We are grateful also for the assistance of Professor J. B. Green in obtaining the spectrum photographs.

DECEMBER 1, 1937 PHYSICAL REVIEW VOLUME 52

Band Spectrum of TiCl

KENNETH R. MORE,* *Sloane Physics Laboratory, Yale University, New Haven, Connecticut*
AND
ALICE H. PARKER, *Pupin Physics Laboratory, Columbia University, New York, N. Y.*
(Received September 13, 1937)

The emission spectrum of TiCl has been excited by both high frequency and low frequency discharges through a continuous flow of $TiCl_4$ vapor in a discharge tube. The spectrum consists of one strong group of bands and several weaker groups, all degraded to shorter wave-lengths. The strong group occurs between 4200 and 4100A and the weak groups between 4100 and 3700A. The strong group is attributed to a transition between doublet electronic levels. The analysis of this system gives the values $\nu_e = 23820.0$ cm^{-1}, $\omega' = 503.4$ cm^{-1}, $x'\omega' = 2.5$ cm^{-1}, $\omega'' = 456.4$ cm^{-1}, $x''\omega'' = 6.3$ cm^{-1}.

Introduction

FOWLER,[1] in 1907, reported three band heads at 4199.5, 4192.7, and 4188.0A which he attributed to the TiCl molecule. This spectrum has been rephotographed and examined in an attempt to make a vibrational analysis. The spectrum was found to extend from 3700 to 4200A, with the strongest bands between 4150 and

* Sterling Fellow.
[1] A. Fowler, Proc. Roy. Soc. **A79**, 509 (1907).

TABLE I. *Wave numbers and intensities of TiCl band heads.*

v',v''	P_1 or P_2					
0,0	23805.6(1)*	23844.5(10)	23864.8(4)	23871.3(8)	23890.8(6)	23906.4(5)
1,1		23899.1(9)	23920.5(4)	23930.8(8)	23946.3(5)	23965.4(3)
2,2		23961.3(9)	23983.4(4)	23995.6(7)	24013.2(5)	24033.7(*bl*)
3,3		24030.1(6)	24057.4(*bl*)	24069.5(5)	24090.0(*bl*)	24112.7(1)
4,4		24106.8(3)	24135.3(3)	24147.4(2)	24178.3(1)	24206.3(0)
5,5		24191.7(*bl*)	24225.2(0)	24233.4(0)	24274.6(0)	
1,0		24342.8(3)				
2,1		24392.3(2)				

* The intensities given in brackets after the wave numbers are visual estimates on a scale of 0–10. Heads which are blended with atomic lines are marked "*bl*."

4200A. The head at 4192.7A reported by Fowler was the strongest one observed.

EXPERIMENTAL

The spectrum attributed to TiCl was excited by two methods. One was the passage of a low frequency discharge between electrodes which were approximately one centimeter apart. The discharge took place in a flask containing $TiCl_4$ at its room temperature vapor pressure. One electrode was a copper cup containing titanium metal. The other was a water-cooled copper rod. The electric power was supplied by a 1 kva Thordarson transformer. The second method used to excite the bands was the passage of a high frequency discharge through a tube containing $TiCl_4$ vapor at a suitable pressure. The discharge tube, which was of the external electrode type, was one centimeter in diameter. The $TiCl_4$ vapor was pumped through the discharge tube from a side tube containing liquid $TiCl_4$. The pressure in the discharge was controlled by varying the temperature of the liquid $TiCl_4$. A temperature of 10°C was found to be satisfactory. The high frequency discharge was much more intense than the low frequency one.

The spectrum excited with the low frequency source was photographed in the second order of a 21-foot grating giving a dispersion of 1.3A per mm, while that excited by the high frequency source was photographed in the third order of a 21-foot grating in a stigmatic mounting. The latter instrument gave a dispersion of 1.5A per mm. In the former case exposures of from 2 to 24 hours were taken, while in the latter 40 minute to 3 hour exposures were sufficient. Iron arc comparison spectra were recorded on all plates.

TABLE II. $\Delta G(v)$ *values for the* P_1 *or* P_2 *heads.*

$\Delta G'(v)$	$v'-v''$	$\Delta G''(v)$
498.3	0−1	443.7
493.2	1−2	431.0

TABLE III. *Isotopic bands.*

$\sqrt{Ti^{48}Cl^{35}}$	$\sqrt{Ti^{48}Cl^{37}}$	$\sqrt{}$ (obs.)	$\sqrt{}$ (calc.)
23961.3 (9)*	23958.8 (1)	2.5	2.2
23983.4 (4)	23980.0 (0)	3.4	2.6
24342.8 (3)	24334.9 (0)	7.9	8.3

Titanium arc spectra were also recorded on many plates. These were used for the identification of the titanium lines which were excited in the discharge.

ANALYSIS

The intense group of bands between 4150 and 4200A can be arranged into six overlapping sequences of rather closely spaced band heads. The wave numbers of the heads are given in Table I. The high intensity of this group relative to the others suggests that the sequences mentioned arise from transitions for which $\Delta v=0$. Since the electronic terms and coupling cases are not known, symbols are not assigned to the different branches. It is probable, however, that the strongest sequence, because of its position relative to the others, consists of P_1 or P_2 heads.

The bands of the $\Delta v=+1$ sequence are fairly weak, while those of the $\Delta v=-1$ sequence are not observed. It is probable that many weak bands of these sequences are masked by strong titanium lines. The weakness of the bands for $\Delta v=\pm 1$ is consistent with the Franck-Condon principle because the difference between ω' and ω'' is relatively small. Band heads which are attributed to the $\Delta v=+1$ sequence of P_1 or P_2 heads are given in Table I. The $\Delta G(v)$ values for the P_1 or P_2 heads are given in Table II. From the values given in Tables I and II the following equation is deduced for the heads of the P_1 or P_2 branches:

$$\nu=23820.0+[503.4(v'+\tfrac{1}{2})-2.5(v'+\tfrac{1}{2})^2]-[456.4(v''+\tfrac{1}{2})-6.3(v''+\tfrac{1}{2})^2].$$

The wave numbers of the last three heads of the $\Delta v=0$ sequence are not used in determining the constants of this equation. It is therefore of im-

portance that the values calculated from the equation agree well with the observed wave numbers.

An interpolation between the ω'' values 535 cm^{-1} and 353 cm^{-1} for the monochlorides of Si[2] and Sn,[3] elements which are respectively above and below Ti in the periodic table, indicates that ω'' for TiCl should be in the range 400 to 490 cm^{-1}. In addition there is evidence that ω'' usually changes slowly in going from compounds of one element to the next as a given electron shell is being built up. The frequencies for the chlorides of Ni,[4] and Cu[5] are respectively 420 and 417 cm^{-1}. Thus a value of the order of 440 cm^{-1} is reasonable for ω'' of TiCl. This leads to a value of about 500 cm^{-1} for ω' because of the observed sequence intervals. Such a value of ω' supports the identification of the bands assigned to the $\Delta v=+1$ sequence because no other bands are observed with a separation from the $\Delta v=0$ heads of less than 700 cm^{-1}.

The bands which have been discussed above are attributed to the molecule $Ti^{48}Cl^{35}$. Since the abundance ratio of the chlorine isotopes is $Cl^{35}:Cl^{37}=100:31.4$, the intensity of the bands due to the $Ti^{48}Cl^{37}$ molecule should be 31 percent of the intensity of the corresponding bands due to the $Ti^{48}Cl^{35}$ molecule. The displacement coefficient $(\rho-1)$ is -0.0158. Band heads which can be attributed to the isotopic molecule are given in Table III, together with the corresponding heads due to the main molecule, the observed and the calculated isotope displacements. Only a few heads due to the isotopic molecule are observed because of the low intensity of many of the bands which are far enough from the system origin for the isotope effect to be appreciable, and because of the masking of weak isotopic bands by stronger bands or by atomic lines.

In addition to the bands which have already been discussed, bands are observed in the regions 4050 to 4000A, 3935 to 3840A, and 3750 to 3720A. These bands, which are all much weaker than the heads of the 4192A system, are not sufficiently well developed for purposes of analysis. It is probable that most of the bands observed are to be attributed to TiCl because the high intensity of the atomic titanium and chlorine lines indicates that a considerable amount of complete dissociation of the $TiCl_4$ occurs in the discharge. It is probable that under such conditions the spectrum of diatomic TiCl would be excited in preference to the spectra of polyatomic fragments formed by the partial dissociation of the $TiCl_4$. This interpretation indicates the presence of more than one excited electronic state of the TiCl molecule.

The ground state of the TiCl molecule is probably a doublet state formed by the combination of the $3d^2\,{}^3F$ ground state of Ti I and the $3p^5\,{}^2P$ ground state of Cl I. The Λ value of the terms can be 0, 1, 2, 3, or 4. The excited states are probably also doublets, built by the combination of excited triplet and singlet states of Ti I with the ground state of Cl I. Again states of high Λ values are possible.

The intensity distribution among the branches of the band group at 4192A furnishes some evidence about the type of electronic transition. The strongest sequence is the one beginning with the band at 4192A. Only the weak sequence beginning at 4199A lies farther to the red. It thus seems necessary to interpret the 4192 sequence as being P_1 or P_2 heads and the 4199 sequence as being weak satellite heads. Even though the other sequences cannot be assigned it is evident that the Q heads are not as strong as the P heads. This suggests that the transitions are probably ${}^2\Pi\rightarrow{}^2\Delta$, or ${}^2\Delta\rightarrow{}^2\Phi$.

[2] W. Jevons, Proc. Phys. Soc. **48**, 563 (1936).
[3] W. Jevons, Proc. Roy. Soc. **A110**, 365 (1926); W. F. C. Ferguson, Phys. Rev. **32**, 607 (1928).
[4] K. R. More, Phys. Rev. **51**, 1019 (1937).
[5] R. Ritschl, Zeits. f. Physik **42**, 172 (1927).

The Low Terms in Cr III, Cr IV, Mn IV and Fe V

I. S. BOWEN
California Institute of Technology, Pasadena, California
(Received October 4, 1937)

Most of the strong lines arising from the d^3, d^34s and d^34p configurations of Cr IV and the d^4, d^34s and d^34p configurations of Cr III, Mn IV and Fe V have been classified. The presence of forbidden lines of these ions in astronomical sources is discussed.

AS previously pointed out[1] the doubly and more highly ionized ions of the elements Cr to Zn are the only astronomically abundant ions whose low metastable terms have not been completely enough located to determine whether forbidden transitions from these terms are represented in the spectra of nebulae, novae, the corona etc. The present paper reports the results of the second of a series[2] of investigations whose purpose is to supply this deficiency.

White has made a fairly extensive analysis of Cr III[3] and Cr IV.[4] He did not, however, locate the stable $d^4\ {}^5D$ terms in Cr III and his very doubtful identification of intercombination lines in Cr IV has since proved incorrect. These earlier analyses did not, therefore, provide information for the location of any forbidden transitions from the metastable states in the astronomically observable range. In both Mn IV and Fe V White[3] identified the lines of one multiplet involving high level terms only.

Table I gives the newly identified lines of Cr IV and Table II the term values fixed both by them and by the lines previously classified by White. The wave-lengths are not of as high an accuracy as might be desired as they were measured on low dispersion (16.7A per mm) plates which were taken for another purpose. The classification of the lines was based on an interpolation between V III and Mn V and Fe VI and could therefore be made with great definiteness. In particular over 25 intercombination lines were available to fix the relative positions of the doublet and quartet terms.

The newly identified lines of Cr III and all classified lines of Mn IV and Fe V are listed in Tables III, IV and V, respectively. In Table VI are given the corresponding term values of these ions. The lines of wave-length less than 625A

[1] I. S. Bowen, Rev. Mod. Phys. **8**, 79 (1936).
[2] I. S. Bowen, Phys. Rev. **47**, 924 (1935).
[3] H. E. White, Phys. Rev. **33**, 914 (1929).
[4] H. E. White, Phys. Rev. **33**, 672 (1929).

TABLE I. *Classified lines of Cr IV.*

Int.	λ	ν	Classification d^3	Classification d^34p	Int.	λ	ν	Classification d^3	Classification d^34p	Int.	λ	ν	Classification d^34s	Classification d^34p
2	573.82	174271	$^4F_{3\frac{1}{2}}$	$-(^3P)\,^4D_{2\frac{1}{2}}$	4	625.08	159980	$^4F_{4\frac{1}{2}}$	$-(^3F)\,^2F_{3\frac{1}{2}}$	2	1722.84	58044	$(^3F)\,^4F_{3\frac{1}{2}}$	$-(^3F)\,^2D_{2\frac{1}{2}}$
5	575.11	173880	$^4F_{4\frac{1}{2}}$	$-(^3P)\,^4D_{3\frac{1}{2}}$	2	625.40	159898	$^4P_{1\frac{1}{2}}$	$-(^3P)\,^4D_{2\frac{1}{2}}$	4	1733.93	57673	$(^3F)\,^4F_{4\frac{1}{2}}$	$-(^3F)\,^2D_{3\frac{1}{2}}$
1	575.88	173647	$^4F_{1\frac{1}{2}}$	$-(^3P)\,^4D_{1\frac{1}{2}}$	4	625.95	159757	$^4F_{3\frac{1}{2}}$	$-(^3F)\,^2F_{2\frac{1}{2}}$	5	1739.17	57499	$(^3F)\,^4F_{1\frac{1}{2}}$	$-(^3F)\,^4D_{2\frac{1}{2}}$
3	576.30	173521	$^4F_{2\frac{1}{2}}$	$-(^3P)\,^4D_{2\frac{1}{2}}$	1	626.58	159597	$^4P_{\frac{1}{2}}$	$-(^3P)\,^4D_{1\frac{1}{2}}$	7	1746.94	57243	$(^3F)\,^4F_{2\frac{1}{2}}$	$-(^3F)\,^4D_{2\frac{1}{2}}$
3	576.68	173406	$^4F_{2\frac{1}{2}}$	$-(^3P)\,^4D_{1\frac{1}{2}}$				$^4P_{2\frac{1}{2}}$	$-(^3P)\,^4D_{2\frac{1}{2}}$	5	1754.74	56989	$(^3F)\,^4F_{1\frac{1}{2}}$	$-(^3F)\,^4D_{1\frac{1}{2}}$
3	595.09	168042	$^2G_{4\frac{1}{2}}$	$-(^1G)\,^2H_{5\frac{1}{2}}$	2	636.92	157006	$^4P_{\frac{1}{2}}$	$-(^3P)\,^4S_{1\frac{1}{2}}$	6	1758.47	56868	$(^3F)\,^4F_{3\frac{1}{2}}$	$-(^3F)\,^4D_{3\frac{1}{2}}$
5	612.70	163212	$^4P_{1\frac{1}{2}}$	$-(^3P)\,^4P_{2\frac{1}{2}}$	3	637.40	156887	$^4P_{1\frac{1}{2}}$	$-(^3P)\,^4S_{1\frac{1}{2}}$	5	1762.79	56728	$(^3F)\,^4F_{4\frac{1}{2}}$	$-(^3F)\,^4D_{4\frac{1}{2}}$
4	613.76	162930	$^4P_{2\frac{1}{2}}$	$-(^3P)\,^4P_{2\frac{1}{2}}$	5	637.64	156828	$^2H_{4\frac{1}{2}}$	$-(^1G)\,^2G_{3\frac{1}{2}}$	2	1775.87	56310	$(^3F)\,^4F_{3\frac{1}{2}}$	$-(^3F)\,^2F_{3\frac{1}{2}}$
4	614.09	162843	$^4P_{\frac{1}{2}}$	$-(^3P)\,^4P_{1\frac{1}{2}}$	5	638.16	156701	$^2H_{5\frac{1}{2}}$	$-(^1G)\,^2G_{4\frac{1}{2}}$	3	1783.98	56054	$(^3F)\,^4F_{2\frac{1}{2}}$	$-(^3F)\,^2F_{2\frac{1}{2}}$
			$^2G_{3\frac{1}{2}}$	$-(^1G)\,^2G_{3\frac{1}{2}}$	3	638.61	156590	$^4P_{2\frac{1}{2}}$	$-(^3P)\,^4S_{1\frac{1}{2}}$	4	1791.04	55834	$(^3F)\,^4F_{4\frac{1}{2}}$	$-(^3F)\,^2F_{3\frac{1}{2}}$
0	614.51	162731	$^4P_{1\frac{1}{2}}$	$-(^3P)\,^4P_{1\frac{1}{2}}$	3	675.14	148117	$^4P_{1\frac{1}{2}}$	$-(^3F)\,^2D_{2\frac{1}{2}}$	1	1796.09	55677	$(^3F)\,^4F_{4\frac{1}{2}}$	$-(^3F)\,^2F_{2\frac{1}{2}}$
4	614.95	162615	$^4P_{\frac{1}{2}}$	$-(^3P)\,^4P_{\frac{1}{2}}$	2	676.47	147826	$^4P_{2\frac{1}{2}}$	$-(^3F)\,^2D_{2\frac{1}{2}}$	1	1910.21	52350	$(^3F)\,^2F_{3\frac{1}{2}}$	$-(^3F)\,^2D_{2\frac{1}{2}}$
			$^2G_{4\frac{1}{2}}$	$-(^1G)\,^2G_{4\frac{1}{2}}$	5	677.60	147580	$^4P_{2\frac{1}{2}}$	$-(^3F)\,^4D_{3\frac{1}{2}}$	0	1918.59	52122	$(^3F)\,^2F_{3\frac{1}{2}}$	$-(^3F)\,^4D_{3\frac{1}{2}}$
3	615.36	162507	$^4P_{1\frac{1}{2}}$	$-(^3P)\,^4P_{\frac{1}{2}}$	4	678.87	147304	$^4P_{1\frac{1}{2}}$	$-(^3F)\,^4D_{2\frac{1}{2}}$	4	1937.65	51609	$(^3F)\,^2F_{3\frac{1}{2}}$	$-(^3F)\,^2D_{3\frac{1}{2}}$
3	615.68	162422	$^4P_{2\frac{1}{2}}$	$-(^3P)\,^4P_{1\frac{1}{2}}$	0	679.19	147234	$^2G_{3\frac{1}{2}}$	$-(^3F)\,^2D_{2\frac{1}{2}}$	2	1939.76	51553	$(^3F)\,^2F_{3\frac{1}{2}}$	$-(^3F)\,^4D_{2\frac{1}{2}}$
5	616.82	162122	$^2H_{5\frac{1}{2}}$	$-(^1G)\,^2H_{5\frac{1}{2}}$	2	680.19	147018	$^2G_{4\frac{1}{2}}$	$-(^3F)\,^4D_{3\frac{1}{2}}$	3	1946.59	51372	$(^3F)\,^2F_{3\frac{1}{2}}$	$-(^3F)\,^4D_{3\frac{1}{2}}$
3	617.06	162059	$^4F_{2\frac{1}{2}}$	$-(^3F)\,^2D_{2\frac{1}{2}}$				$^4P_{2\frac{1}{2}}$	$-(^3F)\,^4D_{2\frac{1}{2}}$	3	1968.42	50802	$(^3F)\,^2F_{3\frac{1}{2}}$	$-(^3F)\,^4D_{2\frac{1}{2}}$
4	618.23	161752	$^4F_{3\frac{1}{2}}$	$-(^3F)\,^2D_{3\frac{1}{2}}$	5B	680.83	146880	$^4P_{\frac{1}{2}}$	$-(^3F)\,^4D_{1\frac{1}{2}}$	0	2033.74	49171	$(^3F)\,^2F_{3\frac{1}{2}}$	$-(^3F)\,^4F_{4\frac{1}{2}}$
1	620.20	161238	$^4F_{3\frac{1}{2}}$	$-(^3F)\,^4D_{3\frac{1}{2}}$	2	681.20	146800	$^4P_{1\frac{1}{2}}$	$-(^3F)\,^4D_{2\frac{1}{2}}$	2	2042.99	48948	$(^3F)\,^2F_{3\frac{1}{2}}$	$-(^3F)\,^4F_{3\frac{1}{2}}$
5	621.41	160924	$^4F_{4\frac{1}{2}}$	$-(^3F)\,^4D_{3\frac{1}{2}}$	3	681.88	146653	$^2G_{4\frac{1}{2}}$	$-(^3F)\,^4D_{4\frac{1}{2}}$	2	2055.51	48650	$(^3F)\,^2F_{3\frac{1}{2}}$	$-(^3F)\,^4F_{3\frac{1}{2}}$
4	622.13	160738	$^4F_{2\frac{1}{2}}$	$-(^3F)\,^4D_{1\frac{1}{2}}$	4	682.82	146451	$^2G_{3\frac{1}{2}}$	$-(^3F)\,^4D_{2\frac{1}{2}}$	0	2058.20	48586	$(^3F)\,^2F_{3\frac{1}{2}}$	$-(^3F)\,^4F_{1\frac{1}{2}}$
3	623.59	160362	$^4P_{2\frac{1}{2}}$	$-(^3P)\,^4D_{3\frac{1}{2}}$				$^4P_{2\frac{1}{2}}$	$-(^3F)\,^2F_{3\frac{1}{2}}$					
			$^4F_{3\frac{1}{2}}$	$-(^3F)\,^2F_{3\frac{1}{2}}$	1	684.35	146124	$^4P_{1\frac{1}{2}}$	$-(^3F)\,^2F_{3\frac{1}{2}}$					

B. Too strong, probably a blend.

TABLE II. *Term values of Cr IV.*

$d^3\,{}^4F_{1\frac{1}{2}}$	0	$d^2(^3F)4p\,{}^4F_{1\frac{1}{2}}$	158515
${}^4F_{2\frac{1}{2}}$	237	${}^4F_{2\frac{1}{2}}$	158880
${}^4F_{3\frac{1}{2}}$	553	${}^4F_{3\frac{1}{2}}$	159341
${}^4F_{4\frac{1}{2}}$	949	${}^4F_{4\frac{1}{2}}$	159855
${}^4P_{\frac{1}{2}}$	14058	${}^2F_{2\frac{1}{2}}$	160299
${}^4P_{1\frac{1}{2}}$	14177	${}^2F_{3\frac{1}{2}}$	160929
${}^4P_{2\frac{1}{2}}$	14476	${}^4D_{1\frac{1}{2}}$	160972
${}^2G_{3\frac{1}{2}}$	15056	${}^4D_{2\frac{1}{2}}$	161486
${}^2G_{4\frac{1}{2}}$	15405	${}^4D_{3\frac{1}{2}}$	162058
${}^2H_{4\frac{1}{2}}$	21067	${}^2D_{2\frac{1}{2}}$	162294
${}^2H_{5\frac{1}{2}}$	21320	${}^2G_{3\frac{1}{2}}$	164905
$d^2(^3F)4s\,{}^4F_{1\frac{1}{2}}$	103983	${}^2G_{4\frac{1}{2}}$	165425
${}^4F_{2\frac{1}{2}}$	104245	$d^2(^3P)4p\,{}^4S_{1\frac{1}{2}}$	171065
${}^4F_{3\frac{1}{2}}$	104620	${}^4D_{1\frac{1}{2}}$	173645
${}^4F_{4\frac{1}{2}}$	105096	${}^4D_{2\frac{1}{2}}$	174074
${}^2F_{2\frac{1}{2}}$	109935	${}^4D_{3\frac{1}{2}}$	174827
${}^2F_{3\frac{1}{2}}$	110685	${}^4P_{\frac{1}{2}}$	176684
$d^2(^3F)4p\,{}^4G_{2\frac{1}{2}}$	157347	${}^4P_{1\frac{1}{2}}$	176903
${}^4G_{3\frac{1}{2}}$	157923	${}^4P_{2\frac{1}{2}}$	177398
${}^4G_{4\frac{1}{2}}$	158619	$d^2(^1G)4p\,{}^2G_{3\frac{1}{2}}$	177895
${}^4G_{5\frac{1}{2}}$	159441	${}^2G_{4\frac{1}{2}}$	178021
		${}^2H_{5\frac{1}{2}}$	183445

were measured on plates which were taken on a 2 meter grazing incidence spectrograph and which have a dispersion from 1.5 to 2A per mm. The longer wave-lengths were obtained with two normal incidence gratings having dispersions of 16.7 and 3.5A per mm. Unfortunately the grating with the 3.5A per mm dispersion formed ghosts of enough strength to prove somewhat troublesome in the analysis of a complicated spectrum.

Because of the overlapping of the $d^3(^4F)4p\,{}^5F$, ${}^5D$ and ${}^3D$ terms the intensities of the lines in the multiplets involving these terms are quite anomalous. Some ambiguity exists therefore as to the assignment of some of these levels. There is also some uncertainty as to whether the terms designated as $d^3(^2H)4p\,{}^3G$ should be given this classification or should be assigned to $d^3(^2H)4p\,{}^3H$.

Tables II and VI provide the data for fixing the wave-lengths of most of the strong forbidden lines corresponding to transitions from the low metastable states of these ions. In general a comparison of these wave-lengths with the observed spectra of various astronomical sources, in which forbidden lines are known to appear, has not yielded significant coincidences. In the case of the 1931–32 spectra of Nova Pictoris,[5] which

[5] H. Spencer Jones, M. N. R. A. S. **92**, 728 (1932).

TABLE III. *Classified lines of Cr III.*

Int.	λ	ν	Classification d^4	Classification d^34p	Int.	λ	ν	Classification d^4	Classification d^34p	Int.	λ	ν	Classification d^4	Classification d^34p
4	920.697	108613.4	${}^5D_2$	$-({}^4P){}^5P_2$	2	1033.944	96717.0	${}^5D_1$	$-({}^4F){}^5F_1$	2	1268.033	78862.3		${}^3P_2-({}^4F){}^5D_3$
6	922.158	108441.3	${}^5D_3$	$-({}^4P){}^5P_3$	4	1035.244	96595.6	${}^5D_2$	$-({}^4F){}^5F_1$	1	1273.314	78535.2		${}^3P_2-({}^4F){}^5D_2$
4	922.527	108397.9	${}^5D_1$	$-({}^4P){}^5P_2$	5	1035.516	96570.2	${}^5D_3$	$-({}^4F){}^5F_2$					${}^3F_4-({}^4F){}^5F_3$
6	923.549	108278.0	${}^5D_2$	$-({}^4P){}^5P_2$	2	1035.743	96549.0	${}^5D_4$	$-({}^4F){}^5F_3$	1	1275.344	78410.2		${}^3F_3-({}^4F){}^5F_2$
2	923.787	108250.1	${}^5D_0$	$-({}^4P){}^5P_1$	8	1035.901	96534.3	${}^5D_2$	$-({}^4F){}^5D_2$	2B	1276.756	78323.5		${}^3F_2-({}^4F){}^5F_1$
7	924.044	108220.0	${}^5D_4$	$-({}^4P){}^5P_3$	8	1036.010	96524.2	${}^5D_4$	$-({}^4F){}^5D_4$	0	1278.676	78205.9		${}^3F_3-({}^4F){}^5D_3$
2	924.307	108189.2	${}^5D_1$	$-({}^4P){}^5P_1$	5	1037.768	96360.7	${}^5D_3$	$-({}^4F){}^5D_3$	2	1279.890	78131.7		${}^3F_4-({}^4F){}^5D_4$
5	925.011	108106.8	${}^5D_3$	$-({}^4P){}^5P_2$	5	1038.124	96327.6	${}^5D_1$	$-({}^4F){}^5D_2$	1	1283.12	77935.0		${}^3F_2-({}^4F){}^5D_3$
3	925.323	108070.4	${}^5D_2$	$-({}^4P){}^5P_1$	0	1039.398	96209.5	${}^5D_2$	$-({}^4F){}^5D_2$	2	1284.108	77875.1		${}^3F_3-({}^4F){}^5D_2$
7	966.216	103496.5	${}^3H_4$	$-({}^2H){}^3G_3$	4	1040.012	96152.7	${}^5D_0$	$-({}^4F){}^5D_1$				d^34s	d^34p
1	966.393	103477.6	${}^3H_4$	$-({}^2H){}^3G_4$	3	1040.131	96141.7	${}^5D_4$	$-({}^4F){}^5D_3$					
8	967.531	103355.9	${}^3H_5$	$-({}^2H){}^3G_4$	0	1040.649	96093.9	${}^5D_1$	$-({}^4F){}^5D_1$					
1	968.010	103304.7	${}^3H_5$	$-({}^2H){}^3G_5$	2	1041.302	96033.6	${}^5D_3$	$-({}^4F){}^5D_2$	0	1986.92	50329.2	$({}^4F){}^5F_4-({}^4F){}^5G_5$	
8	969.255	103172.0	${}^3H_6$	$-({}^2H){}^3G_5$	1	1041.962	95972.8	${}^5D_2$	$-({}^4F){}^5D_1$	1	1989.06	50275.0	$({}^4F){}^5F_3-({}^4F){}^3G_4$	
6	999.332	100066.8	${}^3G_3$	$-({}^2H){}^3G_3$	1	1058.626	94462.0	${}^3H_5$	$-({}^2G){}^3G_5$	1	1999.53	50011.8	$({}^4F){}^5F_3-({}^4F){}^3G_3$	
1	999.513	100048.7	${}^3G_3$	$-({}^2H){}^3G_4$	7	1060.115	94329.4	${}^3H_6$	$-({}^2G){}^3G_5$				$({}^4F){}^5F_4-({}^4F){}^3G_4$	
6B	1000.812	99918.9	${}^3G_4$	$-({}^2H){}^3G_3$	6	1060.999	94250.8	${}^3H_5$	$-({}^2G){}^3G_4$				$({}^4F){}^5F_5-({}^4F){}^3G_5$	
6	1001.010	99899.1	${}^3G_4$	$-({}^2H){}^3G_4$	5	1062.636	94105.6	${}^3H_4$	$-({}^2G){}^3G_3$	0	2010.12	49748.3	$({}^4F){}^5F_4-({}^4F){}^3G_3$	
2	1001.490	99851.2	${}^3G_4$	$-({}^2H){}^3G_5$	4	1072.080	93276.6	${}^3F_4$	$-({}^3G){}^3G_5$	2B	2011.85	49705.5	$({}^4F){}^5F_5-({}^4F){}^3G_4$	
			${}^5D_4$	$-({}^4F){}^3G_5$	4	1073.699	93136.0	${}^3F_3$	$-({}^3G){}^3G_4$	1	2091.43	47814.2	$({}^4F){}^5F_1-({}^4F){}^3D_2$	
4	1002.437	99756.9	${}^5D_3$	$-({}^4F){}^3G_4$	1	1074.508	93065.8	${}^3F_4$	$-({}^3G){}^3G_4$	1	2097.36	47679.0	$({}^4F){}^5F_2-({}^4F){}^3D_2$	
			${}^3G_5$	$-({}^2H){}^3G_4$	5	1076.120	92926.4	${}^3F_2$	$-({}^3G){}^3G_3$	4	2101.14	47593.2	$({}^4F){}^5F_4-({}^4F){}^3D_3$	
8	1002.901	99710.7	${}^3G_5$	$-({}^2H){}^3G_5$	1	1098.849	91004.3	${}^3G_4$	$-({}^3G){}^3G_5$	2	2101.46	47585.9	$({}^4F){}^5F_1-({}^4F){}^3D_1$	
3	1003.370	99664.1	${}^5D_2$	$-({}^4F){}^3G_3$	4	1100.553	90863.4	${}^3G_5$	$-({}^3G){}^3G_5$	4	2106.24	47477.9	$({}^4F){}^5F_3-({}^4F){}^3D_2$	
4	1025.584	97505.4	${}^5D_2$	$-({}^4F){}^3D_2$	3	1101.392	90794.2	${}^3G_4$	$-({}^3G){}^3G_4$	3	2107.48	47450.1	$({}^4F){}^5F_2-({}^4F){}^3D_1$	
3	1027.412	97331.9	${}^5D_3$	$-({}^4F){}^3D_3$	3	1102.847	90674.4	${}^3G_3$	$-({}^3G){}^3G_3$	0	2127.64	47000.5	$({}^4F){}^5F_4-({}^4F){}^3D_4$	
5	1028.293	97248.5	${}^5D_1$	$-({}^4F){}^3D_2$	0	1104.653	90526.2	${}^3G_4$	$-({}^3G){}^3G_3$	7	2141.84	46688.9	$({}^4F){}^5F_3-({}^4F){}^3D_3$	
3	1029.514	97133.2	${}^5D_2$	$-({}^4F){}^3D_2$	0	1204.422	83027.4	${}^3H_5$	$-({}^4F){}^3G_5$	1	2143.28	46657.4	$({}^4F){}^5F_1-({}^4F){}^3D_1$	
4	1029.777	97108.4	${}^5D_4$	$-({}^4F){}^3D_3$	8	1206.433	82889.0	${}^3H_6$	$-({}^4F){}^3G_5$	7	2144.84	46623.5	$({}^4F){}^5F_4-({}^4F){}^3D_3$	
3	1030.065	97081.3	${}^5D_0$	$-({}^4F){}^3D_1$	6	1209.114	82705.2	${}^3H_5$	$-({}^4F){}^3G_4$	5	2147.86	46557.9	$({}^4F){}^5F_3-({}^4F){}^3D_2$	
7	1030.428	97047.1	${}^5D_4$	$-({}^4F){}^5F_5$	5	1211.098	82569.7	${}^3H_4$	$-({}^4F){}^3G_3$	4	2149.35	46525.9	$({}^4F){}^5F_2-({}^4F){}^3D_1$	
4	1030.854	97006.9	${}^5D_3$	$-({}^4F){}^5F_4$	4	1247 826	80139.4	${}^3P_1$	$-({}^4F){}^3D_2$	0	2496.41	40057.5	$({}^4F){}^3F_4-({}^4F){}^3D_3$	
1	1031.418	96953.9	${}^5D_2$	$-({}^4F){}^3D_2$	1	1251.401	79910.4	${}^3P_1$	$-({}^4F){}^3D_1$	0	2504.59	39926.7	$({}^4F){}^3F_3-({}^4F){}^5F_2$	
1	1031.522	96944.1	${}^5D_2$	$-({}^4F){}^5F_3$	5	1252.597	79834.1	${}^3P_2$	$-({}^4F){}^3D_2$	2	2516.65	39735.4	$({}^4F){}^3F_2-({}^4F){}^5D_1$	
0	1031.962	96902.8	${}^5D_2$	$-({}^4F){}^3D_1$	2B	1253.655	79766.8	${}^3P_1$	$-({}^4F){}^5F_2$	3	2517.54	39721.3	$({}^4F){}^3F_3-({}^4F){}^5D_2$	
1	1032.382	96863.4	${}^5D_1$	$-({}^4F){}^5F_2$	0	1256.066	79613.7	${}^3P_1$	$-({}^4F){}^5F_1$	3	2518.99	39698.4	$({}^4F){}^3F_4-({}^4F){}^5F_3$	
8	1033.183	96788.3	${}^5D_4$	$-({}^4F){}^5F_4$	2	1258.517	79458.6	${}^3P_2$	$-({}^4F){}^3D_2$	3	2531.73	39498.7	$({}^4F){}^3F_2-({}^4F){}^5D_1$	
8	1033.389	96769.0	${}^5D_3$	$-({}^4F){}^5F_3$	3B	1261.556	79267.2	${}^3P_2$	$-({}^4F){}^5F_5$	5	2538.47	39393.8	$({}^4F){}^3F_3-({}^4F){}^5D_2$	
			${}^5D_0$	$-({}^4F){}^5F_1$	2	1262.336	79218.2	${}^3P_1$	$-({}^4F){}^5D_2$	4	2545.09	39291.4	$({}^4F){}^3F_4-({}^4F){}^5D_3$	
8	1033.656	96744.0	${}^5D_2$	$-({}^4F){}^5F_2$	1	1264.751	79066.9	${}^3P_2$	$-({}^4F){}^5F_2$					
			${}^5D_3$	$-({}^4F){}^5D_4$	3	1266.021	78987.6	${}^3P_1$	$-({}^4F){}^5D_1$					

TABLE IV. *Classified lines of Mn IV.*

INT.	λ	ν	CLASSIFICATION d^4	CLASSIFICATION d^34p
1	540.102	185150	$^5D_2-(^4P)^5P_3$	
4	540.882	184883	$^5D_3-(^4P)^5P_2$	
2	541.111	184805	$^5D_1-(^4P)^5P_2$	
4	541.666	184616	$^5D_2-(^4P)^5P_2$	
7	541.860	184550	$^5D_4-(^4P)^5P_3$	
			$^5D_0-(^4P)^5P_1$	
4	542.100	184468	$^5D_1-(^4P)^5P_1$	
5	542.453	184348	$^5D_3-(^4P)^5P_2$	
3	542.650	184281	$^5D_2-(^4P)^5P_1$	
4	558.493	179053	$^3H_4-(^2H)^3G_3$	
5	559.232	178817	$^3H_5-(^2H)^3G_4$	
6	560.184	178513	$^3H_6-(^2H)^3G_5$	
0	570.130	175399	$^5D_4-(^4F)^5G_5$	
3	571.793	174888	$^3G_3-(^2H)^3G_3$	
4	572.686	174616	$^3G_4-(^2H)^3G_4$	
0	573.352	174413	$^3G_5-(^2H)^3G_4$	
6	573.697	174308	$^3G_5-(^2H)^3G_5$	
3	579.156	172665	$^5D_3-(^4F)^5D_3$	
6	580.040	172402	$^5D_2-(^4F)^5D_2$	
4	580.385	172299	$^5D_1-(^4F)^5D_2$	
3	581.099	172088	$^5D_0-(^4F)^5D_1$	
			$^5D_2-(^4F)^5D_2$	
			$^5D_4-(^4F)^5D_3$	
7	581.453	171983	$^5D_1-(^4F)^5D_1$	
			$^5D_4-(^4F)^5F_5$	
5	581.652	171924	$^5D_3-(^4F)^5F_4$	
0	581.912	171847	$^5D_2-(^4F)^5D_2$	
0	582.088	171795	$^5D_2-(^4F)^5D_1$	
			$^5D_2-(^4F)^5F_3$	
6	582.785	171590	$^5D_1-(^4F)^5F_2$	
			$^5D_4-(^4F)^5F_4$	
1	665.031	150369	$^3G_3-(^4F)^3G_4$	
6	582.994	171528	$^5D_3-(^4F)^5F_3$	
5	583.384	171414	$^5D_2-(^4F)^5F_2$	
1	583.476	171387	$^5D_0-(^4F)^5F_1$	
2	583.819	171286	$^5D_1-(^4F)^5F_1$	
5	584.059	171216	$^5D_3-(^4F)^5D_4$	
2	584.124	171197	$^5D_4-(^4F)^5F_3$	
5	584.296	171146	$^5D_3-(^4F)^5F_2$	
7	584.443	171103	$^5D_2-(^4F)^5F_1$	
6	584.826	170991	$^5D_2-(^4F)^5D_3$	
8	585.217	170877	$^5D_4-(^4F)^5D_4$	
5	585.582	170770	$^5D_1-(^4F)^5D_2$	
5	585.736	170725	$^5D_3-(^4F)^5D_3$	
4	586.240	170579	$^5D_2-(^4F)^5D_2$	
4	586.881	170392	$^5D_4-(^4F)^5D_3$	
3	587.143	170316	$^5D_2-(^4F)^5D_2$	
2B	594.243	168281	$^3H_4-(^2G)^3G_5$	
6B	594.959	168079	$^3H_5-(^2G)^3G_5$	
6	595.678	167876	$^3H_6-(^2G)^3G_5$	
6	596.169	167738	$^3H_5-(^2G)^3G_4$	
6	597.097	167477	$^3H_4-(^2G)^3G_3$	
5	600.249	166598	$^3F_4-(^2G)^3G_5$	
4	601.147	166349	$^3F_3-(^2G)^3G_4$	
2	601.517	166246	$^3F_4-(^2G)^3G_4$	
4	602.531	165967	$^3F_2-(^2G)^3G_3$	
3	602.824	165886	$^3F_3-(^2G)^3G_3$	
5	610.958	163677	$^3G_5-(^2G)^3G_5$	
5	611.469	163541	$^3G_4-(^2G)^3G_4$	
5	612.303	163318	$^3G_3-(^2G)^3G_3$	

INT.	λ	ν	CLASSIFICATION d^4	CLASSIFICATION d^34p
0	613.162	163089	$^3G_4-(^2G)^3G_3$	
3	642.204	155714	$^3F_3-(^4F)^3F_4$	
6	642.598	155618	$^3F_4-(^4F)^3F_4$	
3	643.976	155285	$[^3F_2-(^4F)^3F_3$	
4	644.294	155209	$^3F_3-(^4F)^3F_3$	
2	644.701	155111	$^3F_4-(^4F)^3F_3$	
6	645.840	154837	$^3F_2-(^4F)^3F_2$	
2	645.943	154812	$^3H_5-(^4F)^3G_5$	
5B	646.152	154762	$^3F_3-(^4F)^3F_2$	
8	646.815	154604	$^3H_6-(^4F)^3G_5$	
4B	647.101	154535	$^3H_4-(^4F)^3G_4$	
8	647.952	154332	$^3H_5-(^4F)^3G_4$	
8	648.722	154149	$^3H_4-(^4F)^3G_3$	
6	652.211	153325	$^3F_4-(^4F)^3G_5$	
4	653.826	152946	$^3F_3-(^4F)^3G_4$	
4	654.005	152904	$^3G_4-(^4F)^3F_4$	
3	654.249	152847	$^3F_4-(^4F)^3G_4$	
7	654.891	152697	$^3G_5-(^4F)^3F_4$	
5	655.152	152636	$^3G_3-(^4F)^3F_3$	
			$^3F_2-(^4F)^3G_3$	
4	655.444	152563	$^3F_3-(^4F)^3G_3$	
6	656.162	152401	$^3G_4-(^4F)^3F_3$	
6	657.083	152188	$^3G_3-(^4F)^3F_2$	
4	660.359	151433	$^3P_0-(^4F)^3D_1$	
6	661.730	151119	$^3P_1-(^4F)^3D_2$	
8B	663.131	150800	$^3P_1-(^4F)^3D_1$	
1	663.395	150740	$^3P_0-(^4F)^3F_1$	
8	663.897	150626	$^3P_2-(^4F)^3D_2$	
8	664.843	150412	$^3G_5-(^4F)^3G_5$	
			$^3P_1-(^4F)^3F_2$	
1	665.031	150369	$^3G_3-(^4F)^3G_4$	
7	666.050	150139	$^3G_4-(^4F)^3G_4$	
6B	666.363	150068	$^3P_2-(^4F)^3D_2$	
8	666.700	149993	$^3F_4-(^4F)^3D_3$	
			$^3G_3-(^4F)^3G_3$	
6	667.009	149923	$^3G_5-(^4F)^3G_4$	
2	667.745	149758	$^3G_4-(^4F)^3G_3$	
			$^3P_2-(^4F)^3D_1$	
			$^3P_2-(^4F)^3F_3$	
4	668.433	149604	$^3F_2-(^4F)^3D_2$	
6	668.512	149586	$^3P_1-(^4F)^3D_2$	
6	668.743	149534	$^3F_3-(^4F)^3D_2$	
3	669.486	149368	$^3P_2-(^4F)^3F_2$	
7	669.799	149299	$^3F_3-(^4F)^3D_1$	
1	670.607	149119	$^3F_4-(^4F)^3F_3$	
6	671.357	148952	$^3P_2-(^4F)^3D_2$	
1	671.891	148834	$^3F_2-(^4F)^3F_2$	
5	673.215	148541	$^3P_2-(^4F)^3D_2$	
0	673.449	148489	$^3F_3-(^4F)^3D_3$	
0	673.804	148411	$^3F_3-(^4F)^3D_3$	
6	674.244	148314	$^3F_4-(^4F)^3D_3$	
6	675.658	148004	$^3F_3-(^4F)^3D_2$	
			d^34s	d^34p
0	1442.40	69329	$(^4F)^3F_2-(^2G)^3G_3$	
0	1444.00	69252	$(^4F)^3F_3-(^2G)^3G_4$	
0	1450.22	68955	$(^4F)^3F_4-(^2G)^3G_5$	
1	1577.17	63405	$(^4F)^5F_4-(^4F)^3G_4$	
			$(^4F)^5F_5-(^4F)^3G_5$	

INT.	λ	ν	CLASSIFICATION d^4	CLASSIFICATION d^34p
1	1586.67	63025	$(^4F)^5F_4-(^4F)^3G_3$	
1	1642.36	60888	$(^4F)^5F_1-(^4F)^3D_2$	
5B	1647.70	60691	$(^4F)^5F_2-(^4F)^3D_2$	
2	1651.78	60541	$(^4F)^5F_4-(^4F)^3D_3$	
4	1653.84	60465	$(^4F)^5F_3-(^4F)^5F_4$	
			$(^4F)^5F_4-(^4F)^5F_5$	
4	1656.10	60383	$(^4F)^5F_3-(^4F)^3D_2$	
4	1656.42	60371	$(^4F)^5F_2-(^4F)^3D_1$	
			$(^4F)^5F_2-(^4F)^5F_3$	
2	1661.19	60198	$(^4F)^5F_1-(^4F)^5F_2$	
5	1664.74	60069	$(^4F)^5F_2-(^4F)^5F_3$	
			$(^4F)^5F_4-(^4F)^5F_4$	
6	1667.05	59986	$(^4F)^5F_2-(^4F)^5F_2$	
			$(^4F)^5F_3-(^4F)^5F_4$	
3	1670.11	59876	$(^4F)^5F_1-(^4F)^5F_1$	
2	1675.35	59689	$(^4F)^5F_3-(^4F)^5F_3$	
1	1675.78	59674	$(^4F)^5F_2-(^4F)^5F_1$	
			$(^4F)^5F_4-(^4F)^5F_3$	
1	1677.91	59598	$(^4F)^5F_4-(^4F)^5F_4$	
6	1698.28	58883	$(^4F)^5F_4-(^4F)^5D_4$	
5	1698.69	58869	$(^4F)^5F_4-(^4F)^5D_3$	
5	1699.08	58855	$(^4F)^5F_3-(^4F)^5D_2$	
1	1705.11	58647	$(^4F)^5F_2-(^4F)^5F_3$	
1	1706.03	58616	$(^4F)^5F_2-(^4F)^5F_4$	
4	1718.29	58197	$(^4F)^5F_2-(^4F)^5F_2$	
6	1720.64	58118	$(^4F)^5F_2-(^4F)^5F_3$	
6	1724.88	57975	$(^4F)^5F_4-(^4F)^5F_4$	
2	1733.94	57672	$(^4F)^5F_3-(^4F)^5F_2$	
4B	1740.07	57469	$(^4F)^5F_4-(^4F)^5F_5$	
7*	1742.12	57401	$(^4F)^5F_5-(^4F)^5G_6$	
7*	1751.60	57091	$(^4F)^5F_4-(^4F)^5G_5$	
7*	1759.82	56824	$(^4F)^5F_3-(^4F)^5G_4$	
6*	1766.34	56614	$(^4F)^5F_2-(^4F)^5G_3$	
5*	1767.11	56590	$(^4F)^5F_3-(^4F)^5G_3$	
5*	1772.20	56427	$(^4F)^5F_4-(^4F)^5G_4$	
5*	1773.57	56384	$(^4F)^5F_1-(^4F)^5G_2$	
4*	1776.58	56288	$(^4F)^5F_2-(^4F)^5G_3$	
3*	1780.01	56180	$(^4F)^5F_2-(^4F)^5G_2$	
4	1786.07	55989	$(^4F)^5F_3-(^4F)^5G_3$	
1*	1789.08	55895	$(^4F)^5F_4-(^4F)^5G_5$	
0*	1789.65	55877	$(^4F)^5F_3-(^4F)^5G_2$	
5	1790.54	55849	$(^4F)^5F_3-(^4F)^5G_4$	
7	1795.77	55686	$(^4F)^5F_4-(^4F)^5G_5$	
0	1811.43	55205	$(^4F)^5F_4-(^4F)^5G_4$	
1	1887.16	52990	$(^4F)^5F_3-(^4F)^3D_3$	
1	1888.47	52953	$(^4F)^5F_3-(^4F)^3D_2$	
3	1899.52	52645	$(^4F)^5F_2-(^4F)^3D_1$	
			$(^4F)^5F_2-(^4F)^5F_3$	
4	1907.14	52435	$(^4F)^5F_3-(^4F)^3D_2$	
4	1910.29	52348	$(^4F)^5F_4-(^4F)^3D_3$	
3	1918.61	52121	$(^4F)^5F_3-(^4F)^5F_3$	
2	1928.95	51842	$(^4F)^5F_3-(^4F)^5D_3$	
2	1932.94	51735	$(^4F)^5F_3-(^4F)^5F_4$	
4	1942.90	51470	$(^4F)^5F_4-(^4F)^5F_5$	
2	1944.23	51434	$(^4F)^5F_2-(^4F)^5D_2$	
2	1948.75	51315	$(^4F)^5F_2-(^4F)^5D_3$	
3	1964.33	50908	$(^4F)^5F_3-(^4F)^5D_2$	
2	1973.43	50673	$(^4F)^5F_4-(^4F)^5D_3$	

* Previously classified by White.

TABLE V. *Classified lines of Fe V.*

INT.	λ	ν	CLASSIFICATION d^4	CLASSIFICATION d^34p
3	364.292	274505	$^5D_2-(^4P)^5P_3$	
4	364.795	274127	$^5D_3-(^4P)^5P_3$	
3	364.973	273993	$^5D_1-(^4P)^5P_2$	
3	365.339	273718	$^5D_2-(^4P)^5P_2$	
6	365.440	273643	$^5D_4-(^4P)^5P_3$	
			$^5D_0-(^4P)^5P_1$	
3	365.634	273498	$^5D_1-(^4P)^5P_1$	
6	365.858	273330	$^5D_2-(^4P)^5P_2$	
3	366.001	273223	$^5D_2-(^4P)^5P_1$	
5	373.720	267580	$^3H_4-(^2H)^3G_3$	
4	374.240	267208	$^3H_5-(^2H)^3G_4$	
2	374.464	267048	$^3H_5-(^2H)^3G_5$	
5	374.864	266763	$^3H_6-(^2H)^3G_5$	
1	379.032	263830	$^5D_4-(^4F)^5G_5$	
3	379.294	263648	$^5D_3-(^4F)^5G_4$	
3	380.664	262699	$^3G_3-(^2H)^3G_3$	
2B	381.152	262363	$^3G_4-(^2H)^3G_3$	
3	381.260	262288	$^3G_4-(^2H)^3G_4$	

INT.	λ	ν	CLASSIFICATION d^4	CLASSIFICATION d^34p
0	381.467	262146	$^3G_4-(^2H)^3G_5$	
0	381.671	262006	$^3G_5-(^2H)^3G_4$	
4	381.881	261862	$^3G_5-(^2H)^3G_5$	
3	383.484	260767	$^5D_2-(^4F)^3D_3$	
3	384.212	260273	$^5D_1-(^4F)^3D_2$	
2	384.610	260004	$^5D_0-(^4F)^3D_1$	
			$^5D_2-(^4F)^3D_2$	
1	384.826	259858	$^5D_1-(^4F)^3D_1$	
6	384.957	259769	$^5D_4-(^4F)^5F_5$	
4	385.023	259725	$^5D_3-(^4F)^5F_4$	
5	385.740	259242	$^5D_4-(^4F)^5F_4$	
			$^5D_1-(^4F)^5F_2$	
5	385.869	259155	$^5D_3-(^4F)^5F_3$	
4	386.156	258963	$^5D_2-(^4F)^5F_2$	
0	386.256	258896	$^5D_0-(^4F)^5F_1$	
1	386.483	258744	$^5D_1-(^4F)^5F_1$	
1	386.585	258675	$^5D_4-(^4F)^5F_3$	

INT.	λ	ν	CLASSIFICATION d^4	CLASSIFICATION d^34p
3	386.737	258574	$^5D_3-(^4F)^5F_2$	
4	386.783	258543	$^5D_2-(^4F)^5D_4$	
4	386.897	258467	$^5D_2-(^4F)^5F_1$	
5	387.199	258265	$^5D_2-(^4F)^5D_3$	
6	387.500	258065	$^5D_4-(^4F)^5D_4$	
4	387.616	257987	$^5D_1-(^4F)^5D_2$	
4	387.775	257882	$^5D_3-(^4F)^5D_3$	
3	387.983	257743	$^5D_0-(^4F)^5D_1$	
2	388.500	257400	$^5D_4-(^4F)^5D_3$	
2	388.607	257329	$^5D_3-(^4F)^5D_2$	
			$^5D_2-(^4F)^5D_1$	
6	392.907	254513	$^3H_6-(^3G)^3G_5$	
5	393.270	254278	$^3H_5-(^3G)^3G_4$	
4	393.911	253864	$^3H_4-(^3G)^3G_3$	
3	395.155	253065	$^3F_4-(^2G)^3G_5$	
2	395.789	252660	$^3F_3-(^3G)^3G_4$	
3	396.773	252033	$^3F_2-(^2G)^3G_3$	

TABLE V.—*Continued.*

Int.	λ	ν	Classification d^4	Classification $d^3 4p$
0	396.902	251951	$^3F_3-(^3G)^3G_3$	
4	400.625	249610	$^3G_5-(^3G)^3G_5$	
2	401.030	249358	$^3G_4-(^3G)^3G_4$	
2	401.639	248980	$^3G_3-(^3G)^3G_3$	
1	402.197	248634	$^3G_4-(^3G)^3G_3$	
1	414.790	241086	$^3F_3-(^4F)^3F_4$	
4	415.006	240962	$^3F_4-(^4F)^3F_4$	
1	415.825	240486	$^3F_2-(^4F)^3F_3$	
3	415.972	240401	$^3F_3-(^4F)^3F_3$	
5B	416.208	240264	$^3F_4-(^4F)^3F_3$	
2	416.910	239860	$^3F_3-(^4F)^3F_2$	
1	417.048	239781	$^3F_3-(^4F)^3F_3$	
6	417.382	239589	$^3H_6-(^4F)^3G_5$	
0	417.516	239512	$^3H_4-(^4F)^3G_4$	
6	418.033	239216	$^3H_5-(^4F)^3G_4$	
5	418.457	238973	$^3H_4-(^4F)^3G_3$	
3	419.915	238143	$^3F_4-(^4F)^3G_5$	
5B	420.546	237786	$^3G_4-(^4F)^3F_4$	
2	420.874	237601	$^3F_3-(^4F)^3G_4$	
5	421.045	237504	$^3G_5-(^4F)^3F_4$	
2	421.682	237146	$^3F_2-(^4F)^3G_3$	
4	421.765	237099	$^3G_4-(^4F)^3F_3$	
6	422.287	236806	$^3G_3-(^4F)^3F_2$	
2	423.833	235942	$^3P_0-(^4F)^3D_1$	
3	424.733	235442	$^3P_1-(^4F)^3D_2$	
1	425.476	235031	$^3P_1-(^4F)^3D_1$	
1	425.589	234968	$^3G_4-(^4F)^3G_5$	
0	425.840	234830	$^3P_0-(^4F)^5F_1$	
5	426.045	234717	$^3P_2-(^4F)^3D_3$	
5	426.097	234688	$^3G_5-(^4F)^3G_5$	
1	426.609	234407	$^3P_1-(^4F)^5F_2$	
			$^3F_2-(^4F)^3D_3$	
3	426.745	234332	$^3F_3-(^4F)^3D_3$	
4	426.814	234294	$^3G_4-(^4F)^3G_4$	
3	426.969	234209	$^3F_4-(^4F)^3D_3$	
3	427.190	234088	$^3G_3-(^4F)^3G_3$	
1	427.320	234017	$^3G_5-(^4F)^3G_4$	
2	427.442	233950	$^3P_2-(^4F)^3D_2$	
1	427.782	233764	$^3G_4-(^4F)^3G_3$	
2	427.918	233690	$^3P_0-(^4F)^5D_1$	
0	428.000	233645	$^3F_2-(^4F)^3D_2$	
3	428.131	233573	$^3F_3-(^4F)^3D_2$	
0	428.292	233486	$^3P_2-(^4F)^5F_3$	
5B	428.763	233229	$^3F_2-(^4F)^3D_1$	
5B	428.909	233150	$^3P_1-(^4F)^5D_2$	
1	429.206	232988	$^3F_4-(^4F)^5F_5$	
1	430.053	232529	$^3F_3-(^4F)^5F_2$	
2	430.624	232221	$^3P_2-(^4F)^5D_3$	
3	431.541	231728	$^3F_4-(^4F)^5D_3$	
3	432.340	231299	$^3F_2-(^4F)^5D_2$	
1	432.919	230990	$^3F_3-(^4F)^5D_1$	
			$d^3 4s$	$d^3 4p$
1	1302.99	76747	$(^4F)^5F_2-(^4F)^3G_3$	
1	1303.59	76711	$(^4F)^5F_4-(^4F)^3G_4$	
			$(^4F)^5F_5-(^4F)^3G_5$	
1	1357.28	73677	$(^4F)^5F_2-(^4F)^3D_2$	
1	1359.41	73561	$(^4F)^5F_1-(^4F)^3D_1$	
5	1361.42	73453	$(^4F)^5F_4-(^4F)^3D_3$	
4	1363.00	73368	$(^4F)^5F_3-(^4F)^5F_4$	
3	1363.72	73329	$(^4F)^5F_4-(^4F)^5F_5$	
3	1365.14	73253	$(^4F)^5F_3-(^4F)^3D_3$	
			$(^4F)^5F_2-(^4F)^3D_1$	
3	1365.73	73221	$(^4F)^5F_2-(^4F)^5F_3$	
4	1371.00	72940	$(^4F)^5F_1-(^4F)^5F_2$	
6	1373.68	72797	$(^4F)^5F_4-(^4F)^5F_4$	
			$(^4F)^5F_3-(^4F)^5F_3$	
6	1376.45	72651	$(^4F)^5F_5-(^4F)^5F_5$	
			$(^4F)^5F_2-(^4F)^5F_2$	
2	1380.18	72454	$(^4F)^5F_1-(^4F)^5F_1$	
1	1384.17	72246	$(^4F)^5F_4-(^4F)^5F_5$	
1	1384.75	72215	$(^4F)^5F_3-(^4F)^5F_3$	
2	1385.32	72186	$(^4F)^5F_3-(^4F)^5D_4$	
0	1386.33	72133	$(^4F)^5F_5-(^4F)^5F_4$	
5B	1388.07	72043	$(^4F)^3F_2-(^4F)^3F_3$	
1	1389.05	71992	$(^4F)^3F_3-(^4F)^3F_4$	
0	1389.97	71944	$(^4F)^5F_2-(^4F)^5D_3$	
3	1394.77	71696	$(^4F)^5F_1-(^4F)^5D_2$	
3	1397.99	71531	$(^4F)^5F_3-(^4F)^5D_3$	
4	1400.30	71413	$(^4F)^3F_3-(^4F)^3F_2$	
6	1402.45	71304	$(^4F)^3F_3-(^4F)^3F_3$	
7	1406.78	71084	$(^4F)^3F_4-(^4F)^3F_4$	
1	1408.19	71013	$(^4F)^5F_3-(^4F)^5D_1$	
6	1409.19	70963	$(^4F)^5F_4-(^4F)^5D_2$	
			$(^4F)^5F_4-(^4F)^5D_3$	
7	1409.51	70947	$(^4F)^5F_5-(^4F)^5D_4$	
3	1420.24	70411	$(^4F)^3F_4-(^4F)^3F_2$	
8*	1430.61	69900	$(^4F)^5F_5-(^4F)^5G_6$	
7*	1440.59	69416	$(^4F)^5F_4-(^4F)^5G_5$	
6*	1448.91	69017	$(^4F)^5F_3-(^4F)^5G_4$	
3*	1454.71	68742	$(^4F)^5F_2-(^4F)^5G_3$	
5	1455.59	68701	$(^4F)^3F_2-(^4F)^3G_3$	
5*	1456.23	68671	$(^4F)^5F_3-(^4F)^3G_3$	
5	1459.85	68500	$(^4F)^3F_3-(^4F)^3G_4$	
2*	1460.86	68453	$(^4F)^5F_4-(^4F)^5G_4$	
3*	1462.67	68368	$(^4F)^5F_1-(^4F)^5G_2$	
6	1464.73	68272	$(^4F)^3F_4-(^4F)^3G_5$	
3*	1465.37	68242	$(^4F)^5F_2-(^4F)^5G_3$	
4B	1479.49	67591	$(^4F)^3F_4-(^4F)^3G_4$	
4B	1532.70	65244	$(^4F)^3F_3-(^4F)^3D_3$	
2B	1533.27	65220	$(^4F)^3F_2-(^4F)^3D_2$	
2	1543.66	64781	$(^4F)^3F_2-(^4F)^3D_1$	
3	1544.50	64746	$(^4F)^3F_3-(^4F)^3F_3$	
2B	1550.80	64483	$(^4F)^3F_3-(^4F)^3D_3$	
1	1554.17	64343	$(^4F)^3F_4-(^4F)^3D_3$	

TABLE VI. *Term values of Cr III, Mn IV and Fe V.*

	Cr III	Mn IV	Fe V
$d^4\,^5D_0$	0	0	0
$^5D_1$	60	92	145
$^5D_2$	180	280	419
$^5D_3$	352	547	804
$^5D_4$	572	880	1285
$^3P_0$		20646	24054
$^3P_1$	17168	21274	24973
$^3P_2$	17852	22321	26466
$^3H_4$	17274	21273	24937
$^3H_5$	17398	21469	25229
$^3H_6$	17534	21676	25527
$^3F_2$	18452	22786	26765
$^3F_3$	18512	22859	26846
$^3F_4$	18584	22957	26973
$^3G_3$	20705	25434	29820
$^3G_4$	20855	25666	30150
$^3G_5$	20997	25875	30429
$d^3(^4F)4s^5F_1$	49494	111502	186437
$^5F_2$	49629	111706	186736
$d^3(^4F)4s^3F_3$	49830	112006	187162
$^5F_4$	50091	112402	187725
$^5F_5$	50409	112877	188401
$^3F_2$	56652	119431	195212
$^3F_3$	56994	119955	195942
$^3F_4$	57424	120599	196845
$d^3(^4F)4p^5G_2$	93768	167885	254805
$^5G_3$	94031	168295	255406
$^5G_4$	94377	168830	256179
$^5G_5$	94802	169492	257142
$^5G_6$	95305	170278	258301
$^5D_1$	96153		257746
$^5D_2$	96387	170861	258134
$^5D_3$	96714	171272	258685
$^5D_4$	97097	171760	259349
$^5F_1$	96776	171381	258887
$^5F_2$	96923	171694	259380
$^5F_3$	97121	172076	259959
$^5F_4$	97360	172471	260528
$d^3(^4F)4p^5F_5$	97619	172863	261054
$^5D_1$	97079	172081	259994
$^5D_2$	97308	172391	260419
$^5D_3$	97685	172948	261182
$^5G_3$	99844	175422	263911
$^5G_4$	100103	175804	264445
$^5G_5$	100424	176283	265117
$^3F_2$	101446	177624	266625
$^3F_3$	101747	178070	267248
$^3F_4$	102102	178573	267932
$d^3(^4P)4p^5P_1$	108250	184560	273643
$^5P_2$	108458	184896	274136
$^5P_3$	108793	185430	274928
$d^3(^2G)4p^3G_3$	111380	188753	278800
$^3G_4$	111648	189207	279507
$^3G_5$	111862	189553	280039
$d^3(^2H)4p^3G_3$	120771	200324	292518
$^3G_4$	120753	200284	292437
$^3G_5$	120708	200186	292291

TABLE VII. *Classified lines of Fe III.*

Int.	λ	ν	Classification
7	1122.65	89075	$d^6\,^5D_4-d^5(^6S)4p\,^5P_3$
5	1125.02	88887	$^5D_3-\ ^5P_2$
3	1126.82	88745	$^5D_2-\ ^5P_1$
3	1128.15	88641	$^5D_3-\ ^5P_3$
3	1128.86	88585	$^5D_2-\ ^5P_2$
3	1129.38	88544	$^5D_1-\ ^5P_1$
3	1130.48	88458	$^5D_0-\ ^5P_1$
3	1131.27	88396	$^5D_1-\ ^5P_2$
1	1132.09	88332	$^5D_2-\ ^5P_3$
8	1895.50	52756.5	$d^5(^6S)4s^7S-d^5(^6S)4p\,^7P_4$
7	1914.06	52245.0	$^7S-\ ^7P_3$
7	1926.27	51913.8	$^7S-\ ^7P_2$
6	2062.30	48489.6	$^5S-\ ^5P_1$
7	2068.94	48333.9	$^5S-\ ^5P_2$
8	2079.70	48083.9	$^5S-\ ^5P_3$

showed some indications of the presence of forbidden Fe VI,[2] the evidence either for or against forbidden Fe V is very inconclusive. Thus the observed line at λ4121.2A agrees satisfactorily with the predicted λ4123.9A of the $^5D_4-{}^3H_6$ transition. Most of the other transitions, which one might expect to be strong, fall at positions where they would be blended with lines already ascribed to other elements.

Table VII lists a few lines of Fe III that can be classified at once because of their great strength.

Energy Levels of Neon and Argon

J. B. SAMPSON
Allegheny College, Meadville, Pennsylvania
(Received September 29, 1937)

The energy levels for the neon $2p^5 3d$ and argon $3p^5 5d$ configurations have been calculated completely from the first-order perturbation theory and compared with the observed values.

THE energy levels for the $n'p^5nd$ configurations have been worked out by Shortley[1] from the first order perturbation theory using intermediate coupling. This method is here applied to neon $2p^5 3d$ and argon $3p^5 5d$.

Shortley obtained 5 secular equations in terms of 6 radial integral parameters. These 5 consist of 2 linear equations corresponding to $J=0$ and $J=4$, 2 cubic for $J=1$ and $J=3$, and a quartic equation for $J=2$. In order to facilitate the solution so he might apply this computation to a number of configurations Shortley made the valid simplification of neglecting the electrostatic interaction between levels derived from different ionic parents, thus reducing his cubic and quartic to linear and quadratic equations. Since this interaction is small for higher values of n, the scheme worked well for these cases.

But for neon $2p^5 3d$, the neglected interaction amounts to about 20 cm^{-1}. Here this configuration is solved completely.

The values of the parameters were obtained by adding the sum of the diagonal terms of the determinants and equating each to the sum of the roots from experimental results recorded in Bacher and Goudsmit. But since there were only 5 equations and 6 parameters, Shortley's value was assumed for the parameter F_0 and the remaining 5 determined from the equations. The secular equations were then solved for the energy levels. Then, since it is possible by the method of least squares applied to this case by Shortley[2] to adjust the parameters somewhat and improve the agreement of the configuration, this was done several times until the improvements became insignificantly small.

The same process was followed in the case of argon $3p^5 5d$ except in the initial evaluation of the parameters. Here since neither Shortley nor anyone else had attempted this configuration before, there was no approximate value to assume for F_0.

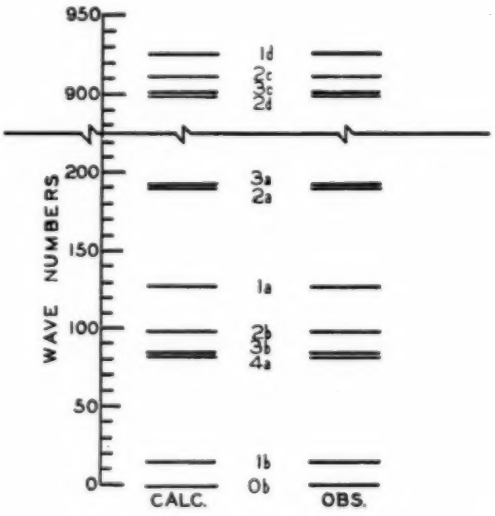

FIG. 1. Energy levels of neon $2p^5 3d$.

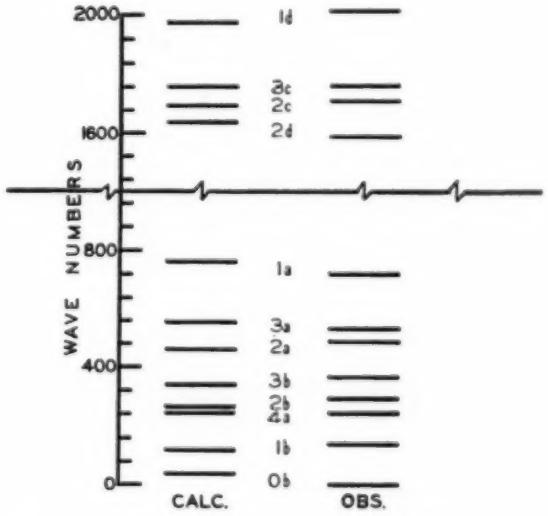

FIG. 2. Energy levels of argon $3p^5 5d$.

[1] George H. Shortley, Phys. Rev. **44**, 671 (1933).

[2] George H. Shortley, Phys. Rev. **47**, 300 (1935).

TABLE I. *Values of the radial integral parameters.*

	NEON $2p^5 3d$	ARGON $3p^5 5d$
F_0	−374.066	−749.42
F_2	16.3841	36.111
G_1	3.02063	44.098
G_3	.031973	3.2809
ζ_p	520.051	887.17
ζ_d	.159007	10.168

Therefore the 5 secular equations were split by Shortley's approximation, yielding 8. Adding the sum of the diagonal terms and equating to the sum of the roots (energy levels) thereby yielded 8 equations for the 6 parameters. The best values of the parameters were found from these 8 equations by the method of least squares. The agreement was then improved by varying the parameters as was done for neon.

Figure 1 shows the results, compared with the observed values, for neon $2p^5 3d$. The difference between any observed and calculated level is less than 1 cm^{-1}. Fig. 2 compares the results for argon $3p^5 5d$ which are not so satisfactory. This may be due to the fact that the $3p^5 7s$ and $3p^5 6d$ configurations overlap $3p^5 5d$ and might interact strongly with it. Table I gives the best values for the radial integral parameters. Table II shows numerically the values of the best solutions of the secular equations compared with the observed values.

TABLE II. *Values of energy levels.*

	NEON $2p^5 3d$			ARGON $3p^5 5d$		
	FORMER NOTATION	CALC.	OBS.	FORMER NOTATION	CALC.	OBS.
$0b$	d_6	−.89	0.0	d_6	38	0
$1b$	d_5	14.53	14.64	d_5	117	139
$1a$	d_2	127.42	127.02	d_2	765	720
$1d$	S_1'	925.65	926.09	S_1'	1,976	2,014
$2b$	d_3	97.63	97.61	d_3	265	293
$2a$	d_1''	190.44	190.05	d_1''	460	488
$2d$	S_1''''	899.25	899.05	S_1''	1,638	1,579
$2c$	S_1''	910.77	910.37	S_1''''	1,692	1,711
$3b$	d_4	82.70	82.55	d_4	339	366
$3a$	d_1'	191.12	191.82	d_1'	557	536
$3c$	S_1'''	900.49	900.61	S_1'''	1,762	1,763
$4a$	d_4'	81.43	80.72	d_4'	244	242

No other $n'p^5 nd$ configurations were done since except for neon, argon $3p^5 5d$ is the only one completely observed.

I am grateful to Professor C. W. Ufford for his keen interest and generous help in this work.

DECEMBER 1, 1937 PHYSICAL REVIEW VOLUME 52

Pressure Effects of Rare Gases on the Second Doublet of Rubidium Principal Series

NY TSI-ZÉ, *Institute of Physics, National Academy of Peiping, Peiping, China*

AND

CH'EN SHANG-YI,* *Physics Department, California Institute of Technology, Pasadena, California*

(Received September 13, 1937)

The displacement, asymmetry, and broadening of the second doublet of the rubidium principal series perturbed by pure helium, neon and argon up to 13 atmospheres are observed. The displacement as well as the broadening of the doublet components are not the same. The $^2P_{\frac{1}{2}}$ component shifts and broadens more conspicuously than the $^2P_{1\frac{1}{2}}$ component (an exception being the broadening by argon). The departure from linear relationship between the shift and the density of the perturbing gas is quite manifest. Both for helium and for neon the line contour shows a distinct asymmetry towards the violet, while for argon the line contour shows a very strong red asymmetry. For helium and neon the violet asymmetries of the $^2P_{\frac{1}{2}}$ component are stronger than that of the $^2P_{1\frac{1}{2}}$ component; the reverse is true for argon. The relationship between the half-width and the relative density is linear for foreign gas concentrations of relative densities up to 8 so far applied.

CERTAIN interesting experiments[1] have been done to test Margenau's theory of the pressure effects of foreign gases on spectral lines.[2] His formula is restricted to resonance lines. In the

* Research Fellow of the China Foundation for the Promotion of Education and Culture.

[1] H. Margenau and W. W. Watson, Phys. Rev. **44**, 92 (1933); G. F. Hull, Phys. Rev. **50**, 1148 (1936); C. Füchtbauer, G. Joos, and O. Dinkelacker, Ann. d. Physik **71**, 204 (1923).

[2] H. Margenau, Phys. Rev. **48**, 755 (1935).

present research the pressure effects of rare gases on the second doublet of the rubidium principal series are studied. The results are compared with the corresponding results for potassium and for caesium as already obtained,[3] thus giving a tentative test of Margenau's theory for lines of higher P states. It is found that the $^2P_{\frac{1}{2}}$ component not only shifts but also broadens much more conspicuously than the $^2P_{1\frac{1}{2}}$ component (with the exception that the broadening by argon is greater for the $^2P_{1\frac{1}{2}}$ component).

Experimental

The absorption tube was similar to that used in the previous research.[4] A Hilger E-1 glass spectrograph (dispersion 5.3A/mm) was employed to register the spectrum on Eastman D.C. OrthoSpectroscopic plates. A point-source incandescent lamp lighted by high capacity batteries was used to supply a continuous spectrum of constant intensity. To calibrate the density gradations in the absorption lines the characteristic curve of each plate was determined by taking five additional spectra on the plate through five standard neutral screens. An Fe arc spectrum was superposed on both sides of the mean exposure as a comparison. The line countour was traced by a Moll type A microphotometer made by Kipp and Zonen and set to the 1 : 49 ratio. Fig. 1(a) gives a superposition of two microphotometer traces of the second doublet of rubidium principal series perturbed by different concentrations of helium, and Figs. 1(b) and 1(c) the corresponding microphotometer traces for neon and argon. The shift of the maxima of the absorption lines and the marked asymmetrical broadening for the high densities of rare gases are shown. The detailed method of analysis was similar to that used by Margenau and Watson.[1]

Table I. *The asymmetrical broadening of the second doublet of Rb principal series perturbed by rare gases.*

t (°K)	p atm.	Relative Density	Half-width (λ4216)	Half-width (λ4202)	Asymmetry (λ4216)	Asymmetry (λ4202)
			(a) Rubidium/Helium			
408	4.01	2.68	7.82 cm^{-1}	5.39 cm^{-1}	0.83	0.90
420	5.73	3.72	10.51	7.71	0.66	0.86
446	8.65	5.29	14.97	—	0.56	—
422	8.47	5.48	15.71	10.2	0.53	0.80
445	10.92	6.71	18.9	12.8	0.50	0.79
424	10.74	6.92	—	13.7	—	0.81
			(b) Rubidium/Neon			
414	1.61	1.06	1.99 cm^{-1}	1.61 cm^{-1}	0.9	0.95
426	1.64	1.03	—	1.10	—	0.96
418	4.02	2.63	3.84	2.91	0.95	0.96
431	6.42	4.07	5.60	—	0.82	—
418	6.33	4.14	—	3.70	—	0.95
436	8.42	5.28	7.67	4.40	0.72	0.96
420	8.28	5.38	—	4.16	—	0.9
438	10.42	6.52	8.80	5.00	0.59	0.92
426	11.88	7.61	—	6.25	—	0.86
440	12.50	7.76	10.76	6.08	0.49	0.85
425	12.15	7.81	—	6.70	—	0.85
			(c) Rubidium/Argon			
396	4.22	2.91	— cm^{-1}	7.32 cm^{-1}	—	2.4
410	4.37	2.91	6.79	—	2.29	—
410	6.61	4.42	—	11.57	—	2.61
418	6.68	4.36	10.83	11.27	1.54	2.34
421	8.43	5.48	12.73	14.65	1.46	1.88
410	8.27	5.50	—	15.73	—	2.11
414	10.49	6.91	—	18.50	—	1.91
424	10.63	6.87	16.38	18.80	1.44	1.85
430	12.18	7.71	17.61	21.46	1.35	1.60
414	11.86	7.83	—	20.61	—	1.64

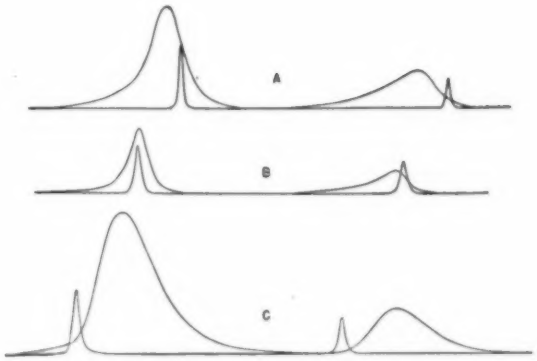

Fig. 1. Microphotometer traces of $^2P_{\frac{1}{2}}$ and $^2P_{1\frac{1}{2}}$. (a) Broadened by helium; pressures 0.12 and 10.92 atmospheres; (445°K). (b) Broadened by neon; pressures 0.2 and 12.5 atmospheres; (440°K). (c) Broadened by argon; pressures 0.1 and 12.18 atmospheres; (430°K). Narrow peaks at the lower pressures.

Results and Discussion

(a) Broadening

The half-widths of the second doublet of the rubidium principal series broadened by helium, neon, and argon are given in Table I. In Fig. 2 the half-widths of the doublet are plotted respectively against the relative densities of these gases. These curves show that up to the highest relative density applied (8) the half-width *vs.* relative density curve is straight, indicating the pre-

[3] W. W. Watson and H. Margenau, Phys. Rev. **44**, 748 (1933); C. Füchtbauer and F. Gossler, Zeits. f. Physik **87**, 89 (1933).

[4] Ny Tsi-Zé and Ch'en Shang-Yi, Phys. Rev. **51**, 567 (1937).

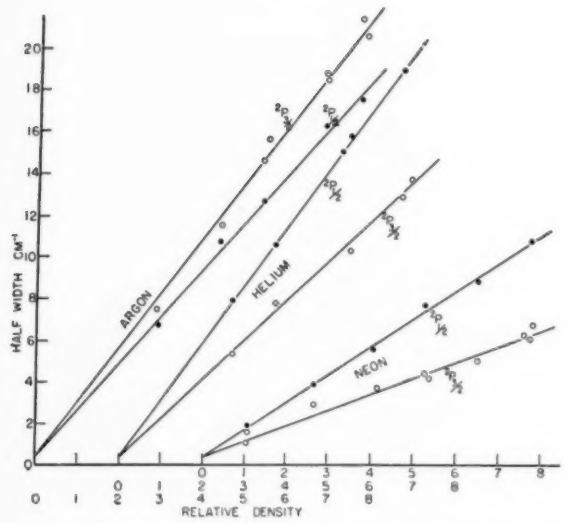

FIG. 2. The broadening of the violet Rb doublet by argon, helium, and neon. (Half-width in cm^{-1} *vs.* relative density.)

dominance of velocity broadening in this pressure region. The slopes of these curves are given in the second column of Table II. It is to be noted that helium and argon produced a much greater broadening than neon, and a marked difference between the half-widths of the doublet components was found. For helium and neon the half-widths of the $^2P_{\frac{1}{2}}$ component is greater than that of the $^2P_{1\frac{1}{2}}$ component, while for argon the half-width of the $^2P_{\frac{1}{2}}$ component is slightly smaller. Thus the effect of broadening by foreign gases that produce violet shift appears to be greater for the longer wave-length component of the doublet and *vice versa*.

Watson and Margenau,[1, 3] and Hull[1] have shown in their results for sodium (with H_2, N_2 and A) and potassium (with N_2 and A) that there is no significant difference between the half-widths of the doublet components for resonance lines and also for the second doublet of the potassium principal series. But Petermann[5] found that the blue Cs doublet and the corresponding potassium doublet show about 20 percent greater broadening for the shorter wave-length component when broadened by hydrogen. Here the results for rubidium with argon are in harmony with Petermann's results, but those with helium and neon for the violet rubidium doublet are true in the reverse sense, i.e., the

[5] Peterman, Zeits. f. Physik **87**, 96 (1933).

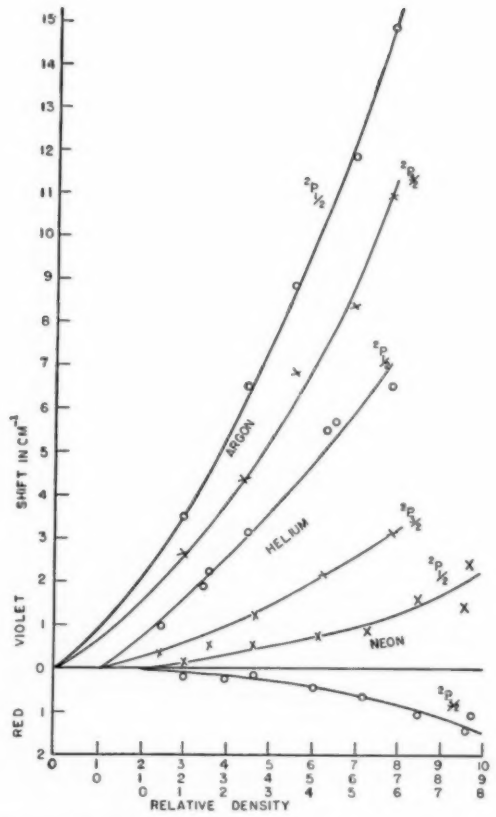

FIG. 3. The displacement of the violet Rb doublet by argon, helium, and neon. (Shift in cm^{-1} *vs.* relative density.)

doublet shows a stronger broadening for the longer wave-length component. These facts indicate that the perturbing effect of foreign gases may be different for different j values.

TABLE II. *Summary of results leading to the value* $\Delta V_{\frac{1}{2}}/\Delta V$.

Spectral Lines and Perturbing Gases	$\Delta V_{\frac{1}{2}}/d$ (in cm^{-1})	$\Delta V/d$ (in cm^{-1})	$\Delta V_{\frac{1}{2}}/\Delta V$	Observers
K 4044–N_2	1.10	0.55	2.0	W. & M.
K 4047–N_2	1.10	0.64	1.72	"
Rb 4216–He	2.77	0.93	3.0	N. & C.
Rb 4202–He	1.88	0.43	4.4	"
Rb 4216–Ne	1.30	0.22	5.9	"
Rb 4202–Ne	0.73	0.16	4.5	"
Rb 4216–A	2.21	1.2	1.8	"
Rb 4202–A	2.56	1.0	2.6	"
Cs 4555–He	1.28	0.39	3.3	F. & G.
Cs 4555–Ne	0.47	0.11	4.3	"
Cs 4555–A	1.27	0.53	2.4	"
Cs 4555–N_2	0.90	0.58	1.6	"
Cs 3876–He	2.88	1.79	1.6	"
Cs 3876–Ne	0.91	0.33	2.7	"
Cs 3876–A	2.69	2.12	1.3	"
Cs 3876–N_2	1.53	0.50	3.1	"

W. & M. = Watson and Margenau, see reference 3.
F. & G. = Füchtbauer and Gossler, see reference 3.
N. & C. = Ny and Ch'en, the present paper.

(b) Shift

Helium and argon produce a much greater shift of the maximum than neon, and the shift of the $^2P_{\frac{1}{2}}$ (λ4216) component is greater than that of the $^2P_{1\frac{1}{2}}$ (λ4202) component in agreement with the results of Margenau and Watson ($K-N_2$) and Hull ($K-N_2$ and A). The shift *vs.* relative density curves for the three gases are shown in Fig. 3. All show noticeable departure from linear relationship. Thus the values of the slopes of the shift *vs.* relative density curves shown in the third column of Table II are rather approximate. The shift appears to be proportional to the square of the relative density.

The shift produced by neon is very small. The $^2P_{\frac{1}{2}}$ component (λ4216) shows a weak shift towards the violet, while the $^2P_{1\frac{1}{2}}$ component (λ4202) shifts slightly towards the red. Helium produces a violet shift of the maximum for both components of the doublet. The shift of the $^2P_{\frac{1}{2}}$ component is nearly twice as much as that of the $^2P_{1\frac{1}{2}}$ component. With argon the shift is towards the red and is the greatest among the three gases.

(c) Asymmetry

So far there is no satisfactory way to figure out the asymmetry of the broadened line. The values given in the 5th column of Table I are the ratios of the red "half" to the blue "half" of the half-widths. Thus a value which is unity indicates a symmetrically broadened line, a value smaller than unity a violet asymmetry, and a value larger than unity a red asymmetry.

Helium and neon produce a violet asymmetry, while argon a red asymmetry. The degree of asymmetry decreases as the concentration of helium and argon decreases. But for argon the effective broadening towards the violet is at first much weaker than that towards the red, so that the line contour exhibits a very strong asymmetry towards the red under a few atmospheres of argon. When the concentration of argon was further increased, the effect of broadening towards the violet is increased appreciably with the increase of broadening towards the red resulting in a value of weaker asymmetry as shown in Table I.

The asymmetry is in general larger for the doublet component that gives the larger shift. A red shift is followed by a red asymmetry, and *vice versa* (the only exception being Cs λ3876 with N_2 observed by Füchtbauer and Gossler[3]).

(d) Comparison with other results

According to Margenau's theory when velocity broadening predominates, the half-width should be about twice as great as the shift. His treatment is based on resonance lines, but as a matter of fact he found his theory approximately true for the second doublet of potassium perturbed by nitrogen.

To observe the validity of his formula for slightly higher P states, tests are made using the results just obtained together with those obtained by various authors using different metals and foreign gases as in Table II. The values of $\Delta V_{\frac{1}{2}}/\Delta V$ as given in the 4th column of the table do not diverge very widely.

The Variation of the Initial Susceptibility with Temperature, and the Variation of the Magnetostriction and Reversible Susceptibility with Temperature and Magnetization in Nickel

DON KIRKHAM
Columbia University, New York, N. Y.*
(Received September 27, 1937)

This research is a sequel to an investigation, previously reported, of the variation of Young's modulus and internal friction with magnetization and temperature in a specimen of annealed, polycrystalline Mond nickel. The specimens used in both researches were cut from the same bar of material and annealed in the same manner. Complete data are given which show the variation of the initial susceptibility with temperature and that of the magnetostriction and reversible susceptibility with temperature, magnetization and magnetizing field between 21°C and the Curie temperature. The course of the initial susceptibility *vs.* temperature curve indicates a transition of the direction of intrinsic magnetization of the elementary domains in nickel from 111 to 100 at about 200°C. Further discussion of the results, in accordance with the domain theory of ferromagnetism, will appear in a subsequent paper by W. F. Brown, Jr.

DR. W. F. BROWN[1] has recently published a generalized development of the domain theory of ferromagnetism, certain formulae of which correlate quantitatively the different magneto-mechanical phenomena exhibited by ferromagnetic substances. It is evident that the adequacy of such formulae can best be tested by comparison with the observed behavior of specimen materials as nearly as possible the same, and that this is particularly true when the substance concerned is polycrystalline.

Siegel and Quimby[2] have measured the variation of Young's modulus and the internal friction with magnetization and temperature between 23°C and 400°C in a specimen of annealed, polycrystalline Mond nickel. The object of the present paper is to report the observed variation of the initial susceptibility with temperature and that of the magnetostriction and reversible susceptibility with temperature and magnetization over the same temperature range, in specimens of nickel cut from the same bar of material and annealed in the same manner.

Specimen Material

The specimen material is Mond nickel containing 0.295 percent impurity distributed as follows:[3] Co, 0.00; Si, 0.01; Cu, 0.02; Fe, 0.11; Mn, 0.00; C, 0.049; Mg, 0.11; S, 0.005. The specimens were annealed at 1100°C for 4 hours in hydrogen at atmospheric pressure and allowed to cool to room temperature in 18 hours.

Magnetostriction Measurements

Figure 1 is a diagram of the magnetostriction extensometer. The specimen, in the form of an ellipsoid of revolution 0.5 inch in diameter and 7.5 inches long,[4] has on its surface two tiny coplanar lateral scratches, one near each end. These scratches engage clear fused quartz knife edges of triangular cross section (*F* and *J*, Fig. 1). One knife edge (*F*) rests on two clear fused quartz rollers 1 mm in diameter, and the other (*J*) on a sliding steatite platform which is loosely connected through a quartz rod to a differential screw not shown in the figure. One of the rollers is an idler, and the other carries a mirror of gold sputtered on fused quartz. Both rest on a fused quartz plate ground to an optical flat. This plate is supported on a Duralumin base, at one end by a knife edge and at the other by a roller. The effective lengths of the quartz plate and Duralumin base are so adjusted that

* Now at Utah State Agricultural College, Logan, Utah.
[1] W. F. Brown, Jr., Phys. Rev. **52**, 325 (1937).
[2] Siegel and Quimby, Phys. Rev. **49**, 663 (1936).
[3] This analysis, together with the specimen material itself, was furnished by the International Nickel Company.
[4] The form effect discussed by Becker (Zeits. f. Physik **87**, 547 (1934)) is negligible for an ellipsoid of these dimensions.

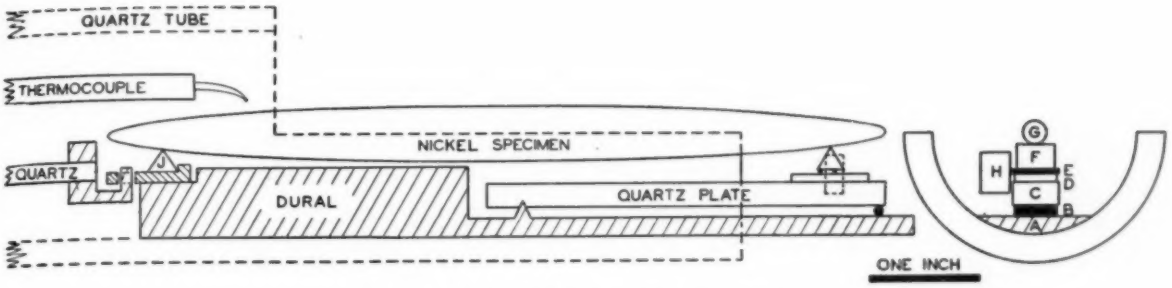

FIG. 1. The magnetostriction extensometer.

the relative thermal expansion of the specimen and its mounting is nearly nil over the operating temperature range. Small adjustments in the position of the mirror are made by sliding the rear knife edge with the differential screw beforementioned.

The extensometer rests in one end of a Vitrosil tube 2.5 inches in diameter and 2 feet long, the other end of which is held in a vibration proofed clamp. This tube projects horizontally into a cylindrical electric furnace,[5] so that the specimen lies at the center. The furnace is surrounded in turn by a water-cooling coil of copper, and a magnetizing solenoid 42 inches long. The whole apparatus is carefully oriented so that the earth's magnetic field lies perpendicular to the long axis of the specimen.

Light from a vertical illuminated scale 4.5 meters distant is reflected from the extensometer mirror, deflected 90° horizontally by a prism, and enters the 3-inch objective of an astronomical transit. One mm scale deflection corresponds to a change in length per unit length of 7.6×10^{-7} in the specimen, and deflections can easily be read with 0.2 mm accuracy. When the deflections are small a filar micrometer eyepiece is employed, and with this observations can be repeated with 0.05 mm accuracy.

The temperature of the specimen is measured with a Pt *vs.* Pt 10 percent Rh thermocouple which nearly touches the specimen at its midpoint. The temperature is constant within 1°C over the length of the specimen, except that during the measurements near the Curie point extra precautions are taken which reduce this variation to less than 0.4°C.

The magnetization is measured with a fluxmeter galvanometer connected to a 34 turn coil of No. 40 chromoxide covered copper wire wound about the specimen ellipsoid at its center.

Figure 2 is a diagram of the arrangements for controlling the magnetizing field. R_1 is a fluid rheostat containing copper sulfate solution. The immersed electrode, C, slides on a track, and can be firmly engaged with a spring contact at each end of its path. It is clear from the figure that a complete excursion of this electrode, from end to end of its path and back, carries the specimen through a complete cycle of magnetization, the amplitude of which is determined by the magnitude of the resistance R_2. Furthermore, the specimen can be demagnetized by oscillating the electrode with continuously diminishing amplitude about the mid-point of the trough. The employment of a fluid rheostat in this manner ensures smooth and therefore certain operation of the extensometer roller system.

The variation of the magnetostrictive change in length per unit length, λ, with magnetization and temperature is given in Table I, in which J_s denotes the (technical) saturation value of the magnetization. The experimental procedure for obtaining these data is as follows: The specimen is demagnetized in the manner described in the preceding paragraph, and the fiducial reading of the extensometer is noted. The specimen is then

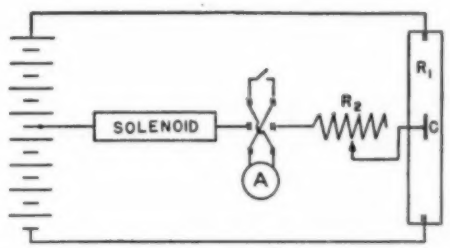

FIG. 2. The circuit for controlling the magnetizing field.

[5] A description of the furnace is given by Williams, Phys. Rev. 46, 1011 (1934).

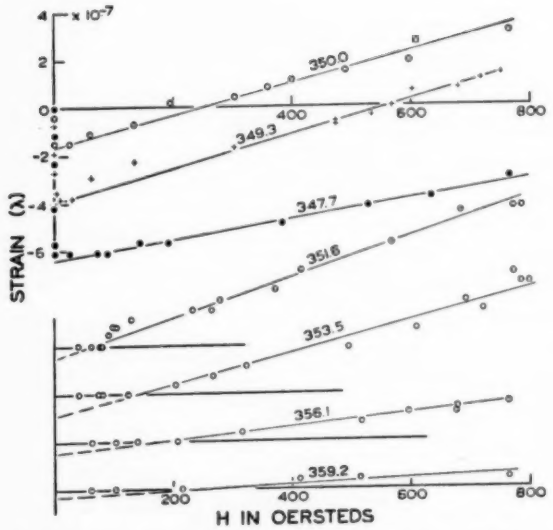

FIG. 3. The variation of the adiabatic strain with magnetizing field near the Curie point.

placed in a chosen cyclic state of magnetization and the corresponding magnetostrictive elongation is observed, the value adopted being the mean of those obtained before and after reversal of the solenoid current. The fiducial reading is checked after each such observation. Repetition of this procedure at a fixed temperature yields data from which is plotted a smooth curve showing the isothermal variation of λ with the magnetizing current. The isothermal variation of the magnetization, J, with magnetizing current is obtained with the fluxmeter in the usual manner. The isothermal variation of λ with J (or J/J_s) follows at once from these two sets of data.

TABLE I. *Variation of magnetostriction with magnetization and temperature.*

J/J_s / T°C	$\lambda \times 10^7$						J_s (H = 740)
	0.2	0.4	0.6	0.8	0.9	1.0	
6.0	7	35	100	207	292	399	487
26.5	6	34	96	201	278	390	483
61.7	8	35	94	191	262	372	468
115.8	8	32	85	172	239	331	443
153.2	6	28	77	155	215	297	422
192.8	6	29	71	142	191	254	398
209.2	4	26	70	137	181	233	387
231.1	4	23	61	120	157	203	370
247.8	4	20	53	107	142	178	354
264.3	4	19	48	95	122	153	335
290.1	2	12	34	68	90	112	295
297.6	2	11	29	59	78	100	282
321.7	1	6	16	33	45	59	228
335.4	0.4	3	8	19	26	33	185
345.9	0.1	1	4	8	11	13	124

Table II shows the variation of λ with temperature and magnetizing field, H. Values of H are computed with the formula, $H=H_0-NJ$, where H_0 denotes the applied field and N ($=0.1508$) is the demagnetization factor of the ellipsoidal specimen.

The experimental arrangements are such that the change in length of the specimen is produced adiabatically. Consequently the observed strain is the resultant of a magnetostrictive contraction and a thermal expansion associated with the magnetocaloric rise in temperature which accompanies the application of the field. The latter contribution is negligibly small, however, except in the neighborhood of the Curie point.

The data plotted in Fig. 3 show the variation of the resultant strain with magnetizing field at a number of temperatures near the Curie point. The presence of the magnetocaloric contribution is evident, and it will further be noted that the variation is linear in fields above 300 oersteds, where the magnetostrictive strain derives from the rotation of the elementary domain magnetizations into the field direction.[6] The intercept of this line on the axis of ordinates determines the strain which would ensue were all the domain magnetizations throughout the specimen to be aligned in the direction of easy magnetization most nearly that of the specimen axis. Accordingly, it is a measure of the intrinsic magnetostrictive deformation of the domains and hence of the domain magnetization itself. It follows

TABLE II. *Variation of magnetostriction with magnetizing field and temperature.*

H / T°C	$\lambda \times 10^7$							
	0.8	1.5	3.0	6.0	20	40	80	140
6	93	118	146	175	228	262	306	358
26.5	90	119	152	184	234	273	320	364
61.7	96	125	157	190	254	298	345	363
115.8	100	133	169	205	274	307	319	323
153.2	104	141	181	215	273	285	288	290
192.8	85	134	183	214	245	248	250	252
209.2	78	125	180	207	225	230	231	232
231.1	73	112	154	180	196	198	199	200
247.8	58	93	132	158	170	174	175	176
264.3	49	79	120	138	148	150	150	151
290.1	41	58	94	104	108	109	110	110
297.6	34	53	82	92	95	96	97	98
321.7	31	42	50	55	56	57	57	58
335.4	15	23	28	30	32	32	33	33
345.9	8	10	11	12	12	13	13	13

[6] This is in accord with the observations of Döring, Zeits. f. Physik **103**, 560 (1936).

that the variation of this quantity with temperature near the Curie point supplies an indication of the variation of the intrinsic domain magnetization with temperature in the same region. The result of the present measurements is given in Fig. 4.

This phenomenon has also been investigated by Döring,[6] who found a very much less abrupt decrease in the magnetostriction as the Curie point is approached, and a considerably higher value above it. It is probable that this discordance may be ascribed, in part at least, to temperature inhomogeneity in Döring's specimen. During the present observations the temperature in the air above the specimen was held constant to better than 0.4°C, so that the variation along the specimen itself must have been considerably less.

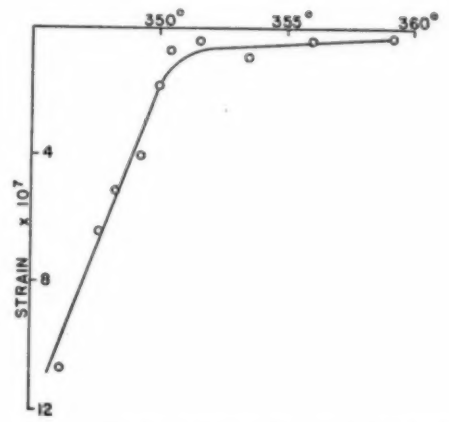

FIG. 4. Variation of the intrinsic domain magnetostriction with temperature near the Curie point.

INITIAL SUSCEPTIBILITY MEASUREMENTS

The specimen upon which the initial susceptibility measurements were made is in the form of a right circular cylinder $\frac{1}{8}$ inch in diameter and 2 inches long, terminated by the end sections of a coaxial ellipsoid of revolution. The form approximates that of an ellipsoid of revolution whose minor axis is $\frac{1}{8}$ inch and major axis 7.5 inches. The specimen material was cut from the bar of Mond nickel which furnished the larger ellipsoid, and the heat treatments of both were identical. The variation of the magnetization with magnetizing field and temperature is given in Table III. It will be noted that, in spite of the effort to secure specimens internally the same, the smaller ellipsoid is magnetically softer than the larger.

The fluxmeter coil consists of 2150 turns of No. 40 chromoxide covered copper wire wound in 4 layers on a Pyrex glass tube 5 mm in diameter and 5 cm long. The layers are separated by sheet mica 0.4 mil thick. One mm deflection of the fluxmeter galvanometer corresponds to 0.18 gauss change in J. The specimen, with the fluxmeter coil about the central cylindrical portion, is placed axially in the furnace solenoid system described above.

TABLE III. *Variation of magnetic field intensity with magnetization and temperature.*

J/J_s / T°C	MAGNETIZING FIELD IN OERSTEDS								J_s (H = 320)
	0.1	0.2	0.4	0.6	0.7	0.8	0.9	0.95	
21.6	0.293	0.389	0.546	0.900	1.82	6.51	35.8	96.0	491
99.0	.180	.242	.358	.601	1.16	3.21	13.0	35.0	471
171.5	.107	.151	.269	.503	.754	1.34	3.16	5.35	428
213.0	.0800	.114	.238	.441	.706	1.05	2.08	3.25	392
252.2	.0792	.110	.220	.482	.740	1 11	1.90	2.68	354
278.4	.0761	.111	.240	.510	.755	1.11	1.87	2.68	318
305.8	.0608	.092	.206	.418	.640	.915	1.63	2.37	274
341.8	.0299	.047	.101	.216	.331	.514	.840	1.30	162

The procedure for measuring the initial susceptibility is as follows: The specimen is demagnetized in the manner previously described and placed in a chosen cyclic state of magnetization. The galvanometer deflection accompanying reversal of the magnetizing current is then noted. These operations are repeated for increasing values of the current, the temperature being held constant. Finally, the magnetization and corresponding magnetic field are calculated in the usual way.

The results are shown in Fig. 5. It will be noted that, over the range of field values there included, the variation of J with H is strictly linear. The lines pass through their respective origins, and their slopes are the initial susceptibilities. The variation of the initial susceptibility with temperature is shown graphically in Fig. 6, and is tabulated in Table IV. The break at about 200°C indicates a transition of the direction of the elementary domain magnetization from 111 to 100.[7]

[7] A suggestion of this phenomenon is discernible in the J *vs.* T curves published by Honda and Nishina, Zeits. f. Physik **103**, 728 (1936), but the accuracy of their measurements does not permit a quantitative comparison with the present data.

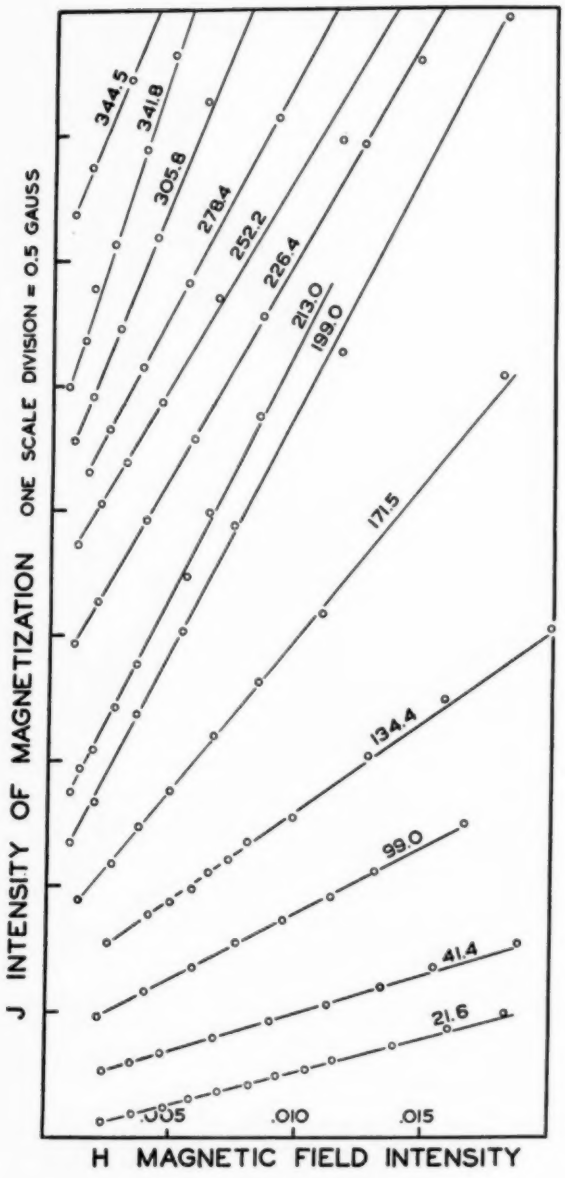

FIG. 5. The variation of magnetization with magnetizing field at low fields.

REVERSIBLE SUSCEPTIBILITY MEASUREMENTS

The experimental arrangements for measuring the reversible susceptibility are the same as for measuring the initial susceptibility, except that the first three layers of the four layer solenoid are used to produce a steady magnetizing field and the fourth layer to supply a small superimposed field of variable magnitude in the opposite direction.

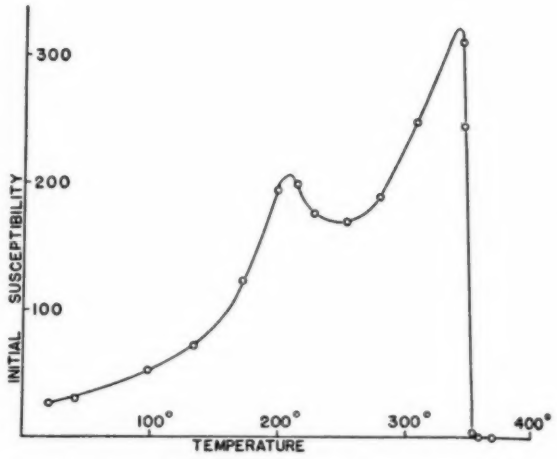

FIG. 6. The variation of the initial susceptibility with temperature in nickel.

The experimental procedure for measuring the reversible susceptibility corresponding to chosen values of the temperature and magnetization is as follows: The temperature is held constant and the required value of J (on the normal induction curve) is obtained by properly adjusting the value of the steady field. The small reverse field is applied and removed several times, until the fluxmeter deflections are the same on application and removal. (The initial deflection is always slightly larger than the final cyclic deflection.) This operation is repeated, with increasing values of the differential field, ΔH, and it is observed that the variation of ΔJ with ΔH is initially linear. Accordingly, the ratio $\Delta J/\Delta H$ is defined as the reversible susceptibility, χ_r. Below the knee of the normal induction curve the maximum value of ΔH for which this linear variation subsists increases from (approximately) 0.014 oersted at 21°C to 0.044 oersted at 306°C. The corresponding values above the knee of the curve are somewhat larger. The observed variation of χ_r

TABLE IV. *The variation of the initial susceptibility with temperature in nickel.*

T°C	χ_0	T°C	χ_0	T°C	χ_0
21.6	26.1	199.0	193	305.8	246
41.4	30.0	213.0	198	341.8	310
99.0	52.1	226.4	175	344.5	244
134.4	70.8	252.2	169	352.0	4.3
171.5	122	278.4	188	357.7	0.2
				368.0	.01

TABLE V. *Variation of the reversible susceptibility with magnetization and temperature.*

J/J_s / T°C	Reversible susceptibility, χ_r								
	0.0*	0.1	0.2	0.4	0.6	0.7	0.8	0.9	0.95
21.6	24.4	24.0	23.0	19.6	13.9	7.6	2.4	0.5	0.4
99.0	46.0	44.2	43.2	37.1	27.1	17.2	7.3	2.0	1.3
171.5	111	110	104	86	63.7	46.7	28.0	9.7	4.1
213.0	205	199	186	150	104	78.0	49.1	18.6	6.8
252.2	152	150	143	121	90.5	71.2	50.0	26.0	9.2
278.4	164	162	156	130	94.0	72.5	50.2	24.0	8.9
305.8	216	209	192	150	106	82.5	54.5	24.0	9.1
341.8	278	264	244	189	128	96.7	60.0	24.8	7.9

* Extrapolated values

with magnetization and temperature is given in Table V. The values corresponding to $J=0$ are obtained by extrapolation.

An interpretation of the data presented in this report, in accordance with the domain theory of ferromagnetism, will appear in a paper shortly to be submitted for publication in this journal by Dr. W. F. Brown, Jr. In conclusion the writer desires to acknowledge his indebtedness to Dr. S. L. Quimby, who suggested this research and followed its progress with helpful counsel and encouragement.

DECEMBER 1, 1937 PHYSICAL REVIEW VOLUME 52

Magnetic Field of a Symmetrical Bundle of Parallel Wires Carrying Equal Currents

C. G. DUNN AND G. L. CLARK
Departments of Physics and Chemistry, University of Illinois, Urbana, Illinois

(Received July 28, 1937)

The radial and circumferential components of the magnetic field outside and inside a bundle of parallel current filaments equally spaced on an infinitely long cylinder are derived in convergent series form. The assumption usually made that the mean circumferential component is a sufficiently good approximation to the actual field at radii of interest is justified by calculation at 12 mm radius from the axis of a bundle containing 36 wires, 6 at 3 mm radius, 12 at 6 mm, 18 at 9 mm. The maximum deviation of the circumferential field from its mean value is here found to be less than one-half percent. A quickly applied primary winding of 36 turns for ring specimens is described. It consists of a central bundle, flat end connecting blocks and external cage. The region of good circular field lies between radii of 12 mm and 60 mm, and is 70 cm in axial length.

THE type of magnetic field produced by a single straight wire infinite in length and carrying an electric current is well known. A compact group of wires would produce a similar field except for the region near the wires where the discontinuous nature of the group would produce fluctuations in the field. By considering a symmetrical group it is possible to determine the amount of the periodic variation in the field, and it turns out to be expressible in terms of a rapidly converging series. The actual details of the derivation are simplified by using complex variables and properties of the roots of unity.

Consider n infinitely long wires each carrying a current I amperes and placed so that the axis of each wire lies on a circle of radius a. The angular separation of the wires will be $2\pi/n$ radians. The average magnetic field at a distance r from the center of the group is

$$\bar{H}=\int Hdl \Big/ \int dl = 0.4\pi nI/2\pi r = 0.2nI/r.$$

The actual magnetic field, however, depends upon the position of the point P on the circle and will be found by adding together the fields obtained by considering each wire separately. Referring to Fig 1, it is seen that wire number 1 gives a magnetic field $0.2I/R$ with components $0.2I\cos\beta/R$ perpendicular to r and $0.2I\sin\beta/R$ parallel to r. It follows that

$$(H_1)_\theta = \frac{0.2I}{r}\,\frac{1-\rho\cos\alpha}{1-2\rho\cos\alpha+\rho^2}$$

and

$$(H_1)_r = \frac{0.2I}{r}\,\frac{\rho\sin\alpha}{1-2\rho\cos\alpha+\rho^2},$$

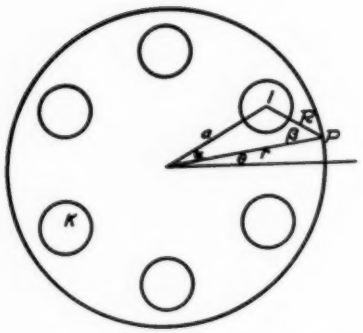

FIG. 1. A symmetrical group of six wires.

where $\rho=a/r$. By writing $H_1=(H_1)_\theta+i(H_2)_r$ in complex variable form the following is obtained:

$$H_1=\frac{0.2I}{r}[1+\rho e^{i\alpha}+\rho^2e^{2i\alpha}+\cdots+\rho^me^{mi\alpha}+\cdots].$$

In general the angular position of the $(k+1)$th wire is

$$\alpha+2\pi k/\mathrm{n},\quad k=0,\,1,\,2,\,\cdots n-1.$$

Therefore

$$H_{k+1}=\frac{0.2I}{r}[1+\rho e^{i\alpha}e^{2\pi ki/n}+\rho^2e^{2i\alpha}e^{2\pi 2ki/n}+\cdots+\rho^me^{mi\alpha}e^{2\pi mki/n}+\cdots].$$

The total field H will be

$$\sum_{k=0}^{n-1}H_{k+1}$$

and will appear in complex variable form. Therefore

$$H=\frac{0.2I}{r}\left[\sum_{k=0}^{n-1}1+\rho e^{i\alpha}\sum_{k=0}^{n-1}e^{2\pi ki/n}+\cdots+\rho^me^{mi\alpha}\sum_{k=0}^{n-1}e^{2\pi mki/n}+\cdots\right].$$

The terms of the sum

$$\sum_{k=0}^{n-1}e^{2\pi ki/n}$$

are the nnth roots of unity; so

$$\sum_{k=0}^{n-1}e^{2\pi ki/n}=0.$$

Consider the general term $e^{2\pi mki/n}$. If m and n have no common factor such as 2, 3, 4, $\cdots$, then the sum is again composed of the nnth roots of unity. If m and n have a factor of 2, one obtains a repeated subgroup of the nnth roots of unity with only $n/2$ roots present. However, these are just the ones that correspond to the $n/2$ roots of unity so

$$\sum_{k=0}^{n-1}e^{2\pi mki/n}=0.$$

If m and n have a common factor of 3, 4, etc., the arguments are similar. However, if $m/n=1$, 2, 3, etc., then

$$\sum_{k=0}^{n-1}e^{2\pi mki/n}=n.$$

Consequently, most of the powers of ρ drop out of the series. The result is

$$H=\frac{0.2nI}{r}+\frac{0.2nI}{r}(\rho^ne^{ni\alpha}+\rho^{2n}e^{2ni\alpha}+\cdots)$$
$$=\bar{H}+\bar{H}(\rho^ne^{ni\alpha}+\rho^{2n}e^{2ni\alpha}+\cdots).$$

The component of H perpendicular to r is

$$H_\theta=\bar{H}+\bar{H}(\rho^n\cos n\alpha+\rho^{2n}\cos 2n\alpha+\cdots).$$

The imaginary part gives the other component H_r. Since $\rho<1$, $(r>a)$, it is seen that the series will tend to converge very rapidly for n fairly large and furthermore the second term gives the variation of H_θ with α.

If a circular path is taken within the group $(r<a$ and $\rho=r/a)$, then the average field is zero. The addition of the fields obtained by considering each wire separately gives directly the variation in the field. The procedure is the same as that used above. The following expression is obtained:

$$H_1=(0.2I/\rho a)(\rho e^{i\alpha}+\rho^2e^{2i\alpha}+\cdots).$$

Adding all the fields gives

$$H=(0.2nI/a)(\rho^{n-1}e^{ni\alpha}+\rho^{2n-1}e^{2ni\alpha}+\cdots).$$

The real part gives

$$H_\theta=(0.2nI/a)(\rho^{n-1}\cos n\alpha+\rho^{2n-1}\cos 2n\alpha+\cdots).$$

Application

In a previous paper[1] one of the authors described a form of primary winding that was being used in testing ring specimens. This type of winding has been improved from a two dimensional form to a symmetrical three dimensional form which produces a good circular field along the entire central region. The fundamental principle of the device is not essentially new. A prototype is described by Mollinger[2] and various "bird-cage" windings have been in use. Kelsall[3] devised a one-turn winding for high frequency a.c. which was an improvement over earlier models.

The frame consists of two hard rubber ends and four brass rods. The magnetizing coil is made of copper wire of B and S gauge No. 12. Bakelite guides are used in the closely packed central group to form three symmetrical layers of six, twelve, and eighteen wires respectively. The No. 12 wire also enables one to make socket type connections in such a way as not to interfere with the use of small specimens. Rings of inside diameters of twenty-four millimeters may be slipped onto the central group after first compressing the brush-like group at the top and sliding the brass ring well up towards the end. Symmetry arrangements and slight differences in the lengths of the wires makes it possible to correctly connect the thirty-six wires in series. If only eighteen wires are desired, a shift in one lead removes a symmetrical group of eighteen. Thus, the primary winding can be applied to one or many specimens in just a few minutes. Suitable specimen holders may be placed anywhere along the central region.

[1] C. G. Dunn, Rev. Sci. Inst. **7**, 359 (1936).
[2] Mollinger, *Gumlich—Leitfaden der magnetischen Messungen* (1918), p. 149.
[3] Kelsall, J. O. S. A. **8**, 329 (1924).

In regard to the uniformity of the magnetic field, it is fairly easy to see that the main variation in H near the center is produced by the central group—the ends and sides producing negligible effects. On a circle of radius r taken anywhere along the central group the average magnetic field $\bar{H}$ is $0.2\times 36I/r$. To compute the variation in H, it is sufficiently accurate to consider these wires as infinite in length. Hence,

$$H_\theta=\bar{H}+\bar{H}(\rho^n\cos n\alpha+\rho^{2n}\cos 2n\alpha+\cdots),$$

which is a maximum when $H_\theta=\bar{H}(1+\rho^n+\cdots)$. For the three layers of wires the maximum value of ρ is $\frac{1}{4}$, $\frac{1}{2}$, and $\frac{3}{4}$ respectively and n is 6, 12, and 18, respectively. (The three layers of wire have mean radii of 3, 6, and 9 mm and r is equal to or greater than 12 mm.) Therefore,

$$(H_\theta)_6=(\bar{H}/6)[1+(1/4)^6+\cdots]$$
$$=\bar{H}[1/6+1/6(1/4)^6+\cdots$$

and $$(H_\theta)_{12}=(\bar{H}/3)[1+(1/2)^{12}+\cdots]$$
$$=\bar{H}[1/3+1/3(1/2)^{12}+\cdots$$

and $$(H_\theta)_{18}=(\bar{H}/2)[1+(3/4)^{18}+\cdots]$$
$$=\bar{H}[1/2+1/2(3/4)^{18}+\cdots.$$

If all three were to become a maximum together, then

$$(H_\theta)_{\max}=(H_\theta)_6+(H_\theta)_{12}+(H_\theta)_{18}=\bar{H}[1.003].$$

Consequently, the variation of H_θ is less than one-half of one percent. With respect to the apparatus described above, it may be stated that a good circular field occurs over a region of about seventy centimeters along the central part and radially outward to a distance well beyond six centimeters.

The authors are indebted to Dr. D. G. Bourgin, department of mathematics and Dr. J. Kunz, department of physics, for valuable advice.

X-Ray and Magnetic Analyses of Deformed Silicon Steel Rings

G. L. CLARK AND C. G. DUNN
Departments of Chemistry and Physics, University of Illinois, Urbana, Illinois
(Received July 28, 1937)

Flat rings cut from sheet silicon steel by grinding and etching, so as best to preserve the properties of uncut sheet, were clamped between dies that bent them to fit more or less closely over a toroidal plunger and allowed, under these conditions, testing of circumferential magnetization and taking of x-ray diffraction patterns (Laue type) at one point on the most deformed circle. Slight deformation temporarily shifts and elongates the Laue spots and depresses the magnetization curve. More severe deformation permanently displaces some Laue spots, although the crystals in their new orientations are not permanently strained. The magnetization curve is permanently depressed, and it is suggested that this is due to changes at grain boundaries not recorded by the x-ray method. Very severe deformation leaves some crystals strained, as shown by x-rays, and the permanent changes in magnetic properties are nearly as great as the temporary changes. The changes in shape of Laue spots in coarse-grained rings agrees at all stages with bending of strained crystals about axes lying in the original plane of the sheet. Specimens cut from partly annealed sheets that had previously been given various reductions in thickness by cold rolling showed parallel but rather erratic changes in magnetic hardness, measured by inverse maximum permeability, and x-ray strains, measured by range in angles of incidence on single crystals.

IN 1925 Clark[1] first showed a correlation between crystal grain size determined from x-ray patterns and hysteresis loss in commercial silicon steel, the loss increasing with decreasing size. Clark and Beckwith[2] devised a modulus from an x-ray pattern serving as a measure of slight residual distortion in grains, and showed that the magnetic permeability was a very sensitive function of this residual deformation.

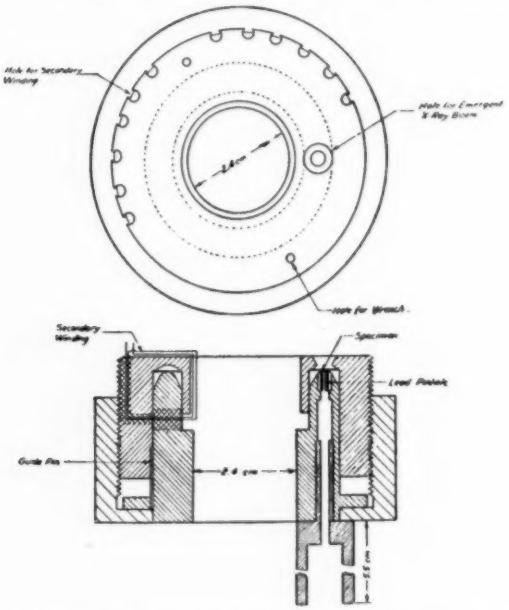

FIG. 1. Combined specimen holder, straining machine and x-ray pinhole system.

However, since previous work has been fragmentary, a quantitative correlation between crystal grain structure and deformation and magnetic properties is highly desirable. Because of the fundamental interest in such an investigation from both academic and practical points of view, the present work is concerned with obtaining the effects upon magnetic properties produced by small distortions of crystals in ferromagnetic sheet material.

EXPERIMENTAL PROCEDURE

At low fields the ring type specimen is particularly suitable. The problem of overcoming to a large extent the labor involved in the winding of such specimens was solved by constructing a permanent primary winding which is described in another paper.[3]

It was found possible to grind out flat ring samples from annealed sheet steel which had a maximum permeability of more than 6000, and therefore were subjected to much less cold work than were those obtained by any shearing operation.

The unique feature of the present work consists in the use of a single specimen which could be strained by varying amounts, and simultaneously

[1] G. L. Clark, *Applied X-Rays*, first edition (McGraw-Hill Book Company, 1926), p. 238.
[2] G. L. Clark and M. M. Beckwith, Zeits. f. Krist. **90**, 392 (1935).
[3] C. G. Dunn and G. L. Clark, Phys. Rev. **52**, 1167 (1937).

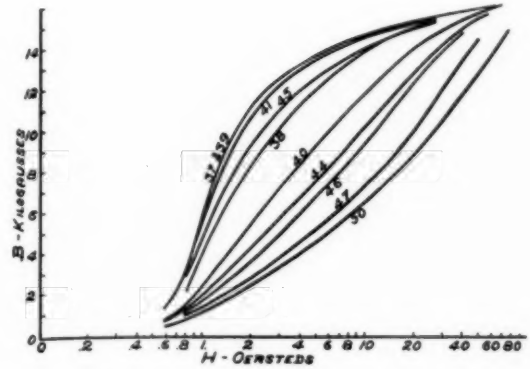

FIG. 2. *B-H* curves for different bending strains for 3.2 percent silicon steel (S series).

without removing from the straining machine subjected to x-ray diffraction analysis and magnetic testing.

Apparatus for producing strains

The straining machine, which is shown in some detail in Fig. 1, was made entirely of brass so that there would be no ferromagnetic materials present besides the specimen. The dotted lines in the top view indicate the position of the ring specimen. The side cross-sectional view shows three movable parts. One part called the plunger,

TABLE I. *Results of magnetic measurements on strained sample of small grain 3.2 percent silicon steel.* B_2 *is the magnetic induction in gausses at a magnetic field of 2 oersteds;* μ_m, *maximum permeability;* H_m, *the magnetic field at maximum permeability. The percentage drops in* B_2 *and* μ_m *are with reference to the unstrained sample S37. The strained condition is indicated by the rotation of the outer part of the straining machine; a rotation of 360° corresponds to an advance of the screw of 1/24 inches.*

No.	B_2	% Drop in B_2	μ_n	% Drop in μ_m	H_m	Condition of Strain (Screw Rotation)
S37	11,100	..	6460	..	1.27	0
S38	8,150	26.5	4430	31.5	1.40	40
S39	11,100	none	6460	none	1.27	0
S40	5,350	51.8	2720	57.9	1.55	65
S41	10,600	4.5	6100	5.6	1.28	0
S44	4,270	61.5	2150	66.7	1.60	90
S45	9,300	16.2	5200	19.5	1.35	0
S46	3,500	68.5	1810	72.7	1.67	103
S47	2,750	75.2	1430	77.9	1.75	163
S48	5,450	51.0	3090	48.5	1.54	0
S50	2,450	78.0	1250	80.7	1.80	240
S51	3,650	67.1	1850	71.4	1.67	0

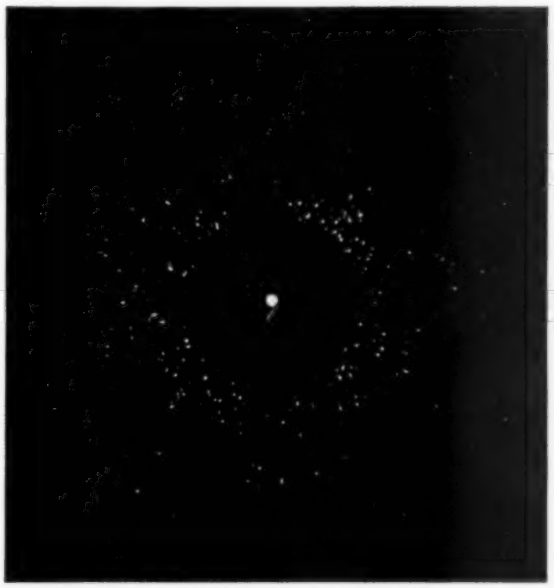

FIG. 3. Typical diffraction pattern for S44.

contains a lead pinhole which is one millimeter in diameter. A guide pin prevents the plunger from rotating as the plunger advances against the specimen. The outer part is knurled and can be held by hand; but the inner part must be held by a wrench. As may be inferred from the diagram, this type of straining frame bends the sample and puts it into a cupped form. The inner diameter of 2.4 cm, shown in the figure, allows the machine to be placed on the specimen support of the primary winding. In order to provide for a secondary winding which would not interfere with the straining operations, twelve holes were put through the plunger and smaller holes continued on through and around the stationary part. They are capable of handling 350 to 400 turns of fairly fine silk insulated wire. As the plunger advances, it is clear that these secondary windings will not be sheared or interfered with.

The open structure of the primary windings makes it possible to carry out straining operations while the straining machine is on the primary winding. Then without changing this condition the machine can be removed from the primary winding and transferred to the x-ray machine. The tube of 5.5 cm length shown in the figure slips into a slightly larger tube, which contains the second lead pinhole, and is directly lined up with an x-ray beam for taking transmis-

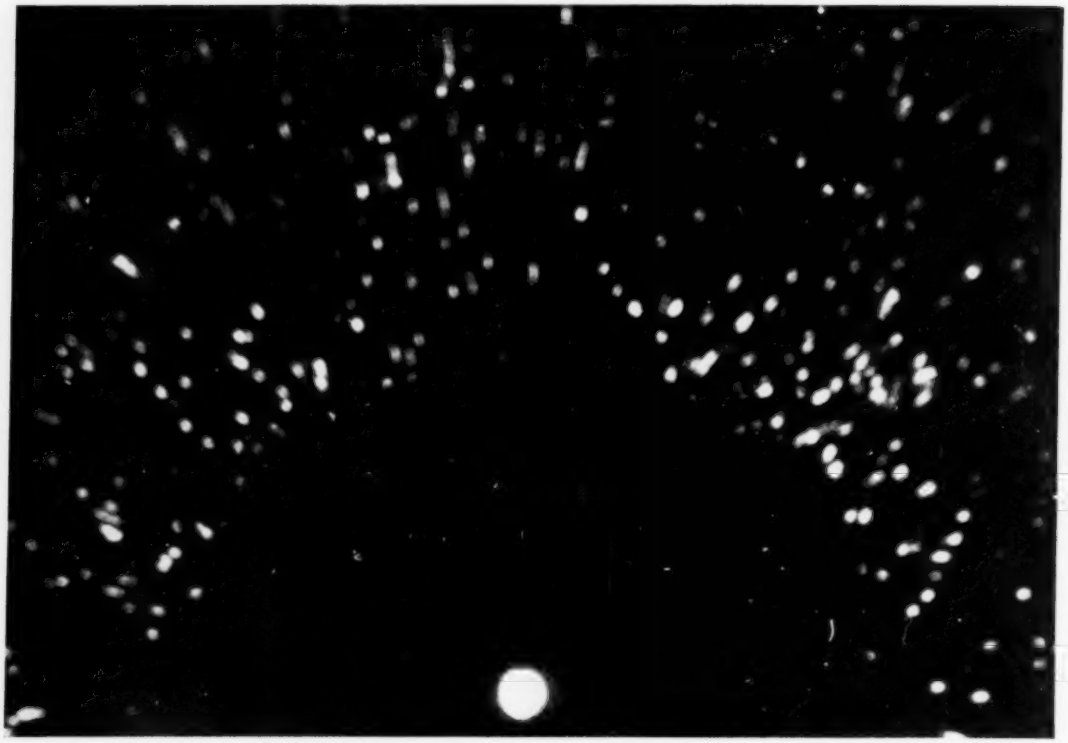

FIG. 4. Magnified pattern for S44 (strained).

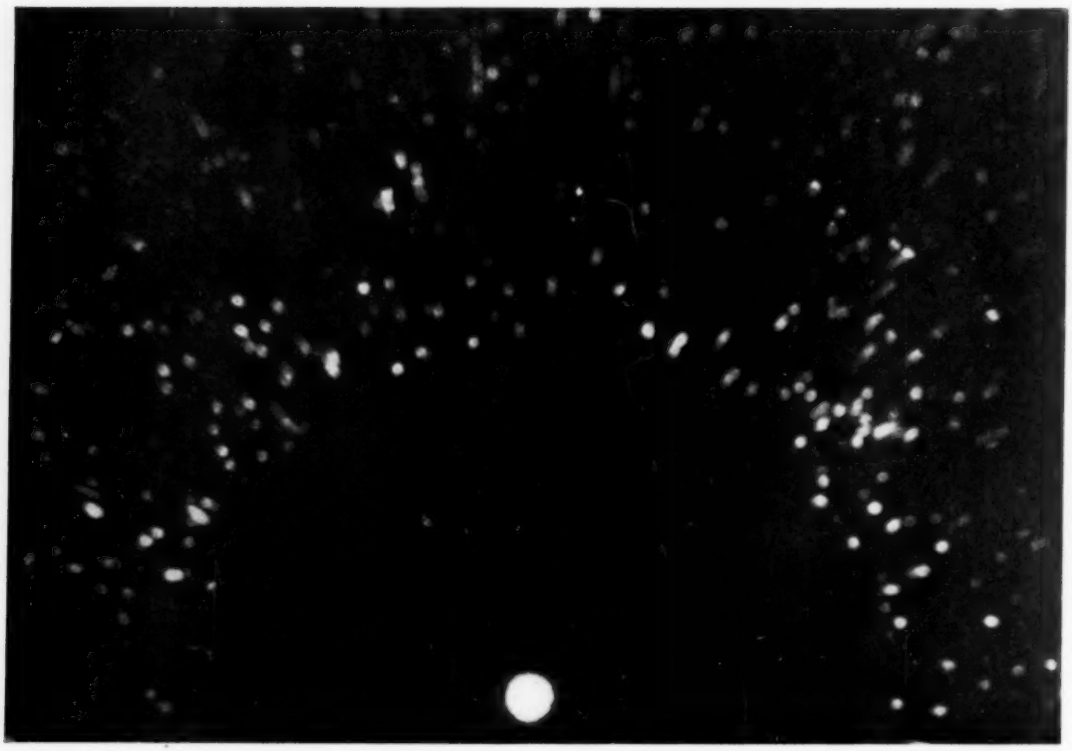

FIG. 5. Magnified pattern (4×) for original state in S series.

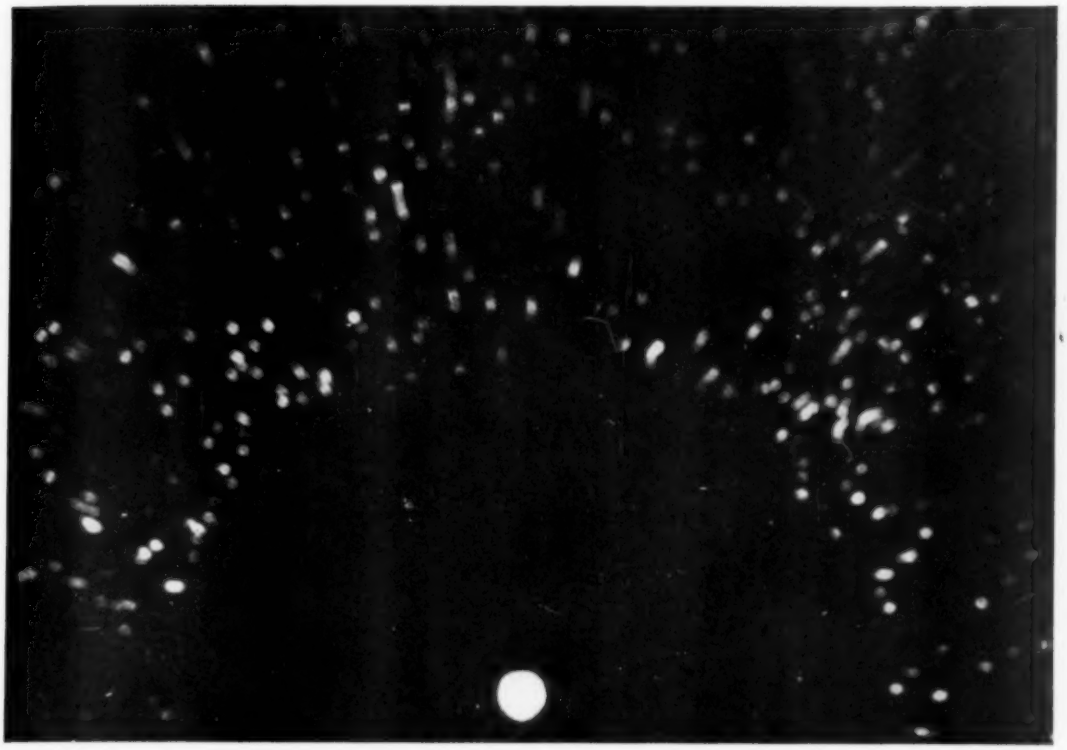

FIG. 6. Magnified pattern for S45 (stress removed).

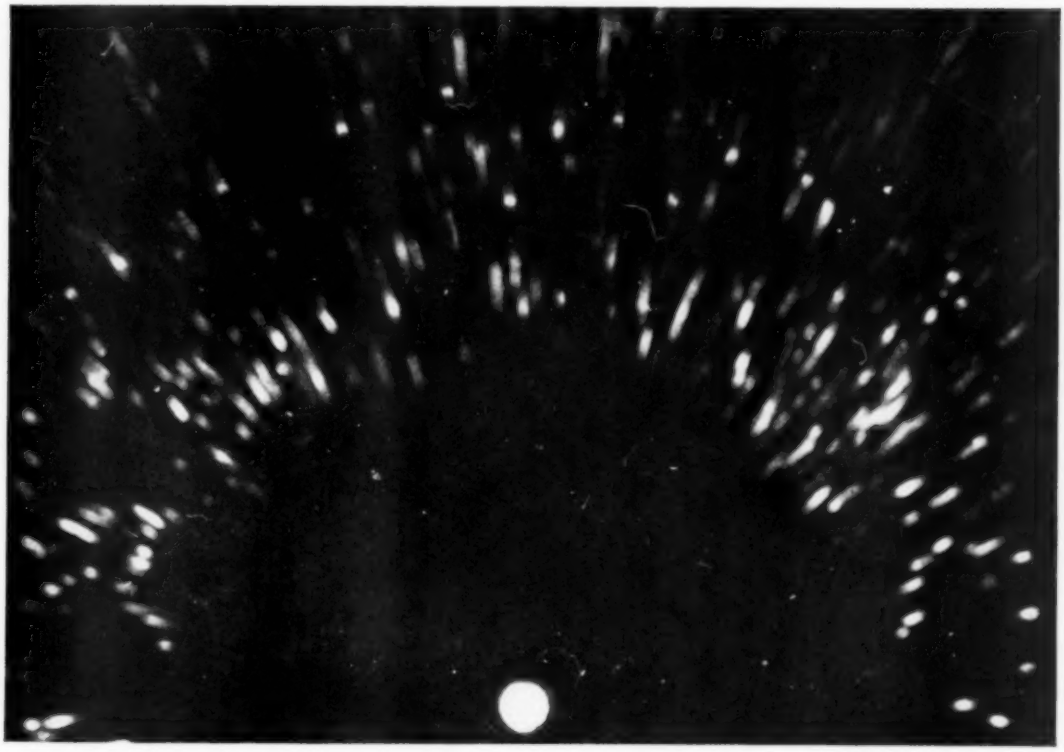

FIG. 7. Magnified pattern for S47 (with large residual distortion).

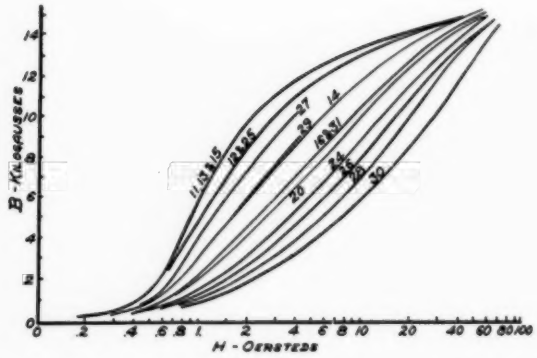

FIG. 8. *B-H* curves for different bending strains for 4.5 percent silicon steel.

sion Laue type patterns. By using a cassette that is screwed down, the film distance of 5 cm is never changed. Rotation of the outer part of the straining machine does not change this film distance Hence, a complete series of x-ray patterns can be taken and readily compared.

DISTORTION EFFECTS IN A SMALL GRAIN 3.2 PERCENT SILICON STEEL SAMPLE (S SERIES)

(a) Magnetic measurements

A 3.2 percent silicon steel sample was prepared from cold rolled sheet material of 0.033 cm thickness. It was then etched with aqua regia to a thickness of about 0.020 cm. and then given an anneal of two hours at a temperature ranging from 750 to 780°C. After furnace cooling, the sample was again carefully etched in order to obtain a clean surface. The final mass was 0.9020 grams, the mean radius 1.857 cm, and the cross-sectional area 0.01004 cm². Since the radial width of the sample was approximately 6 mm, this meant that the x-ray beam had to pass through a distance of 0.017 cm or about 0.007 inches.

TABLE II. *Results of magnetic measurements on strained sample of large grain 4.5 percent silicon steel.*

No.	B_2	H_m	μ_m	% DROP IN μ_m	SCREW ROTATION	$\Delta\theta$
Q11	9720	1.16	5960	..	0	None
Q12	8400	1.17	4940	17.1	66	None
Q14	5750	1.35	3110	47.8	103	None
Q16	4450	1.40	2310	61.2	120	0.6
Q20	4000	1.43	2030	65.9	128	.8
Q24	3060	1.50	1530	74.3	150	1.6
Q26	2550	1.55	1280	78.5	172	2.1
Q28	2200	1.60	1100	81.6	210	3.5
Q30	1750	1.65	885	85.2	290	5.0
Q13	9720	1.16	5960	None	0	None
Q15	9700	1.16	5900	1.0	0	None
Q17	9500	1.16	5820	2.3	0	None
Q21	9280	1.16	5600	6.0	0	None
Q25	8400	1.17	5000	16.1	0	None
Q27	7550	1.20	4250	28.5	0	0.3
Q29	6100	1.30	3300	44.5	0	1.0

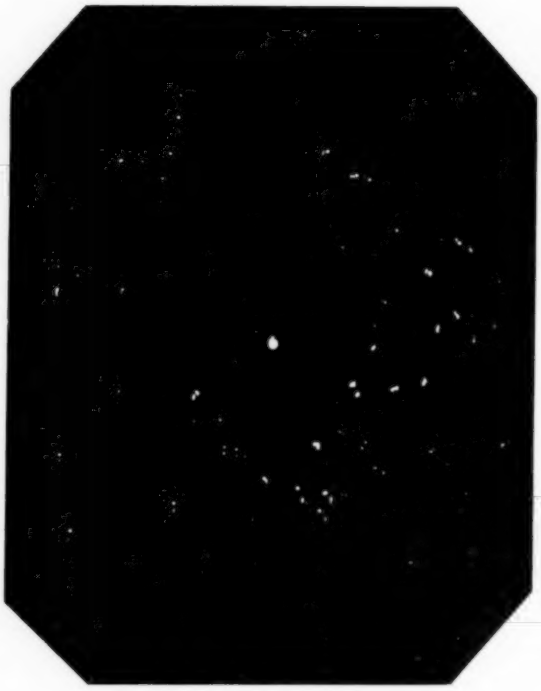

FIG. 9. Double exposure pattern for specimen stressed and unstressed (Q16–17) showing change in shape of spots.

For the sample in the unstressed condition (S37) a galvanometer deflection of 100 mm was obtained at a field of two oersteds. At 60 oersteds a deflection of 220 mm was obtained. In the small deflection range it was possible to estimate fractions of a millimeter; so the data obtained were good in general to within one percent.

Table I gives some of the numerical results. The order in which the data were obtained is the same as that of the designation numbers. That is, data on S39 were taken directly after those on S38, etc. For this reason some numbers, such as S42, do not appear because the data presented were considered sufficient to show the trend of changes within the specimen.

As may be seen from the curves of Fig. 2, it is possible to have large elastic recoveries. S37 and S39 are the same to within the accuracies of measurement. When the stresses are not too large, the curves tend to converge at about 70

oersteds. S47 and S50, however, are still much below the other curves. Since the rotation of the screw for S50 was 240, the sample was cupped enough to produce a radius of curvature of 5 mm. This amount of bending would very probably introduce internal air gaps or small cracks which would account for the slow convergence in the high magnetic field range. Test S51, which represents the final condition of the specimen, was considerably bent. In the low field range S51 was nearly the same as S46. At higher fields the curve of S51 lies below that of S46. S48 and S51 tend to converge together much less than do the curves of S40 and S46. It appears then that the sample has become inhomogeneous, some parts being slightly strained and other parts strained to a high degree.

(b) X-ray data

The x-ray interference patterns were obtained by using unfiltered molybdenum radiation from a tube operating at 26 kv and 23 ma. To stop fogging of the film due to scattered radiation, a tin filter in the form of a thin foil was placed in front of the x-ray film.

Figure 3 shows a typical pattern for the specimen in question in the state of strain S44. An enlarged print (magnification of four) of S44 in Fig. 4 indicates the great possibilities of detecting very small changes in the positions and definitions of spots, especially by comparison with enlarged prints of the original unstressed ring specimen (S37) (Fig. 5); of S45 (Fig. 6) which represents release of stress immediately following S44; and of S47 for a high stress with complete lack of recovery (Fig. 7).

The magnetic measurements show that S39 represents a complete recovery from S38 where the drop in B_2 was 26.5 percent. Referring to the x-ray pictures of S39 and S38, little difference is seen in the *shapes* of corresponding spots, but there are some groups which show relative shifting of the spots. This means that there has been some elastic rotation of the crystals relative to one another.

The pattern for S40 shows the change in relative positions within the selected group of spots to be much larger.

The magnetic tests show that S44 was strained so that B_2 dropped 61 percent. Upon removing the applied stress it was found (S45) that B_2 was still 16 percent below S37. Internal strains were introduced. The x-ray pictures show considerable relative shifting of spots in S44 but still no noticeable change in original sharp Laue spots. S45 shows that considerable recovery in the position of spots has occurred, but there are a number of differences between S45 and S39.

S46–S47 show marked distortions in the crystals because the original sharp Laue spots are now definitely elongated. Additional relative rotation of crystals is observed. These results indicate beginning stages of the fragmentation of the larger crystals. If the crystals are held mechanically in a bent form either by internal or external stresses, then they would also give the types of radial streaks observed in S47.

Upon removing the external stress, B_2 of S48 was found to be 51 percent below S37. The x-ray picture of S48 shows considerable distortions of the spots. When the maximum stress was applied (S50) very marked radial streaks occurred. These streaks are away from the axis of bending of the sample; and could be fit to a Leonhardt curve.[4]

Distortion Effects in a Large Grain 4.5 Percent Silicon Steel Sample (Q Series)

(a) Magnetic measurements

The measurements were made in the same manner as those in the S series. The sample in this case was prepared from 4.5 percent silicon sheet steel which had first been annealed for four hours at 800°C, then given a light pickle, and finally cold reduced by 10 percent. The ring specimen was then etched to a thickness of less than 0.020 cm. By annealing the ring for several hours at a temperature between 850 and 870°C and then gradually cooling down to room temperature, a sample of fairly large grains was obtained. This sample was further etched to remove the surface layers formed in the furnace.

The final ring sample had a mass of only 0.606 grams and a cross-sectional area of 0.00679 cm². The mean radius was 1.862 cm. In this case the x-ray beam would have a thickness of 0.004 to 0.005 inches to traverse. Because of the smallness of the sample, 360 secondary turns were applied.

[4] J. Leonhardt, Zeits. f. Krist. **61**, 100 (1924).

At a magnetic field of 54 oersteds a galvonometer reading of 332 mm was obtained, the air core part contributing 146 mm of this. At maximum permeability the correction due to the air core was about 4 percent.

Figure 8 shows curves connecting B and H for various states of strain as represented in Table II. From measurements on the disotrtions of the Laue spots the amount of bending of a crystal ($\Delta\theta$) was also computed.

In some of the work two patterns were taken on the same film (Fig. 9). This was done as follows: While on the primary winding the sample was strained to a suitable extent and the magnetic measurements made. It was then transferred to the x-ray machine. Without moving any apparatus, the stress was removed from the specimen after taking the first exposure. Another was then taken on the same film. To further aid in the study, one or both of the separate diffraction patterns were usually taken. When the stress was removed, a small amount of rotation occurred about the x-ray, beam as an axis. Consequently, with these double pictures it was possible to study relative shifting of spots

In the initial unstressed condition, Q11, the sharp Laue spots indicate good crystals. Double patterns of the specimen with and without small deformation show a small shift in the spots which may be due to a rotation of a group and therefore does not show clearly any relative rotation of crystals. The complete recovery magnetically indicates only elastic processes. Since Q15 did not return completely to the condition of Q11 (a 1 percent drop in μ_m occurred), it seems reasonable to suppose that just before the large crystals became distorted to an appreciable extent the crystallites between the larger crystals either are forced into new stable positions or broken into smaller grains. Further bending of the sample would bring the large crystals into more direct contact and they would become bent.

Figure 9 for tests Q16–17 shows directly the change in shape of the Laue spots when the larger stress is applied. This pattern also shows that there was elastic rotation of at least one crystal in the path of the x-ray beam because the relative shifting of spots (allowing for the rotation about the direction of the beam) could not be produced by a group rotation about the axis of bending.

For Q20 the distortions of the Laue spots are considerably larger than those in Q16, but the distortions occurred largely in an elastic way. Table II shows the remarkable recovery in the maximum permeability.

For Q24 asterism spots were still more definitely formed with the sample stressed so that μ_m dropped by 74 percent. However, when the stress was removed the asterism disappeared. Comparing with the original pattern of Q11, the x-ray pattern has not changed much from a standpoint of large deformations. The difference in relative intensities of spots is quite noticeable. When negatives of Q11 and Q25 are compared directly by superposing one on the other, then relative displacements of spots are immediately noted. It appears that crystals have failed to rotate back into their initial positions. Since no asterism appears, the larger crystals seem to be fairly free from stress.

With higher stresses radial streaking of spots occurs to a still greater extent. These asterism spots correspond to a bending of the crystal by 2 to 3.5°. Upon removal of the stress, these spots recovered to a large degree but still remained distorted to the extent of 0.3 to 1.0°.

The highest stress obtainable by the straining machine was applied in test Q30. The pattern shows pronounced radial streaks. In order to study the nature of the bending of the crystals, use was made of Leonhardt's curves as was previously described.[4]

The results of the Q series show that crystals in a polycrystalline sheet can be elastically rotated and also elastically bent. This bending of the crystal produced the well known radial streaks or asterism. Hence, data are presented which confirm other work on elastic deformations in silicon steel.[5] Furthermore, the magnetic measurements show that internal strains which are indicated by asterism reduce the quality of the material. Since internal air gaps or cracks tend to form when crystals rotate relative to one another, and since such air gaps have a great effect on magnetic properties, it seems that the x-ray and magnetic data presented point to a certain amount of crack formation upon bending of the material.

[5] G. L. Clark, *Applied X-Rays*, second edition (McGraw-Hill Book Company, 1932), p. 400.

Some Results on the Effect of Cold Rolling (H Series)

Samples of 4.5 percent silicon sheet steel were annealed for four hours at 800°C. These sheets were then given cold reductions of 2, 3, 4, 6, 8 and 10 percent, respectively. From each sheet a specimen was ground out as previously described. These were then given an anneal of several hours at a temperature of 750°C which was not high enough to remove all strains. By the use of a machine, about 300 turns of secondary wire were put on each ring. All six specimens were then mounted in the primary winding and the tests made.

Table III gives some results in the neighborhood of the maximum permeability.

From these data the maximum permeabilities are found. Table IV shows the maximum permeability and the percent reduction in area of the original sheet.

These results point to some periodicity in the process of deformation produced by cold work. X-ray work on the shape of Laue spots led Clark and Beckwith[2] to conclude that cold work, in the form of cold rolling, of 4 percent silicon steel produced a periodic fragmentation of the crystals. In Fig. 10 are reproduced curves relating the modulus, obtained from measurements on Laue spots and the percent reduction in area. The reciprocal of the maximum permeability multiplied by 10^4 plotted on the same graph gives the same general type of curve. It would be reasonable to conclude that this is evidence for a relationship between the shape of Laue spots and the magnetic quality of the material, and that asterism streaks in an x-ray diffraction pattern indicate an inferior magnetic quality, other things being the same.

Table III. *Magnetic measurements in the neighborhood of maximum permeability which show the effect of cold rolling.*

	H2a		*H3a*		*H4a*	
H	*B*	μ	*B*	μ	*B*	μ
0.706	1540	2030	1800	2550	2420	3430
.803	2530	3150	3370	4200	3400	4235
.895	3400	3800	4840	5410	4200	4690
1.002	4230	4220	6250	6240	5010	5000
1.255	5650	4500	8250	6570	6450	5140
1.464	6570	4490	9340	6380	7420	5050
1.750	7230	4130	9930	5670	8080	4610
2.020	7790	3860	10370	5130	8700	4310
2.510	8600	3430	10910	4350	9540	3800
3.000	9220	3070	11270	3760	10110	3370
59.4	14470	243	14300	241	14450	243

	H6a		*H8a*		*H10a*	
H	*B*	μ	*B*	μ	*B*	μ
0.501	3120	6230	3460	6910	2850	5690
.600	4440	7400	4900	8170	4070	6780
.705	5560	7880	6040	8560	4970	7050
.808	6450	7980	6870	8500	5750	7120
.905	7210	7970	7550	8340	6390	7060
1.002	7850	7830	8070	8060	6940	6930
1.250	8980	7190	9060	7250	8030	6420
1.498	9730	6490	9720	6480	8840	5900
1.738	10170	5860	10120	5830	9380	5400
2.005	10520	5250	10440	5210	9850	4910

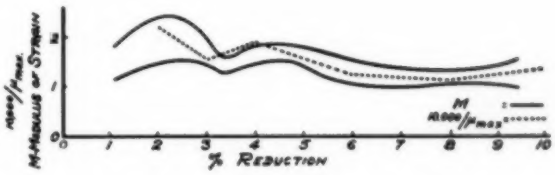

Fig. 10. Periodicity as a function of cold rolling of x-ray modulus and of 10,000/maximum permeability.

The Dependence of the Divergence of a Diffracted X-Ray Beam on Distortion

An attempt was made to determine that part of the divergence of a diffracted x-ray beam which was due to crystal distortion and not crystal size. By making measurements on the pinhole system and knowing the film distance, it was a fairly easy matter to calculate the divergence of the beam expected for a given size of crystal. In order to measure the total experimental divergence of the x-ray beam, x-ray pictures were taken with film distance of 5 cm and 2.5 cm, respectively.

Table IV. *Maximum permeability and percent reduction in area in cold rolled specimens.*

No.	μ_{max}	Percent Reduction in Area
H2a	4500	2
H3a	6550	3
H4a	5150	4
H6a	7980	6
H8a	8550	8
H10a	7100	10

These results indicate essentially no divergence along the periphery of a characteristic ring. The presence of asterism, however, shows that there is distortion present in the crystals. The only distortions that could produce peripheral widening of spots would be those arising from the bending of crystals about axes parallel to the incident x-ray beam. Since no divergence appeared, the results indicate that the axes of bending were fairly well confined to the plane of the sheet.

DECEMBER 1, 1937 PHYSICAL REVIEW VOLUME 52

On the Anisotropy of Cubic Ferromagnetic Crystals

J. H. VAN VLECK
Harvard University, Cambridge, Massachusetts
(Received October 18, 1937)

It is shown that the dependence of the intensity of magnetization on direction in cubic single crystals probably results from the interplay between orbital valence and spin-orbit interaction. Because of the spin-orbit coupling, the spin vectors responsible for the ferromagnetism feel slightly the anisotropic electrostatic forces which connect the orbital angular momenta of different atoms and whose bonding effect is called orbital valence. In consequence there is apparent dipole-dipole coupling between the spins of different atoms with a constant of proportionality about fifty times larger than results from pure magnetic forces between spins. The same mechanism also gives rise to apparent quadrupole-quadrupole coupling, but it is shown very generally that the latter is possible only if the spin quantum numbers of the atoms are greater than $\frac{1}{2}$. Although dipole-dipole coupling is well known not to contribute to cubic anisotropy when the elementary magnets are all parallel, there is an appreciable contribution in the second approximation of perturbation theory in which complete parallelism is not assumed. The perturbation calculations can be carried through for both the dipole or quadrupole models, provided a Weiss molecular field is used to portray exchange interaction. Both lead to a constant K_1 of about the observed order of magnitude in the expression $F_0+K_1(\alpha_1^2\alpha_2^2+\alpha_2^2\alpha_3^2+\alpha_3^2\alpha_1^2)+K_2\alpha_1^2\alpha_2^2\alpha_3^2$ for the free energy. The temperature variation of K_1 is given correctly in so far as K_1 vanishes much more rapidly than the intensity of magnetization near the Curie point, but the calculations are not sufficiently refined to give quantitative details of the temperature dependence, such as, for example, the different behavior of iron and nickel. The empirical values of K_2 seem somewhat larger than one would expect provisionally from dimensional considerations, but higher order calculations are needed before this point can be definitely settled. Our model is admittedly somewhat phenomenological, but in our opinion comes closer to physical reality than others in the literature, which are criticized. An explanation is given of why the so-called lattice sums in magnetostriction have larger magnitude, and sometimes different sign, than computed for pure magnetic coupling between the spins. In the final section a brief discussion is included on the anisotropy of hexagonal crystals.

PART I. DESCRIPTIVE SURVEY AND CRITIQUE

1. Introduction

IT is well known that even in cubic crystals there is some ferromagnetic anisotropy, i.e., the ease of magnetization is dependent on the choice of axes. The magnetization curves for the 100, 010, and 001 axes are of course completely equivalent because of the cubic symmetry, but the latter does not require a similar behavior for the 100, 110, and 111 directions, and it is indeed found that nickel is more readily magnetized along the 111 than the 100 axis, while the reverse is true of iron. The empirical results are best expressed in terms of a free energy function F. It is shown in the literature[1] that the observed anisotropy is explicable in terms of a free energy of the form

$$F=F_0+F_1+F_2, \tag{1}$$

where F_0 is purely isotropic, but where F_1 and F_2 involve the direction cosines α_1, α_2, α_3 of the field relative to the principal cubic axes in the fashion

$$F_1=K_1(\alpha_1^2\alpha_2^2+\alpha_2^2\alpha_3^2+\alpha_3^2\alpha_1^2), \tag{2}$$

$$F_2=K_2\alpha_1^2\alpha_2^2\alpha_3^2. \tag{3}$$

We suppose the field powerful enough so that

[1] For an excellent resumé of this part of the subject, and references, see. R. M. Bozorth, J. App. Phys. **8**, 575 (1937), Phys. Rev. **50**, 1076 (1936), also Stoner, *Magnetism and Matter*, pp. 385–401.

it is unnecessary to distinguish between the direction of the applied field and that of local magnetization.

The selection of the best values of K_1, K_2 to represent the experimental magnetization curves is not an easy task, and constitutes the so-called subject of technical magnetization.[1] However, it is not the part of the problem with which we shall be concerned. Rather, we shall confine our attention to the theoretical explanation of the existence of nonvanishing constants K_1, K_2 of the proper order of magnitude, in other words, the origin of the anisotropy on the basis of atomic theory.

The forces between atoms which are primarily responsible for ferromagnetism are the exchange interactions. However, they are well known not to lead to any anisotropy,[2] provided the atoms are considered to be effectively in s states. To explain the fact that the susceptibilities do depend somewhat on direction, it is necessary to superpose some other coupling on the large exchange forces. The most obvious type of such other interaction is that represented by the mutual energy of two dipoles.

2. Dipole-dipole coupling

The conventional treatment of this coupling is one in which all the elementary dipoles are regarded as mutually parallel. It has often been pointed out that under these circumstances, dipole-dipole forces[3] are unable to give any anisotropy in cubic crystals. The reason is quite simple. The mutual potential energy of a collection of parallel dipoles transforms like a quadratic form under a rotation of axes. The distinction between complete isotropy and cubic symmetry can be represented by a form of no lower order than the fourth, i.e., the expression (2). A quadratic form, on the other hand, yields either perfect isotropy (equal coefficients of α_1^2, α_2^2, and α_3^2), or no more than rhombic or perhaps axial symmetry.

However, when the dipoles are not all perfectly parallel, it is no longer true that dipole-dipole coupling is incapable of yielding any anisotropy. Instead, it will be shown in Section 10, that when a perturbation calculation is carried to the second order, there is a dependence on direction except in the case of complete parallelism. The latter case is, of course, an ideal one not achieved practically except at $T=0$. It is obviously necessary to carry the perturbation calculation to the second rather than first approximation, since a quadratic form can simulate a biquadratic one only when raised to the second power.

3. Quadrupole-quadrupole coupling—the necessity of $S>\frac{1}{2}$ for this

The most frequently employed model of cubic anisotropy is that wherein each magnet is somehow supposed to carry with it a quadrupole moment.[4] A dependence on direction of the form (2) is then achieved even when the quadrupoles are all perfectly parallel. Irrespective of the question of the mechanism responsible for the quadrupole-quadrupole coupling, there is a fundamental difficulty with all quadrupole models as applied to nickel. Quite possibly, here the spin of each elementary magnet is $\frac{1}{2}$,—at least this is the value which gives the best interpretation of the variation of the magnetization of nickel with temperature.[5] However, the most general potential coupling together two spins of quantum number $\frac{1}{2}$ and symmetrical in them is

$$V=V_0-2J(S_{xi}S_{xj}+S_{yi}S_{yj}+S_{zi}S_{zj})$$
$$+C(2S_{zi}S_{zj}-S_{xi}S_{xj}-S_{yi}S_{yj})+D(S_{xi}S_{xj}-S_{yi}S_{yj})$$
$$+E(S_{xi}S_{yj}+S_{xj}S_{yi})+F(S_{xi}S_{zj}+S_{xj}S_{zi})$$
$$+G(S_{yi}S_{zj}+S_{zj}S_{yi}), \quad (4)$$

inasmuch as any polynomial in S_{xi}, S_{yi}, S_{yi} can be expressed as identically equal to a linear form $a_0+a_1S_{xi}+a_2S_{yi}+a_3S_{zi}$ because with $S=\frac{1}{2}$ the matrices S_{xi}, S_{yi}, $\cdots$, S_{zj} are all of the second rank, and so satisfy simple algebraic equations

[2] The so-called Dirac vector model shows that the exchange forces between equivalent electrons are formally equivalent to a coupling energy of the form $-\frac{1}{2}Jn_in_j-2J\mathbf{S}_i\cdot\mathbf{S}_j$ between the spins, where J is the exchange integral and n_i, n_j are the number of electrons outside closed shells in atoms i, j. (See P. A. M. Dirac, Proc. Roy. Soc. **A123**, 714 (1929), or J. H. Van Vleck, Phys. Rev. **45**, 405 (1934).) The additive constant $-\frac{1}{2}Jn_in_j$ is unimportant for present purposes and hence omitted in our Eqs. (9) and (45). The dot product $\mathbf{S}_i\cdot\mathbf{S}_j$ is clearly invariant under rotation, and so cannot lead to anisotropy.

[3] Cf., for instance, R. Becker, Zeits. f. Physik **62**, 253 (1930), or Mahajani, reference 4.

[4] G. S. Mahajani, Phil. Trans. Roy. Soc. **228**, 63 (1929); N. S. Akulov. Zeits. f. Physik **57** 249; **59** 254 (1929); R. Gans and E. Czerlinsky, Ann. d. Physik **16**, 625 (1933).

[5] Cf. F. Tyler, Phil. Mag. **9**, 1026 (1930); E. Stoner, Phil. Mag. **10**, 27 (1930).

which permit the degree to be depressed, e.g.

$$S_{z_i}^2=\tfrac{1}{4},\quad S_{z_i}^3=\tfrac{1}{4}S_{z_i},\quad S_{x_i}S_{y_i}+S_{y_i}S_{x_i}=0,$$
$$S_{x_i}S_{y_i}-S_{y_i}S_{x_i}=iS_{z_i},\quad (S=\tfrac{1}{2}). \quad (5)$$

We throughout suppose our angular momentum vectors to be expressed as multiples of the Bohr unit $h/2\pi$. If we take the z axis as that of the radius vector r_{ij} joining magnets i and j, the coefficients D, E, F, G will vanish if the interaction is invariant with respect to rotation about r_{ij}. We will henceforth therefore neglect the corresponding part of (4). (Even if these terms did not vanish, (4) would be essentially a second order rather than quadrupole-quadrupole proposition.) The first term of (4) is a trivial constant, while the J term is merely the Heisenberg isotropic coupling. The factor -2 is included in its definition in order to make the coefficient J identical with the conventional exchange integral.[2] The C term is of the dipole-dipole type as far as the dependence on spin-alignment is concerned. We thus see that with spins of $\frac{1}{2}$ (one uncompensated electron per atom), dipole-dipole coupling is the most general type of nonisotropic interaction. The constant of proportionality C need not, however, have the value

$$C=g^2\beta^2/r_{ij}^3,\quad (\beta=he/4\pi mc) \quad (6)$$

characteristic of the mutual energy of two magnets separated by a distance r_{ij}. Here β is the Bohr magneton, and g is the Landé factor,[6] equal to two for spins. We throughout use the term "dipole-dipole" as allowing an arbitrary proportionality factor. When C is to be restricted to (6), we shall speak of "true magnetic coupling."

As a specific example of this theorem that spins of $\frac{1}{2}$ cannot generate quadrupole coupling, let us consider the simplest type of quadrupole-quadrupole potential, *viz.*

$$V=V_0+\gamma S_{z_i}^2S_{z_j}^2. \quad (7)$$

When we utilize the first relation of (5), the right side of (7) reduces to a trivial constant $V_0+\frac{1}{16}\gamma$. Eq. (7) is, of course, not the most general expression quadratic in each of the spin components, but for our purposes is sufficiently typical of the workings of quadrupole-quadrupole interaction provided we take the z axis to be the line joining the two atoms. Then (7) is a quite general form which is invariant under rotations about this line and whose mean value is nonvanishing in the first approximation.

If the anisotropy of nickel is to be explained otherwise than with essentially dipole-dipole coupling, it is necessary that the carriers of the magnetic moment in nickel have spins of 1 or greater. A model of this type has indeed been proposed by Wolff and by Mott and Jones from other evidence[7] but we find it rather difficult to believe that the atomic spin have such a large value in nickel. At the absolute zero, the value of the saturation magnetization of nickel is 0.6 Bohr magnetons per atom. Presumably this behavior means that 60 percent of the nickel ions are in the magnetic configuration d^9 and 40 percent in the nonmagnetic configuration d^{10}, with 0.6 conduction electrons per atom in $4s$ bands which are wide enough so that the magnetism of their spins is annihilated because of the Pauli principle. With Mott's model, there would be 30 percent of the ions in d^8, 70 percent in d^{10}, with still 0.6 conduction electrons per atom. Since very much greater energy is required to ionize an atom twice rather than once, it is hard to see why the ions should prefer to be in d^8 rather than d^9. At the same time, we are not unmindful of the fact that Mott and Jones have listed certain arguments favoring a spin $S=1$ for nickel. Possibly the difficulty regarding the high ionization energy of d^8 is overcome by some of the $4s$ conduction electrons being sucked in towards the d^8 ions, so that the mean charge cloud around these ions corresponds to considerably less than twofold ionization.

In the case of iron, there appears to be no

[6] As we are dealing with media where practically all the magnetism comes from spin, the g factor can immediately be equated to 2. However, we prefer to carry an undetermined g factor because the calculations in Part II may have some future application to other problems in which the angular momentum vectors of the different atoms coupled together do not arise solely from spin. The analysis in Part II is immediately adapted to such problems merely by replacing the spin vector **S** by the total angular momentum **J**, and the spin quantum number S by the inner quantum number J.

[7] A. Wolf, Zeits. f. Physik **70**, 519 (1931); also especially N. F. Mott and H. Jones, *The Theory of the Properties of Metals and Alloys*, pp. 224–227. Attempts to deduce the configuration of the nickel ions from the formula $\chi=Ng^2\beta^2(S^2+S)/3k(T-T_c)$ for the susceptibility above the Curie point are in our opinion inconclusive, since this formula is valid theoretically only if $T\gg T_c$ whereas in practice it is used in regions where T is not much greater than T_0.

objection to granting a spin of unity, or perhaps even $\frac{3}{2}$, as the Fe atom has two electrons less than Ni, and so is further from a completed d shell. The most general potential coupling together two spins of unit quantum number is a polynomial of the second degree in S_{xi}, S_{yi}, S_{zi}, and also of this degree in S_{xj}, S_{yj}, S_{zj}. The proof is based on the fact that S_{xi}, S_{yi}, S_{zi} are three-rowed matrices when $S=1$, and is similar to that used in establishing that (4) is the most general potential with dipole-dipole coupling. Consequently, the most general interaction between two spins of unit quantum number consists of quadrupole-quadrupole and lower order (dipole-dipole, dipole-quadrupole) terms, inasmuch as dipoles and quadrupoles are respectively linear and quadratic in vectorial properties. If the spins or quadrupole axes are all parallel, the most general dependence on direction is of the form (2). This is true even when the spins are not all parallel, provided only a first-order perturbation calculation is made, as will be shown in sections 11–12. The additional term (3) would require apparent hexapole-hexapole coupling. This can mean that either (*a*) the spin is greater than unity, or else that (*b*) the elementary magnets are not perfectly parallel. In case (*b*) the angular dependence (3) is yielded if the perturbation calculation is carried to a sufficiently high approximation, *viz.* the second order with dipole-quadrupole coupling, or the third order with dipole-dipole interaction. That these are the proper orders can be seen from the powers to which the direction cosines are raised, on remembering that each spin transforms like a vector.

4. Origin of the coupling terms

So far we have introduced the interaction between atoms more or less *ad hoc*, and we must now inquire into its physical causes. One possibility is that we have to do with *bona fide* magnetic coupling, so that the constant C in (4) has the form (6). The resulting value of K_1 is, however, too small by a factor 10^3 (see fine print, Section 6).

In our opinion, the most likely explanation of the origin of the anisotropic terms is to be found in the concept of *orbital valence*. By the latter term, we mean the fact that the mutual electrostatic energy of two atoms depends on the way their orbital angular momenta as well as on the way their spins are aligned. The orbital coupling involves in general not merely the orientation of the orbital angular momentum vectors relative to each other, but also their orientation relative to the axis joining the two atoms. The latter ingredient, on the other hand, does not appear in the Heisenberg exchange interaction, which is formally equivalent to isotropic spin-spin coupling. Expressed in formulas, the energy of orbital valence is of the form $f(\mathbf{L}_i\cdot\mathbf{L}_j, L_{zi}, L_{zj})$ whereas the exchange energy is $F(\mathbf{S}_i\cdot\mathbf{S}_j)$. Here $\mathbf{L}_i$ is the angular momentum vector of atom i, and the z axis is supposed that joining the two atoms. In other words, orbital valence is anisotropic, but exchange energy is isotropic because $\mathbf{S}_i\cdot\mathbf{S}_j$ is unaffected if similar rotations are given to $\mathbf{S}_i$ and $\mathbf{S}_j$. Since practically all the ferromagnetism arises from the spin, anisotropy in the orbital moment may at first sight seem to be of little consequence. However, the effect of spin-orbit coupling is not entirely negligible even when the orbital moment is largely quenched, and so the energy will not be entirely independent of how the spins are oriented relative to the figure axis. The situation may be likened to that in the spectra of diatomic molecules, where the energies of Σ_1, Σ_0, Σ_{-1}, the three components of a "ρ type triplet." are not quite the same even though a Σ state has zero mean orbital angular momentum.[8] If only one orbital state need be considered for each atom, the most general potential representing the dependence of energy on spin alignment is given by a function of the form (4) in case the spin of each atom is $\frac{1}{2}$. If the spin of each atom is 1, we must add to (4) some quadrupole-quadrupole terms, analogous to (7), and also perhaps some quadrupole-dipole coupling, linear in one spin and quadratic in the other. Similarly with $S=\frac{3}{2}$ hexapole terms must be included. These results are consequences of the limited rank of the spin matrices, which make polynomials of low degree the most general function, as explained in Section 3. Thus the superposition of spin-orbit coupling and orbital valence leads directly to potentials which simulate true magnetic dipole-dipole or quadrupole-quadrupole coupling, except for the

[8] M. H. Hebb, Phys. Rev. **49**, 617 (1936).

proportionality factor, but have in reality an entirely different origin.

The one weak point in the argument is that actually more than one orbital state surely does come into play for each atom. In reality, the orbital as well as spin vectors probably readjust themselves considerably when the temperature is varied. We do not wish to enter into any detail as to what the orbital states look like, since this would require us to delve into the intricate question of just how the orbital angular momentum is destroyed or "quenched," a subject imperfectly understood at present. The mechanism of quenching is probably not the same as the crystalline potential operative in paramagnetic salts.[9] If it were, the g factor should be different for different cubic ferromagnetic materials, due to inversion of the Stark pattern. Namely, in a cubic field, sometimes a degenerate and sometimes a nondegenerate orbital state is deepest, depending upon the number of electrons. The g factor should be much nearer 2 in the latter than in the former event. The inversion of the Stark pattern[10] explains, for instance, why the paramagnetic salt cobalt chloride has a g factor 1.54 as compared with 1.95 for chromic chloride. The g factors for ferromagnetic metals, on the other hand, are always remarkably near 1.9 (except for the freak case of pyrrhotite), showing that the quenching mechanism cannot be the same as the crystalline fields acting in paramagnetic salts. It is, of course, not surprising that the quenching machinery should be completely different in conducting metals than in nonconducting ionic salts. In the case of the ferromagnetic metals the quenching mechanism is probably the coupling between the orbital angular momentum vectors of different atoms, of antiferromagnetic sign as suggested by Sommerfeld and Bethe.[11] The coupling is not so strong but that a large number of orbital states are inhabited at room temperatures. The behavior is then exceedingly complicated, as rigorously the whole crystal rather than one atom ought to be treated as a single quantum mechanical unit. Another way of stating the difficulty is that the factors C and γ in (4) or (7) are matrices in the orbital quantum numbers rather than ordinary numbers. Since we treat them as ordinary numbers (which would be rigorous were there only one orbital state), our use of a potential such as (4) or (7) to represent the interplay between orbital valence and spin-orbit interaction must be regarded as somewhat phenomenological. In consequence it is possible that the constants C and γ should be regarded as functions of the temperature. They represent, so to speak, the mean effect of the interplay, which can vary with temperature because the Boltzmann distribution among the orbital states varies with T.

5. Representation of exchange coupling by means of a molecular field

A further approximation is necessary before the calculation can be started. Even when the orbital problem has been simplified by use of (4) or (7), there is still the ordinary Heisenberg exchange coupling, which must be included in the unperturbed part of the energy, as the isotropic ferromagnetic action is much larger than the small perturbations causing anisotropy. However, the determination of the characteristic values of the exchange energy $-2\Sigma_{i>}{}_j J_{ij}\mathbf{S}_i\cdot\mathbf{S}_j$ for the entire crystal is well known to be a hopeless task. We therefore resort to the usual artifice of regarding the exchange energy as equivalent to a molecular or inner field proportional to the intensity of magnetization. The constant of proportionality κ may, if desired, be a function of T. This use of a Weiss field is, again, somewhat phenomenological, but has been shown to have a quantal basis in Heisenberg's theory of ferromagnetism. Namely, he shows that an inner field with the constant of proportionality independent of temperature results if identity of energy is assumed for all states with the same resultant crystalline field.[12] Empirically, this approximation is quite a good one. In fact, Weiss[13] used his inner field model with great success long before the advent of quantum mechanics to explain the variation of the saturation intensity with tem-

[9] For a survey of work on the influence of the crystalline field on paramagnetic susceptibilities, see Chapter X of Stoner's *Magnetism and Matter*, especially p. 292 ff.

[10] J. H. Van Vleck, Phys. Rev. **41**, 208 (1932).

[11] A. Sommerfeld and H. A. Bethe, *Handbuch der Physik*, second edition, Vol. 24/2, p. 613.

[12] W. Heisenberg, Zeits. f. Physik **49**, 619 (1928); presentation in terms of the vector model in Chapter XII of J. H. Van Vleck, *Theory of Electric and Magnetic Susceptibilities*.

[13] For a resumé of the original Weiss theory and its relation to the more modern Heisenberg quantum-mechanical model, see Stoner, *Magnetism and Matter*, pp. 350–361.

perature. This simple model with κ independent of T works better than the more refined model in which a Gaussian distribution is assumed. Partial theoretical explanations of why this is so have been given along different lines by Fay[14] and by Opechowski.[15]

We thus base our calculations in Part II on a Hamiltonian function of the form

$$\mathcal{H} = -g\beta\kappa \mathbf{I}\cdot\Sigma_i \mathbf{S}_i + \Sigma_{j>i} C_{ij}[\mathbf{S}_i\cdot\mathbf{S}_j - 3r_{ij}^{-2}(\mathbf{S}_i\cdot\mathbf{r}_{ij})(\mathbf{S}_j\cdot\mathbf{r}_{ij})] + \Sigma_{j>i}\gamma_{ij} r_{ij}^{-4}(\mathbf{S}_i\cdot\mathbf{r}_{ij})^2(\mathbf{S}_j\cdot\mathbf{r}_{ij})^2, \quad (8)$$

where I is the intensity of magnetization. We shall see that a nonvanishing anisotropy constant K_1 is obtained when the C and γ terms are regarded as perturbations, and the development is carried to the second approximation in C or first approximation in γ. It is to be emphasized that (8) is to be regarded as a substitute for the more exact secular problem, which would involve a Hamiltonian of the form

$$\mathcal{H} = -2\Sigma_{j>i} J_{ij}\mathbf{S}_i\cdot\mathbf{S}_j + A\Sigma_i \mathbf{L}_i\cdot\mathbf{S}_i + \Sigma_{j>i} f_{ij}(\mathbf{L}_i\cdot\mathbf{L}_j, \mathbf{L}_i\cdot\mathbf{r}_{ij}, \mathbf{L}_j\cdot\mathbf{r}_{ij}) \quad (9)$$

where f_{ij} is some polynomial function.[16] The first or molecular field term of (8) replaces the exchange or first member of (9). The remainder of (8) is regarded as representing the constraints on the spin which would be obtained if the interplay between the second and third, i.e., spin-orbit and orbital valence terms of (9) could be treated exactly.

It would, of course, be desirable if the calculations could be based directly on (9) rather than (8) but the labor involved appears prohibitive. Even if (9) is simplified by replacing the first member by an inner field, the partition function would have to be developed to at least the fifth order for any anisotropy to appear. This order is required because cubic anisotropy is achieved only if the spin-orbit parameter A is raised to at least the fourth power; also the f term must be utilized at least once in the expansion, giving an additional power. The anisotropy exists only in virtue of f_{ij} because here $\mathbf{L}_i$ and $\mathbf{L}_j$ are coupled to $\mathbf{r}_{ij}$ as well as simply to each other whereas the rest of (9) is isotropic. If f_{ij} is linear in $\mathbf{L}_i\cdot\mathbf{r}_{ij}$ and $\mathbf{L}_j\cdot\mathbf{r}_{ij}$ it would have to be raised to the fourth power to make the direction cosines appear in the fashion (2), and then an eighth-order development would be required.[17] Such a procedure obviously is out of the question. Even if the eighth order computation could be made, the approximation would not be a particularly good one, inasmuch as f_{ij} and A are of the same order of magnitude as kT, so that series expansion of the partion function does not converge adequately. The fact that any development has to be carried a long way means, of course, many powers of T in the denominator, and so it is qualitatively understandable why the temperature dependence may be more rapid than can be depicted by our model (8) if C and γ are regarded as constant with respect to T. We believe, however, that with C and γ functions of temperature, our model (8) has a fairly general significance as a phenomenological approximation. In particular, it need not be confined to the Heitler-London method, since the orbital states may not necessarily be anchored to each atom, but instead can be of the itinerant Bloch-Slater variety.

6. Results of calculations based on the Hamiltonian (8)

The model embodied in the Hamiltonian function (8) is not too difficult to handle analytically, and can be tested by reckoning out the constants K_1 and K_2. The mathematical detail is presented in Part II, and at this stage we shall simply summarize the conclusions. The three possible checks are on the sign, magnitude, and temperature variation of K_1 and K_2.

Sign of K_1.—There is no feasible way of determining the sign of K_1 if it is due to the quadrupole-quadrupole or last part of (8). If, however, K_1 is due to dipole-dipole or second

[14] C. H. Fay, Proc. Nat. Acad. Sci. **21**, 537 (1935).
[15] W. Opechowski, Physica **4**, 181 (1937).
[16] Part of f_{ij} in (9) may be linear in $\mathbf{S}_i\cdot\mathbf{S}_j$ since the exchange integrals themselves depend on how the orbital angular momentum vectors are aligned when the atoms are not in s states. In other words orbital valence affects the exchange as well as Coulomb energy. This complication is of no particular interest to us, for the validity of (8) as a substitute for (9) is not much influenced by whether f_{ij} involves $\mathbf{S}_i\cdot\mathbf{S}_j$.
[17] It is to be emphasized that consideration of transformation properties show that three distinct quantities must each be raised to at least the fourth power. The necessity of this power of A is seen by imagining the $\mathbf{S}_i$ to rotate with the $\mathbf{L}_i$ held fast; that of $\mathbf{L}_i\cdot\mathbf{r}_{ij}$ by rotating $\mathbf{L}_i$ relative to the crystal; that of H^4 by rotating the external field.

member of (8), then K_1 is negative for a face or body-centered lattice, and positive for a simple cubic one. The reason why the sign can be determined in one case but not in the other is the following. It does not appear practical to determine the sign of either C or γ in (8), as detailed specification of atomic wave functions would be necessary. Now K_1 is linear in γ, but involves C only through its square, since dipole-dipole effects enter only in the second approximation (cf. Eqs. (30) and (44)). Hence the dipole-dipole contribution to K_1 is of determinate sign even though there is ambiguity in C itself. The dipole-dipole coupling gives a K_1 of the proper sign for nickel, since the latter has a face-centered lattice and negative K_1. This agreement is gratifying, inasmuch as nickel is the material which is most likely to have $S=\frac{1}{2}$, and we saw in Section 3 that with $S=\frac{1}{2}$, the quadrupole contribution to K_1 vanishes so that only the dipole explanation can be used. When we come to iron, the observed sign (positive with a body-centered lattice), does not check with the dipole-dipole model, but is not inconsistent with $S>\frac{1}{2}$ and quadrupole-quadrupole coupling. It is probable that iron has a spin of at least unity. If so, here, both causes of K_1 enter simultaneously. The right sign is possible only if the quadrupole effect is more important than the dipole one. It is not clear theoretically why this should be the case, as in the next paragraph we estimate very crudely the two effects to be of the same rough order of magnitude when they are both present. It is thus impossible to tell *a priori* which should be the larger, and so the best that can be done is to appeal to the empirical evidence.

Order of magnitude of K_1.—The constant K_1 should be of the order $A^4/10kT_c h^2\nu^2$, or thereabouts, per atom if due to dipole-dipole interaction, and of the order $A^4/h^3\nu^3$ if due to the quadrupole-quadrupole effect. The basis of these estimates is set forth in fine print below. Here A is the usual spin-orbit constant, T_c is the Curie temperature, and ν is a quantity of the order of magnitude of the separation of energy levels caused by interaction of the orbit with the crystalline field (or alternatively, of the coupling energy between the angular momentum vectors of adjacent atoms, something presumably of the same order of magnitude). A reasonable estimate is perhaps[18] $A^2/h\nu=10$ cm^{-1}, $\nu=10^4$ cm^{-1}, $kT_c\sim 10^3$ cm. If so, then when due to either effect, K_1 is of the order 10^{-2} cm^{-1} per atom or 10^5 ergs/cm^3. It is not surprising that both the dipole and quadrupole mechanisms should lead to the same order of magnitude for K_1, as there is little distinction between them from the standpoint of the more fundamental equation (9) although they appear differently in (8). This estimate $K_1\sim 10^5$ is of the order of the experimental values. Namely iron has $K_1=6\times 10^5$ at room temperatures, while nickel has $K_1=-3\times 10^4$ at this temperature, but about -3×10^6 at liquid hydrogen.[19] Thus with the model which we propose, there is no difficulty in understanding the existence of anisotropies as large as are observed.

To derive the above estimates of K_1, we first note that the calculations of Section 10 show that the constant K_1 is of the order $C^2/10kT_c$ per atom if ascribed to dipole-dipole coupling. The factor 10 does not follow from dimensional considerations, but is included because the purely numerical factor involved in Table I of Section 10 is rather small. The quantity C is the constant of proportionality in the second member of (8). It should be of the same order of magnitude $A^2/h\nu$ as the spin-orbit splitting in a molecular state devoid of mean angular momentum (cf. Hebb's calculations[8] on ρ type tripling in $^3\Sigma$ states). The splitting is of this order rather than simply A because it disappears in the first approximation for such a state. If the dipole-dipole constant C arose primarily from a pure magnetic interaction rather than spin-orbit coupling, C would be of the order of magnitude. 2 cm^{-1} given by (6) with $r_{ij}^{-3}\sim 10^{23}$ rather than $C\sim A^2/h\nu\sim 10$ cm^{-1}, and K_1 would be too small by a factor about 10^{-3}.

If K_1 is due to our quadrupole-quadrupole coupling, it should be of the same order of magnitude as γ (cf. Section

[18] The expression $C\sim A^2/h\nu$ should be of the same order of magnitude as the constant term in the width of a ρ type triplet in band spectra. This term is 1.99 cm^{-1} for the oxygen molecule (R. Schlapp, Phys. Rev. **51**, 342 (1937)), and an extra power of at least ten seems in order in extrapolating to heavy elements like nickel. The quantity C can also be gauged by $^3\Pi_0^+-{}^3\Pi_0^-$ intervals in molecular spectra, with similar results. Another quite different method of estimation is furnished by considering the multiplet splitting in the configuration d^5 of say Cr II, which is again about 10 cm^{-1} (cf. page 162 of Bacher and Goudsmit's tables). This splitting is of the order $A^2/h\nu_1$, where ν_1 is the coupling energy between l vectors of the same atom rather than of different atoms and is probably somewhat greater than our ν. So, if anything, 10 cm^{-1} is an underestimate of C, and hence it is not too surprising that $|K_1|$ should sometimes reach almost 10^7 ergs/cm^3, as appears to be the case for nickel at very low temperatures.

[19] The experimental values of K_1 quoted here and in the tables of Part II are taken from Bozorth, reference 1, and are based ultimately largely on Japanese work on magnetization curves; Honda, Masumoto, Kaya, and Shirakawa, Sci. Rep. Tohoku Univ. **17**, 111 (1928); **24**, 391 (1935).

11, especially Table III) and γ is of the order $A^4/h^3\nu^3$. At first sight it might seem that γ should be of the same order of magnitude $A^2/h\nu$ as C, but to obtain a splitting like (7) which involves the spins all told to the fourth degree, it is necessary that the perturbing potential be raised to the fourth power, which involves a fourth rather than second order perturbation calculation. (In this connection, the third term of (9) is to be regarded as the unperturbed energy, and the second member $\Sigma_i A\mathbf{l}_i\cdot\mathbf{s}_i$, summed over two atoms, is to be treated as the perturbing potential.)

Temperature variation of K_1.—As regards the dependence of K_1 on T, our model proves correct only in a rough qualitative way in that it does indeed predict that the anisotropy should fade out much more rapidly than does the intensity of magnetization itself when the temperature is raised towards the Curie point. However, the predicted variation with temperature is still not as drastic as is found experimentally. In the case of iron, the observed anisotropy varies approximately as I^{10} near the Curie point,[20] whereas the computed values given in Table III simulate more nearly I^6 or I^5. Here we use the quadrupole-quadrupole calculations in order not to be in conflict on the sign of K_1. In the case of nickel, K_1 is actually over fifty times larger at 17° than at 293°K, whereas according to our calculations K_1 should increase but very little in numerical magnitude when T is reduced below room temperatures. This statement is true regardless of whether the dipole or quadrupole model is used, since either one gives qualitatively about the same variation with T (cf. Tables I and III of Part II). For the latter reason, no explanation is obtained of why it is that dK_1/dT is very much larger in absolute value at low temperatures for nickel than for iron, so that the absolute zero is approached in a quite different way for the two materials.

We believe that the failure of the models based on the Hamiltonian function (8) to give the proper quantitative temperature dependence should not be regarded as too serious a difficulty, since (8) presupposes a somewhat phenomenological treatment of the orbital part of the problem. In fact, we mentioned at the end of Section 5 that (8) might not give a rapid enough variation with T. As stressed in Section 5, C and γ ought really to be regarded as undetermined functions of the temperature, rather than as constants as we have taken them to be in obtaining the theoretical predictions mentioned in the preceding paragraph. Another, but probably less important source of error, is the use of the Weiss inner field as a method of depicting the workings of exchange interactions between the spins. Additional leeway is obviously obtained if the proportionality factor κ in the molecular field is regarded as a function of temperature, rather than constant, as we take it to be. To examine how serious are the deficiencies of the Weiss field approximation, we give in Section 12 an alternative method of calculation of the quadrupole-quadrupole effect in which the exchange interactions in the pair under consideration are taken into account rigorously and only the effect of outside atoms represented by means of the molecular field. The difference between this perhaps improved method of calculation and the original one given in Section 11 is unimportant (cf. Table III). Unfortunately, it does not appear feasible to carry out the computations with the Bloch "spin-wave" type of approximation which is particularly suitable for low temperatures.

Magnitude of K_2.—We have not carried the perturbation calculations to a high enough order to permit saying anything on either the sign or temperature variation of K_2. Dimensional considerations, such as those given in fine print above, suggest that K_2 would differ from K_1 by a factor $A^2/h^2\nu^2$ or perhaps $A^2/h\nu kT_c$ and hence be about 10^{-3} to 10^{-2} as great as K_1. Actually K_2 is comparable with K_1. For instance, K_2 almost equals K_1 in iron above 500°K, while K_2 is about 30 percent of K_1 in nickel at 123°K. This difficulty is not merely one characteristic of the particular model (8) which we use, since with any type of calculation the spin-orbit parameter must be raised to the sixth rather than fourth power to generate an angular dependence of the form (3) rather than (2). As suggested to me by Dr. Bozorth, part of the apparent discrepancy may be associated with the different size of the angular factors in (2) and (3). The maximum of $\alpha_1^2\alpha_2^2\alpha_3^2$ is only 1/27, as compared with $\frac{1}{3}$ for $\alpha_1^2\alpha_2^2+\alpha_1^2\alpha_3^2+\alpha_2^2\alpha_3^2$, while the difference in mean value is even greater, *viz.* a factor 21. Whether the dimensional considerations on magnitudes relate more exactly to the expressions (2)

[20] Cf. N. Akulov, Zeits. f. Physik **100**, 197 (1936).

and (3) inclusive or exclusive of the directional factors cannot be determined without a rather laborious explicit calculation of K_2. Of course one must bear in mind that because of the small angular factor mentioned above, the constant K_2 is not easy to measure with precision, and so the experimental values may not be very accurate. However, the observed magnetization curves are so complicated that it is scarcely conceivable that they can always be depicted by a dominant fourth order form F_1 without the admixture of comparable F_2 terms. In fact in some cases appreciable higher harmonics F_3 and F_4 may be required.

In nickel, K_1 apparently changes sign at about 420°K. To be sure, this is in a region where the anisotropy is so small that the experimental data may not be reliable. If the change in sign is real, it would perhaps indicate that excited states of nickel can have $S>\frac{1}{2}$ and so manifest quadrupole coupling even though the normal states, which determine the sign at low temperatures, have $S=\frac{1}{2}$ and so only the dipole effect. Another more likely possibility is that the higher order perturbation terms are for some reason abnormally important, as they would need to be to generate a K_2 much larger than K_1, such as is apparently shown in nickel at high temperature. These terms will make some contribution to the angular structure (2) as well as (3).

7. Relation to other models of ferromagnetic anisotropy in the literature

Bloch and Gentile's theory and the one atom model.—A large number of papers have already been written on the same subject as the present article, *viz.* the origin of the anisotropy constants K_1, K_2 in atomic theory, but usually in our opinion on the basis of models which cannot be regarded as a close or satisfactory approximation to physical reality. Considerable resemblance, however, appears at times between the preceding discussion and that given by Bloch and Gentile.[21] This statement is particularly true regarding the way in which the constants enter dimensionally, and the idea that cubic anisotropy exists primarily in virtue of spin-orbit interaction, but only after the spin-orbit parameter is raised to the fourth power. In a certain sense, all our calculations in Part II may be regarded as simply an attempt to put their general scheme of things on a firmer and more tangible basis. Nevertheless, there is one respect in which our approach seems to differ from theirs in principle. Their explanation for ferromagnetic anisotropy appears to be the interplay between spin-orbit interaction and the quantization of a single atom in a crystalline field. It is perhaps not entirely fair to make this statement definitely, as their paper is couched in such general language that it is impossible to extract from it exactly the type of orbital quantization which is implied. However, they do talk of the "s state of an atom," "excitation of one atom," etc. and so would seem to imply that each orbit can be quantized in a crystalline field. Such a picture we shall call the "one-atom model," as it would imply that magnetic anisotropy can be deduced from a secular problem involving only one atom, provided exchange is represented by an inner field. In other words, the Bloch-Gentile Hamiltonian function differs from ours in that the last, or orbital valence term of (8), is replaced by the sum $\Sigma_i V_i$ of the individual crystalline potentials of the separate atoms. However, we advance in the next paragraph reasons for believing that such a model is incapable of yielding any appreciable anisotropy. We maintain that the coupling between orbital angular momentum vectors of different atoms is a vital ingredient, rather than the interaction of a single vector with the crystalline field.

The reason why the one-atom model cannot give appreciable cubic anisotropy is the degeneracy whereby many levels coincide in a cubic field. If we have a nonmagnetic, nondegenerate orbital level (type Γ_1 or Γ_2 in Bethe's[22] notation) in a cubic field, and add the spin, then group theory shows that the resulting levels are completely degenerate[23] so long as the spin quantum number S is less than 2, as is altogether probable.

[21] F. Bloch and G. Gentile, Zeits. f. Physik **70**, 395 (1931).

[22] H. Bethe, Ann. d. Physik **3**, 133 (1929).

[23] The appropriate relations in the language of group theory are the following formulas for the reduction of the "direct products" of the spin and orbital representations:

$$\Gamma_6\times\Gamma_1=\Gamma_6, \quad \Gamma_6\times\Gamma_2=\Gamma_7, \quad \Gamma_4\times\Gamma_1=\Gamma_4,$$
$$\Gamma_4\times\Gamma_2=\Gamma_5, \quad \Gamma_8\times\Gamma_1=\Gamma_8\times\Gamma_2=\Gamma_8$$

inasmuch as $S=\frac{1}{2}$, 1, $\frac{3}{2}$ have the cubic transformation properties of Γ_6, Γ_4, Γ_8 respectively. There is no splitting when the reduced product contains only one irreducible representation, as in the above cases.

This result is intimately connected with the fact that the most general polynomial in the spin vector is an expression of the first, second, or third degree according as S equals $\frac{1}{2}$, 1, or $\frac{3}{2}$, whereas cubic anisotropy requires the fourth degree. In consequence of this fact, the atom will be isotropically bound as long as one considers only matrix elements of the Zeeman energy (i.e., energy of the atom in the Weiss molecular field) connecting the different components of the ground level. As soon as one includes matrix Zeeman components joining the ground state and excited orbital levels based on other representations than Γ_1 or Γ_2, cubic anisotropy can appear. However, as shown in fine print below, a very high order perturbation development is required, and the resulting value of K_1 is too small to be significant.

In Section 6 we saw that a K_1 of about the right order of magnitude is obtained if K_1 is dimensionally of the structure $[A^4/h^2\nu^2 10kT_c]\varphi$ or $[A^4/h^3\nu^3]\varphi$. Here φ is a function only of the dimensionless argument $g\beta\kappa I/kT$. ($10f$ or f_1+f_2 in our later Eqs. (32), (38) are examples of essentially φ functions.) Any portion of the free energy leading to the angular structure (2) must involve the spin-orbit parameter A and the molecular field $H=\kappa I$ each to at least the fourth power. The requisite fourth power of κI was previously tacitly contained in φ which was not mentioned in Section 6 as φ is of the order of magnitude unity. However, the appearance of the argument $g\beta\kappa I/kT$ is as a rule possible only in virtue of nonisotropic "low frequency" matrix elements connecting energy levels split by intervals small compared with kT. When the Zeeman components leading to anisotropy join normal and excited states, the dimensionless factor[24] usually becomes instead $\kappa I/h\nu$, and K_1 is of the order $A^4\kappa^4 I^4/h^7\nu^7$ or perhaps $A^4\kappa^4 I^4/h^6\nu^6 kT_c$, and then K_1 would be about 10^2 ergs/cm^3 rather than the observed 10^5 to 10^6.

If there is a spin of unity or greater, and if the ground orbital state of the atom happens to be Γ_3, the orbital level is degenerate but by exception nonmagnetic. Then there is no difficulty with g-factors. Also the introduction of the spin causes a small splitting of the ground level (as embodied in the group theory relation $\Gamma_3\times\Gamma_4=\Gamma_4+\Gamma_5$, if $S=1$, or $\Gamma_3\times\Gamma_5=\Gamma_6+\Gamma_7+\Gamma_8$ if $S=\frac{3}{2}$), so that the desired small lifting of the degenerary is available. Conceivably this situation is part of the explanation of the anisotropy of iron. It will not work for nickel if the latter has $S=\frac{1}{2}$, as the formula $\Gamma_3\times\Gamma_6=\Gamma_8$ shows that the degeneracy persists even after insertion of the spin. However, we doubt if it is an accurate picture of things to use the crystalline field mechanism in conductors, as explained in Section 4. So it is rather academic to discuss at length any specific details of the one atom model.

Powell's model.—In an interesting paper, Powell[25] secures the desired angular structure (2) by introducing an anisotropic Weiss field. The dissymmetry in the latter is somehow to be associated with the effects of spin-orbit interaction, and should perhaps be regarded as a phenomenological substitute for the last two terms of (9). However, the relation of Powell's model to the actual workings of spin-orbit coupling is apparently such a remote and heuristic one that it cannot yet be regarded as a real explanation of ferromagnetic anisotropy.

Akulov's calculation of the temperature variation of K_1.—There are numerous papers by Mahajani, Akulov and others[4] based on rather arbitrary quadrupole-quadrupole models, but as far as we know, in only one of them, by Akulov,[20] is any attempt made to compute theoretically the temperature dependence of K_1. His results are in better agreement with experiment than ours, as he finds the anisotropy varying as the tenth power of the intensity of magnetization near the Curie point. However, he regards the spins of adjacent atoms as all parallel, and all precessing together about the axis of resultant magnetization. According to statistical mechanics, the elementary magnets tend less and less to be mutually parallel as the temperature is raised, and it is hard to believe that the assumption of complete parallelism is a better approximation to the true workings of exchange coupling than is the Weiss molecular field. The latter, to be sure, probably does not take sufficient cognizance of the tendency of magnets to coagulate locally into parallel clusters, but the modified calculation

[24] Powers of kT in the denominator of the free energy or partition function arise in general from perturbing matrix elements involving energy changes $h\Delta\nu$ small compared to kT, because kT replaces $h\Delta\nu$ in the perturbation denominators when terms are paired in appropriate fashion (cf. K. F. Niessen, Phys. Rev. **34**, 253 (1929); J. H. Van Vleck, *The Theory of Electric and Magnetic Susceptibilities*, Section 46). Hence a small splitting of the ground state by the crystalline field is necessary. (For formal purposes a zero splitting can be regarded as a small splitting, but in the cases under consideration zero splitting gives essentially the same transformation properties as free rotation and so does not cause anisotropy.) In the text we have listed one power of $1/kT$ in K_1 as possible even when the ground level does not split, because sufficiently high perturbation calculations involving the interaction with excited states may ultimately lead to anisotropic low frequency matrix elements.

[25] F. C. Powell, Proc. Roy. Soc. **130**, 167 (1930); with R. H. Fowler, Proc. Camb. Phil. Soc. **27**, 280 (1931). An anisotropic Weiss field is also suggested by Mahajani, reference 4.

given in Section 12 appears to indicate that the temperature dependence is probably not greatly modified by this tendency, although the latter admittedly works in the right direction.

Bozorth and McKeehan's model.—Practically all the papers using quadrupole-quadrupole coupling are open to the objection that they introduce this mechanism more or less *ad hoc* without supplying any basis in atomic theory. An attempt to circumvent this difficulty has been given in a recent article by Bozorth and McKeehan.[26] They neatly point out that spin dipoles can give rise to quadrupole and still higher order moments when it is remembered that the spin is not anchored to the nucleus but instead travels around with the electron. Thus on taking the time average, i.e., matrix elements diagonal in the electronic orbital quantum numbers, there is a dipole of finite extent, which will introduce quadrupole moments as long as there is a correlation between the direction of the electronic spin and the directions of anisotropy in the "time exposure" electronic charge cloud. Also it is necessary that the spin quantum number S be $>\frac{1}{2}$, since (4) is the most general potential when $S=\frac{1}{2}$. With complete correlation and with pure magnetic interaction the constant K_1 would then be of the order of magnitude $R^2g^2\beta^2/r_{ij}^5$, where R is the atomic radius. If we take $R^2/r^2\sim 1/10$, $r_{ij}^3=10^{-23}$ the resulting value of the constant K_1 is indeed of the order of magnitude observed experimentally. For this reason they suggest that true magnetic coupling (6) is sufficient to explain anisotropy, and dismiss the possibility of the electrostatic interaction between the charge clouds of different atoms, represented essentially by the last term of (9), as of uncertain magnitude and unnecessary. However, in our opinion, the correlation between spin and orbital alignment is slight, i.e., the electronic charge cloud does not orient very much with the spin, since the observed g factors of nearly 2 indicate that the orbital angular momentum is largely quenched and decoupled from the spin. So with pure magnetic interaction, the anisotropy would be too weak by a factor 1000 or so. The loss in magnitude is recovered when the Bozorth-McKeehan model is so amended that the primary coupling between different atoms is electrostatic, as seems inevitable since the orbital valence terms are surely much larger than the pure magnetic ones. (For the latter reason, incidentally, the anisotropy would be much too large were there anything like complete correlation between spin and orbital orientation.) With this modification, there is at least a vague resemblance between the Bozorth-McKeehan model and our use of the quadrupole potential (7) for $S>\frac{1}{2}$, though the approaches are entirely different. The gist of the matter is that enough fo the orbital anisotropy "sticks" to the spins to create apparent quadrupole forces between them.

[26] R. M. Bozorth and L. W. McKeehan, Phys. Rev. **51**, 210 (1937); L. W. McKeehan, Phys. Rev. **52**, 18 (1937).

8. Magnetostriction

It is not our main purpose to discuss magnetostriction, but we can note in passing how our theory has some bearing on this subject. There is a considerable literature on magnetostriction,[27] the essence of which is that it is possible to understand many of the phenomena, especially those concerned with spatial variation, if one assumes that besides the ordinary elastic energy, there is the energy of a dipole lattice which is strained due to the magnetic field, and which so loses its perfect cubic spacing. However, there is the difficulty usually stated in the form that the theoretical so-called "lattice sums" do not have the proper value, being sometimes too small, sometimes even of the wrong sign. Another way of saying the same thing is that empirically the constant of proportionality C in the dipole-dipole potential (4) (or rather its derivatives with respect to r_{ij}) does not have the value (6) corresponding to pure magnetic coupling. Fortunately in Section 4 it was shown that most of C probably does not arise from this cause, but rather from the interplay between orbital valence and spin-orbit interaction, so that C has an order of magnitude $A^2/h\nu$ about fifty times larger than (6). (As a matter of fact, even the pure exchange coupling gives rise to magnetostriction, but the resulting contribution is isotropic, and we shall consider only the spatial variation.) Hence it is clear why the so-called lattice sums should usually turn out considerably larger than given by

[27] N. S. Akulov, Zeits. f. Physik **52**, 389 (1928); **59**, 254 (1930); **69**, 78 (1931); Becker, reference 3; R. Gans and J. v. Harlem, Ann. d. Physik **16**, 162 (1933); W. Heisenberg, Zeits. f. Physik **69**, 287 (1931); F. C. Powell, Proc. Camb. Phil. Soc. **27**, 561 (1931).

(6), and not necessarily with the sign demanded by (6). According to Powell [27, 28] the anomaly in iron amounts to a factor 13, in sufficient agreement as regards order of magnitude with our rough estimate 50. Quantitative comparison of the values of C obtained from the anisotropy in the intensity of magnetization and from magnetostriction immediately suggests itself, but is not very feasible, since the former involves C itself, while the latter depends on the derivatives with respect to r_{ij}.

One thing which the magnetostriction data clearly show is that the first order dipole energy is larger than the quadrupole. In cubic systems we have seen that as far as anisotropy is concerned, the dipole energy appears only in the second order and cannot be resolved from the quadrupole contribution, as both effects enter additively when $S>\frac{1}{2}$. With magnetostriction, however, it is different. The dipole-dipole effects can come into play in the first order because the strain makes the crystal cease to be cubic. The magnetostriction data show that in (8) the constant C is certainly larger than γ. Namely, if one assumed that the magnetic energy of strain were of the order $\gamma\delta l/l$ rather than $C\delta l/l$, where l and δl are respectively the lattice spacing and strain therein, the magnetostriction would not be as large as the observed by a factor about 100. Also it is doubtful if its angular dependence would be correct, because strain of quadrupole lattices would lead to different spatial behavior than would that of dipole ones. Since C is thus so much larger than γ, it is once again hard to see why K_2 is as large as is observed, for from crude dimensional considerations one would expect the ratio of K_2 to K_1 to be about the same as that of γ to C.

It is possible that the "one-atom model" has some importance and relevance for magnetostriction even though it does not for ferromagnetic anisotropy. When a cubic crystal becomes strained, it acquires only tetragonal symmetry, and the bottom states can split, provided $S>\frac{1}{2}$. So under strain the one-atom crystalline potential can materially hamper the free alignment of the spins, and conceivably it might be possible to explain magnetostriction with this mechanism instead of the coupling (8) or (9). No doubt the two effects, crystalline potential and orbital valence, are superposed in reality.

Part II. Mathematical Analysis

9. Preliminary details

We now proceed to the mathematical calculation of the partition function $Z=\Sigma_\lambda e^{-W_\lambda/kT}$ for our model. Once this has been computed, the free energy is supplied immediately by the relation $F=-kT\log Z$. Our Hamiltonian function is

$$\mathfrak{H}=-g\beta H\Sigma_i S_{zi}+\Sigma_{j>i}w_{ij}, \tag{10}$$

where i, j refer to the various atoms of the crystal, w_{ij} is in the interaction energy between atoms i, j, and H is supposed directed along the z axis. The total effective field H is composed of the external field H_{ext} and the Weiss internal field, which is supposed to depict the ordinary exchange interaction as explained in section 5, and which is presumably proportional to the intensity of magnetization I, so that

$$H=H_{\text{ext}}+\kappa I. \tag{11}$$

For the purposes of the present paper, only the second term of (11) is of importance, but by taking H to be solely the external field, it is easily possible to adapt the calculation of section 10 to two other entirely different problems, *viz.* the adiabatic demagnetization of titanium alum, and the Gaussian fluctuations in the Heisenberg theory of ferromagnetism, as we shall show in two later papers.

Let us now regard the first member of (10) as the unperturbed system. A system of representation can then be used in which each atom is space-quantized separately, the corresponding characteristic

[28] Akulov and Becker, reference 27, obtained factors 2 and 5 respectively rather than 13, but Powell showed that this apparent discrepancy was because they used different boundary conditions or demagnetization corrections, not appropriate to the shape of the specimens usually employed experimentally.

value of S_{zi} being denoted by m_i. The unperturbed energy is then

$$W_0 = -g\beta H\Sigma_i m_i. \tag{12}$$

The second part of (10) is the perturbing potential.

10. Second-order effect of dipole-dipole coupling

Equation (8) shows that the interaction energy w_{ij} contains both dipole and quadrupole terms (provided $S>\frac{1}{2}$). However, the two terms contribute additively to K_1 to the approximation under consideration (second order in C, first in γ), and so may be treated separately. The consideration of the quadrupole part will therefore be reserved until Section 11. In the present case of dipole-dipole coupling, the interaction is thus

$$w_{ij} = \sum_{q,q'=x,y,z} a_{ij}{}^{qq'} S_{qi} S_{qj'} \quad (a_{ij}{}^{qq'} = a_{ij}{}^{q'q}). \tag{13}$$

For the sake of increased generality, needed in connection with other problems, a quadratic form has been used in (13) which is somewhat less specialized than the second member of (8). In fact, except for a trivial additive constant, (13) has the same generality as all of (4).

The matrix elements of the perturbing potential may readily be computed with the aid of the well-known formulas

$$S_{zi}(m_i; m_i') = m_i\delta(m_i; m_i'), \quad (S_{xi} \mp iS_{yi})(m_i; m_i') = (S^2+S-m_i^2 \mp m_i)^{\frac{1}{2}}\delta(m_i \pm 1; m_i'), \tag{14}$$

where δ is the Kronecker delta, and S is the spin quantum number of the atom, which we suppose the same for all atoms, but which need not necessarily be $\frac{1}{2}$. Because (13) involves the product of only two spins, Σw_{ij} is never off-diagonal in more than two quantum numbers. A typical element is, for example

$$\Sigma_{j>i} w_{ij}(m_k m_l; m_k+1, m_l-1) = \tfrac{1}{4}(a_{kl}{}^{xx}+a_{kl}{}^{yy})(S^2+S-m_k^2-m_k)^{\frac{1}{2}}(S^2+S-m_l^2+m_l)^{\frac{1}{2}}. \tag{15}$$

Here we have listed only those quantum numbers which are different in the initial and final states. In the particular case (15), these two states involve the same energy, so that in the notation of a previous article,[29] the transition (15) is one of the type indicated by the superscript$^{=}$. Another example, not of this type, is

$$\Sigma_{j>i} w_{ij}(m_l; m_l-1) = \tfrac{1}{2}\Sigma_k(a_{kl}{}^{zx} - ia_{kl}{}^{zy})m_k(S^2+S-m_l^2+m_l)^{\frac{1}{2}}. \tag{16}$$

In this instance the energy change is $g\beta H$.

The partition function can now be calculated to terms in $w_{ij}{}^2$ inclusive by means of formulas (64), (65), (68–72) given in Section 6 of a previous paper,[29] which we shall call *l.c.* In fact the present calculation resembles in many ways that given in detail in sections 1–2 of *l.c.* However, there is the distinction that we there supposed the field strength small, so that we could stop with second powers thereof. In the present ferromagnetic case, the effective, inner field is not small, and saturation cannot be neglected. Cubic anisotropy first appears in the approximation H^4. So it is necessary to use a more general theory in which all powers of the field strength are retained. The requisite skeleton mathematical basis is supplied by Eqs. (64) etc. of Section 6 of *l.c.*, which have the desired generality, and serve as a starting point for the present calculation. The inclusion of a crystalline field, allowed in Section 6 of *l.c.* is, however, not necessary for present purposes. When the formulas of *l.c.* for the partition function are utilized, there are still sums over the various quantum numbers to be evaluated. Fortunately they can all be factored into sums over individual quantum numbers of the type

$$B_n = \sum_{m=-S}^{S} m^n e^{m\theta} / \sum e^{m\theta} \quad \text{with} \quad \theta = g\beta H/kT. \tag{17}$$

[29] J. H. Van Vleck, J. Chem. Phys. **5**, 320 (1937).

The function B_n defined by (17) may be evaluated explicitly by means of the relation

$$B_n = Q^{-1}d^nQ/d\theta^n \quad \text{where} \quad Q=\sum e^{m\theta}=e^{-S\theta}(1-e^{(2S+1)\theta})/(1-e^{\theta}).$$

With the aid of *l.c.*, one thus finally finds that

$$\begin{aligned} Z/Z_0 = 1 &- \tfrac{1}{2}Nk^{-1}T^{-1}\Sigma_j a_{ij}{}^{zz}B_1{}^2+\tfrac{1}{2}NB_1{}^2B_2k^{-2}T^{-2}[(\Sigma_j a_{ij}{}^{zz})^2-\Sigma_j(a_{ij}{}^{zz})^2] \\ &+\tfrac{1}{8}Nk^{-2}T^{-2}B_1{}^4[(N-4)(\Sigma_j a_{ij}{}^{zz})^2+2\Sigma_j(a_{ij}{}^{zz})^2]+(NB_1{}^3/2kTg\beta H)[(\Sigma_j a_{ij}{}^{zz})^2+(\Sigma_j a_{ij}{}^{yz})^2 \\ &-\Sigma_j(a_{ij}{}^{zz})^2-\Sigma_j(a_{ij}{}^{yz})^2]+\tfrac{1}{4}NB_2{}^2k^{-2}T^{-2}\Sigma_j(a_{ij}{}^{zz})^2+\tfrac{1}{2}(NB_2B_1/kTg\beta H)[\Sigma_j(a_{ij}{}^{zz})^2+\Sigma_j(a_{ij}{}^{yz})^2] \\ &+\tfrac{1}{32}Nk^{-2}T^{-2}(S^2+S-B_2+B_1)(S^2+S-B_2-B_1)\Sigma_j(a_{ij}{}^{zz}+a_{ij}{}^{yy})^2 \\ &+\tfrac{1}{8}(NB_1/2kTg\beta H)(S^2+S-B_2)\Sigma_j[(a_{ij}{}^{zz}-a_{ij}{}^{yy})^2+4(a_{ij}{}^{xy})^2]. \end{aligned} \tag{18}$$

Here Z_0 is the partition function in the absence of the perturbing potential $\Sigma_{j>i}w_{ij}$. The contribution of the factor Z_0 to the free energy $F=-kT\log Z$ is simply the free energy corresponding to an ideal gas in a magnetic field, and consequently isotropic as far as the latter's orientation is concerned. This part of F is obviously of no interest for us. In writing (18), we have replaced $\Sigma_{j>i}$ by $\frac{1}{2}N\Sigma_j$. This is legitimate because the atoms are all alike in behavior in the cubic gratings we are considering.

Equation (18) involves the a_{ij} relative to a system of coordinate axes such that the applied field is always in the z direction. To study anisotropy, it is necessary to express the interaction energy w_{ij} in terms of similar constants A_{ij} for a system of axes fixed relative to the crystal, which are denoted by capital letters, i.e.,

$$w_{ij}=\Sigma_{q,q'=X,Y,Z}A_{ij}{}^{qq'}S_{qi}S_{qj}. \tag{19}$$

The reason that the results must be expressed in terms of the A's rather than the a's is, of course. that the A's are constants independent of the direction of the applied field, whereas the a's are not, Since w_{ij} must be invariant of the coordinate system, and since the S_i transform like vectors, comparison of (14) and (19) shows that the transformation relations connecting the a's and A's are

$$a_{ij}{}^{qq'}=\Sigma_{p,p'=XYZ}\lambda_{qp}\lambda_{q'p'}A_{ij}{}^{pp'}, \tag{20}$$

where the λ_{qp} are direction cosines. We now substitute (19) in (18). A large number of terms coalesce or drop out if we assume, as we do, that there is cubic symmetry. In virtue of the latter, sums like $\Sigma A^{XY}A^{YZ}$ in which a letter (here X or Z) appears only once, must vanish for there is nothing to distinguish between the positive and negative X (or Y or Z) directions. If such sums did not vanish they would not be invariant under the substitution $X=-X$, inasmuch as $A^{-XY}=-A^{XY}$. Also because of the parity of all coordinate axes in a cubic system, we must have

$$\Sigma_j(A_{ij}{}^{zz})^2=\Sigma_j(A_{ij}{}^{zz})^2, \quad \Sigma_j A_{ij}{}^{zz}A_{ij}{}^{yy}=\Sigma_j A_{ij}{}^{zz}A_{ij}{}^{zz}, \quad \text{etc.}$$

Similar relations also apply in the x, y, z system. They would not be true were the summation over j removed, as the interaction between any given pair of atoms certainly does not have cubic symmetry. With the summation, however, the full cubic symmetry of an atom's environment is manifested. Thus it is finally found that (18) becomes

$$\begin{aligned} Z/Z_0 = 1 &- \tfrac{1}{2}Nk^{-1}T^{-1}\Omega_0B_1{}^2+\tfrac{1}{8}Nk^{-2}T^{-2}[B_1{}^4(N-4)+yB_1{}^2B_2]\Omega_0{}^2 \\ &+\tfrac{1}{5}Nk^{-2}T^{-2}[\tfrac{1}{4}B_1{}^4-\tfrac{1}{2}B_1{}^2B_2+\tfrac{1}{4}B_2{}^2+\tfrac{1}{16}(S^2+S-B_2)^2-\tfrac{1}{16}B_1{}^2+\tfrac{1}{8}(S^2+S-B_2)(B_1kT/g\beta H)]\Omega_1 \\ &+\tfrac{1}{5}Nk^{-2}T^{-2}(kT/g\beta H)[\tfrac{1}{4}B_1(S^2+S-B_2)-B_1{}^3+B_2B_1]\Omega_2 \\ &+\tfrac{1}{5}Nk^{-2}T^{-2}[\tfrac{1}{16}(S^2+S-B_2)^2-\tfrac{1}{16}B_1{}^2-\tfrac{1}{8}(S^2+S-B_2)(B_1kT/g\beta H)]\Omega_3 \\ &-Nk^{-2}T^{-2}[\tfrac{1}{2}B_1{}^4-B_1{}^2B_2+\tfrac{1}{2}B_2{}^2+\tfrac{1}{16}(S^2+S-B_2)^2-\tfrac{1}{16}B_1{}^2 \\ &+\tfrac{1}{8}(kT/g\beta H)(S^2+S-B_2)B_1+(kT/g\beta H)(B_1{}^3-B_2B_1)]\Omega_4(\alpha_1{}^2\alpha_2{}^2+\alpha_1{}^2\alpha_3{}^2+\alpha_2{}^2\alpha_3{}^2-\tfrac{1}{5}), \end{aligned} \tag{21}$$

where $\Omega_0=\frac{1}{3}\Sigma_j(A_{ij}{}^{XX}+A_{ij}{}^{YY}+A_{ij}{}^{ZZ})$ and

$$\Omega_1=3b+2c+4d,\quad \Omega_2=b-c+3d,\quad \Omega_3=b+4c-2d,\quad \Omega_4=b-c-2d$$

$$b=\Sigma_j b_{ij}=\tfrac{1}{3}\Sigma_j\{(A_{ij}{}^{XX})^2+(A_{ij}{}^{YY})^2+(A_{ij}{}^{ZZ})^2\},\quad c=\tfrac{1}{3}\Sigma_j(A_{ij}{}^{XX}A_{ij}{}^{YY}+A_{ij}{}^{YY}A_{ij}{}^{ZZ}+A_{ij}{}^{ZZ}A_{ij}{}^{XX}),\quad (22)$$

$$d=\tfrac{1}{3}\Sigma_j\{(A_{ij}{}^{XY})^2+(A_{ij}{}^{YZ})^2+(A_{ij}{}^{ZX})^2\}.$$

In (21), the notation α_1, α_2, α_3 has been used in place of λ_{zX}, λ_{zY}, λ_{zZ}, respectively. The additive constant $-\frac{1}{5}$ is included in the angular factor in the last term of (21) in order to make this term average to zero, inasmuch as the mean or power value of (21) will be needed in a later paper.

Formula (21) is valid for any value of the spin. In the important special case $S=\frac{1}{2}$ one has

$$B_1=\tfrac{1}{2}\tanh(g\beta H/2kT),\qquad B_2=\tfrac{1}{4},\qquad (23)$$

and the analytical form of (21) is really rather simple, merely a polynomial in B_1.

Demagnetization corrections.—In case the test body is not molded in the shape of a sphere, the boundary conditions do not in general exhibit cubic symmetry even though the crystal belongs to the cubic classification. Then it is not allowable to suppose that the part of the A's due to the pure magnetic coupling (6) satisfy the relation

$$\Sigma_j A_{ij}{}^{XX}=\Sigma_j A_{ij}{}^{YY}=\Sigma_j A_{ij}{}^{ZZ}.\qquad (24)$$

Instead, because (5) varies only as the inverse cube of the distance, the way the specimen is molded makes itself felt in a complicated way, giving rise to the so-called demagnetization corrections. It is well known that a rigorous theory of the latter is feasible only if the body is cut in an ellipsoidal form. Otherwise the various atoms cannot be regarded as equivalent in their grating sums and it would not be allowable to replace $\Sigma_{j>i}$ by $\frac{1}{2}N\Sigma_j$, as presupposed in (18) and (21). For this reason (18) and (21) are not rigorous when the body is molded in a cube or some other nonspherical shape compatible with cubic symmetry even though the full validity of (24) is then restored. The expression (21) can be used not merely for a spherical specimen, but also for a body cut in an ellipsoid of revolution with axis parallel to the field, provided Ω_o is defined not as before (22) but as

$$\Omega_o=\Sigma_j a_{ij}{}^{zz}=-Ng^2\beta^2\Phi+\tfrac{1}{3}\Sigma_j(A_{ij(o)}{}^{XX}+A_{ij\,(o)}{}^{YY}+A_{ij\,(o)}{}^{ZZ}).\qquad (25)$$

Here Φ is the demagnetization plus Lorentz factor fully explained in Section 4 of *l.c.* The value of Φ for a sphere is 0, while Φ equals $4\pi/3$ and $-8\pi/3$ respectively for very prolate and very oblate ellipsoids. The subscript (o) attached to A_{ij} in (25) means that the part of A_{ij} due to the pure magnetic coupling is to be omitted. On the other hand this part of A_{ij} should still be included in computing Ω_1, Ω_2, Ω_3, Ω_4. These expressions all involve the A_{ij}'s quadratically, so that in the sums (22) the pure magnetic coupling (6) gives rise only to inverse sixth powers and there is no trouble with boundary conditions regardless of shape. The orbital valence portion $A_{ij\,(o)}$ which we saw in Section 4 doubtless constitutes the bulk of A_{ij} does not introduce shape complications even in the linear relation (25) since $A_{ij\,(o)}$ varies much more rapidly with distance than the inverse cube and so satisfies (24). The demagnetization factor Φ makes no contribution to the anisotropy if the body is always cut in the same direction relative to the field. This is what appears to be done experimentally; e.g., three specimens are cut in the form of long rods along the 100, 110, and 111 axes respectively, and their magnetization curves measured separately. The demagnetization correction for a long rod is presumably about the same as for a very prolate ellipsoid. Anyway, these corrections are not very important for our present purposes, since the extreme range $-8\pi/3$ to $4\pi/3$ in the Φ factor is very small compared with the constant of proportionality $\kappa\sim10^5$ of the Weiss molecular field.

Numerical checks.—There are three simple checks on the arithmetical correctness of (21) which should be mentioned, and which we have verified. One is that if the functions B_1, B_2 be expanded as Taylor's series in $\theta=Hg\beta/kT$, *viz.*

$$B_1=\tfrac{1}{3}\theta x-\theta^3(2x^2+x)/90,\quad B_2=\tfrac{1}{3}x+\theta^2(4x^2-3x)/90,\quad (x=S^2+S)\qquad (26)$$

then the coefficient of Ω_4 in (21) vanishes unless one goes to the fourth power of H. This must be the case, for since H transforms like a vector, only terms in H^4 or higher can exhibit a dependence on the direction cosines of the form $\alpha_1^2\alpha_2^2+\alpha_1^2\alpha_3^2+\alpha_2^2\alpha_3^2$. A term in H^2, for instance, could only give quadratic dependence and because of cubic symmetry, can only contribute to the constant part of Z. The second check is that the coefficient of Ω_4 also vanishes in the limit $H=\infty$, which corresponds to complete parallelism of the dipoles; here $B_1=\sqrt{B_2}=S$.

The third check is that the direction-independent part of (21) should reduce to (53) and the unnumbered equation after (55) of *l.c.* when the development is terminated with H^2, and when the potential w_{ij} is specialized to exchange plus true magnetic-dipole coupling so that w_{ij} has the form given in (13) of *l.c.* (The notation J rather than S was used in *l.c.* for the angular momentum vector and the exchange integral was denoted by K rather than J, while v_{ij} is the same as our $-2J_{ij}r_{ij}^3/g^2\beta^2$.) Then

$$\Omega_0=Ng^2\beta^2(-\Phi+z'v),\quad \Omega_1=N^2g^4\beta^4(2Q_0+5Q_1),\quad \Omega_2=\tfrac{1}{2}N^2g^4\beta^4\cdot3Q,\quad \Omega_3=N^2g^4\beta^4(-Q_0+5Q_1),\qquad (27)$$

where $Q_0=2N^{-2}\Sigma r_{ij}^{-6}$, $Q_1=Q-Q_0=4N^{-2}g^{-4}\beta^{-4}\Sigma_i J_{ij}^2$, $z'v=-2Ng^{-2}\beta^{-2}\Sigma_i J_{ij}$. The first relation of (27) follows from (25). The easiest way to establish the rest of (27) is to note that Ω_1, Ω_2, Ω_3 are independent of the choice of coordinate axes. So it is allowable to place the z axis along r_{ij} for each term in the lattice sums involved in the definitions (22), even though a different choice of axes is then required for each term. With (27), Eq. (21) reduces properly to (53) of *l.c.* Incidentally, (53) and other relations of *l.c.* apply when the dipole-dipole coupling is due to orbital valence, rather than of true magnetic origin, provided $g^2\beta^2/r_{ij}^3$ be replaced by C_{ij} in definatory relations such as (8) or (18) of *l.c.*

The structure factor Ω_4 in the anisotropic part of the partition function (21–22) is conveniently expressed in terms of a set of axes ξ_j, η_j, ζ_j which are so selected that ζ_j always is along r_{ij}, and whose choice hence varies with each term j in the sum. Then

$$\Omega_4=\sum_j[b_{ij}'-c_{ij}'-2d_{ij}'][1-5(\lambda^2 x_{\xi j}\lambda^2 y_{\xi j}+\lambda^2 y_{\xi j}\lambda z_{\xi j}^2+\lambda^2 z_{\xi j}\lambda^2 x_{\xi j})], \tag{28}$$

where the λ's are direction cosines and where b_{ij}', c_{ij}', d_{ij}' are similar to b_{ij}, c_{ij}, d_{ij} except for being computed relative to the ξ_j, η_j, ζ_j rather than X, Y, Z axes. Thus b_{ij}', c_{ij}', d_{ij}' are defined by (22) except that ξ_j, η_j, ζ_j throughout replace X, Y, Z. The advantage of (28) is that it employs the simplest choice of axes for each individual pair of atoms in the sum.

If w_{ij} has the dipole-dipole form given by the second member of (8), the expression (28) becomes

$$\Omega_4=3\sum_j C_{ij}^2[1-5(\lambda^2 x_{\xi j}\lambda^2 y_{\xi j}+\lambda^2 y_{\xi j}\lambda^2 z_{\xi j}+\lambda^2 z_{\xi j}\lambda^2 x_{\xi j})]. \tag{29}$$

To determine sign behavior, no harm will be done if the summation in (29) is restricted to the immediate neighbors of the given atom i. In the first place C_{ij} varies rapidly with r_{ij}, as the inverse sixth power if caused by the true magnetic effect (6), and still more drastically if due to the interplay of orbital valence and spin-orbit interaction. Also, especially, as one gets very far from a given atom, the distribution approaches effectively more and more that of a continuum. As soon as the summation can be replaced by an integral over a sphere, it vanishes, as the bracketed factor in (29) integrates to zero. By restricting ourselves to the nearest neighbors we probably overestimate slightly the numerical value of the sum (29), since the sign of the angular factor in (29) for the next-to-nearest neighbors, which presumably contribute the next-most-important terms, is the opposite to that for the leading terms. Possibly, but not very likely, this fact explains why K_2 is as large as it is relative to K_1, for the cancellation of the first and second zones is not as complete in K_2 as in K_1. With the restriction to nearest neighbors, the values of (29) are as follows for the various lattices.

simple	face-centered	body-centered
$\Omega_4=+18\ C^2$,	$-9\ C^2$,	$-16\ C^2$,

(30)

where C is the value of C_{ij} connecting adjacent atoms. To a sufficient approximation the free energy is

$$F=-kT\log Z=-kT\log Z_0-kT(Z_1/Z_0)+kT(Z_1/Z_0)^2-kT(Z_2/Z_0)+\cdots \tag{31}$$

if Z_1 and Z_2 denote respectively the parts of (21) of the first and second degree in the A_{ij}. Consequently the anisotropy constant K_1 in (2) has the value

$$K_1=Nk^{-1}T^{-1}f(g\beta H/kT)\Omega_4, \tag{32}$$

where $f(g\beta H/kT)$ denotes the long factor inclosed by square brackets in the last or Ω_4 term of (21).

Before we can compute with (32), it is necessary to agree on how to select the effective field H. We shall neglect the applied field H_{ext} in comparison with the inner field, an approximation which is completely warranted for our purposes inasmuch as the factor of proportionality κ by which the intensity of magnetization is multiplied to get the effective Weiss field is so very large. It is, however, at the same time tacitly supposed that the external field is adequate to make the inner field coincide in direction with it, or in other words to produce saturation. Our computed values of the free energy thus relate to $-\int I dH_{ext}$ integrated out to a field H_{ext} adequate to produce saturation, but at the

TABLE I. *Anisotropy for dipole-dipole model with* $S=\frac{1}{2}$.

$g\beta\kappa I/kT$	∞	6	4	3.2	2.6	2	1.6	1.2	0.8
$I/I_0=\frac{1}{2}B_1$	1	0.996	0.96	0.92	0.86	0.76	0.66	0.54	0.38
T/T_c	0	.33	.48	.58	.66	.76	.825	.9	.95
K_1kT_c/NC^2 (calc.)	−.140	−.139	−.126	−.102	−.076	−.046	−.028	−.011	−.003
T (nickel)	0[30]	210	305	365	420	480	525	570	605°K
K_1 (obs., nickel)	-3×10^6	-1.6×10^6	-3×10^4	-5×10^3	0	$+10^4$	$+10^4$	$+10^4$	$+10^4$ ergs/cm³

same time small compared with κI.[31] We shall assume that the factor of proportionality κ in the molecular field is independent of temperature. Then the Heisenberg theory[32] shows that

$$H=\kappa I=3kT_cI/I_0g\beta(S+1), \qquad T_c=2Jz(S^2+S)/3k, \tag{33}$$

where I/I_0 is the ratio $I/g\beta S$ of the saturation intensity of magnetization at the given temperature to the complete saturation at the absolute zero. T_c is the Curie temperature, z is the number of neighbors, and J is the exchange integral. In computing the tables we take $g=2$, as the difference between 2 and the experimental value 1.9 is inconsequential. In order to record dimensionless expressions, we give the theoretical values of K_1kT_c/NC^2 rather than of K_1 itself. To evaluate (21) it is necessary to determine the values of T to be correlated with each value of I. It proves unimportant whether one uses the experimental correlation or the theoretical one $I=g\beta B_1$ given by the Weiss-Heisenberg theory, since the latter reproduces the observed $I-T$ curves sufficiently well for our purposes.

In Section 6, it was shown that the values of NC^2/kT_c by which the calculated K_1kT_c/NC^2 must be multiplied through to yield the observed K_1 at room temperatures and lower are of a reasonable order of magnitude. If C^2 is regarded as constant with respect to T, the calculated variation of K_1 with T is not sufficiently rapid; reasons why this should be so are also discussed in Section 6. Comparison of Tables I and II show that the behavior of K_1 for $S=\frac{1}{2}$ and $S=1$ is very similar except for a constant proportionality factor. Hence it matters little what atomic spin is assumed in the present qualitative status of the theory. For possible significance of the small positive experimental values of K_1 at high temperatures, see the very end of Section 6.

11. First-order effect of quadrupole-quadrupole interaction

We now consider the case where the coupling between atoms is of the quadrupole rather than dipole type. Referred to axes fixed relative to the field, the interaction between two atoms is of the type form

$$w_{ij}=\Sigma_{q,q',q'',q'''=x,y,z}\, a_{ij}{}^{qq'q''q'''}S_{qi}S_{q'i}S_{q''j}S_{q'''j}, \tag{34}$$

which is, of course, biquadratic in the two spins, considered together, or quadratic in the individual spins, considered separately. Without loss of generality, we may suppose (34) symmetric not merely

TABLE II. *Anisotropy for dipole-dipole model with* $S=1$.

$g\beta\kappa I/kT$	∞	3	2	1.6	1.3	1	0.8	0.6	0.4
$I/I_0=B_1$	1	0.95	0.85	0.77	0.69	0.58	.48	.38	.26
T/T_c	0	.48	.64	.72	.79	.87	.91	.95	.97
K_1kT_c/NC^2 (calc.)	−.75	−.68	−.50	−.35	−.24	−.13	−.05	−.02	−.01

Values of K_1T_c/NC^2 given in Tables I and II are calculated for face-centered lattice; for body-centered and simple cubic lattices, they should be multiplied by 16/9 and −2, respectively.

[30] The experimental values of K_1 given in Tables I and III are for $T=21$°K and $T=93$°K respectively rather than $T=0$. Extrapolation indicates that in nickel $|K_1|$ is probably much larger than 3×10^6 at the absolute zero.

[31] In very weak fields, the direction of the spontaneous magnetization no longer coincides with the applied field, and is distributed in accordance with a statistical theory developed by Heisenberg (reference 27, not to be confused with his better known exchange theory, reference 12, of ferromagnetism). Heisenberg's ideas have been applied by Bozorth to ferromagnetic anisotropy in weak fields, especially the difference in direction between the vectors **B** and **H**. (Phys. Rev. **42**, 882 (1932)). Such investigations, of course, do not aim to explain the atomic origin of the anisotropy.

[32] Cf., for instance, J. H. Van Vleck, *The Theory of Electric and Magnetic Susceptibilities*, Chap. XII, Eqs. (34), (37) and (29).

as regards permutation of the two atoms, but also as regards permutation of indices relating to the same atom, whence

$$a_{ij}{}^{qq'q''q'''}=a_{ij}{}^{q''q'''qq'}, \quad a_{ij}{}^{qq'q''q'''}=a^{q'qq''q'''}. \tag{35}$$

(If there were any unsymmetrical terms contrary to the second relation of (35), they could immediately be reduced to lower degree by the familiar relations $S_xS_y-S_yS_x=iS_z$, etc.)

We suppose, as before, that the exchange interaction can be represented by means of an inner field (33), and regard (34) as a perturbation. As often previously mentioned, with quadrupoles the perturbation calculation need by carried only to the first order to bring out the cubic anisotropy (2). To this approximation the free energy is then identical with the mean interaction energy; i.e.,

$$F=-kT\log Z_0+\sum_{j>i}(w_{ij})_{Av}. \tag{36}$$

The average denoted by the subscript Av is, of course, proportional to the diagonal sum in the system of representation, described in Section 9, in which each spin is separately space-quantized.

We now pass from axes x, y, z fixed relative to the field to axes X, Y, Z fixed in the crystal, denoting by capital letters the coefficients corresponding to (34) in the X, Y, Z system. The transformation equations connecting the two sets of coefficients are

$$a_{ij}{}^{qq'q''q'''}=\Sigma_{QQ'Q''Q'''=X,Y,Z}\,\lambda_{qQ}\lambda_{q'Q'}\lambda_{q''Q''}\lambda_{q'''Q'''}A_{ij}{}^{QQ'Q''Q'''}. \tag{37}$$

In precisely the same way that (21) was obtained from (18), it is found on using the cubic symmetry of the lattice that (36) becomes

$$F=F_0+\Omega_5[f_1+f_2][\alpha_1{}^2\alpha_2{}^2+\alpha_2{}^2\alpha_3{}^2+\alpha_3{}^2\alpha_1{}^2], \tag{38}$$

where F_0 is a purely isotropic term and where

$$\Omega_5=-N\Sigma_j[A_{ij}{}^{ZZZZ}-A_{ij}{}^{XXYY}-2A_{ij}{}^{XYXY}]. \tag{39}$$

The expressions f_1 and f_2 appearing in (38) are dimensionless functions of the argument $g\beta H/kT$, defined by

$$f_1=(S_{zi}{}^2S_{zj}{}^2)_{Av}+(S_{yi}{}^2S_{yj}{}^2)_{Av}+(S_{zi}{}^2S_{zj}{}^2)_{Av}-(S_{xi}{}^2S_{yj}{}^2)_{Av}-(S_{yi}{}^2S_{zj}{}^2)_{Av}-(S_{zi}{}^2S_{xj}{}^2)_{Av} \tag{40}$$

$$f_2=-\tfrac{1}{2}[(S_{xi}S_{yi}+S_{yi}S_{xi})(S_{xj}S_{yj}+S_{yj}S_{xj})+(S_{yi}S_{zi}+S_{zi}S_{yi})(S_{yj}S_{zj}+S_{zj}S_{yj})$$
$$+(S_{zi}S_{xi}+S_{xi}S_{zi})(S_{zj}S_{xj}+S_{xj}S_{zj})]_{Av}. \tag{41}$$

Although Ω_5 is evaluated in the X, Y, Z system, the averages of the spin vectors involved in (40–41) relate to the x, y, z system. Since each atom is separately spaced quantized in the system of representation being used (cf. Section 9), the averages may be taken over atoms i and j separately. In virtue of (14) and (17), Eqs. (40–41) may be written

$$f_1=[\tfrac{1}{2}(S^2+S)-\tfrac{3}{2}B_2]^2, \qquad f_2=0, \tag{42}$$

with B_2 as in (17). If $S=\frac{1}{2}$, then $B_2=\frac{1}{4}$, and f_1 vanishes, in agreement with our statement in section 3 that a quadrupole model is capable of yielding anisotropy only if $S>\frac{1}{2}$. If the quadrupole interaction energy has the form given by the third member of (8), which is sufficiently general for our purposes, then in the same way that (29) was obtained, it is found that

$$\Omega_5=-N\Sigma_j\gamma_{ij}[1-5(\lambda^2{}_{X\zeta_j}\lambda^2{}_{Y\zeta_j}+\lambda^2{}_{Y\zeta_j}\lambda^2{}_{Z\zeta_j}+\lambda^2{}_{X\zeta_j}\lambda^2{}_{Z\zeta_j})], \tag{43}$$

where the ζ_j axis is directed along r_{ij}. If γ_{ij} has a nonvanishing value γ only between neighbors, (43) yields

	face-centered	body-centered	simple cubic
Ω_5/N	$+3\gamma$	$+(16/3)\gamma$	-6γ

(44)

TABLE III. *Anisotropy for quadrupole-quadrupole model with* $S=1$.

$g\beta\kappa I/kT$	∞	4	3	2.5	2	1.6	1.3	1	0.8	0.6
$I/I_0=B_1$	1.0	0.98	0.95	0.91	0.85	0.77	0.69	0.58	.48	.38
T/T_c	0	.38	.48	.55	.64	.72	.79	.87	.91	.95
$K_1/N\gamma$ (calc.)	1.333	1.20	.98	.81	.56	.34	.20	.10	.04	.02
T (iron)	0[33]	400	500	575	670	750	820	910	950	990°K
K_1 obs (iron)	6×10^5	3.6×10^6	2.7×10^6	2×10^6	1.3×10^6	$.7\times10^6$	$.4\times10^6$	$.1\times10^6$	0	0 ergs/cm³
$K_1/N\gamma$ (sec. 12)	1.333	1.13	.89	.76	.47	.27	.16	.07	.03	.01

Values of $K_1/N\gamma$ in Table III are calculated for body-centered lattice; for face-centered and simple cubic lattices, they should be multiplied respectively by 9/16 and $-9/8$, respectively.

The numerical values of K_1/γ given by (38,) (42), (44) for various temperatures are shown in Table III for the case $S=1$.

Nothing can be said at present from pure theory concerning the sign of γ. For discussion of the relation of the calculated to observed values of K_1 see Section 6. The general lay of the land is about the same as in the dipole-dipole case; *viz.* the order of magnitude of γ required to fit the experimental data is reasonable, but the calculated temperature variation of K_1 is not rapid enough if γ is regarded as a constant. However, the discrepancy is not as great as in the case of nickel. For instance, the table shows that experiment gives a reduction in K_1 by a factor 50 in going from low temperatures to 910°K, and theory also yields a fairly large reduction factor, *viz.* 13, or 19 with the improved calculation given in the next section.

12. Alternative, perhaps improved calculation of first order quadrupole-quadrupole interaction

It is obviously only an approximation to represent the exchange coupling by a molecular field. It is therefore advisable to see if substantially the same results are obtained with somewhat different approximations. We therefore now describe a somewhat modified and slightly more intricate calculation, in which we take into account rigorously the exchange interaction between the two particular atoms i, j whose anisotropy we are computing, but we still employ an appropriately chosen Weiss field to represent the exchange coupling of atom i with all other atoms than j, or of j with all others but i. Instead of being separately space quantized the two atoms i, j have a quantum number $S'=0, 1, \cdots, 2S$ which quantizes their total resultant spin, and another quantum number $M'=-S', \cdots, S'$ which determines the spatial orientation of S'. The choice of the system of quantization thus is different for each pair of atoms in the sum, but this procedure is allowable, because we are at liberty to approximate to the mean value of each individual term in (36) in the best fashion possible. Although we are still using the artifice of an inner field to represent the interplay of an atom with all but one of its z neighbors, the present procedure probably constitutes an improvement over Section 11 as far as the calculation of the anisotropic interactions is concerned. The reason is that if we are computing the mean value of a given perturbing term w_{ij}, it seems more important to take into account rigorously the interaction between atoms i and j than that between atoms i or j and other atoms, since w_{ij} is particularly sensitive to the relative alignment of atoms i and j. With our amended model, Eqs. (38)–(41) are still applicable, but the averages over atoms i and j can no longer be computed independently, inasmuch as with our new system of quantization there is a correlation between the motions of atoms i and j. Consequently f_1 and f_2 no longer have the values (42). The matrix elements of S_{x_i}, etc. appropriate to the present system of representation may be found in the literature.[33] They are then multiplied out to form the expressions (40)–(41) with each state weighted with its appropriate Boltzmann factor $e^{-[W(S')-M'g\beta H]/kT}$. The mutual exchange energy $W(S')$ of atoms i, j has the value[3]

$$W(S')=-2J\mathbf{S}_i\cdot\mathbf{S}_j=-J[S'^2+S'-2S^2-2S], \tag{45}$$

where J is the exchange integral connecting i and j. Henceforth we shall consider only the special case $S=1$ of one quantum unit of spin per atom. Then

$$W(2)=-2J, \quad W(1)=2J, \quad W(2)=4J,$$

and it is found that

$$f_1+f_2=\tfrac{1}{2}[\cosh 2\theta-4\cosh\theta+3]/D, \tag{46}$$

where $\theta=g\beta H/kT$ and

$$D=(2\cosh 2\theta+2\cosh\theta+1)+(2\cosh\theta+1)e^{-4J/kT}+e^{-6J/kT}. \tag{47}$$

The result (46) may be easily deduced by the following argument instead of resorting to the rather laborious compounding of the matrix elements to compute the individual terms of (40)–(41) explicitly. All the cubic anisotropy must come from the different Zeeman components of the state $S'=2$, since the angular dependence (2) is impossible for a single system with resultant spin $S'=1$ or $S'=0$. (Cf. remarks under Bloch-Gentile theory in Section 7). In this connection

[33] See, for example, Condon and Shortley, *The Theory of Atomic Spectra*, pp. 63–67.

atoms i and j are to be regarded together as a one unit, inasmuch as the interaction energy w_{ij} involves a dynamical system of two atoms. (Hence the spin of an individual atom, which is only a component part of the system, can still be only unity.) Furthermore, the contributions of the various Zeeman components of $S'=2$ to the anisotropy is easily seen to be independent of the sign of M'. Consequently f_1+f_2 must have the form $a\cosh 2\theta+b\cosh\theta+c$, where D is defined as in (47), and where a, b, c are independent of T, H, and J. The explicit values of a, b, c given in (46) follow immediately from the requirement that (46) must reduce to (42) when $J=0$.

The inner field must now be taken as

$$H=2J(z-1)I/I_0g\beta \tag{48}$$

rather than as $2JzI/I_0g\beta$, the usual Weiss-Heisenberg value, since one of the z interactions is taken into account rigorously rather than incorporated in this field. The formula for the ratio I/I_0 of the intensity of magnetization to its maximum value at $T=0$ is

$$I/I_0=\tfrac{1}{2}[(4\sinh 2\theta+2\sinh\theta)+2\sinh\theta e^{-4J/kT}]/D. \tag{49}$$

The Curie temperature T_c is the temperature at which (48) has a double root in I at $I=0$, or what is the same, the temperature at which the susceptibility becomes infinite when a small external field is added to the right side of (48). Hence T_c is determined by the transcendental equation

$$kT_c=2J(z-1)(5+e^{-4J/kT_c})/(5+3e^{-4J/kT_c}+e^{-6J/kT_c}). \tag{50}$$

The Curie temperature given by (50) is almost identical with that $T_c=4zJ/3k$ (cf. Eq. (33) with $S=1$) given by the ordinary Heisenberg model, e.g. 10.4 as compared with 10.7 if $z=8$. Henceforth in applying formula (46) no appreciable harm will be done if we use the correlation of I/I_0 with T/T_c given by the conventional Weiss formula $I/I_0=B_1$, rather than by (49).[34] The values of $K_1/N\gamma$ computed from (46) are shown in the last line of Table III, Section 11. The difference between the new values and those originally computed in Section 11 is unimportant in the present status of the theory. For this reason it does not seem worth while to apply the present method to the second-order effect of dipole-dipole interaction, which would be more difficult.

13. Hexagonal crystals

We shall now in closing digress briefly on hexagonal instead of cubic lattices. It is found empirically that with a hexagonal structure, the dependence on the free energy on the angle φ between the applied field and the hexagonal axis is of the form

$$F=F_0+K'\sin^2\varphi+K''\sin^4\varphi. \tag{51}$$

With our model, the constant K' results primarily from dipole-dipole interaction, which, owing to the loss of cubic symmetry, no longer vanishes in the first approximation. Instead, in exactly the same way that (38) was obtained, it is found on using (36), (19), (20), (14), (17) and the hexagonal symmetry that

$$F=F_0+\Omega_6B_1^2\sin^2\varphi, \tag{52}$$

where

$$\Omega_6=-\tfrac{1}{2}N\Sigma_{j>i}[A_{ij}{}^{ZZ}-\tfrac{1}{2}(A_{ij}{}^{XX}+A_{ij}{}^{YY})], \tag{53}$$

with Z directed along the hexagonal axis. Since B_1 is the same as SI/I_0 the variation of B_1^2 with temperature can be found simply by squaring the values of I/I_0 given in Table I for $S=\frac{1}{2}$ or Table II for $S=1$. The theoretical variation with T is thus somewhat less rapid than in the case of fourth order or cubic anisotropy. (In Table II, the anisotropy was more nearly proportional to I^3). Experimentally the dependence on temperature is again greater than given by theory if Ω_6 is regarded as a constant. In fact in cobalt $K'+K''$ is even found to change sign at 550°K. The discrepancy must once more be attributed to the fact that Ω_6 is a function of temperature. As regards orders of magnitude one might at first thought expect Ω_6/N to be comparable with the constant C in (8). For instance, if the only important coupling is to six neighbors in the same equatorial plane as the given atom, (53) becomes $\Omega_6=-9NC/2$. In section 6 we estimated C to be of the order $A^2/h\nu\sim 10\ \text{cm}^{-1}$. Then K' would be about 10^9 ergs/cm^3, whereas the experimental values are only of the order 10^7. As suggested

[34] It is clearly to be understood that in using the formula $I/I_0=B_1$, the value (33) should be employed for H, as then this formula gives about the same $I-T$ curves as (49) with the field (48). The field (48) is still to be used in (46). The difference between the arguments (33) and (48), rather than the difference between the functional forms of (42) and (46), accounts for most of the divergence between the two sets of values of $K_1/N\gamma$ in Table III. The first line of Table III gives the field (33) instead of (48).

by Bloch and Gentile,[21] the explanation is probably that the arrangement of atoms in the hexagonal gratings does not deviate too greatly from cubic form. With strict cubic symmetry, the expression (53) would vanish, and with hexagonal the various members of (53) may nearly cancel, so that Ω_6 is considerably smaller than NC in magnitude. There is no corresponding cancellation in the fourth-order coefficient, which one should thus expect to be of about the same order 10^6 ergs/cm³ as the cubic anisotropy coefficient K_2 in (1). This is indeed what is found experimentally in cobalt,[35] as at room temperatures K'' is 2.2×10^6 ergs/cm³, or about one-half as large as $K'=5.1\times10^6$. The two terms of (51) are thus comparable even though they involve the spin-orbit parameter A to different powers (*viz.* the second and fourth).

It must be mentioned that the "one-atom model" of Bloch and Gentile described in Section 7 may have some significance for hexagonal crystals, since with only axial symmetry the crystalline field can lift the degeneracy if $S>\frac{1}{2}$. In fact the effective magneton number and g-factor can be different in different directions. Conceivably this fact has some connection with the anomalous behavior of pyrrhotite, which is ferromagnetic along certain axes but only paramagnetic along others.

The writer wishes to express his thanks to Dr. R. M. Bozorth and Professor F. Bitter for helpful comments.

[35] These values of K', K'' are calculated in unpublished work of Bozorth, from the data of Honda and Masamuto, Sci. Rep. Tohoku Univ. **20**, 323 (1931). Gans obtained $K'=1.1\times10^6$, $K''=4.4\times10^6$ from previous work by Kaya, Sci. Rep. Tohoku Univ. **17**, 1157 (1928). Dr. Bozorth asks me to record the following errata in the discussion of cobalt in his recent paper (J. App. Phys. **8**, 575 (1937)). The statement on p. 585 that the higher power term K_2 in his formula $E=K_0+K_1S_1^2+K_2S_1^4$ is negligible is incorrect, as vanishing K_2 is not required by the absence of anisotropy in the plane perpendicular to the hexagonal axis. The ordinate of Fig. 18 is K_1+K_2 rather than K_1. Bozorth's K_0, K_1, K_2 for cobalt are the same as our $F_0+K'+K''$, $-K'-2K''$, and K'' respectively since his S_1^2 is $1-\sin^2\varphi$.

DECEMBER 1, 1937 PHYSICAL REVIEW VOLUME 52

On the Nature of Cosmic-Ray Particles

Y. NISHINA, M. TAKEUCHI, AND T. ICHIMIYA
Institute of Physical and Chemical Research, Tokyo

(Received August 28, 1937)

VARIOUS authors[1] have taken the view that cosmic-ray particles consist of two or more kinds of corpuscles. According to Compton and Bethe, and Auger,[1] the soft component near sea level is thus composed of electrons and the penetrating one of protons. Assuming the theory of showers by Bhabha and Heitler[2] and by Oppenheimer and Carlson[3] to be correct, we ought to be able to distinguish cosmic-ray electrons from protons, if they exist at all, by observing whether or not the particles suffer a large loss of energy and often produce showers on colliding with a lead plate of a suitable thickness.

We carried out such experiments with a lead bar 1.5 cm thick mounted in the middle of a Wilson chamber 40 cm in diameter, which is placed in a magnetic field of about 17,000 oersteds. The operation of the chamber is actuated by the coincidence of two Geiger-Müller tube counters mounted above the chamber, the distance between the counters being about 50 cm. The results showed that at sea level near Tokyo (geomag. lat. 25.4°N) about 10 to 20 percent of cosmic-ray particles of energies, high enough to produce coincidence in the strong magnetic field and pass through the Wilson chamber, consist of electrons and positrons, the rest being heavy particles, since they do not produce showers nor suffer much loss of energy in passing through the lead bar. Among the latter, however, we were

[1] A. H. Compton and H. A. Bethe, Nature **134**, 734 (1934); P. Auger, J. de phys. **6**, 226 (1935); C. D. Anderson and S. H. Neddermeyer, Int. Conf. on Physics, London **1**, 182 (1934); Phys. Rev. **50**, 268 (1936); J. Clay, Physica **3**, 338 (1936); L. Leprince-Ringuet, J. de phys. **7**, 70 (1936); J. Crussard and L. Leprince-Ringuet, Comptes rendus **204**, 240 (1937).

[2] H. J. Bhabha and W. Heitler, Proc. Roy. Soc. **A159**, 432 (1937).

[3] J. F. Carlson and J. R. Oppenheimer, Phys. Rev. **51**, 220 (1937).

surprised to find that there are some particles of both signs, which have much greater penetrating power for lead than protons of the same momentum ($H\rho$) would have. The specific ionization of some tracks is also much smaller than that of protons of the observed $H\rho$. These results can most naturally be explained, if one assumes the existence of new particles of a mass heavier than that of an electron and lighter than that of a proton. At about this time we received the paper of Street and Stevenson[4] and then that of Anderson and Neddermeyer[5] and saw that these authors had obtained similar results. Crussard and Leprince-Ringuet[6] also recognized the existence of particles, which lose less energy through matter than expected for electrons on the theory of showers and produce smaller specific ionization than protons of the same $H\rho$.

We have since then been trying to find a more exact value of the mass of the new particle. Since this seems hardly to radiate in collision with matter, we may for the moment assume that the loss of its energy in passing through lead is entirely due to ionization, although this is probably not always the case as will later be mentioned. In this respect the new particle behaves more like protons than electrons, and especially for energies higher than 10^9 ev we cannot discriminate between the two by specific ionization, because it becomes nearly the same for both. The range in lead, however, as a function either of $H\rho$ or of energy is sensitive to the difference of mass of the particles. We can thus draw a series of mass $H\rho$ curves for various values of ranges. By means of these curves, we can determine the mass of a particle, if we know its range and $H\rho$ from Wilson tracks. As the range we chose 3.5 cm of lead mounted in the middle of our Wilson chamber. In order to filter the electronic component of cosmic rays, a lead block 20 cm thick was inserted between the two controlling counter tubes, placed above the Wilson chamber as described before.

Until now we have obtained only one track which can probably be used for the determination of the mass. The initial value of $H\rho$ of the particle was 7.4×10^5 gauss-cm and after passing through lead it became 4.9×10^5 gauss-cm, showing the loss of about a half of the energy. The loss of energy by ionization and the range in lead calculated from the thickness of the lead bar and the final $H\rho$ are consistent, if we assume the mass in question of the particle to be 1/7 to 1/10 that of the proton. The above values of $H\rho$ and the specific ionization shown by the corresponding tracks are in accordance with the assumed mass. This value must necessarily be provisional and subject to a possible alteration. For accurate determination we need more tracks of appropriate energies.

From our present experimental results we cannot conclude whether the penetrating component of cosmic rays at sea level consists exclusively of these new particles or in part of protons. There are observed some particles which are stopped by 3.5 cm of lead and can be interpreted as protons on the mass $H\rho$ curve. On the other hand we observe some particles of high $H\rho$ which seem to be stopped by the lead plate. The ionization alone cannot account for such a large loss of energy, even if they are protons. We do not know as yet whether we have here to do with the presence of particles heavier than protons or with a certain type of loss of energy other than ionization for the new particles or for protons. The disintegration of lead nuclei caused by these particles must be taken into account in the problem, as can be seen from one of our photographs. Although the exact determination of the composition of the penetrating component of cosmic-ray particles has thus not yet been possible, its large part no doubt consists of the above new particles, through the existence of which various difficulties in connection with cosmic-ray phenomena e.g., ionization, radiative effect,[7] penetrating power, etc. now find a natural explanation.

We should like to express our gratitude to the Imperial Japanese Navy for kind assistances in carrying out these experiments and to Hattori Hokokwai Foundation for a financial grant. We are indebted to Mr. M. Kobayasi for theoretical discussions.

[4] J. C. Street and E. C. Stevenson, Bull. Am. Phys. Soc. **12**, No. 2, 13 (1937).
[5] S. H. Neddermeyer and C. D. Anderson, Phys. Rev. **51**, 884 (1937).
[6] J. Crussard and L. Leprince-Ringuet, J. de phys. **8**, 215 (1937).
[7] E. J. Williams, Phys. Rev. **45**, 729 (1934); *Kernphysik*, (Berlin, 1936), p. 123.

LETTERS TO THE EDITOR

Prompt publication of brief reports of important discoveries in physics may be secured by addressing them to this department. Closing dates for this department are, for the first issue of the month, the eighteenth of the preceding month, for the second issue, the third of the month. Because of the late closing dates for the section no proof can be shown to authors. The Board of Editors does not hold itself responsible for the opinions expressed by the correspondents.

Communications should not in general exceed 600 words in length.

Contact Potential of Cleavage Face of Zinc Crystal Cleaved in Vacuum

The rate of change of the contact potential of a freshly cleaved face of a single crystal of zinc was observed by Zisman and Yamins.[1] Their curves show a rapid initial drop for a period of about 15 minutes, followed by a slow downward drift at a uniform rate for over an hour. These results suggest the possibility that if the same experiment were repeated in a vacuum, the initial rate of change might be greatly reduced. A negligible rate of change in the contact potential and hence in the work function of the surface would demonstrate the possibility of cleaving a crystal in a vacuum for the purpose of measuring the photoelectric properties of the material. The investigation described here was undertaken for the purpose of examining the feasibility of such measurements.

Single crystal bars of zinc grown with the principal cleavage plane normal to the axis of the bar can be broken by the application of a very small force. Because of this property, they can be cleaved easily in a vacuum by using the device sketched in Fig. 1. One end of the crystal is clamped in a brass tube pivoted at *A* and the other end is clamped in a longer tube which lies on a support at *B*. A weight released by an electromagnet so that it strikes at *C* after falling from a height of 10–20 cm will cleave the crystal at some point between the two tubes. A clean break is obtained in about one trial out of four. The weight *D* rotates the crystal into a vertical position, and measurements are made of the contact potential difference between it and a platinum reference surface which is lowered from above. Zisman's method is used for measuring the contact potential difference.[2]

Crystals were grown at atmospheric pressure in H_2, CO_2, and N_2, and in vacuum at a pressure of 0.1 mm of mercury. Contact potentials were measured at atmospheric pressure and in vacuum at pressures of 5×10^{-3} and 10^{-5} mm and plotted as a function of time measured from the instant at which the crystal was cleaved. For vacuum measurements, the crystal and the platinum reference surfaces were allowed to remain in the vacuum for 24 hours before cleaving in order that the platinum surface might reach a state of equilibrium.

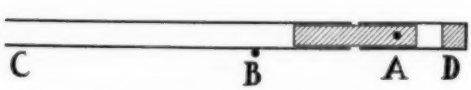

FIG. 1. Arrangement for breaking crystal in vacuum.

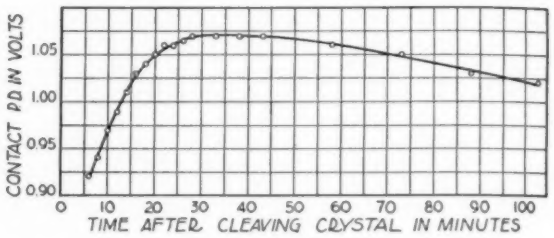

FIG. 2. Contact potential change with time after cleaving crystal. Pressure about 10^{-5} mm.

The crystals broken in air at atmospheric pressure showed a slow drop in contact potential difference of about 0.1 volt per hour for the first hour. Although the first measurement was made within ½ min. after cleaving, no trace was found of the rapid initial drop observed by Zisman and Yamins. At a pressure of 5×10^{-3} mm, the contact potential difference dropped at the rate of 0.05 volt per hour for the first hour. At pressures in the neighborhood of 10^{-5} mm, the contact potential difference varied as shown in the curve (Fig. 2). This curve was taken with a crystal grown in H_2, but all of the crystals showed the same qualitative behavior, the only difference being in the rate of the initial rise. The maxima of the various curves agreed to within 0.03 volt.

A possible explanation of the phenomena observed is that the rapid initial rise, which corresponds to a decrease in the work function of the zinc, is due to the formation of a surface layer of gas, and that the subsequent drop is due to the gradual diffusion of this surface layer into the crystal.

FRED B. DANIELS
M. Y. COLBY

Department of Physics,
University of Texas,
Austin, Texas,
November 8, 1937.

[1] W. A. Zisman and H. G. Yamins, Physics **4**, 7 (1933).
[2] W. A. Zisman, Rev. Sci. Inst. **3**, 367 (1932).